Temperature and Solvent Effects, Rate Constants and Activation Parameters for the Reactions of the Excited States of Substituted Benzene Compounds

By

Carlos Miguel Gonzalez

Submitted in partial fulfillment of the requirements
for the degree of Doctor of Philosophy

at

Dalhousie University
Halifax, Nova Scotia
May 2006

Your file Votre référence
ISBN: 978-0-494-19601-4
Our file Notre référence
ISBN: 978-0-494-19601-4

DALHOUSIE UNIVERSITY

To comply with the Canadian Privacy Act the National Library of Canada has requested that the following pages be removed from this copy of the thesis:

Preliminary Pages
- Examiners Signature Page (pii)
- Dalhousie Library Copyright Agreement (piii)

Appendices
- Copyright Releases (if applicable)

Table of Contents

Chapter 1

Introduction to the Kinetic Study of Reactions Occurring from Excited States

Chapter 2

Temperature and Solvent Effects, Rate Constants and Activation Parameters for the Reactions of the Excited States of Substituted Benzenes

Chapter 3

Steric Effects in the Phototransposition Reaction of Dialkylbenzenes

Chapter 4

A Mechanistic Study of the Photochemical Addition of Alcohols to Methoxy-Substituted 1,2-Diphenylethyne Derivatives

List of Figures

List of Schemes

List of Tables

Abstract

The rate constants of decay of the excited singlet states (k_d) of the *o*-, *m*- and *p*-isomers of cyanotoluene **1**, arylboranate ester **2**, trifluoromethyltoluene **3** (photochemically reactive isomers) and methylanisole **4** (photochemically stable even at 50 °C), were determined by the measurement of the lifetimes of S_1 (τ_s) in acetonitrile (AN) over a range of temperatures. In addition, measurements of τ_s were carried out in 2,2,2-trifluorethanol (TFE) for the *o*-, *m* -and *p*-isomers of cyanotoluene and arylboranate ester over the same range of temperatures. By fitting the experimental values of k_d vs. T to a non-linear expression (the Arrhenius plot method), that includes rate constants for reaction (k_r), fluorescence (k_f), and intersystem crossing (k_{isc}), the values for the rate constants for all of the processes of S_1 were obtained reliably. Measurements of τ_s in AN and TFE indicated that the values of k_r for S_1 are greater when the ionization power of the solvent increases. The influence of the solvent on k_d suggests that the prefulvene intermediates are polar. The values of k_{isc} and k_f obtained are essentially the same in both solvents. The dependence of τ_s on temperature for the isomers of methylanisole suggests that an activated intersystem crossing process may also take place.

Dialkylsubstituted cyanobenzenes **5** and **6**, and their cyclic analogues (indans **7** and **8**, and tetralins **9** and **10**) were studied in order to understand the geometric changes required to form the prefulvene intermediates, as well as the influence of ortho-methyl substitution on the photochemistry of cyano-substituted benzene compounds. The reactivity of S_1 decreased (absence of photoproducts) for both of the compounds containing the neighbouring ring and the cyano substituted benzene compounds with an ortho-methyl group. The values of k_{isc} and k_r for S_1 were again determined by the Arrhenius plot method.

The photochemical addition of TFE to methoxy-substituted tolans **11** – **14** was also investigated. Solvent studies, including isotopic substitution experiments, were carried out to elucidate the reaction mechanism. The mechanism is consistent with a rate-determining proton transfer process, followed by a trapping of the resulting carbocation by the solvent. Compared to the parent tolan, *m*-methoxy and 3,4-dimethoxytolan display a larger quantum yield for fluorescence, as well as an increased photochemical reactivity toward the addition of TFE. The *p*-methoxy compound was also found to be more reactive photochemically toward TFE than tolan.

List of Abbreviations and Symbols Used

Photochemistry

S_0	singlet ground state
S_1	first singlet excited state
S_2	second singlet excited state
T_1	first triplet state
τ_s	singlet excited state lifetime
$h\times\nu$	electromagnetic energy (light)
A	absorvance
ϵ	extinction coefficient
ϵ_{max}	extinction coefficient for the absorption maximum
λ	wavelength for both the electronic and the emission spectra
λ_{max}	wavelength for both the electronic and the emission spectra for the maximum
ν	frequency for the electromagnetic radiation (light)
ν'	frequency for the emitted light (emission spectrum)
I_f	intensity of the fluorescence
I_{abs}	intensity of the absorbed radiation.
I_o	intensity of the light beam arriving from the source of light
Φ_i	quantum yield for the i process
Φ_r	quantum yield for reaction

Φ_f	quantum yield for fluorescence
Φ_f^o	quantum yield for fluorescence when [Q] = 0
Φ_{isc}	quantum yield for intersystem crossing
Φ_p	quantum yield for phosphorescence
Φ_{prod}	quantum yield for product formation
Φ_i	efficiency for the formation of a particular excited state
ϕ_{RI}	efficiency of formation of the reactive intermediate from S_1
M*	excited molecule
$E_{0,0}$	energy of the zero-zero band
f	oscillator strength
$\Delta\mu$	dipole moment of the $S_0 \rightarrow S_n$ transition

Kinetics

k_i	rate constant for the i process
k_d	rate constant of deactivation for S_1
k_r	rate constant for reaction
k_f	rate constant for fluorescence
k_f^{calc}	rate constant for fluorescence calculated by the Strickler / Berg equation (eq. 1.12)
k_{isc}	rate constant for intersystem crossing
k_{ic}	rate constant for internal conversion
k_p	rate constant for phosphorescence

k_{prod}	rate constant for product formation
k_{abs}	rate constant for absorption of electromagnetic radiation (light)
k_Q	rate constant for a quenching process
k_H	rate constant for a proton transfer reaction
k_D	rate constant for a deuterium transfer process
R_{M*}	rate for deactivation of M*
R_{abs}	rate for absorption of electromagnetic radiation (light)
R_f	rate for the fluorescence process
R_{isc}	rate for the intersystem crossing process
R_{ic}	rate for the internal conversion process
RI	reactive intermediate
Q	quencher
E_{act}	activation energy
A	pre-exponential factor
C_{sv}	Stern-Volmer coefficient
$\Delta S^{\neq}$	activation entropy

n	the refractive index of the solvent
A_{nm}	Einstein coefficient for induced emission
B_{nm}	Einstein coefficient for spontaneous emission
ε	solvent dielectric constant
ε_o	permittivity of vacuum
m_e	electron mass
N	Avogadro constant
e	elementary charge
μ	dipole moment
h	Plank's contant
c	speed of light
R	gas constant
k	Boltzmann constant
δ	electron density
$\langle\nu\rangle$	the expectation value for the frequency of the fluorescence spectrum
g_i	multiplicity of the i state
g_u	multiplicity of the g state
pH	acidity scale defined as: $-\log [H^+]$
α	Bronsted coefficient
K_{HA}	dissociation equilibrium constant for the acid HA

V	wavefunction for the coordinates of the nuclei
$<V(S_1)\|V(S_0)>$	Franck-Condon factor
ΔE	energy gap between the zero points of S_0 and S_1
e	standard error

Solvents

AN	acetonitrile
TFE	2,2,2-trifluoroethanol
TFED	deuterated 2,2,2-trifluoroethanol
THF	tetrahydrofuran

Experimental Techniques

UV	ultraviolet
GC-MS	gas chromatography, mass selective detector
GC-FID	gas chromatography, flame ionization detector
m/z	mass to charge ratio
^{1}H NMR	proton magnetic resonance
^{13}C NMR	carbon-13 magnetic resonance
δ	chemical shift

Acknowledgements

My PhD student experience has been the most important part of my life so far. Without any doubt, having come from Havana City to the Halifax to pursue my PhD education was a crucial decision. In writing my acknowledgments, I could not help but reflect seriously on what my life has been in these last five years. I conclude mainly that life has provided me with the best scenario that I could have chosen for the completion of my graduate studies. First, Halifax very soon became a place that I with no hesitation call home. After a couple of years, I felt very confortable living in Halifax. The way of the Haligonians; kind, polite, joyful, contributed to help me feel at home. Second, Dalhousie University has been the best place to complete my education as a chemist. I believe the most important factor that has influenced my performance as a PhD student remarkably was the role that my supervisor, Professor James Pincock, and his research group have played in my life. I must say that it has been an honour and a pleasure to have gotten to know Dr. Pincock. As a clever and wise man, he directed my investigation to a fruitful end. His advice and suggestions were invaluable for the results that are presented in this thesis. His experience and knowledge helped me save time and resources in the experiments that I had to carry out during these years. Very soon, I realized that Dr. Pincock was the type of chemist that masters several disciplines in Chemistry with equal ability. It is customary in the acknowledgements part of a thesis to say how grateful one is regarding supervisors and co-workers; in my case, I truly mean it. I could not have been more fortunate in having Dr. Pincock as my supervisor. Not only is he a very skillful chemist, but more importantly, he is a kind man, with a huge heart, and

a deep knowledge of human nature. From the bottom of my heart: Thank you, Dr. Pincock. I will never forget the years I have spent working in Dr. Pincock's research group. I also want to thank Alex Pincock for all her support. In the most generous way, she passed on to me a great part of her lab experience. She always has taken care of the smallest details in Dr. Pincock's lab and has given me a great deal of help with the computer programs. Alex has been that guardian angel that one can count on when things get tough. From a personal point of view, I want to tell Alex how much I enjoyed our little chats. These were enjoyable moments that I still look forward to having. I also had the pleasure of working with Dr. Jeff Roberts, a former graduate student of Dr. Pincock. For four years he was my lab-mate, the best one I could have had; kind, cooperative and sensitive. He was always conscious of my research needs by accommodating his own experiments in such a way that we both could efficiently use the instruments. Having more experience than me with respect to experimental chemistry, Jeff always gave me his support and generously shared his knowledge. I truly appreciated our chemistry talks and our discussions about the nature of things.

The research described in this thesis has been possible thanks to the generous donations of chemicals by Sepracor to Dr. Pincock's research program. I must thank Cory Beshara for his help with the hydrogenation reactions described in Chapter 4, and for our valuable talks in which I became aware of his knowledge of the synthetic organic chemistry and his potential as a chemist. I must also thank Reinaldo Moya, for his support with the NMR programs and for having taken the time to explain to me all the details required to be able to work with the 500 MHz NMR instrument at the ARMR center. In addition, I must acknowledge Lisandra Cubero for having provided me with the

mass spectra reported in the NIST Library, for her helpful explanations, and for being a great friend. Finally, I want to mention the pleasant relationship that the members of Dr. Pincock's group has with the research groups of Dr. Norman Schepp and Dr. Frances Cozens. I wish to acknowledge Dr. Mike Lumsden and Dr. Bob Berno for having carried out the 2D NMR spectra presented in Chapter 4.

I would like to thank professors Philip Pacey and Peter Wentzell for having taken the time to answer my questions with great patience.

I sincerely thank the Graduate Studies Faculty and the Department of Chemistry for their generous economic support during these years

I must thank also the members of the Department of Chemistry, staff and researchers, for having been kind, polite and cooperative co-workers. I want to especially mention the spirit of cooperation that exist in our department. I believe that this is the type of human behaviour that is precious to humankind, and gives hope for a future of harmony and peace.

Finally, I want to mention that my family was very supportive during these five years and that I am eternally indebted to them.

Chapter 1

Introduction to the Kinetic Study of Reactions Occurring from Excited States

1.1. Overview of thesis

The study of a reaction mechanism often requires, in addition to the identification of the intermediates that are formed during the chemical process, the estimation of kinetic parameters such as the activation energy (E_{act}) and the pre-exponential factor (A). These kinetic parameters provide a powerful tool for understanding the dynamics of the chemical processes occurring from either the ground state or an excited state. Kinetic studies allow us to understand and predict the effect of the changes in both the structure of the reactants and the solvent on the generation, reactivity, stability and type of the intermediates.

The first part of this thesis will provide a comparison between the classical method of determining the kinetic rate constants of the chemical processes occurring from the ground state (S_0), and of those occurring from the first singlet excited state (S_1). Section 1.2 will give an overview of the physical and chemical processes that provide de-activation pathways for electronically excited molecules formed by absorption of electromagnetic radiation. The relation between the lifetime (τ_s) of the lowest energy

singlet excited state, S_1, and the rate constant for all the processes of decay will be then discussed. Section 1.3 will present a discussion of quantum yields for the same processes. Section 1.4 will present a historical overview of the development of the photochemistry of benzene compounds, followed in Section 1.5 by a discussion of the intermediates involved. Section 1.6 will present a brief summary of the photochemistry in protic solvents of benzene compounds conjugated to acetylene units (1-arylalkynes).

The discussion of the investigation begins in Chapter 2, with a report of the influence of the temperature on the τ_s of the excited sates for the *o-*, *m-* and *p-* isomers of the methylbenzonitriles (**1o, 1m, 1p**); 2-(4', 4', 5', 5'-tetramethyl-1', 3', 2'-dioxaborolanyl)toluenes [arylboronate esters], (**2o, 2m and 2p**); trifluoromethyltoluenes, (**3o, 3m and 3p**) and methylanisoles, (**4o, 4m and 4p**). The estimated values of kinetic rate constants (k_i) and quantum yields (Φ_i) for all processes of S_1 in both acetonitrile (AN) and 2,2,2-trifluoroethanol (TFE) will be presented and discussed.

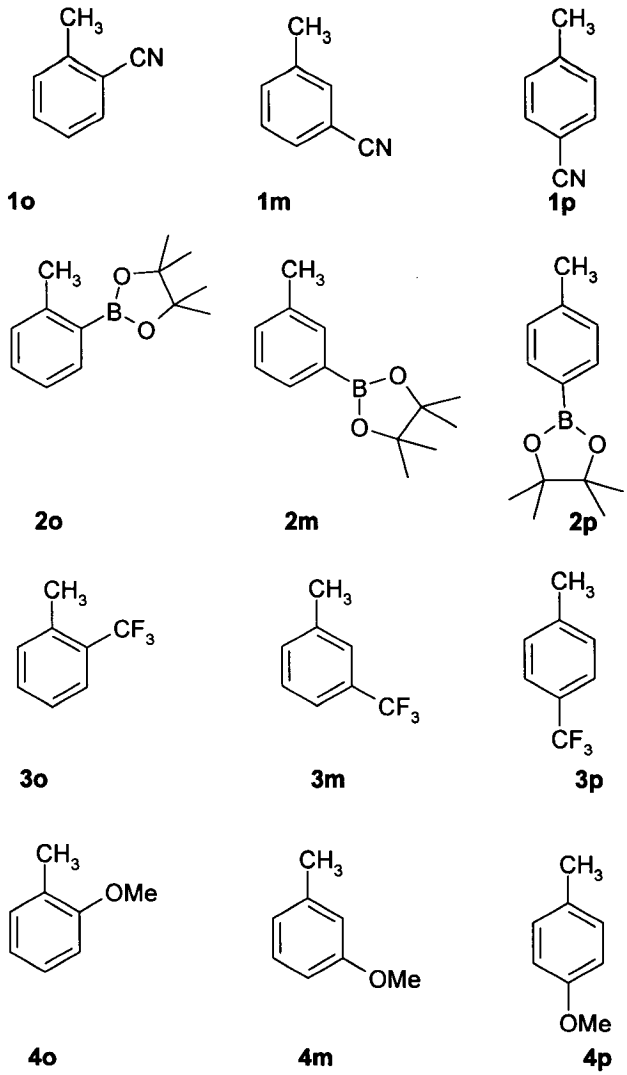

Chapter 3 will present a report on the influence of the substitution pattern on the photochemical behavior of dialkylbenzonitrile compounds. A comparative study of the photochemistry of 2,3- and 3,4-dimethylbenzonitrile (**5, 6**) with respect to the photochemsistry of 4- and 5-cyanoindane **(7, 8)** and 5- and 6-cyano-1,2,3,4-tetrahydronaphtalene **(9, 10),** as more rigid analogues of **5** and **6,** will be described in order to understand the influence of the methyl or methylene substituents on the photochemical behavior of the dimethylbenzonitriles. The objective of these experiments is to investigate if the neighboring ring can hinder intramolecular motions of S_1 that

might produce isomers. The multiplicity of the reactive excited state for **5** and **6** will also be established.

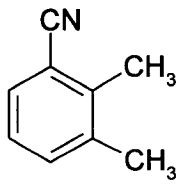

5

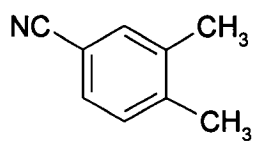

6

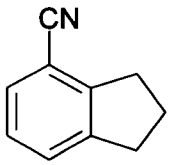

7

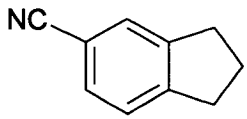

8

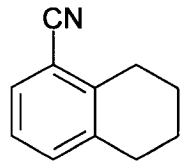

9

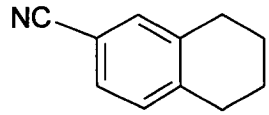

10

Chapter 4 will present a mechanistic study on the photochemical addition of alcohols to diphenylacetylene **11** and methoxy-substituted diphenylacetylenes (**12**, **13**, **14**). The influence of meta-methoxy substituents on the photochemistry and photophysics of these compounds will be discussed.

11

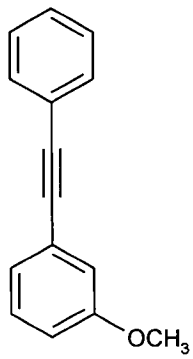

12

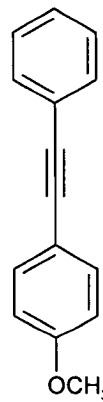

13

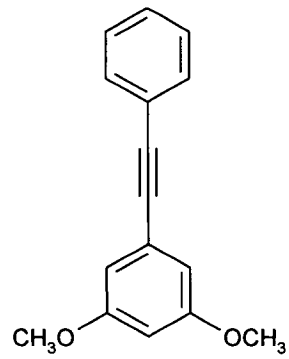

14

Chapter 5 will provide the experimental details for the projects reported.

1.2. Chemical kinetics

1.2.1. Scope of chemical kinetics

Chemical kinetics deals with the rates of chemical processes and how the rates depend on factors such as reactant structure, concentration, temperature, and the solvent. Such studies are important in providing evidence as to the dynamics and, consequently, the mechanisms of chemical processes. The kinetic study of chemical reactions may also include investigations into the detection of reactive intermediates, the determination of the influence of the temperature on rate constants (calculation of E_{act} and A), the study of the influence of the substituents on the rate constants (linear free energy relationship),[1] and the study of the influence of the solvent on the relative energy of the transition state (TS) and the reactants,[2] as well as studies that use isotopes, either as kinetic or structural probes.

Chemical reactions can occur in many media, including the gas phase, in solution in a variety of solvents, in liquid and solid states, and at gas-solid, and liquid-solid interfaces. These processes can be initiated using thermal energy or electromagnetic radiation (microwave energy, gamma rays and UV radiation). The goal of this thesis is to use the kinetic investigation of the excited states as a tool for understanding the dynamics of the excited states' processes.

1.2.2. Dynamics of excited states

This section will give a brief explanation of excited states processes as discussed in a classic textbook.[3] Absorption of electromagnetic radiation initially leads to the formation of an excited state. A molecule does not persist in the excited state indefinitely, since this is an unstable situation with respect to the ground state. Electronic de-excitation must somehow occur; the excess energy can be released as thermal or radiation energy. Transitions involving the de-excitation of electronically excited states that do not involve the emission of radiation are called non-radiative transitions, whereas those that give rise to the emission of radiation are called radiative transitions. The emitted radiation is called fluorescence if it originates from an excited state with the same spin multiplicity as the ground state. Since all closed shell molecules have singlet ground states, fluorescence is most frequently observed from singlet excited states, most commonly, $S_1 \rightarrow S_0$. The emission is called phosphorescence if it originates from an excited state of spin multiplicity different from that of the ground state (for example, most commonly, $T_1 \rightarrow S_0$).

All of the possible transitions that may occur between the different energy levels can be presented by the Jablonski diagram, Figure 1.1, which is actually a state diagram. This diagram is simplified from the general case by showing only the lowest energy excited state of two different multiplicities, singlet S_1 and triplet T_1. This simplification is appropriate for most of the excited-state reactions of organic compounds in solution. Transitions that involve electromagnetic radiation (both absorption and emission) are indicated as straight arrows and non-radiative transitions as wiggly arrows. It is also important to illustrate the possibility of generating differing vibrational states associated

with each electronic energy level. Non-radiative transitions involve conversion from one state to another with the evolution of thermal energy. Non-radiative conversion between states of the same spin multiplicity is called internal conversion (ic). For states of different spin multiplicity the term intersystem crossing (isc) is used. Intersystem crossing from the first excited singlet state S_1 to the first excited triplet state T_1 leaves the molecule with some excess vibrational energy above the lowest T_1 level. In solution, this excess energy is rapidly removed by collisions with solvent molecules, *i.e.* vibrational relaxation (vr). The de-activation by a chemical reaction is a process that can occur from any of the excited states, including the triplet state, and is characterized by the rate constant k_r. Therefore, in contrast to ground state kinetic studies, excited-state reactivity is complicated by the possibility of both excited singlet and triplet states reacting. Selective quenching of the triplet states, because of their longer lifetimes, or selective generation of the triplet state by sensitization techniques have been the historical methods of determining which of the two states reacts, or whether both states are reactive. Rate constants can be determined experimentally for many of the processes shown in Figure 1.1 using methods that usually monitor the emitted light (fluorescence and/or phosphorescence) as a way to determine the concentration of excited molecules with respect to time.

Figure 1.1. Jablonski diagram

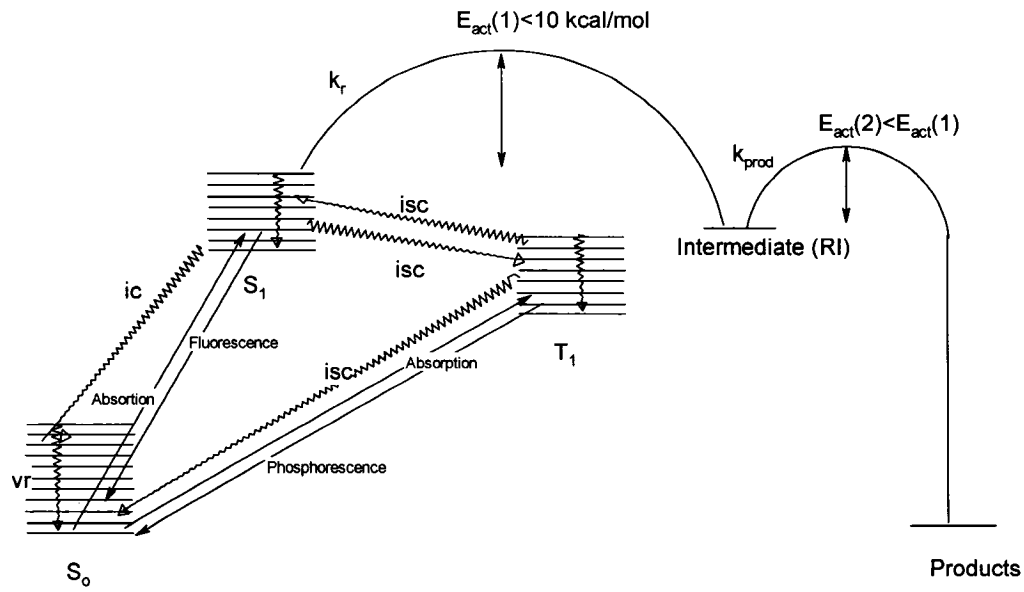

ic: Internal conversion
isc: Intersystem crossing
vr:Vibrational relaxation

$S_1 \longrightarrow S_o + h\nu'$	k_f	Fluorescence
$S_1 \longrightarrow T_1 + \text{heat}$	k_{isc}	Intersystem crossing
$S_1 \longrightarrow S_o + \text{heat}$	k_{ic}	Internal conversion
$S_1 \longrightarrow RI + \text{heat}$	k_r	Chemical reaction
$T_1 \longrightarrow S_o + h\nu''$	k_p	Phosphorescence
$RI \longrightarrow P + \text{heat}$	k_{prod}	Formation of products
$RI \longrightarrow S_o + \text{heat}$	k_{icr}	Thermally activated internal conversion

The usual experimental limits of the rate constant of fluorescence, k_f, are from 10^9 sec^{-1} to 10^5 sec^{-1} and for intersystem crossing, k_{isc}, from 10^{12} sec^{-1} to 10^5 sec^{-1}. The de-activation by internal conversion k_{ic} for aromatic molecules is usually a minor pathway for decay, as the values of the kinetic rate constant for this process range from 10^5 sec^{-1} to 10 sec^{-1}. A chemical reaction of the singlet excited state, k_r, might be a main pathway for deactivation, with rate constants having a range of values from 10^{15} to 10^{-6} sec^{-1}. In order

for a chemical reaction to be a dominant pathway k_r must be greater than k_f, k_{ic} and k_{isc}. For substituted benzene compounds, phosphorescence occurs with kinetic rate constants ranging from 10^6 sec^{-1} to 10^{-1} sec^{-1}.

1.2.3. Reactions of the singlet excited state

The absorption of electromagnetic radiation offers the possibility of initiating chemical processes that usually have no analogue in thermal chemistry. In most photochemical reactions, the necessary energy for starting the transformation comes in the form of ultraviolet radiation. Absorption of this energy initiates promotion of an electron from the highest occupied bonding molecular orbital to an unoccupied antibonding orbital. The photon energy ($E = h\nu$) is therefore "matched" to the energy difference between these two levels. The electronic transition frequency spans a narrow range of values as the electronic spectrum of aromatic compounds in solution features bands instead of lines. Chemists can make use of a substantial portion of the electromagnetic spectrum to reveal details of molecular structure and motion, including infrared (vibrational) and microwave (rotational) spectroscopy. However, organic photochemists are primarily concerned with energies provided by absorption in the ultraviolet (UV) and visible (VIS) portion of the electromagnetic spectrum, from 200 nm (approximately 600 kJ/mol) to 700 nm (approximately 170 kJ/mol).

The choice of the excitation energy depends on the electronic spectrum of the compounds being studied. Moreover, it provides us not only with the experimental data on which we base our theories of electronic structure, but also with the information required regarding suitable excitation wavelengths. The excitation energy is, thus,

dictated by the nature of the electronic energy levels that determine the absorption spectrum of the reactant. Evidently, the "first law of photochemistry" is that only radiation that is absorbed by a molecule can lead to chemical change.

For most reactions of excited states, the reaction leads to a reactive intermediate (RI), Scheme 1.1. The lifetimes of such reactive intermediates may vary from picoseconds to seconds. Often RI's can be studied by, for example, laser flash photolysis so that their reactivity is well understood for many cases. However, their rates of formation are not easily determined without very fast probe techniques (pico- or femtosecond lasers). The traditional way of estimating k_r values has been by measuring quantum yields of products Φ_{prod}. Unfortunately, this method ignores the internal return of the reactive intermediate (RI) to S_0, Scheme 1.1.

Scheme 1.1. Basic dynamics of a singlet excited state

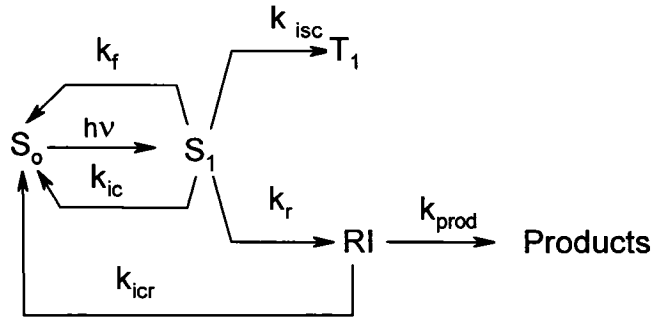

An excited molecule can undergo a unimolecular photoisomerization or photofragmentation due to the high content of absorbed energy. If there are no other molecules to react with the excited state (bimolecular process) or if the excited molecule does not undergo any unimolecular reactions, it will simply emit radiation as either fluorescence or phosphorescence and thus return to the ground state. The presence of a

molecule, called a quencher, with which the excited state can interact, or the occurrence of a unimolecular reaction may allow processes that will compete with emission or radiationless decay.

Information about the excited state reactivity can be obtained by the study of the emission of light, which can be characterized in terms of its intensity and its dependence with respect to time. Such studies can provide, for example, the lifetime of the excited state.

1.2.4. The radiative lifetime

For a radiative process from a molecule in isolation, the concentration of the electronically excited molecules [M*] will decay to zero as a function of time due to the spontaneous emission of radiation: M* → M + hν', where hν' is usually a lower energy photon compared to the one initially absorbed by the ground state molecule. This emission process follows first order kinetics, defined by a rate constant of decay k_d, eq. 1.1.

$$\frac{-d[M^*]}{dt} = k_d\,[M^*] \tag{1.1}$$

The lifetime of a molecule in the excited state is simply the reciprocal of the emission rate constant, eq. 1.2. If the only process that the molecule undergoes is fluorescence, k_d in eq. 1.2 can be substituted by k_f, eq. 1.3.

$$\tau_s = \frac{1}{k_d} \tag{1.2}$$

$$\tau_s = \frac{1}{k_f} \tag{1.3}$$

This expression is oversimplified, because it is only correct in the absence of all other processes by means of which the excited molecule could return to the ground state. Therefore, the lifetime τ_s is equal to the reciprocal of the sum of all rate constants for the processes that deactivate S_1, both radiative and non-radiative ones, including rate constants of chemical reactions, eq. 1.4.

$$\tau_s = \frac{1}{k_d} = \frac{1}{\sum k_i} \tag{1.4}$$

Experimentally, values of τ_s can be determined by measurement of the decay of S_1 as a function of time. In the case of S_1, the most convenient method to monitor the concentration of [M*] is to measure the fluorescence intensity emitted from the S_1 state.

1.2.5. Singlet lifetimes

Experiments can be performed in which the ground state molecule is electronically excited by a radiation of an appropriate wavelength. Examination of the emitted electromagnetic radiation as a function of time, Figure 1.2, permits us to determine the radiative lifetime by means of the rate of decay, eq. 1.5.

Figure 1.2. Exponential decay of the concentration of electronically excited molecules

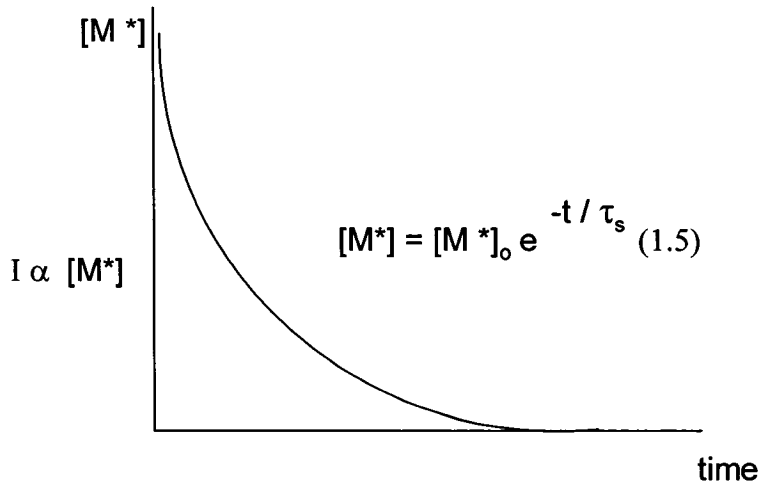

As stated before, k_d, although measured by fluorescence decay, cannot be identified as k_f because additional processes contribute to the decay of the excited state. For unreactive excited states, the fluorescense of M* is in competition with internal conversion (which results in vibrationally excited S_0) and with intersystem crossing (which gives T_1). Therefore, the overall rate of decay has to include all the kinetic laws of such processes, eqs. 1.6-1.10.

$$M^* \rightarrow M_0 + h\nu \qquad R_f = k_f[M^*] \tag{1.6}$$

$$M^* \rightarrow T_1 + \text{heat} \qquad R_{isc} = k_{isc}[M^*] \tag{1.7}$$

$$M^* \rightarrow M_0 + \text{heat} \qquad R_{ic} = k_{ic}[M^*] \tag{1.8}$$

$$R_{M^*} = \frac{-d[M^*]}{dt} = k_f[M^*] + k_{isc}[M^*] + k_{ic}[M^*] \tag{1.9}$$

$$R_{M^*} = \frac{-d[M^*]}{dt} = (k_f + k_{isc} + k_{ic})[M^*] = k_d[M^*] \tag{1.10}$$

The decay of M* will still obey first order kinetics, but now the rate constant for the deactivation process is taking into account the actual dynamics of S_1.

1.2.6. The Strickler and Berg equation of the radiative lifetime[4]

In 1962, Strickler and Berg derived a theoretical equation for aromatic molecules that relates the rate constant of fluorescence to the absorption spectrum. Einstein initially pointed out that two processes needed to be considered in emission of radiation: induced emission, defined by the factor B_{nm}, and spontaneous emission, defined by the factor A_{nm}, where m denotes the lower energy level and n the higher. In UV spectroscopy, spontaneous emission is usually much more efficient than stimulated emission and therefore, k_f is defined only as a function of A_{nm}. Therefore, the fluorescence rate constant k_f is equal to the Einstein coefficient for spontaneous emission summed over the entire range of the fluorescence spectrum.[3,4]

$$k_f = \sum_{nm} A_{nm} \tag{1.11}$$

A_{nm} can be estimated on the basis of the theory of the Boltzmann distribution of populations, and the resulting eq. 1.12 can be derived:

$$k_f^{calc} = 2.88 \times 10^{-9} n^2 < v^{-3} >^{-1} g_i / g_u \int \epsilon \, d \ln v \tag{1.12}$$

where n is the refractive index of the solvent, $\langle \nu^{-3} \rangle^{-1}$ is the expectation value for the frequency of the fluorescence spectrum, g_i and g_u are the multiplicity of the lower and upper electronic levels and $\int \epsilon \, d\ln\nu$ is proportional to the integrated absorption spectrum.

Three early independent studies have been carried out to test the validity of eq. 1.12 for the fluorescence rate constant, by Strickler and Berg,[4] Birks and Dyson[5] and Ware and Baldwin.[6] The values of the fluorescence rate constant were determined experimentally from observations of τ_s and Φ_f in dilute solution. The theoretical fluorescence rate constant was obtained by fitting both the emission and electronic spectrum to the theoretical eq. 1.12. This expression has been demonstrated by these authors to be valid for a number of compounds in which the transition studied is strongly allowed, and the geometry of the ground and excited state are very similar, as indicated by the fact that the absorption and emission spectra exhibit good mirror image symmetry. However, an increasing number of successful calculations of k_f for aromatic compounds whose $S_0 \rightarrow S_1$ transitions are symmetry forbidden have been reported.[7, 8] Table 1.1 shows some of the calculated values and the experimental ones.

Table 1.1. Comparison of experimental fluorescence rate constants and theoretical fluorescence rate constants for anthracene, perylene and fluorescein

Compound	Solvent	k_f(exp.) / 10^7 s^{-1}	k_f^{calc} /10^7 s^{-1}
Anthracene	Benzene	6.4	7.0[4]
	Benzene	6.0	7.4[6]
	95 % ethanol	5.2	5.6[4]
Perylene	Benzene	18.2	19.6[4]
	Benzene	18.6	20.7[5]
	Benzene	17.7	19.8[6]
Fluorescein	0.1 M NaOH (H_2O)	20.2	21.3[6]

1.3. Quantum yields for excited state processes

The photochemist needs to have some measure of the efficiency of the various photochemical pathways of decay that is, to quantify the yield of a process relative to the total photons absorbed. For a photochemical reaction, eq. 1.13, the quantum yield for formation of the product B can be defined as in eq. 1.14.

$$M + h\nu \rightarrow M^* \rightarrow B \tag{1.13}$$

$$\Phi_B = \frac{No.\ of\ molecules\ of\ B\ formed\ per\ unit\ of\ time\ per\ unit\ of\ volume}{No.\ of\ quanta\ absorbed\ per\ unit\ of\ time\ per\ unit\ of\ volume} \tag{1.14}$$

The photochemical transformation requires that a molecule of M absorbs a photon (First Law of Photochemistry). If there is the probability that light absorption will produce 100% of the reactive state M* with respect to its ground state, and if then M* is converted into B every time that it absorbs a photon, the photochemical process will be 100% efficient and Φ_B will be equal 1. If the excited state M* has other decay pathways than the photochemical reaction, then the quantum yield for B is lower than 1 and the conversion is no longer 100% efficient.

A quantum yield can be defined for any process, including the physical ones, radiative and non-radiative. For example, the quantum yield for fluorescence can be defined as follows, eq. 1.15.

$$\Phi_f = \frac{No.\ of\ molecules\ fluorescing\ per\ unit\ of\ time\ per\ unit\ of\ volume}{No.\ of\ quanta\ \ absorbed\ \ per\ unit\ time\ per\ unit\ of\ volume} \qquad (1.15)$$

As the number of photons absorbed or emitted is related to the intensities, an alternative expression for Φ_f, which is very useful in practice, can be written, eq. 1.16.

$$\Phi_f = \frac{I_f}{I_{abs}} \qquad (1.16)$$

I_f is the intensity of the fluorescence and I_{abs} is the intensity of the absorbed radiation. I_{abs} is distinct from the intensity of the light beam arriving from the source of light, I_o, as all the photons incident on the sample may not be absorbed by it. Eq. 1.16 is used for experiments in which the excitation energy is supplied continuously in order that

a steady state concentration of M* is reached, generating a constant fluorescence intensity.

1.3.1. The fluorescence quantum yield

The previous definition of Φ_f denotes the concentration of fluorescence photons emitted (h ν') as a function of time and relates this to the concentration of photons absorbed (h ν) in the same time. Therefore, an expression for Φ_f can be written in terms of the rates of absorption and fluorescence, eq. 1.17.

$$\Phi_f = \frac{\frac{d[h\nu']}{dt}}{\frac{-d[h\nu]}{dt}} = \frac{k_f\,[M^*]}{k_{abs}\,[M]\,[h\nu]} \tag{1.17}$$

As Φ_f can be determined by steady state measurements, then eq's. 1.18 and 1.19 apply, where the first term is the rate of absorption and the second one the total rate of decay, including fluorescence.

$$-\frac{d[M^*]}{dt} = k_{abs}\,[M]\,[h\nu] - \Sigma k_i\,[M^*] = 0 \tag{1.18}$$

$$\text{then, } [M^*] = \frac{k_{abs}\,[M]\,[h\nu]}{\sum k_i} \tag{1.19}$$

Substitution of eq. 1.19 into 1.17 gives

$$\Phi_f = \frac{k_f}{\sum k_i} \tag{1.20}$$

Because $\tau_s = \frac{1}{k_d} = \frac{1}{\sum k_i}$

(1.4)

then Φ_f can be written as eq. 1.21.

$$\Phi_f = k_f \tau_s \qquad (1.21)$$

This expression allows the calculation of k_f from the experimental quantum yield for fluorescence and the experimental lifetime.

1.3.2. The experimental study of radiative transitions

A considerable amount of detailed kinetic and mechanistic information can be obtained from the study of radiative processes. This information is important for organic photochemistry, because the study and knowledge of photochemical routes requires an understanding of how the excited states behave.

Emission spectroscopic methods offer a way to determine the radiative lifetime of an emitting molecule and, therefore, to gain an understanding of the dynamics of such excited states when variables such as temperature and solvent vary. Flash photolysis techniques, generating a high concentration of excited molecules, provide a way to monitor the concentration of excited molecules as a function of time. τ_s can be determined using this technique. This method is used as well to produce photochemical transients (excited states, radicals, complexes, ions, etc.). The concentration and kinetics of such unstable species can then be determined by monitoring their concentration as a function of time.

Time correlated single-photon-counting fluorescence spectroscopy, which is also a flash technique, is a useful way to determine the lifetime of an excited singlet state. This technique uses multiple pulses to excite a molecule, and the resulting decay profiles are summed together. The cycle is repeated thousands of times per second. The decay profile generated by a singlet lifetime apparatus represents a sum of many absorption-emission processes. The decay profiles can give very precise estimates of radiative lifetimes.

The determination of quantum yields provides the efficiency of the different photochemical events occurring from the excited state. Emission quenching methods offer a way to determine second-order rate constants for both chemical and physical processes, and give an indirect method for determining τ_s. The presence of a quencher Q requires including the rate law for this interaction in the dynamics of an excited state. A quencher can interact with an excited state by exchanging energy, by way of a mechanism of deactivation called energy transfer, or by a chemical reaction. The method consists of the measurement of the quantum yield of one of the processes of S_1, often the fluorescence quantum yield, at different quencher concentrations, and finally comparing these changed quantum yields with the quantum yield of the process at [Q] = 0. The Stern-Volmer equation, eq. 1.22, is used:

$$\frac{\phi_f^o}{\phi_f} = 1 + \tau_s k_Q [Q] \tag{1.22}$$

This equation is linear with respect to the quencher concentration, with an intercept of unity and a slope that includes the product of both the lifetime and the second

order kinetic rate constant of the quenching process. Independent measurements of τ_s, for instance by single-photon-counting fluorescence decay, gives k_Q, the bimolecular quenching rate constant

1.4. The photochemistry of benzene compounds

As late as the 1950's, benzene was actually suggested as a useful solvent for photochemical reactions because of its stability to ultraviolet irradiation. By 1960, however, such statements on the photostability of aromatic compounds had been totally discredited by the publication of several reports describing photoinduced isomerization and addition reactions of benzene rings and substituted benzenes.[9,10,11] These accounts encouraged an important number of investigations into all aspects of the photochemistry of aromatic compounds. A prominent feature that emerged is that while the thermal reactions of substituted benzenes are, with a few exceptions, restricted to substitution processes with the retention of aromaticity, the photoexcitation of the benzene ring leads to a wide variety of reactions, frequently yielding non-aromatic compounds. This difference between the ground and the excited-state chemistries of benzene compounds results not only from the changes in electron distribution and electron donor-acceptor properties produced upon excitation, but also from the energy of the $S_0 \rightarrow S_1$ transition (426 kJ/mol), which is almost three times greater than the classical resonance energy (150 kJ/mol). The energy of electronic excitation promotes the formation of unstable and highly reactive compounds, which are inaccessible from benzene compounds by conventional thermal routes.

1.4.1. Photochemistry of benzene

The electronic spectrum of benzene features three maxima centered at 254, 203 and 180 nm, corresponding to electronic transitions from S_0 to S_1, S_2 and S_3, respectively. Irradiation of benzene in the $S_0 \rightarrow S_1$ band, either in the vapour or in condensed phase, gives a mixture of fulvene **15** and benzvalene **16**, Scheme 1.2. Dewar benzene has not been detected in this process.[9] These photoproducts are thought to arise from the biradical intermediate **17,** which is often called the prefulvene biradical. Its formation occurs by way of a bonding interaction between carbon atoms 1 and 3, in a process called meta-bonding.

Scheme 1.2. The meta-bonding process in the first singlet excited state of benzene

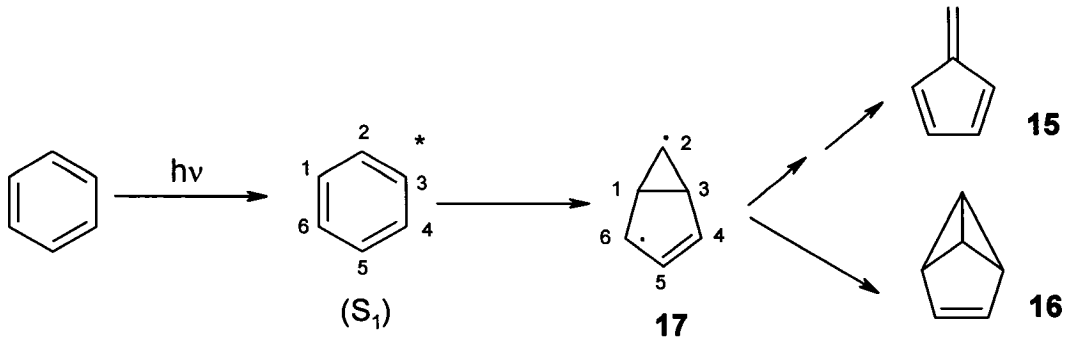

Neither benzvalene nor fulvene are particularly stable, and benzvalene isomerises rapidly back to benzene.[10,11] The participation of benzvalene as an intermediate has been inferred from labelling studies.[11] Scheme 1.3 shows the general case for phototransposition *via* benzvalene, a process that leads to switching of the positions of carbon atoms 1 and 2. These phototranspositions are indicated by the fact that the carbons 1 through 6 in the starting material are altered in the products. Benzene also

undergoes photoisomerization to give Dewar benzene when irradiated in the 200 nm region.[12] This wavelength corresponds to excitation from $S_0 \rightarrow S_2$.

Scheme 1.3. Phototranspositions in benzene

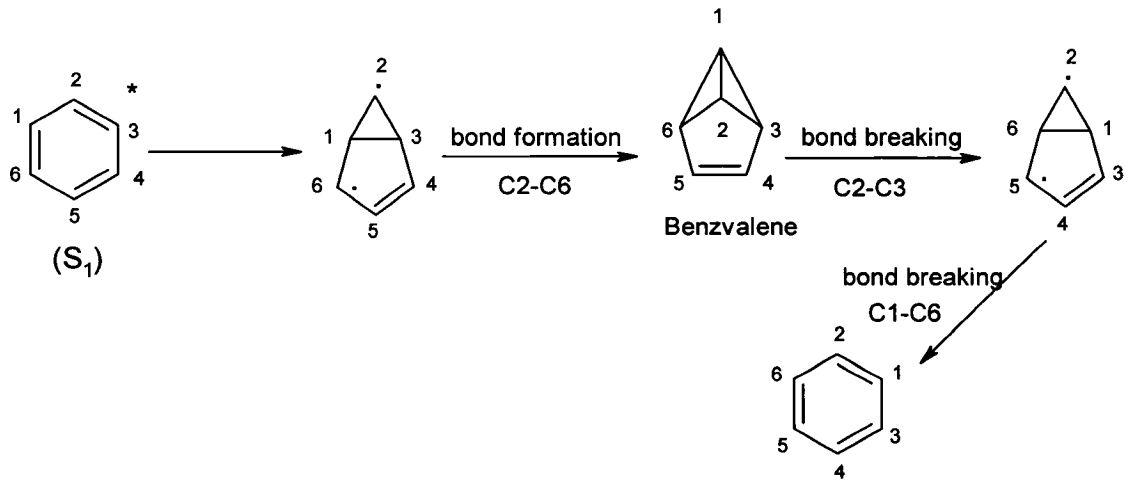

1.4.2. Photochemistry of alkyl-substituted benzene compounds

The first photochemical rearrangement of substituted aryl compounds was reported in 1964 for *o*-xylene **18**.[11] When *o*-xylene is irradiated at 254 nm, both *m*-xylene **19** and *p*-xylene **20** are formed.

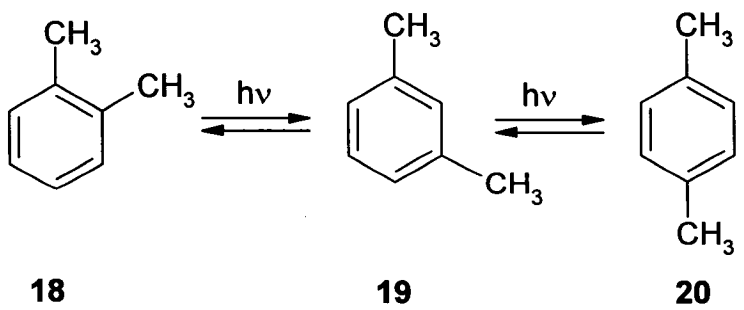

18 **19** **20** (1.23)

For this rearrangement, the evidence indicates that the mechanism involves methyl-substituted tricyclo[3.1.0.0^{4,6}]hex-3-enes (benzvalenes) as intermediates, as shown in Scheme 1.4.[13,14,15] Although four different dimethylbenzvalenes are possible, only the first one leads to a phototransposition. The process is again a transposition reaction rather than a migration of methyl groups. Letters, rather than numbers, are used to label the carbon atoms to avoid confusion with nomenclature numbering.

Scheme 1.4. Pathway for the rearrangement of o-xylene

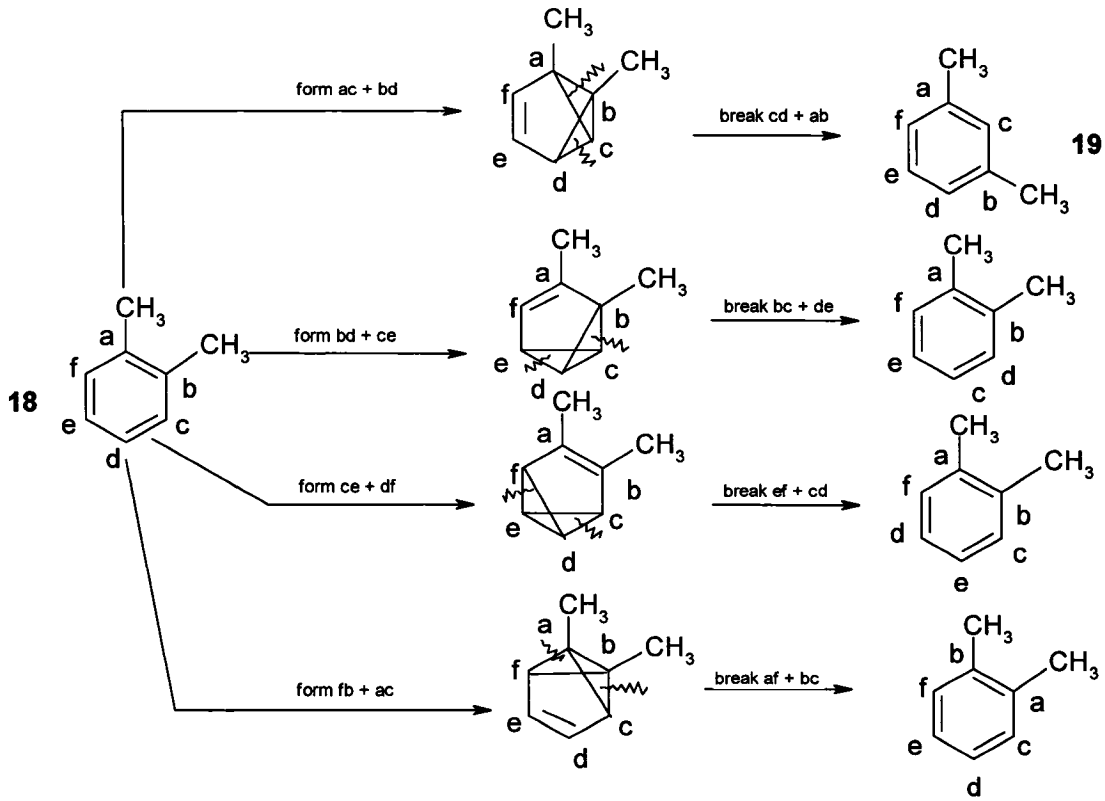

An indication of the possible mechanism of these processes was provided by the study of the photolysis of 1,3,5-trimethylbenzene (mesitylene) **21**. Using the substituents as labels for the carbons, the rearrangement of isotopically labelled mesitylene-1,3,5-^{14}C

produced 1,2,4-trimethylbenzene **22** exclusively, as shown in eq. 1.24, demonstrating that during the phototransposition process the carbons interchange positions.[11]

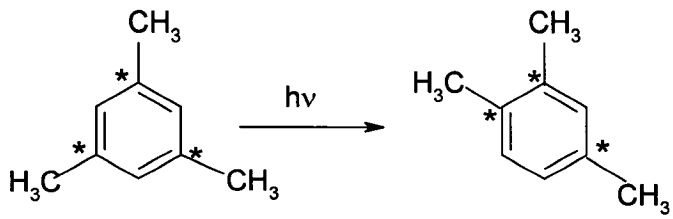

(1.24)

21 **22**

1.5. The intermediate for the phototransposition reaction of benzene compounds

There are a number of experiments that can be used in proposing the mechanism of a chemical process. Among these are the characterization of products (including reaction stereochemistry), the determination of the kinetic law and the activation parameters, the study of the influence of the solvent, the substituents and the temperature on the kinetics of the reaction, and testing for suspected intermediates. Proving the existence of an intermediate is, perhaps, the most difficult experiment to support a reaction mechanism. The preparation of the suspected intermediate by an independent synthesis, the isolation and characterization of the intermediate, the detection of the intermediate by spectroscopy techniques, isotopic labelling experiments and the trapping of the intermediate are all common techniques that are used for reaction mechanism studies.

The proposed intermediate for the phototranspositon reaction of benzene derivatives is a prefulvene biradical. Several experiments have been reported that support this proposal.[11-18]

The photochemical addition of alcohols to benzene and alkylbenzenes was first reported by Kaplan *et al.* in 1966.[19] Thus, irradiation of benzene (0.02 M) at 254 nm in 2,2,2-trifluoroethanol (TFE) resulted in the formation of two major products, **23** and **24** in a ratio of 2 : 1, eq. 1.25.

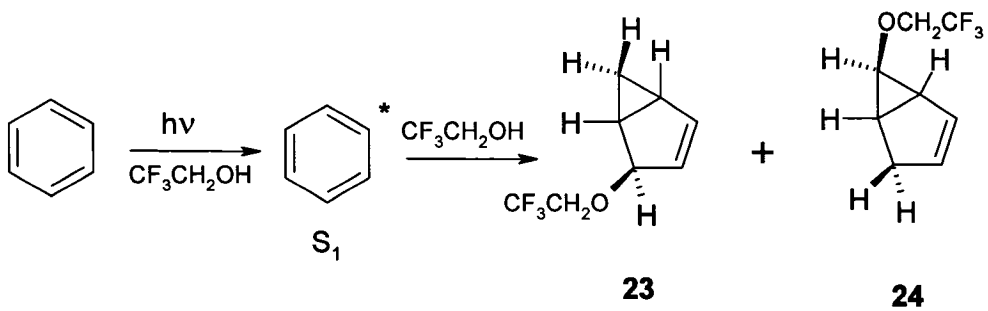

(1.25)

Similarly, irradiation of 1,3,5-tri-*tert*-butylbenzene **25** in methanol gave, as the only detectable product, the methyl ether, **26**, eq. 1.26. Moreover, the positional isomerization of this substrate was suppressed in favor of the addition reaction. The endo stereochemistry of the hydrogen at C6 in **26** was established by ^{1}H NMR coupling constants to the two other cyclopropyl hydrogens. The mechanistic conclusion reached was that these products result from ground-state addition of the alcohol to the expected benzvalene primary photoproduct. Therefore, it is logical to state that the prefulvene biradical **27** is the best candidate as a precursor for **26**.

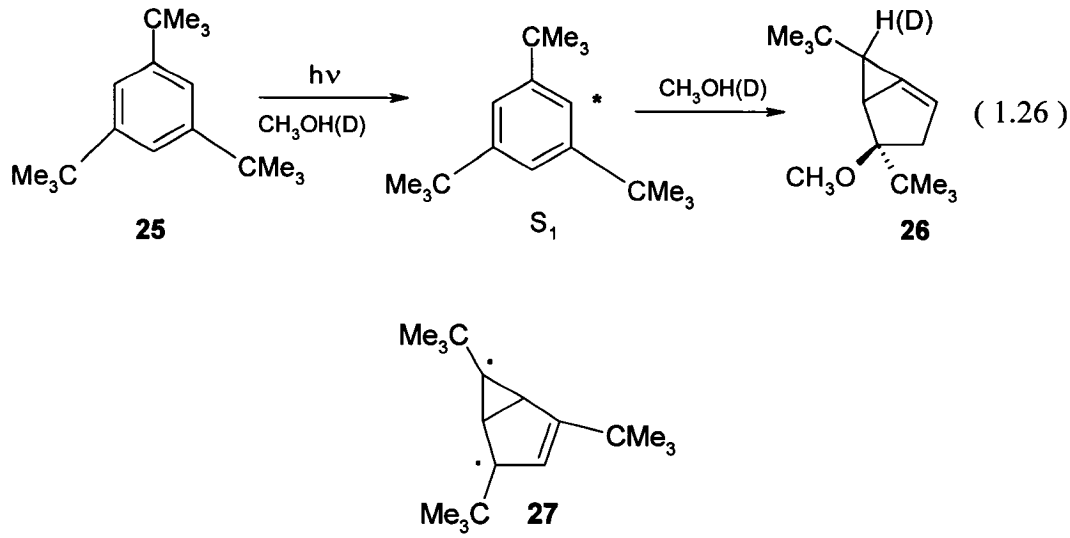

(1.26)

Similar additions of acetic acid and water (0.1 M in phosphoric acid) to benzene were observed in the same year.[20]

These conclusions were further supported by Berson and Hasty from the photolysis of benzene at 254 nm in D_2O (0.1 N D_3PO_4), eq. 1.27.[21] Analysis of the ^1H NMR of the isolated alcohol, **28**, indicated that the deuterium at C6 was exclusively endo. The stereochemistry of the hydroxy group at C2 was exo, but any of the endo alcohol formed would have rapidly epimerized to the exo-alcohol in the acidic solution.

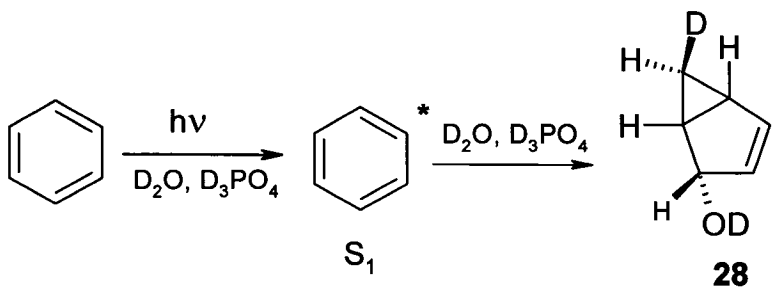

(1.27)

As well, irradiation of benzene in acetic acid produced all four possible regio- and stereoisomers of the bicyclo[3.1.0]hex-3-en-2-yl addition products,[22] **29-32**. In the earliest sample analyzed (after 2 hours of irradiation), the ratio was approximately 40 : 41 : 4 : 16 (estimated from a plot in reference 21). Assuming rapid endo to exo ground-state conversion of the products, *i.e.*, **30** to **29**, the major primary photoproduct is the endo adduct. Therefore, both the protonation and nucleophilic attack were predominantly endo, as expected for an addition to benzvalene on the basis of previously observed additions to one other bicyclobutane derivative.[23] After 48 hours of irradiation the product ratio was 23 : 13 : 15 : 48. The photoequilibration of the products was proposed to occur by a vinylcyclopropane rearrangement, as in eq. 1.28, involving cleavage of the C1-C5 bond.

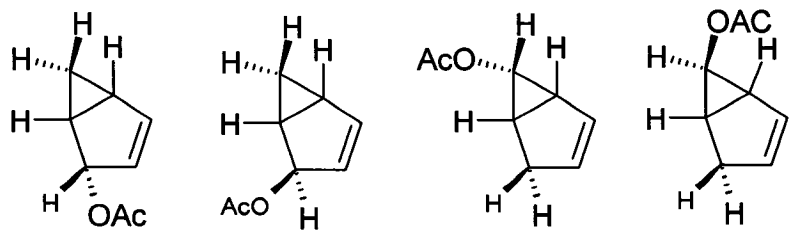

29 **30** **31** **32**

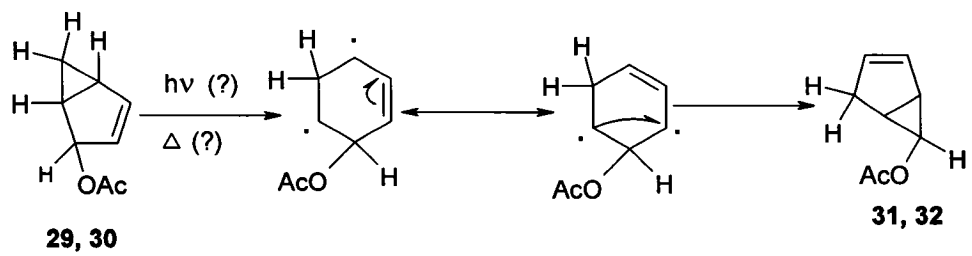

29, 30 **31, 32** (1.28)

The participation of benzvalene as an intermediate in these photoaddition reactions received even stronger support after it became available in abundant quantities as a result of a non-photochemical synthesis developed by Katz and co-workers.[24] Reaction of benzvalene in ether with D_2O/D_3PO_4 for 30 minutes gave a quantitative yield of **28**.

Finally, Kaplan and co-workers,[9] using benzene-1,3,5-d_3 and benzene-d_6 as substrates, proved that:

1. The photoaddition products **29-32** did come from the protonation of benzvalene.

2. **29** and **30**, the primary photoproducts, were formed by the nucleophilic trapping of the cation **33**.

3. Both **31** and **32** were formed from **29** and **30** by benzene-sensitized secondary photolysis involving C1-C5 bond cleavage as in eq. 1.28.

4. **31** and **32** were equilibrated, probably photochemically, although a thermal pathway could be an alternative route, either by C1-C5 bond cleavage or C1-C6 cleavage, this latter pathway being dominant.

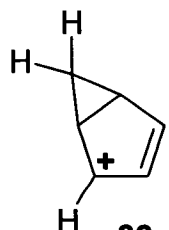

33

1.6. Overview of the photochemical reactivity/stability of benzene compounds

A wide number of aromatic molecules has been shown to undergo photochemical rearrangement as well as photochemical addition of alcohols under UV irradiation. In contrast, many benzene compounds, both mono- and disubstituted, are photochemically unreactive to the same processes, Table 1.2.[25, 26, 27] As explained before, the reactive benzene compounds yield compounds that are not accessible from the ground state, particularly the photoaddition products.

Table 1.2. Summary of phototranspositions (PT) in AN and photoadditions (PA) of TFE for substituted benzenes, C_6H_4XY[25]

Substituents	Isomer	PT	PA
-H	-	Yes, with 1,3,5-d_3	Yes, endo[a] (eq 1.27)
$-CH_3$	-	-	Yes, endo[a]
$-OCH_3$	-	-	No
-F	-	-	No
$-CF_3$	-	-	Yes, only detected by GC/MS
$-CO_2CH_3$	-	-	No
$-CH_3$, $-CH_3$	ortho	meta : para = 11 : 1[b]	Yes, endo[a]
	meta	ortho : para = 6.0 : 1[b]	Yes, but the PA products are not stable
	para	meta : ortho > 25 : 1[b]	Yes, but the PA products are not stable
		ortho : meta : para = 1 : 1.4 : 0.3[c]	
-CN, $-CH_3$	ortho	meta : para = 7.1 : 1[b]	No
	meta	ortho : para = 1.7 : 1[b]	Yes
	para	meta : ortho = 4.2 : 1[b]	Yes
		ortho : meta : para = 1 : 4 : 32[c]	

Table 1.2 (Continued)

$-OCH_3$, $-CH_3$	o, m, p	No	No
$-OCH_3$, -CN	o, m, p	No	No
-CN, -CN	o, m, p	No	No
SO_2CH_3, CH_3	para	No	No
$-CF_3$, $-CH_3$	ortho	meta : para > 10 : 1[c]	Yes, only detected by GC/MS
	meta	ortho : para = 0.25[b]	Yes, only detected by GC/MS
	para	meta : ortho > 20 : 1[b]	No
		ortho : meta : para = 1 : 0.67: 0.16[c]	
$-CF_3$, -CN	ortho	meta : para = 1.7 : 1[b]	No
	meta	ortho : para = 0.81 : 1[b]	No
	para	meta : ortho = 7.2 : 1[b]	No
		ortho : meta : para = 1 : 2.7 : 3.1,[c] in both AN and TFE	

Table 1.2 (Continued)

-F, -CH_3	ortho	Very slow	No
	meta	ortho : para = 5.0 : 1[b]	No
	para	Very slow	No

a. Stereochemisty of the proton at C6 of the bicylo[3.1.0]hexene products, implies a benzvalene intermediate.
b. Product ratio at very low conversion. High values from the ortho or para starting material suggest that 1,2-transpositions dominate.
c. Relative reactivity

After the examination of the substitution pattern of the compounds given in Table 1.2, the conclusion reached is that no clear trends are apparent that would permit reliable predictions for the photochemical reactivity of new compounds. However, electron-withdrawing groups (-CN, -CF_3) seem to favour the processes of both phototransposition and photoaddition of TFE.

1.7. Photochemistry in protic solvents of benzene compounds that contain acetylene units

The photochemistry in protic solvents of compounds containing double bonds is well understood; however, the corresponding photochemistry of compounds that feature carbon-carbon triple bond has received much less attention. The photochemistry of phenylacetylenes has been limited to cycloaddition,[28, 29] oxidation,[30] photochemical addition of simple nucleophiles such as alcohols[31, 32] and water,[33] and photochemical reduction reactions.[31, 32]

1.7.1 Photochemical reactions of diphenylacetylene in methanol[31]

Roberts, Ardemagni and Shechter reported in 1969 that the photochemical addition of methanol to diphenylacetylene **11** resulted in the formation of *cis*- and *trans*-1,2-diphenylvinylethers **34, 35**, Scheme 1.5.[31] An important result of this study was that the photoproducts of reduction, *cis*- and *trans*-stilbene **36, 37** were also detected. Phenanthrene **38** was also detected, presumably by a photochemical cyclization of **36** followed by oxidation, eq. 1.29. The photolysis of **11** in methanol occurred slowly to give *trans*-1,2-diphenyl-1-methoxyethene **34** as the major photoproduct, the ratio of **34 : 35 : 36 : 37** being 62 : 1 : 21 : 10 after 10 hours, Table 1.3.

Scheme 1.1. Photochemical reactions of diphenylacetylene in methanol

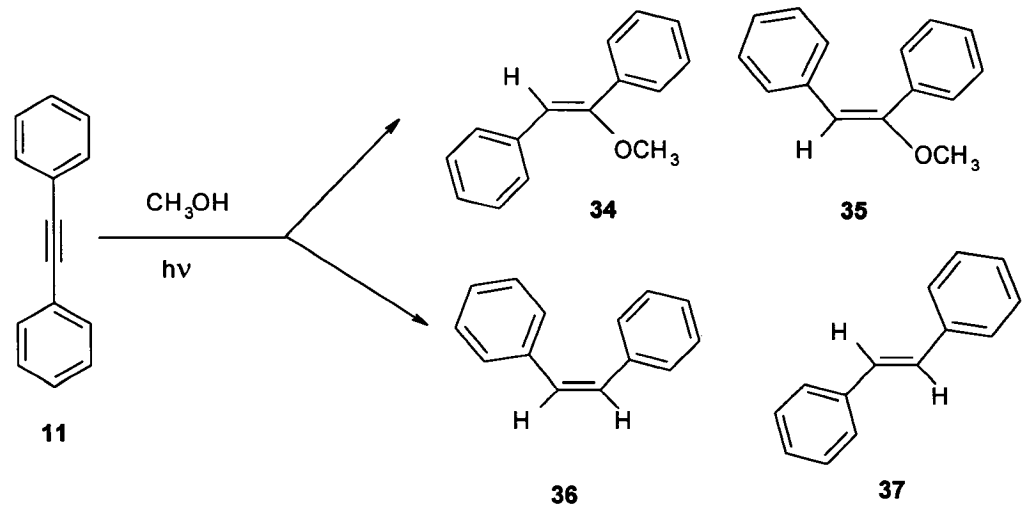

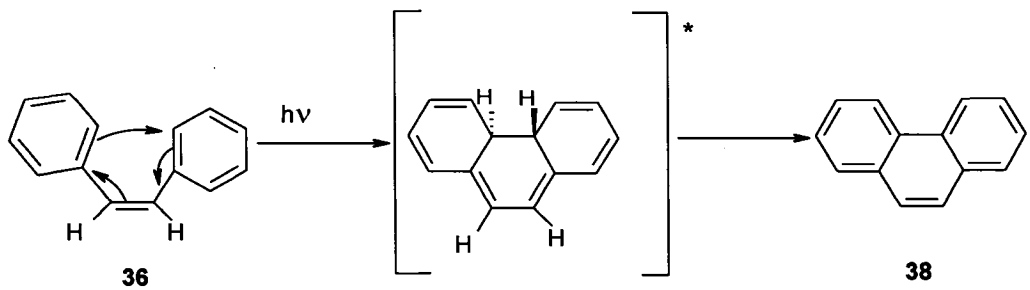

(1.29)

Table 1.3. Photolysis of diphenylacetylene in methanol[31]

Time/ hr	% reaction	% **34***	% **35***	% **36***	% **37***	% **38***
10	33	62	1	21	10	6
20	35	60	2	19	11	8
40	73	63	3	17	6	10
88	88	62	6	13	6	14

* The percentage of products was calculated with respect to the chemically transformed starting material.

1.7.2. Photochemistry of mono- and diacetylenic systems

In 1973, Zimmerman and Pincock reported on the photochemistry 3,3-dimethyl-1,3-diphenyl-1,4-pentadiyne **39** using tert-butanol and isopropyl alcohol as solvents.[32] As a result of the considerable number of examples of the di-π-methane rearrangements involving two carbon-carbon double bonds connected through an sp^3 hybridized carbon,[34, 35, 36] a problem of interest became the study of methane derivatives containing two acetylenic moieties.

Irradiation of **39** in isopropyl alcohol generated two products, cyclopentadiene **40** and enyne **41**, eq. 1.30. No di-π-methane rearrangements were observed in these experiments.

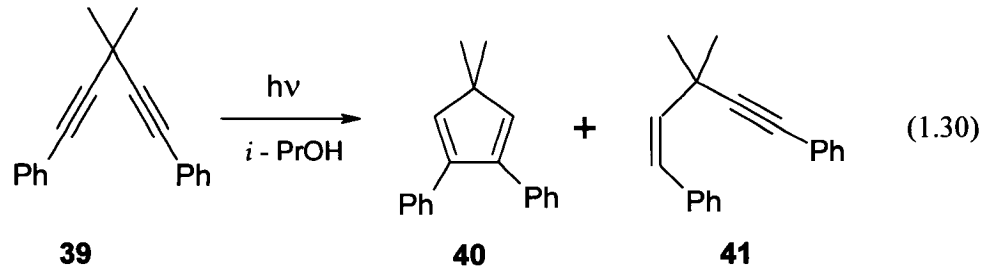

(1.30)

In contrast to the results in isopropyl alcohol, irradiation of **39** in *tert*-butanol gave only cyclopentadiene **40**.

To gain a better understanding of the photochemical processes of **39**, the same reactions were carried out using a model compound with just one acetylenic unit. This was done in order to learn if the formation of **41** required the presence of two triple bonds. For this study phenyl *t*-butylacetylene **42** was selected. In *tert*-butanol, irradiation of this alkyne gave no photoproducts. However, in isopropyl alcohol the geometric isomers of 3,3-dimethyl-1-phenyl-1-butene (*cis*-**43** and *trans*-**43**) were the major products, with the cis isomer being kinetically favoured. Additionally, 2-hydroxy-2,5,5-trimethyl-3-phenyl-3-hexene **44** was also formed, eq. 1.31.

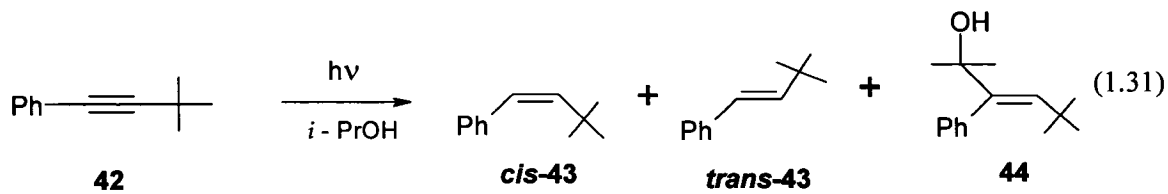

(1.31)

The result of interest for this thesis is that photoadditions of alcohols involving oxygen and suggesting ionic intermediates were not observed.

1.7.3. Photohydration of phenylacetylenes[37]

The thermal acid-catalyzed hydration of phenylacetylenes has been studied extensively.[38, 39, 40] This ground state reaction has been found to be extremely slow, k_{H^+} ~10^{-5} – 10^{-7} M^{-1} s^{-1}, and also subject to general acid catalysis in an important number of cases.[41, 42] The photohydration of phenylacetylenes, **45-50**, is also catalyzed by H_3O^+. If electron-donor substituents are present in the ring, they react via their lowest singlet excited state and the reactions are regiospecific in a route that agrees with Markonikov's rule.[43, 44, 45]

Scheme 1.2. Mechanism for the photochemical hydration of phenylacetylene

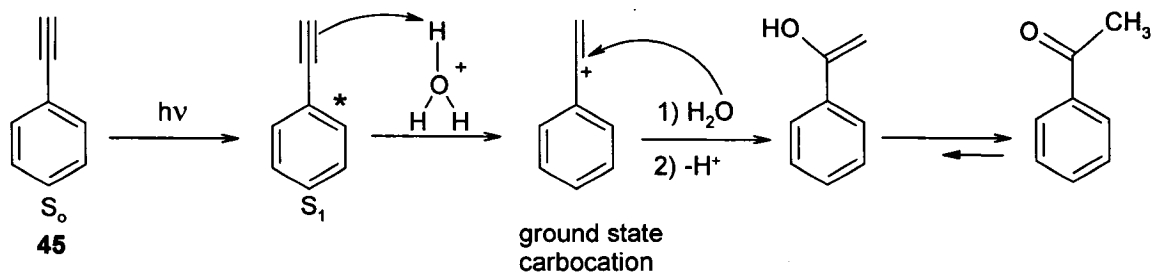

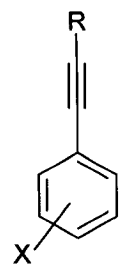

45: X= H; R = H
46: X = *p*-CH_3; R = H
47: X = *p*-OCH_3; R = H
48: X = 2,3-C_4H_4; R = H
49: X = 3,4-C_4H_4; R = H
50: X = H; R = Ph

Values of the rate constant for the proton transfer process, k_{H^+}, from H_3O^+ to S_1, demonstrate that these photochemical reactions are very fast.[43, 44, 45] The reported values for k_{H^+} are in the order of 10^6–10^7 $M^{-1}s^{-1}$. The authors of this study proposed a mechanism in which the rate-determining step is the protonation of S_1, followed by a rapid attack of H_2O on the intermediate carbocation. The kinetic isotope effect, k_H / k_D was found to be about 1.3–1.8.

The quantum yield for reaction of these alkynes at pH = 7 is not zero, and the amount of ketones formed at pH = 7 and higher is considerable. The authors state that the process is subject to water catalysis and, therefore, raises the interesting possibility that this photohydration reaction might be subject to general acid catalysis.

The photohydration processes described [37] are orders of magnitude faster than the catalyzed thermal hydration. For these experiments, the authors used buffers of pH > 2. This suggests that the excited states of these compounds are considerably more polar than the ground state. Recently, a number of articles have been published in which it has been reported that the excited states of benzene compounds containing subtituents with multiple bonds, such as styrenes, stilbenes and diphenylacetylenes, are considerably more polar than S_0.[46, 47, 48]

In addition, the authors used the values of rate constant for the acid-catalyzed reaction in a Brønsted fit ($\log k_{HA} = \alpha \log K_{HA}$ + constant), with respect to the dissociation equilibrium constant of the acidic catalysts used. The Brønsted plots were curved downward in every case. The calculated α coefficients were smaller than those obtained for the same reactions in the ground state. This means that the transition state is an early one. Taking into account the α values and the k_H/k_D ratios obtained for the

photohydration of phenylacetylenes, the authors concluded that the proton is much less than half-transferred at the transition state, and that the rate limiting step is the hydrogen transfer process.

Chapter 2

Temperature and Solvent Effects, Rate Constants and Activation Parameters for the Reactions of the Excited States of Substituted Benzenes

2.1. Introduction

A very important objective in the kinetic study of excited states is to gain the same depth of understanding of structure/reactivity relationships as those that are established in ground-state chemistry. This requires the measurement of rate constants of reactions that occur from excited states, and is one of the goals of the experiments reported in this thesis.

As discussed in Chapter 1, in contrast to the mechanistic studies of ground-state chemistry, excited–state reactivity is complicated by the possibility of both singlet and triplet state reactions, photophysical processes that de-activate the excited state and quenching processes with high rate constants that compete with both the photophysical deactitivation and the chemical reaction. The excited states of some benzene derivatives undergo chemical reaction, Table 1.2. The products are formed by a mechanism in which a reactive intermediate (RI) is formed. This reactive intermediate rearranges extremely

quickly, either resulting in products or returning to the ground state of the reactant by means of an activated pathway.

The conventional way of obtaining k_r values has been by measuring the quantum yield of product formation, eq. 2.1.

$$\Phi_{prod} = \Phi_r = \frac{k_r}{k_r + k_f + k_{isc} + k_{ic}} \tag{2.1}$$

Taking into account Scheme 1.1, which represents the basic dynamics of a singlet excited state, eq. 2.1 ignores the activated internal conversion of the excited state S_1 to a reactive intermediate RI that returns to S_0. Therefore, eq. 2.1 can not be used to obtain k_r if there is an activated route for internal conversion. The main reason is that, in this situation, the yield of products as a function of time does not reflect the rate at which the RI is formed.

Ermolaev's rule[49] for S_1 of organic compounds, which has been basic in the progress of organic photochemistry, states that the sum of the quantum yield of fluorescence and intersystem crossing equals unity ($\Phi_f + \Phi_{isc} = 1$). This rule applies very well to polycyclic aromatics such as anthracene (0.30 + 0. 71 = 1.01),[50] naphthalene (0.19 + 0.75 = 0.94)[50] and phenanthrene (0.13 + 0.85 = 0.98).[50] However, it fails for benzene and many of its derivatives: benzene (0.06 + 0.25 = 0.31),[50] toluene (0.14 + 0.51 = 0.65),[50] and *o*-xylene (0.15 + 0.58 = 0.73).[50] The reason for this apparent violation of the law of conservation of photons is well-established; processes that are not considered in this rule (internal conversion and chemical reaction) contribute to the de-activation of S_1. In fact, as stated in Chapter 1, many experimental studies of the photochemistry of

benzene compounds report a chemical reaction where the RI is a prefulvene radical.[11-18] In addition, for many photochemical reactions, especially for those involving a radical pair or ion pair intermediate as the RI, internal return, as a result of a recombination process, has been demonstrated to be an efficient process. For that reason, eq. 2.1 is not correct for simple benzene compounds. A correct but more complicated equation is necessary for the determination of k_r from the quantum yield for product formation, eq. 2.2, where the second term is the efficiency of product formation from the RI.

$$\Phi_{prod} = \phi_{RI} \frac{k_{prod}}{k_{prod} + k_{icr}} = k_r \tau_s \frac{k_{prod}}{k_{prod} + k_{icr}} \tag{2.2}$$

ϕ_{RI} is the efficiency of formation of the reactive intermediate from S_1, k_{prod} is the rate of product formation from RI and k_{icr} is the rate constant of return of the RI to S_o. Eq. 2.2 indicates that obtaining k_r will be complicated due to the experimental difficulties in estimating the fraction of RI that yields the products.

As stated in Section 1.2, the rate of formation of the RI's is estimated conveniently using very fast probe techniques or fluorescence methods, such as flash-lamp nanosecond single-photon counting. Fortunately, for the excited states of benzene compounds, it is possible to use florescence decay as a way of monitoring $[S_1]$ as a function of time. The measurements of the singlet lifetime of S_1, and the quantum yield of fluorescence, eq. 1.21, are easily done for benzene compounds.

2.1.1. Project proposal

The general goal of the work described in this chapter is to determine all the rate constants for the deactivation of S_1 of benzene compounds, such as intersystem crossing and chemical reaction. This research focused on the dependence of the lifetime as a function of temperature as a vehicle for understanding the dynamics of the first-singlet excited state S_1 of these compounds. By a relatively simple mathematical model (Arrhenius plot method, to be discussed in section 2.5) that describes conveniently the processes of this excited state, it is possible to estimate rate constants for the temperature dependent process (reaction) and the independent ones (fluorescence and intersystem crossing). The experimental determination of these rate constants is usually a difficult and time-consuming process. By using the Arrhenius plot method, these rate constants can be obtained reliably in a timely fashion. This work will show how the kinetic study of the processes taking place from the excited states is a powerful tool for understanding the changes in geometry and electron distribution that occur for the excited-state processes of substituted benzene compounds.

2.2. Phototransposition reaction of cyanotoluenes,[8] arylboronate esters[51] and trifluoromethylbenzenes[52]

2.2.1. Photochemistry of 1, 2, 3o, m, p in acetonitrile (AN)

Pincock and collaborators have published a series of papers on the photochemistry of disubstituted benzene compounds: cyanotoluenes in AN (**1o**, **1m** and **1p**),[8] the arylboronate esters in AN (**2o**, **2m** and **2p**),[51] the trifluoromethyltoluenes (**3o**,

3m and **3p**),[52] and dialkylasubstituted trifluoromethylbenzenes (**51-56**) in AN.[53] These compounds have been shown to undergo phototranspositions when irradiated in acetonitrile, Scheme 2.1.[8, 51, 52, 53]

Scheme 2.1. Phototransposition reactions for compounds 1, 2, and 3 in AN

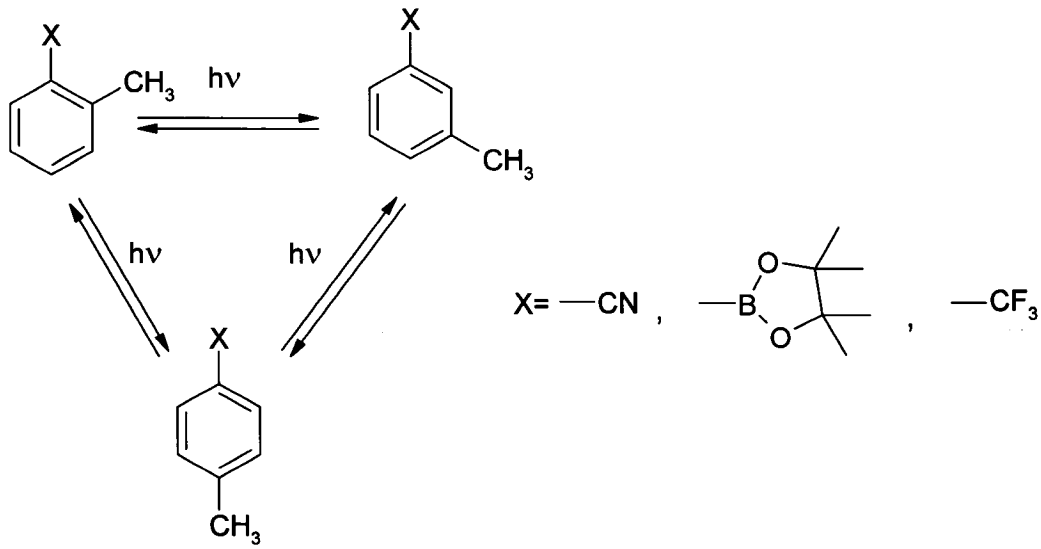

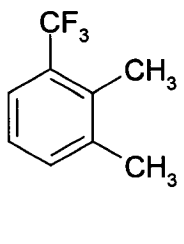

51

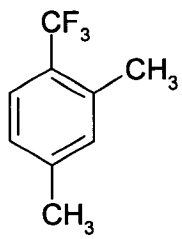

52

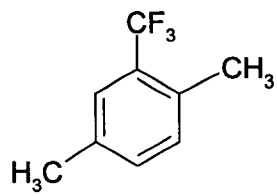

53

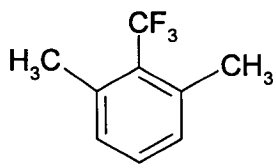

54

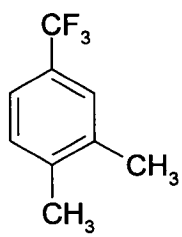

55

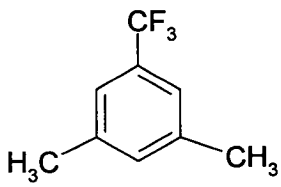

56

Each compound is converted to the other isomers by both 1,2- and 1,3-phototranspositions in a unimolecular photochemical process initiated by meta-bonding. The relative efficiencies of the phototransposition reaction for **1** in AN were determined: **1o** : **1m** : **1p** = 1 : 4 : 32, which correctly explains the photostationary state obtained after complete photoequilibration: **1o** : **1m** : **1p** = 67% : 26% : 7%.[8] The most reactive isomer **1p** has the lowest final yield, as expected. The quantum yields of product formation, $\Phi_{prod,}$ also follow this order: **1m** : **1p** = 0.003 : 0.025. The ortho-isomer was too unreactive to measure its quantum yield of disappearance. Similary, for the phototransposition reactions of **2** in AN, values of isomer composition were calculated using the steady-state approximation, giving **2o** : **2m** : **2p** = 76% : 19% : 5%.[51] The most reactive isomer **2p** has the lowest yield at equilibration, as expected. For **3**, the steady-state composition is essentially reversed from that observed for the cyanotoluenes **1**, **3o** : **3m** : **3p** = 7% : 32% : 61%. The ortho-isomer is now the most reactive.[8, 52]

All the compounds above have fluorescence spectra that overlap with their absorbance bands at the expected zero-zero transition. Therefore, their S_1 states are spectroscopic minima, and this suggests that the chemical reaction occurs from the same minimum as the fluorescence.

The multiplicity of the reactive excited state was determined for both *meta*- and *para*-cyanotoluene by doing simultaneous quenched and unquenched irradiations. Fluorescence quenching studies were done using 2,3-dimethyl-1,3-butadiene. From the linear Stern-Volmer plot obtained, it is possible to establish that, at a quencher concentration of less than $1x10^{-3}$ M, the fluorescence is not quenched. With this in mind, the aim of this experiment was to verify if the isomer composition varied as a result of

the quenching of the triplet state T_1, which was assumed to be longer lived. Because phototransposition still occurred with the same efficiency, the conclusion drawn was that these substrates rearrange from the S_1 state.[8] The multiplicity of the reactive state for the boronate esters **2** was established by a similar experiment but only for the meta isomer. Photolysis in the absence or presence of 2,3-dimethyl-1,3-butadiene (again $1x10^{-3}$ M) gave essentially the same conversion (16% versus 14%) after 180 minutes of photolysis in AN. The isomer composition after photolysis gave the same ratio of isomers with and without quencher. Again, the conclusion reached was that the singlet excited-state is the reactive one.[52]

In order to understand the mechanism for the cyanotoluene phototransposition reactions, deuterium labelling experiments were performed.[8] The photolysis of 3,5-dideuterio-4-cyanotoluene **57** was done in AN. The deuterated isomer **57** was prepared from the deuterated hydrochloric salt of *p*-aminotoluene, by a Sandmeyer reaction with CuCN.

For the para-isomer, there are four possible meta-bondings that could lead to the prefulvene biradical and then, possibly, to a benzvalene, **58-61**. Scheme 2.2 for *p*-cyanotoluene deuterated in the ortho positions, **57**, shows that pathway (a), with the meta-bonding occurring between C2 and C6 would give **62** and therefore the cyano group must be on the single carbon bridge of the possible prefulvene biradical. In pathway (b), the meta-bonding takes place between C3 and C5, giving **66**, and the methyl group is situated on the single-carbon bridge. Pathway (a) also allows rearrangement of **62** to **63**, and then to 4,5-dideuterio-3-cyanotoluene **64**. Further rearrangement then gives the 4,5-dideuterio-2-cyanotoluene **65**. In contrast, pathway (b) gives the isomeric 2,4-dideuterio-

3-cyanotoluene **68** and then 3,6-dideuterio-2-cyanotoluene **69**. If these and the other two possible pathways (not shown) occurred simultaneously, a complex mixture of labelled isomers would be formed.

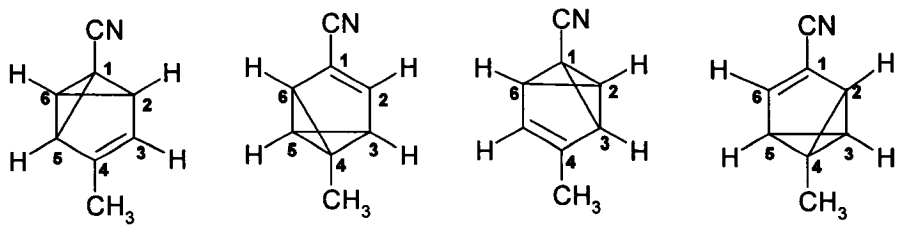

58 **59** **60** **61**

Scheme 2.2. Possible meta-bondings in the phototranspositions of deuterated 4-cyanotoluene

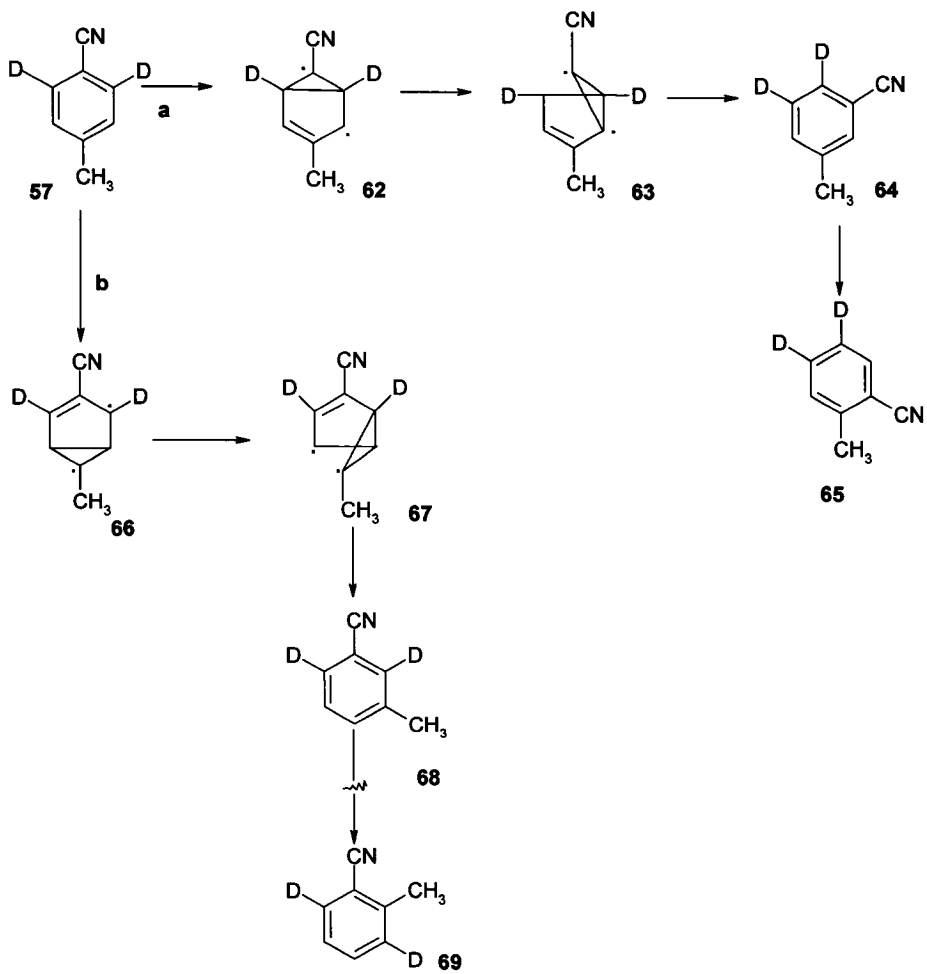

After photolysis of **57** in AN, the position of the deuterium labels was assigned by ^{13}C-NMR. This analysis revealed that the cyano-substituted carbon is the active one in the process and that pathway (a) was the dominant one. The general mechanism can be presented as shown in Scheme 2.3. Excitation of 4-cyanotoluene gives the S_1 state; this is obviously a minimum on the energy surface because fluorescence can still be observed. In order to form the biradical **70**, which results from selective meta-bonding between C2 and C6, assuming that the cyano-substituted carbon is C1, the energy barrier that separates S_1 of *p*-cyanotoluene from this biradical must be surmounted. The 1,2- and 1,3-transpositions can be explained as primary photochemical events; **70** must isomerise by migration of the cyano-substituted carbon to give the biradicals **71** and **72**. The relative stabilities of **70**, **71**, and **72** and the energy barrier between them are not easy to predict. **71** should be the most stable of the three biradicals because one of the carbons in the allylic system should be stabilized by the methyl substitutent. The other biradicals, **70** and **72**, are probably similar in stability. All three of these biradicals could have some zwitterionic character due to the presence of two substituents of different polarity. No evidence has been obtained for the possible benzvalenes **73–75** as intermediates.

Scheme 2.3. General mechanism for the photoisomerization of 1o, 1m, 1p

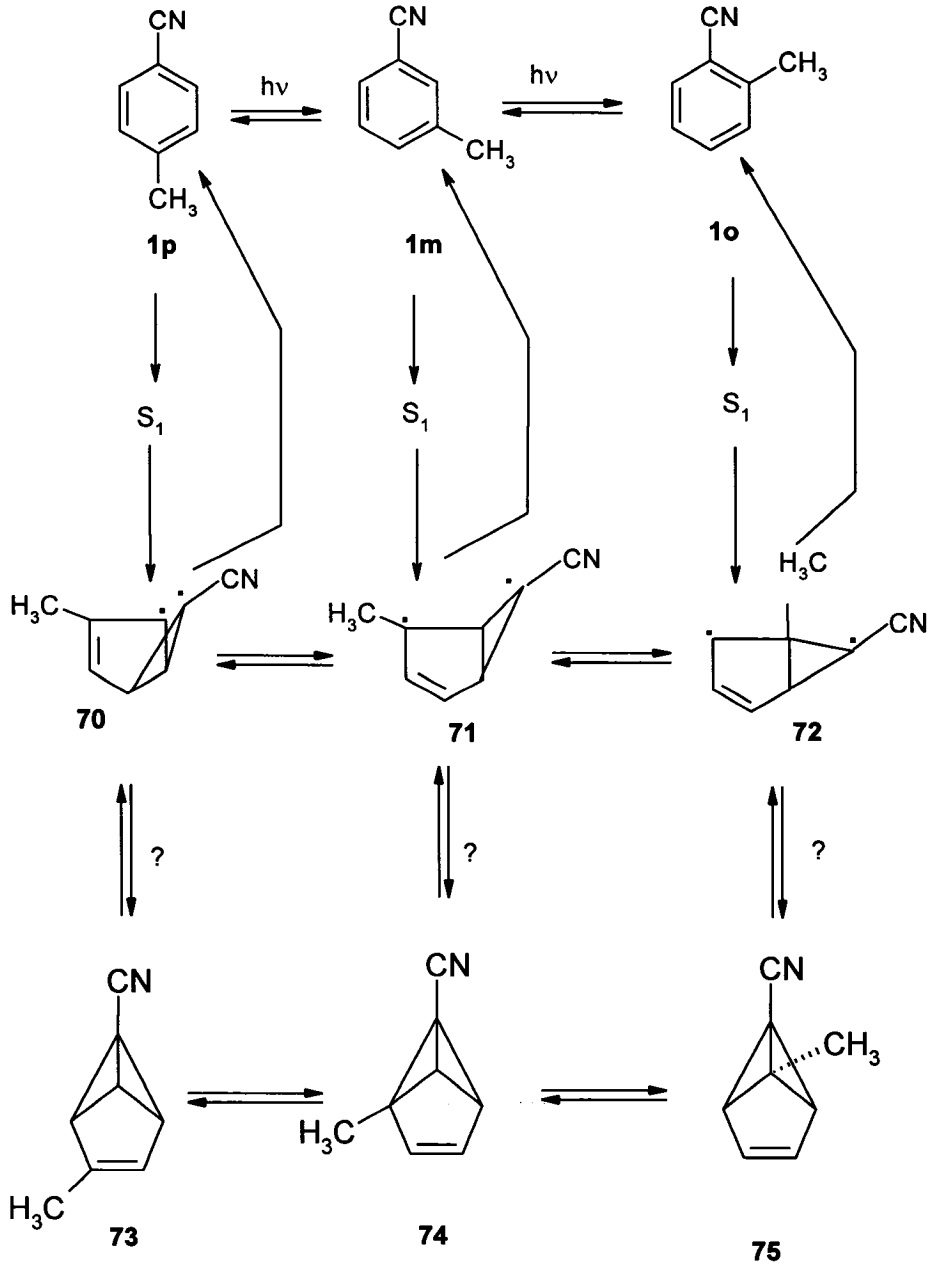

For the boronate esters, analysis of ^{13}C NMR spectrum of the product mixture was also obtained after photolysis in AN of the *p*-boronate ester selectively deuterated at C2 and C6. This analysis showed that the boron-substituted carbon is the active one in the phototransposition reaction of **2p**. Once again, the process is a phototransposition and not a migration of the substituent. It is important to note that no evidence was obtained

for a pathway for the phototranspositon of the methyl-substituted carbon, despite the well known phototransposition reactions of methyl-substituted benzene.[54]

Scheme 2.4. Proposed mechanism for the phototransposition reactions of the p-boronate ester 2p in acetonitrile

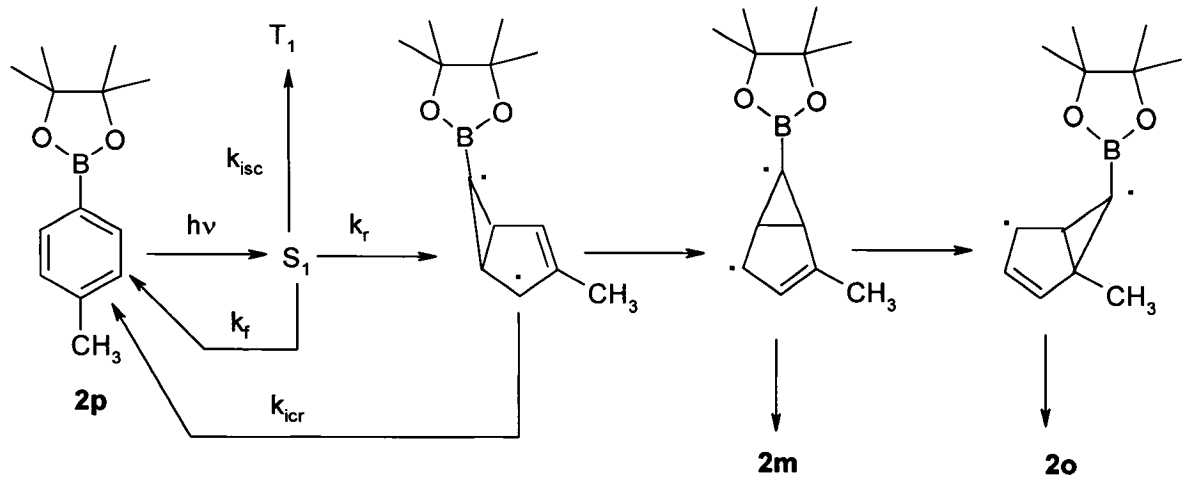

The reactivities of the cyanotoluenes and boronate esters follow the order para > meta > ortho. However, for the trifluoromethyltoluene the order is reversed and the isomer composition at the stationary state was **3o** : **3m** : **3p** = 7% : 32% : 61 %.[53] For this case, the para isomer is the least reactive. Another interesting feature is that the photostationary state is reached more quickly in AN, about 10 times faster than for *p*-cyanotoluene,[53] and about 3 times faster than for *p*-boronate ester. The photolysis of *p*-trifluoromethyltoluene deuterated, at C2 and C6, was performed in order to obtain details on the mechanism, as before. This compound was synthesized starting from 2,6-dideuterio-methylanilinium hydrochloride, followed by diazotation, reaction with KI and finally replacement of the iodide by a CF_3 group. Thus, all the carbons were labelled and could be tracked during the irradiation of the sample. The analysis of the ^{13}C NMR of the

irradiated samples showed that the trimethyl-substituted carbon is the active one. In addition, the results for the dialkyl-trifluoromethylbenzene compounds, which can be considered homologues of **3o**, **3m**, **3p**, support this result.[53] Photolysis of any of the dialkyl-trifluoromethylbenzenes **51–56** resulted in a photoisomerization process. The dominant processes for this photochemical reaction separated the isomers into two triads, a fact which agrees very nicely with the mechanism proposed for the photorearrangement of benzene compounds. The analysis of the GC-FID plots for the photolysis sample of **51 – 56** indicated again that the trifluoromethyl-substituted carbon is the migratory one.

Scheme 2.5. Phototransposition reactions of 51–56 in AN

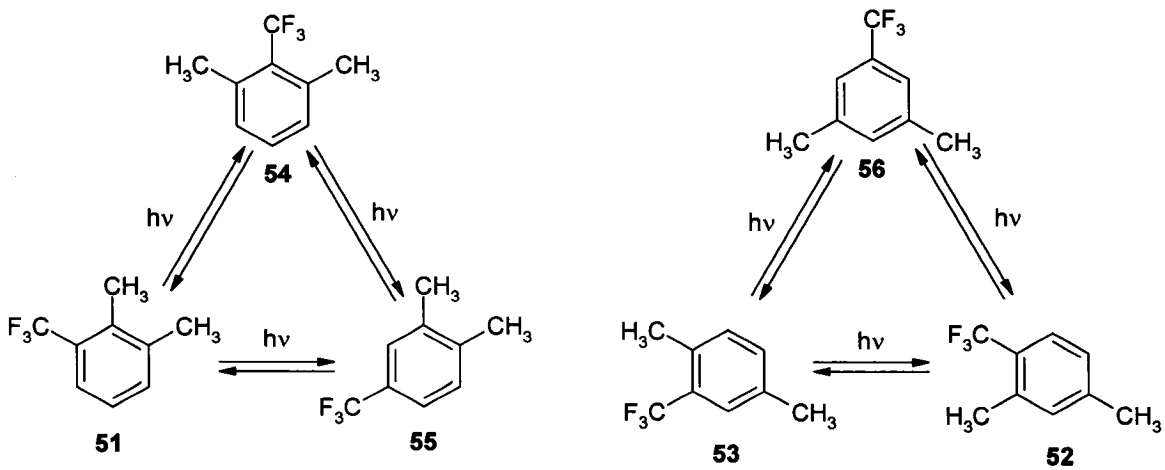

2.2.2. Photochemistry of compounds 1,[55] 2,[51] and 3[52, 53] in 2,2,2-trifluoroethanol (TFE)

A better understanding of the molecular connectivity of the intermediates of the phototransposition reactions reported in reference 8 has been be obtained by trapping the intermediates. Photolysis of benzene in TFE resulted in a mixture of two isomeric

photoadducts, **23** and **24,** eq. 1.25.[19, 20, 21] On the basis of these previous studies, 2,2,2-trifluoroethanol was chosen as the trap. When the cyanoderivatives **1o, 1m** and **1p** were irradiated in TFE, phototransposition reactions no longer occurred. Instead, isomeric bicycle[3.1.0]hexene adducts were formed. Photolysis of benzonitrile **77** in TFE also resulted in the formation of four addition products, **78 - 81**.

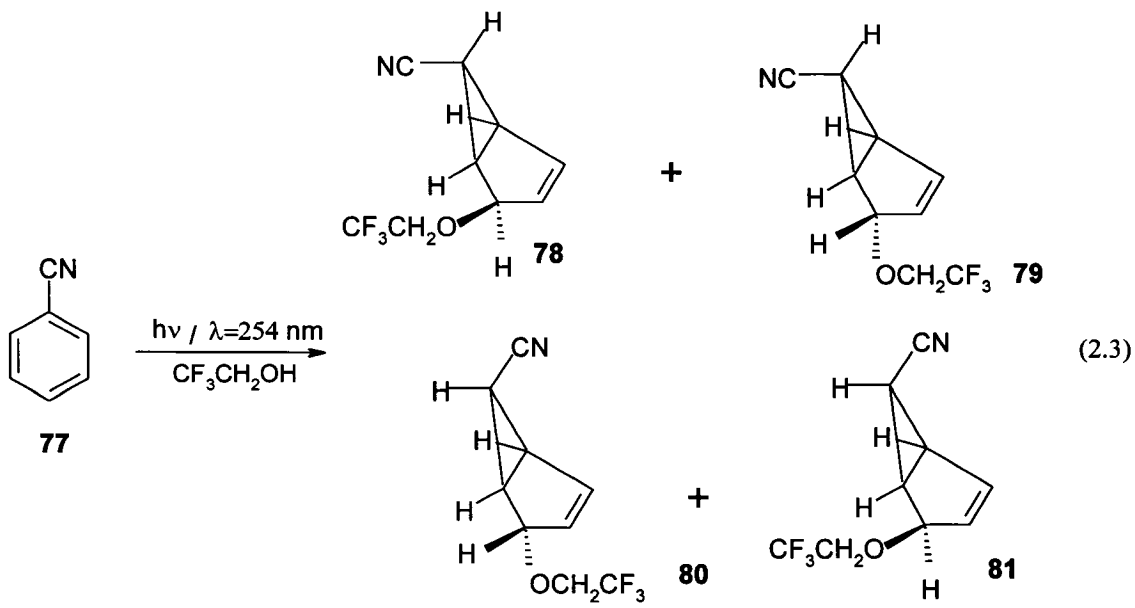

(2.3)

The photolysis of 2,6-dideuterio-4-cyanotoluene **57** in TFE proved to be helpful in understanding the pathways for the addition reactions. These pathways are shown in Scheme 2.6. The proposed mechanism begins by formation of the zwitterion **82** from S_1, and then **85** and possibly **88**, although no evidence was obtained for products derived from **88**. In TFE, the intermediates **82** and **85** are trapped by both endo- and exo-protonation to give **83** and **84**. The cations **83** and **84** then undergo a 1,4-sigamatropic rearrangement in order to yield the more stable cations **86** and **87**, followed by trapping of such species by the solvent, resulting in two different regioaddition pathways. The

products **89 - 94** are derived from them. In conclusion, for the isomers **1o, 1m**, and **1p,** the proposed mechanism is endo- and exo- protonation by TFE of the first formed zwitterions, followed by a rapid trapping of the cations by TFE. The 1,4-sigmatropic rearrangement of the cations stops at the most stable structures, the *endo*- and *exo*-6-cyano-2-methylbicyclo[3.1.0]hex-3-en-2-yl cations **86** and **87**, and all of the product are derived from them.

Scheme 2.6. Photoaddition of trifluorethanol to the cyanotoluenes

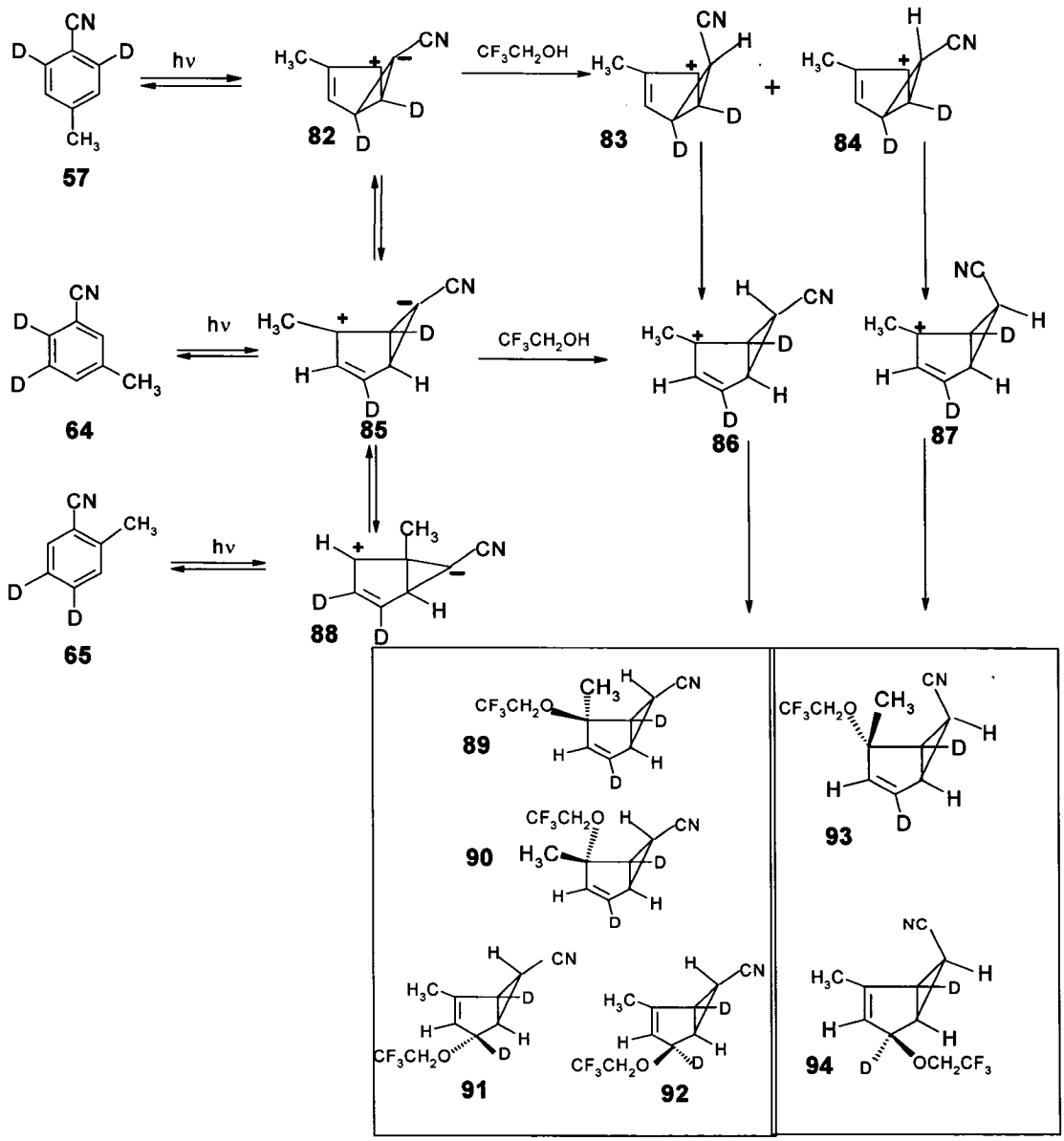

The phototransposition reactions of the boronate esters **2o**, **2m**, **2p** were also observed to occur more efficiently in TFE than AN.[51] Trapping of the substrates by TFE was now not the main process. The least efficient process arises from the photorearrangement of the ortho isomer, the ortho to para photorearrangement being the least efficient. The values for the isomer composition at the photostationary state were again calculated by applying the steady-state approximation, giving a ratio **2o** : **2m** : **2p** = 8% : 57% : 35%. The observed values when the photolysis processes were stopped were **2o** : **2m** : **2p** = 12% : 54% : 34%, in excellent agreement with the prediction using the steady state approximation. GC-MS analysis of the photolysis samples showed that a photoaddition process of TFE occurred as well, but to a minor extent. This indicates that a competition between the photoisomerization process and the trapping of the zwiterrion intermediates takes place. Isolation and characterization of the TFE adducts was not possible. By analogy with the reaction of the cyanotoluenes, Scheme 2.3, they are presumably bicycle[3.1.0]hex-2-ene derivatives.

To confirm that the boron substituted carbon was the active one, the para isomer deuterated in positions 3 and 5 was then irradiated in TFE. The analysis of the ^{13}C NMR spectrum for the mixture obtained indicated that the dominant process for the process involves the boron substituted carbon.[51]

The photolysis of the trifluoromethyltoluenes **3o**, **3m**, **3p** in TFE resulted in photoaddition products as well. The phototransposition reactions did not take place for any of the three isomers in this solvent, as was the case of the cyanotoluenes. The irradiated samples resulted in a complex mixture of photoaddition products, and ^{1}H NMR

revealed broad bands, suggesting the presence of oligomers or polymers. Specific structures could not be assigned.[55]

2.3. The dependence of the lifetime of S_1 on temperature as a tool to reveal details of the dynamics of this state

2.3.1. The rate constant of decay of S_1 for benzene compounds

The lifetime of the first excited singlet state was defined in eq. 1.4 as the reciprocal of the summation of the rate constants of all the processes taking place from S_1. This sum of all the rate constants is often referred to as the total rate constant for decay, k_d.

$$\tau_s = \frac{1}{k_d} = \frac{1}{\sum k_i} \tag{1.4}$$

k_d can be written in terms of the rate constants of all the processes that deactivate S_1.

$$k_d = k_{ic} + k_{isc} + k_f + k_r \tag{2.4}$$

Because k_r is the rate constant for a unimolecular rearrangement, it will be temperature dependent. Both k_{ic} and k_{isc} might depend on the temperature, but k_f is assumed to be temperature independent. k_{ic} can be neglected from eq. 2.4 due to its small value in comparison with the rate constants for the other processes. This last assumption is reasonable for benzene compounds as the S_1 to S_0 energy gap is large, leading to unfavourable Franck-Condon overlap, $\langle V(S_1)|V(S_0)\rangle \approx 0$, where V is the wavefuntion that describes the coordinates of the nuclei. This is a consequence of the energy gap law, which establishes that the rate constant for the vertical jump between two surfaces, in this

case k_{ic}, is proportional to $\exp(-\alpha\Delta E)$, where α is a proportionality constant and ΔE is the energy gap between the zero points of both states. For simple benzene compounds, ΔE is generally about 400 kJ/mol, which means that the probability for the vertical jump between the surfaces of the S_0 and S_1 states has a low value. Estimates of this rate constant for benzene compounds range between 10^2 s^{-1} and 10^5 s^{-1}. Taking into account the two considerations explained above, we can write a new equation for k_d, eq. 2.5.

$$k_d = k_{isc} + k_f + k_r(T) \qquad (2.5)$$

This mathematical model is applied to processes occurring only from S_1. Any reaction taking place from T_1 will not affect the estimated values of the kinetic parameters which are determined from observations of fluorescence decay. As will be described in the next three sections, this method has been used recently by several other research groups.

2.3.2. Kinetic study of the photochemistry of styrene and derivatives[56]

The geometric isomers of substituted styrenes undergo a cis-trans isomerization upon irradiation. The process starts by absorption of electromagnetic radiation, followed by the formation of both singlet and triplet twisted intermediates, which form both geometric isomers. Studies on the chemical behaviour of styrene **95** concluded that the S_1 state is, like its ground state, planar and has a C=C torsional barrier greater than 16 kJ/mol.[57] Computational studies have suggested that this barrier is greater than 57 kJ/mol, a value that would effectively prevent C=C torsion as a viable pathway for a

singlet state decay.[58] In fact, the singlet lifetime and fluorescence quantum yield for S_1 of styrene increases only slightly upon cooling from room temperature to 77 K,[59] in accordance with the absence of a low-barrier activated pathway for singlet state non-radiative decay. Triplet styrenes have no barrier to C=C torsion.[60]

The isomeric 1-phenylpropenes **95-101** were selected for the study of phenylalkene photoisomerization. Fluorescence decay times and isomerization quantum yields were measured over an extended range of temperatures. Assuming that both singlet and triplet twisted intermediates decay with equal probability to cis and trans ground states, the total isomerization rate constant $k_{iso}(T)$, can be calculated using eq. 2.6. An equivalent equation that considers the kinetic rate constants of all the processes that participate in the isomerization process must be considered in order to describe completely the dynamics of the isomerization, eq. 2.7. This equation contains two parts, a temperature-dependent singlet component and a temperature-independent triplet component.

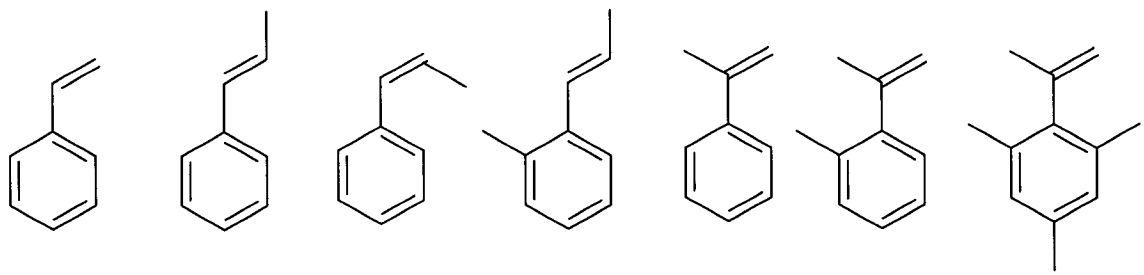

95 **96** **97** **98** **99** **100** **101**

$$k_{iso}(T) = 2\,x\,\frac{\Phi_{iso}(T)}{\tau_s(T)} \qquad (2.6)$$

$$k_{iso}(T) = k_{isc} + A\,exp\left(\frac{-E_{act}}{RT}\right) \tag{2.7}$$

The $k_{iso}(T)$ values were calculated using the experimental values of Φ_{iso}, and τ_s at different temperatures. A non-linear fitting was done using eq. 2.7. The resulting barriers for C=C torsion of *trans*- and *cis*-1-phenylpropene, **96** and **97,** were calculated to be 36.8 and 19.1 kJ/mol, respectively. The former barrier, although lower than theoretical predictions for styrene, is sufficiently high to render C=C torsion a minor pathway for the geometric isomerization at room temperature and below. However, C=C torsion is the dominant singlet decay process for the cis-isomer.

A simple solution to calculate the barrier of the styrenes, **95 - 101**, is provided by a non-linear fitting of the temperature-dependent singlet lifetimes, eq. 2.8.

$$\tau_s(T) = \frac{1}{\sum k_i + A\,exp\left(\frac{-E_{act}}{RT}\right)} \tag{2.8}$$

$\Sigma\, k_i$ is the sum of all non-activated decay processes, fluorescence and intersystem crossing. A and E_{act} are the pre-exponential factor and the activation energy for the activated processes. The values of A and E_{act} for the *trans*-2-phenylpropenes are similar to those for styrene, which indicates that the trans methyl-substitution in **96** and **98** has little effect on the C=C torsional barrier. This result indicates that there is no steric acceleration from the ortho substituent that could result in a reduction of the torsional barrier. The activation energy for the other isomers is calculated to be lower than 23 kJ/mol, in comparison to values of 50 kJ/mol for the trans isomers. The calculated values

for the pre-exponential factor are higher for the trans-isomer, log A ~12.6 (trans) and 9.7 (cis).

2.3.3. Temperature-dependent photochemistry of 1,3-diphenylpropenes[61]

Lewis and collaborators have studied the photochemical behaviour of 1,3-diphenylpropene and several of its 3-substituted derivatives, **102-105**, over a wide range of temperatures.[61] The singlet excited state of these alkenes is found to decay via two activated processes: trans-cis isomerization, and a phenyl-vinyl bridging process by a di-π-methane rearrangement, Scheme 2.7,[62] and two non-activated processes: fluorescence and intersystem crossing. A kinetic modeling of the temperature-dependent rate constants for decay, combined with the quantum yields of fluorescence, intersystem crossing, and both of the photochemical processes, provided a method to estimate the rate constants for all the processes of S_1, including the Arrhenius parameters for the activated ones.

Scheme 2.7. Photochemical reactions of 1,3-diphenylpropenes

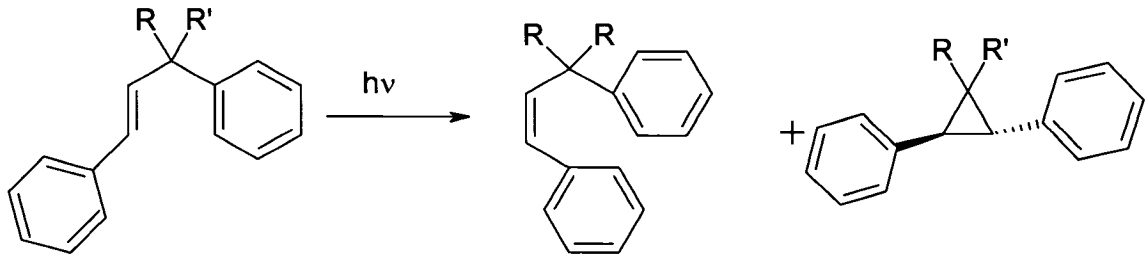

	R	R'
102	H	H
103	CH_3	H
104	CH_3	CH_3
105	Ph	H

The temperature dependence of the quantum yields for the trans-cis isomerization (Φ_{iso}) and for the di-π-methane rearrangement ($\Phi_{di\text{-}\pi}$) were determined over the range 140 - 352 K. The study of the isomerization of **104** established that these processes can occur via an activated singlet state pathway (k_{twist}) and intersystem crossing (k_{isc}), the latter dominating at room temperature or below, and the former dominating at higher temperatures. Both pathways lead to twisted intermediates, singlet or triplet, depending on the route, which decay with equal probability to the ground state of both the cis and the trans isomers. According to these facts, the total isomerization quantum yield can be described by eq. 2.9. Eqs. 2.9 - 2.11 describe phenomenologically the dynamics of the isomerization process.[63] The rate of isomerization increased with bulky substituents because of compression of the internal angle between these groups.[64] Thus, the rate enhancement observed is a consequence of complex changes in the entropy and enthalpy of activation.

$$\Phi_{iso} = \frac{1}{2} k_{twist} \tau_s + \frac{1}{2} k_{isc} \tau_s \tag{2.9}$$

$$k_{iso} = \frac{\Phi_{iso}}{\tau_s} \tag{2.10}$$

$$k_{iso} = \frac{1}{2}\left[A_{twist} \exp\left(\frac{-E_{twist}}{RT} \right) + k_{isc} \right] \tag{2.11}$$

k_{twist} is the rate constant for the singlet state isomerization, k_{isc} is the rate constant for intersystem crossing, A_{twist} is the pre-exponential factor, and E_{twist}, the activation

energy for the process. The kinetic parameters were obtained from a nonlinear fitting of the values of k_{iso} with respect to temperature.

Another interesting result of these fits is that the Zimmerman rearrangement process features lower pre-exponential factors and activation energies than for the cis - trans isomerization. The lower pre-exponetial factors are consistent with a decrease in entropy, as would be expected for the formation of a cyclopropane ring.

The values obtained for k_{isc} were similar to values previously reported in the literature (~ 4.6 x $10^7 s^{-1}$). The values of A_{twist} for the diphenylpropenes are larger than for the value reported for 1-phenylpropene (0.63 x 10^{12} s^{-1}), but the values of E_{twist} for the diphenylpropenes are slightly lower than for 1-phenylpropene (36.8 kJ/mol in hexane). These values decrease with the bulk of the 3-substituent probably, as explained before, due to a steric acceleration of the substituent.

The mathematical model of the processes of S_1 for **102** is complicated by the fact that the chemical reaction takes place from the same excited state as geometric isomerization. The rate constant for the Zimmerman rearrangement process, eq. 2.12, can be described by a rate constant equation that is analogous to eq. 2.10.

$$k_{di\text{-}\pi} = \frac{\Phi_{di-\pi}}{\tau_s} \tag{2.12}$$

Activation parameters for the di-π-methane rearrangement ($k_{di\text{-}\pi}$), the cis–trans isomerization (k_{twist}), and the intersystem crossing rate constant (k_{isc}), can be obtained from a non-linear fitting of the temperature dependence of the S_1 decay time according to

eq. 2.13. For this expression, the previously determined values of k_f, A_{twist}, and E_{twist}, were used.

$$\tau_s = \frac{1}{k_f + k_{isc} + A_{di-\pi}\, exp\left(\frac{-E_{di-\pi}}{RT}\right) + A_{twist}\left(\frac{-E_{twsit}}{RT}\right)} \qquad (2.13)$$

This expression considers the cis-trans isomerization and the Zimmerman rearrangement. The values of $k_{di\text{-}\pi}$ at room temperature increased upon introduction of 3-methyl substituents, following the order **103** < **104** < **105**. This increase in the calculated rate constant for the Zimmerman rearrangement was attributed to the *gem*-dialkyl effect on the biradical intermediate. The values of the pre-exponential factor are lower than those for the cis-trans isomerization, consistent with the formation of a three-membered ring at the transition state. As a consequence of the lower activation energies, values of $\Phi_{di\text{-}\pi} > \Phi_{iso}$ were found for **103** and **104** at temperatures higher than 180 K. At temperatures lower than 160 K, the activated processes become slower and the main deactivation pathways are the photophysical processes, fluorescence and intersystem crossing. At temperatures higher than 440 K, the calculated rate constant for the cis-trans isomerization is greater than for the di-π-methane rearrangement, in agreement with the experimental observations.

2.3.4. Internal conversion for 4-aminobenzonitriles in alkane solvents[65]

In non-polar alkane solvents, the emission spectra of 4-dimethylaminobenzonitrile **106** and related molecules **107 - 109** present a single fluorescence band. The authors do not specify which excited state fluoresces, but given the very well understood

photochemistry of benzene compounds, it is logical to state that the fluorescence occurs for the first excited singlet state S_1. The fluorescence decay of both **106** and **107** in alkane solvents are single exponential.[66] Internal conversion for these compounds was a negligible process in comparison with other typical modes of decay.

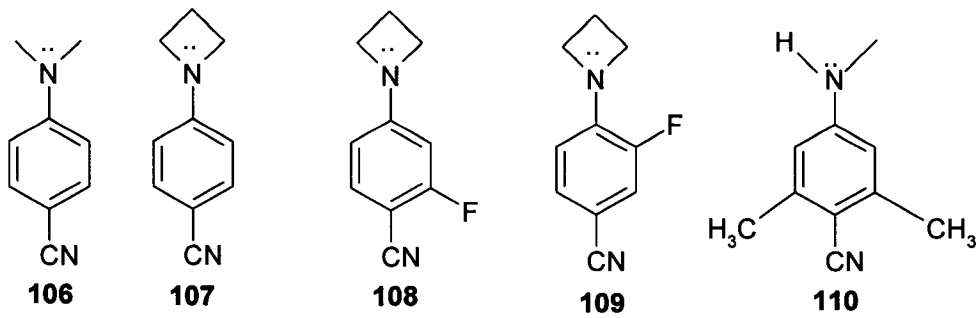

For **107** in n-hexane at 25°C, the sum of the fluorescence quantum yield Φ_f and the intersystem crossing yield Φ_{isc} is close to unity,[67] showing that internal conversion is not an important deactivation pathway for the decay of S_1. However, efficient thermally-activated internal conversion has been observed with other aromatic amines: 3,5-dimethyl- 4 -(methylamino)benzonitrile **110**,[68] 1-(dialkylamino)naphthalenes,[69, 70, 71] 4-substituted-1-(dimethylamino)naphthalenes,[71] and 9-(dimethylamino)anthracenes.[72] It has been shown that the occurrence of this activated internal conversion is governed by the twist angle of the amino group relative to the plane of the benzene moiety, as well as by the energy gap, ΔE (S_2-S_1), between the two lower excited states.[72] The internal conversion process has been assumed to proceed from S_1 to S_0 via a conical intersection.[71, 73]

During the investigation of the influence of fluoro substitution on the benzene ring of the aminobenzonitriles on the efficiency of intramolecular charge-transfer process in the singlet excited state, Zachariasse and collaborators found that, for **108** and **109,** the F-substitution opens up an efficient activated internal conversion decay process.

The quantum yields for fluorescence of **106-109** were determined over a broad range of temperatures (-92 °C to 45 °C). The Φ_f for **108** was considerably smaller than for **107** over the entire range of temperatures, decreasing form 0.17 at -92 °C to 0.01 at 45 °C, whereas the Φ_f for **107** decreased from 0.39 to 0.26 over the same temperature range. The Φ_f for **109** decreased from 0.24 to 0.09 between these two temperatures, whereas the Φ_f for **110** did not have a significant dependence on the temperature.

The yields of the intersystem crossing process, Φ_{isc}, for the S_1 to T_1 conversion were measured by T-T absorption techniques, using a method based on triplet-triplet energy transfer with perylene as the acceptor, and N-methyl-1,8-naphthalimide as a reference.

Fluoro substitution in the benzene ring resulted in changes in the absorption spectra of the compounds studied. In the spectrum of **108,** the S_1 band was clearly visible as a shoulder on the lower energy side of the absorption band of S_2.[74, 75] However, for **109**, the band corresponding to the $S_0 \rightarrow S_1$ was completely covered by the S_2 band. This indicates that the energy gap between both states is probably reduced by the fluoro substitution. In addition, fluoro substitution on the benzene ring leads to a considerable lowering of the fluorescence quantum yield as the temperature increases.

In order to establish the nature of the non-radiative decay processes for **107**, **108** and **109,** the quantum yields for intersystem crossing were determined at 25 °C. The sum

of the quantum yields of fluorescence and intersystem crossing was, in all the cases, less than 1. There was no evidence that a photochemical reaction was responsible for this apparent abnormality. From the data reported,[65] it was found that internal conversion was the major deactivation pathway for **108**, suggesting that an interaction between the ortho-relation of the cyano and fluoro substituents might be responsible for this result. For the other aromatic amines, the intersystem crossing process was the main process of decay. The rate constant for all the processes was calculated using eq. 2.14, equivalent to eq. 1.21

$$\Phi_i = k_i \tau_s \qquad \text{(where i = f, isc, ic)} \tag{2.14}$$

The Arrhenius parameters for internal conversion and intersystem crossing were calculated for **107**, **108**, and **109,** from the temperature dependence of the fluorescence decay. The τ_s for all of these amines were measured as a function of temperature in cyclopentane, n-hexane and n-hexadecane. The decays were single exponential. From the lifetimes and the calculated rate constants for fluorescence from Φ_f's, the Arrhenius parameters for internal conversion and intersystem crossing were both determined by fitting the experimental data to eq. 2.15.

$$k_d = k_f + k_{ic} + k_{isc} = k_f(0)n^x + k_{ic}^0 \exp\left(\frac{-E_{ic}}{RT}\right) + k_{isc}^0 \exp\left(\frac{-E_{isc}}{RT}\right) \tag{2.15}$$

The conclusion reached was that activated internal conversion dominates at the higher temperatures and intersystem crossing becomes more important at the lower temperatures.

The occurrence of efficient internal conversion from S_1 to S_0 for **108** and **109** must be due to a change in geometry in the excited state from that reached by electromagnetic excitation of S_0. The kinetic barrier for ic is reduced as a result of the fluoro substitution. The influence of this substituent on the value of the kinetic barrier for internal conversion shows that the difference in electronic distribution of the S_1 and S_0 states plays an important role in the magnitude of the E_{ic} barrier. In addition, the fluoro substituent decreases the quantum yield of fluorescence and shortens the lifetime of these species with respect to the aromatic amine **106**.

The important conclusion reached from the examples presented in Sections 2.3.3 to 2.3.5 is that the temperature-dependence of singlet excited-state lifetimes can be used as a tool to estimate kinetic rate constants for the process of S_1.

2.4. Results[7, 76]

As stated before, compounds **1-3** rearrange by means of a pathway that requires the formation of a reactive intermediate (RI) from S_1. This intermediate arises from a meta-bonding process upon excitation. In addition, the product distribution has been shown to be dependent on the solvent and the substitution pattern. These characteristics make these compounds ideal substrates for a study of temperature and solvent effects.

2.4.1. Photophysical properties of 1 - 3

All nine compounds have the usual two bands in the electronic spectra, with the former one being at longer wavelengths and with lower molar absorptivities (ϵ), and the latter being at shorter wavelengths and with higher molar absorptivities. All these compounds also have fluorescence spectra that overlap with the absorbance bands at the expected zero-zero transition (for $S_1 \rightarrow S_0$ deactivation). Photophysical data are given in Table 2.1. The values of ϵ indicate that the $S_0 \rightarrow S_1$ transition is symmetry forbidden, and the $S_0 \rightarrow S_2$ transition is symmetry allowed.

Table 2.1 Photophysical properties of 1-3 in AN and TFE

compound	λ_1/nm($S_0 \rightarrow S_1$)[a]	λ_2/nm($S_0 \rightarrow S_2$)[a]	ϵ_1/ $M^{-1}cm^{-1}$	ϵ_2/ $M^{-1}cm^{-1}$	$E_{0,0}$/ $kJmol^{-1}$
1o					
CH_3CN	275	227	1380	11400	417
CF_3CH_2OH	276	227	1430	11900	417
1m					
CH_3CN	275	227	1150	11000	419
CF_3CH_2OH	275	227	1140	13428	419
1p					
CH_3CN	267	232	570	16100	426
CF_3CH_2OH	267	232	664	17600	426
2o					
CH_3CN	273	224	868	13500	438
CF_3CH_2OH	273	222	780	10000	438
2m					
CH_3CN	272	224	988	13900	421
CF_3CH_2OH	273	223	778	11000	421
2p					
CH_3CN	264	227	322	14100	429
CF_3CH_2OH	264	227	422	14900	429
3o					
CH_3CN	265	206	940	9380	435
3m					
CH_3CN	265	208	690	7730	435
3p					
CH_3CN	258	211	330	5980	440

a. λ values are λ_{max}.

For the compounds **1-3,** similar values of both λ and ϵ were obtained in AN and TFE. This indicates that there is not a significant interaction between the protic solvent TFE and the ground state of the substrates, and that both solvents solvate in a similar manner the excited states S_1 and S_2 of these compounds.

High values of molar absorptivities were found for the isomers **1o, m, p**. This is a consequence of the increase of delocalization due to the resonance effect arising from the cyano group. The red shift of the λ_{max} of the $S_0 \rightarrow S_1$ band for the boronate esters **2o, m, p** with respect to the parent compound toluene indicates that the substituent $-B(OR)_2$ is also conjugated to the benzene ring.

2.4.2. Effect of the temperature and the solvent on the deactivation rate constant for the singlet excited state S_1 of compounds 1 - 3

The influence of temperature and the solvent on the singlet lifetimes (τ_s) of compounds **1-3** was studied. Singlet lifetimes were determined by monitoring fluorescence decay using a nanosecond single photon counting apparatus with a hydrogen lamp of pulse width at about 1.8 ns. All samples were degassed by three freeze-pump-thaw cycles. The absorbance of the samples was measured to guarantee a value lower than 0.3 at the excitation wavelength. For the temperature-dependent measurements, the cell compartment was thermostated with circulating water from a constant temperature bath. The temperature was measured with a thermocouple. The τ_s's were measured from approximately -45/-30 °C to 65 °C in both AN and TFE. Plots of the deactivation rate constant k_d are used to show graphically the effect of the temperature on the deactivation rate. The rate constants for deactivation, k_d, were calculated using eq. 1.4. The k_d (s^{-1})

data as function of T (K) for the compounds are shown graphically in Figures 2.1–2.15, and numerically in Appendix 1.

Figure 2.1. Dependence of the deactivation rate constant on the temperature for *o*-cyanotoluene 1o in AN

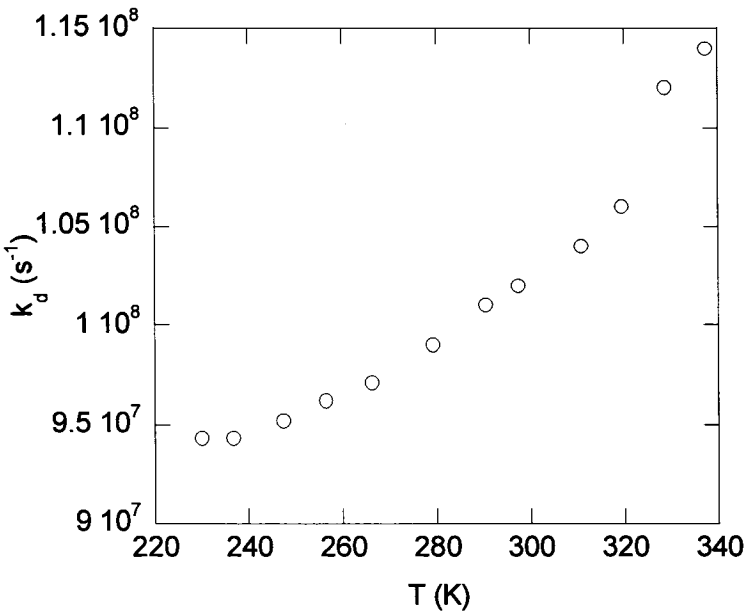

Figure 2.2. Dependence of the deactivation rate constant on the temperature for *o*-cyanotoluene 1o in TFE

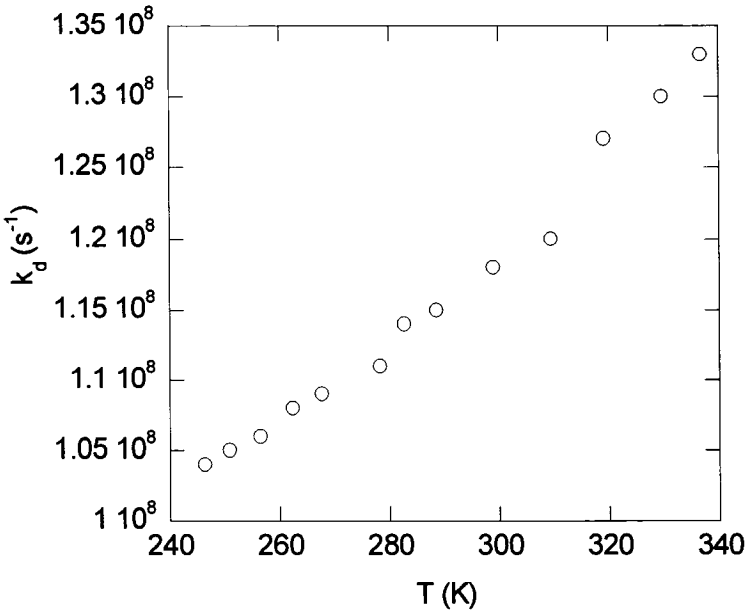

Figure 2.3. Dependence of the deactivation rate constant on the temperature for *m*-cyanotoluene 1m in AN

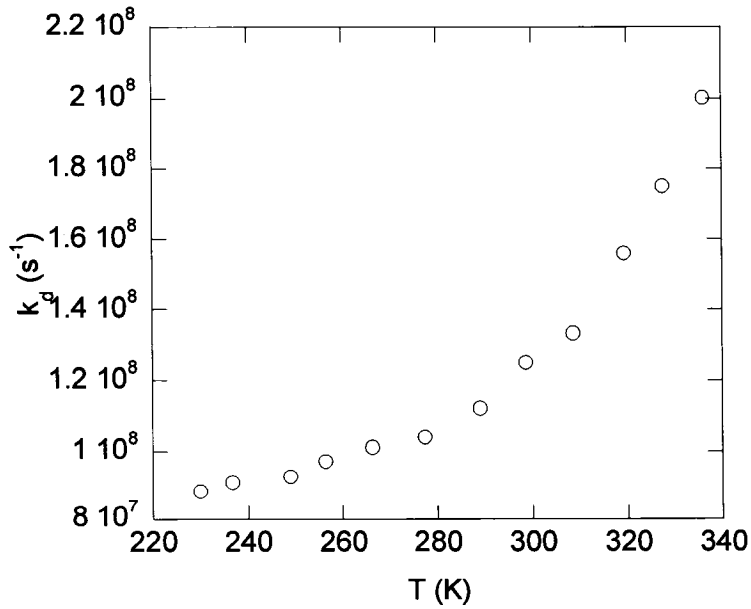

Figure 2.4. Dependence of the deactivation rate constant on the temperature for *m*-cyanotoluene 1m in TFE

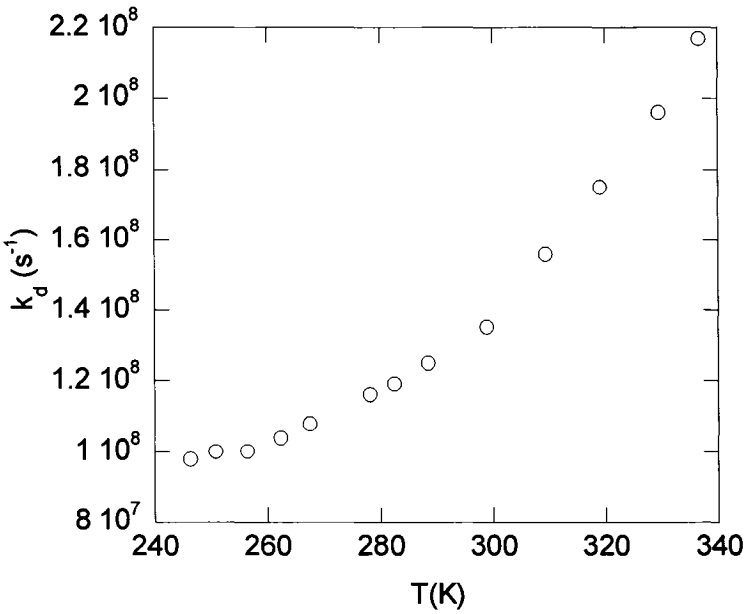

Figure 2.5. Dependence of the deactivation rate constant on the temperature for *p*-cyanotoluene 1p in AN

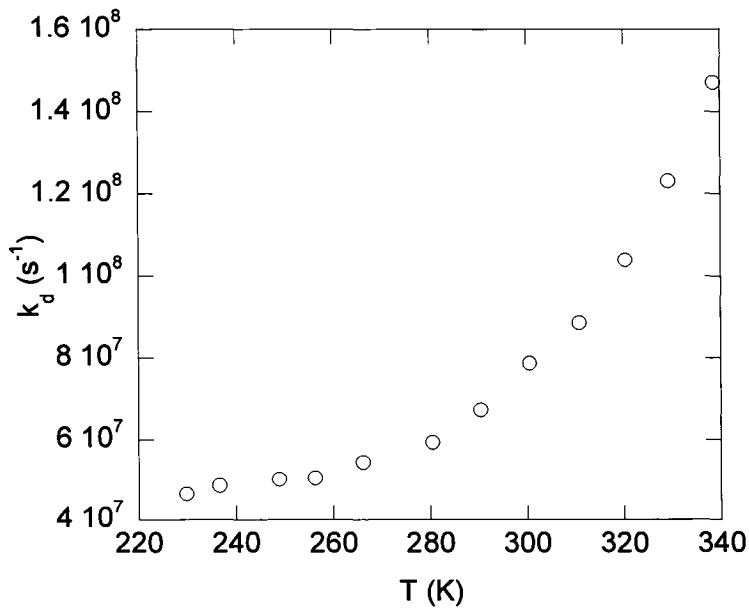

Figure 2.6. Dependence of the deactivation rate constant on the temperature for *p*-cyanotoluene 1p in TFE

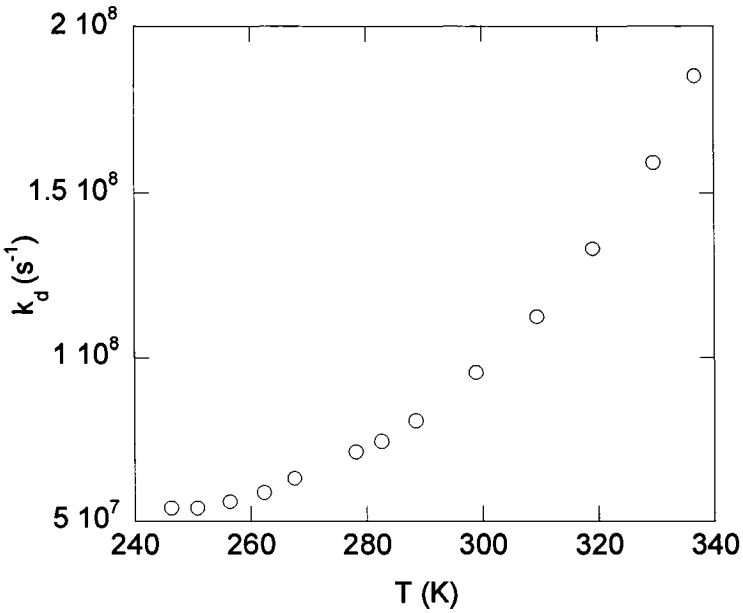

Figure 2.7. Dependence of the deactivation rate constant on the temperature for *o*-boronate ester 2o in AN

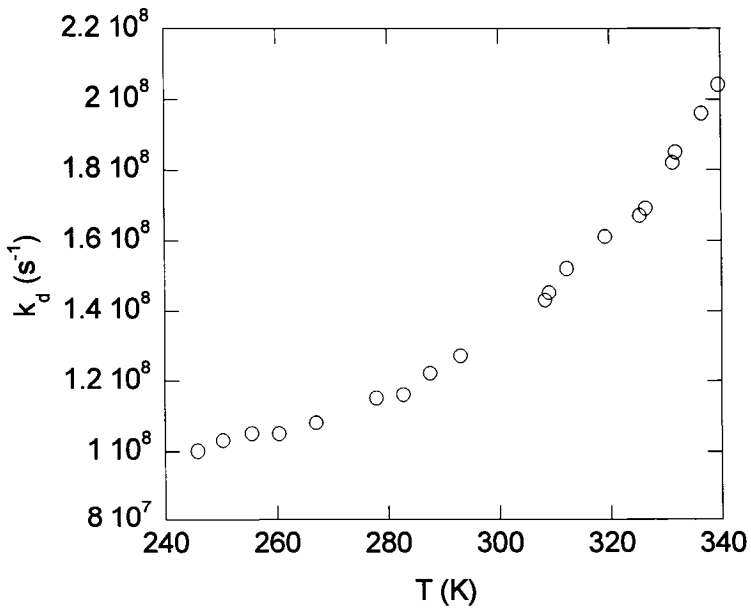

Figure 2.8. Dependence of the deactivation rate constant on the temperature for *o*-boronate ester 2o in TFE

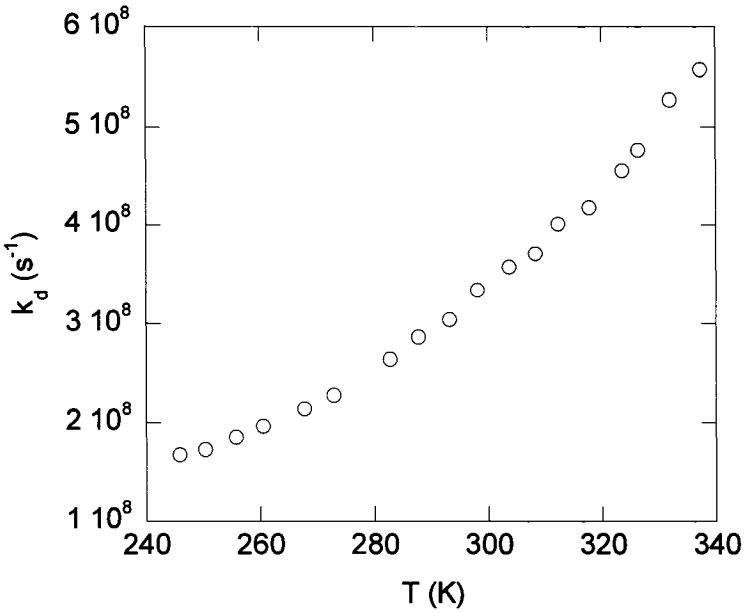

Figure 2.9. Dependence of the deactivation rate constant on the temperature for *m*-boronate ester 2m in AN

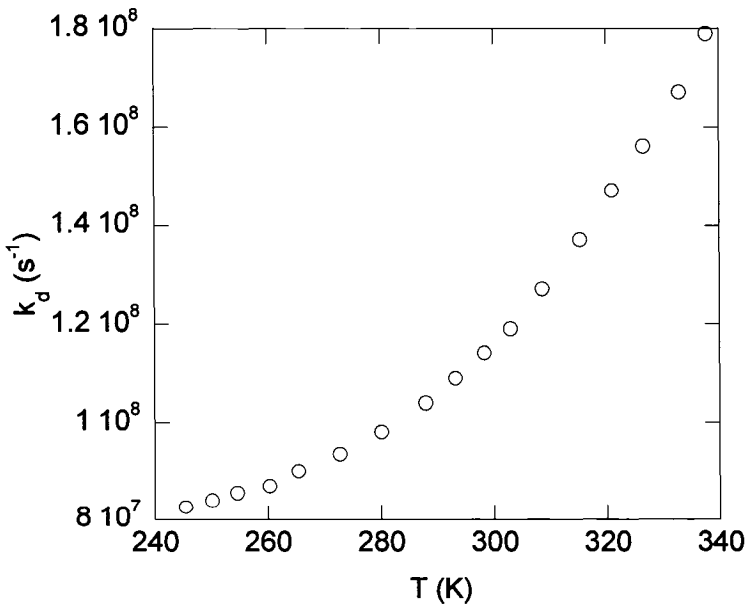

Figure 2.10. Dependence of the deactivation rate constant on the temperature for *m*-boronate ester 2m in TFE

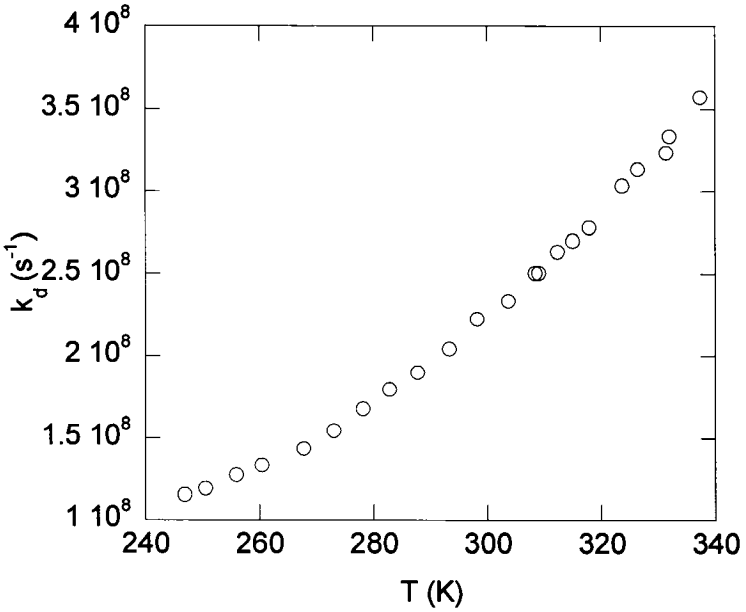

Figure 2.11. Dependence of the deactivation rate constant on the temperature for *p*-boronate ester 2p in AN

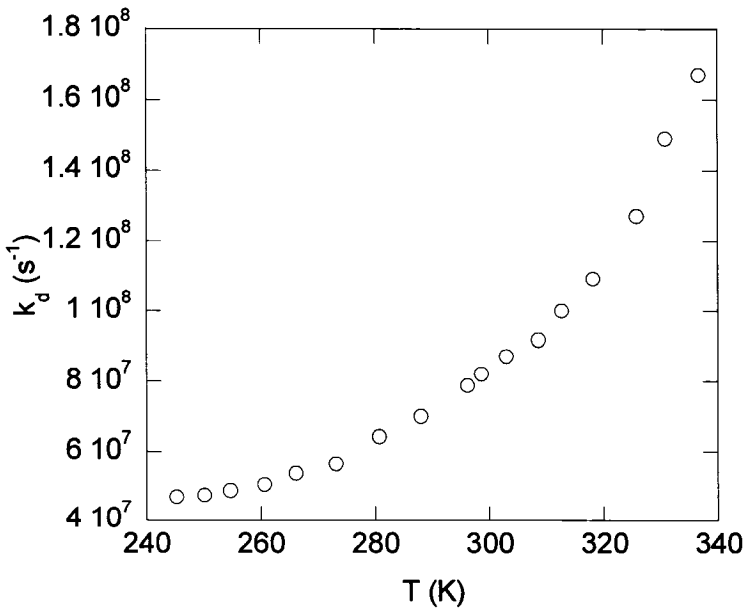

Figure 2.12. Dependence of the deactivation rate constant on the temperature for *p*-boronate ester 2p in TFE

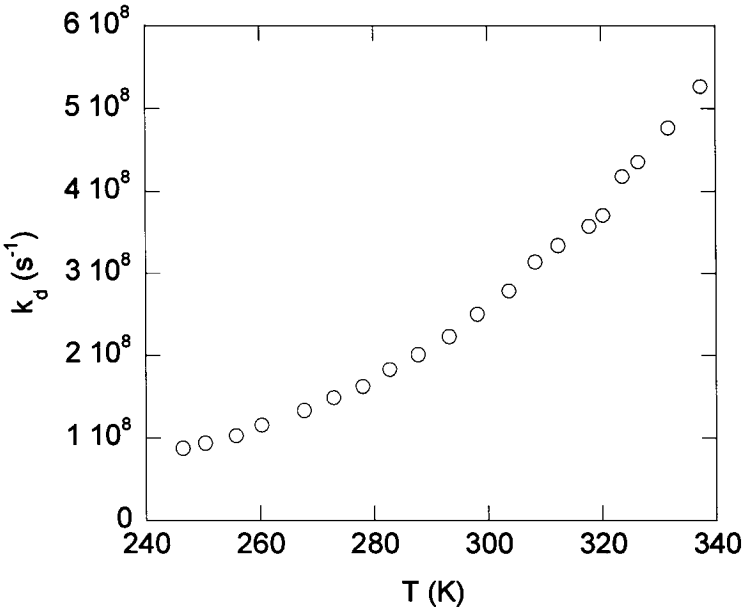

Figure 2.13. Dependence of the deactivation rate constant on the temperature for *o*-trifluoromethyltoluene 3o in AN

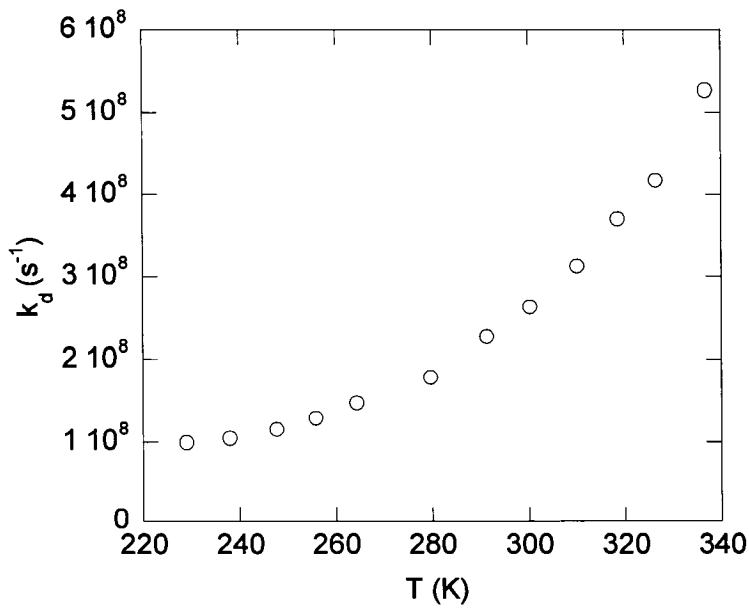

Figure 2.14. Dependence of the deactivation rate constant on the temperature for *m*-trifluoromethyltoluene 3m in AN

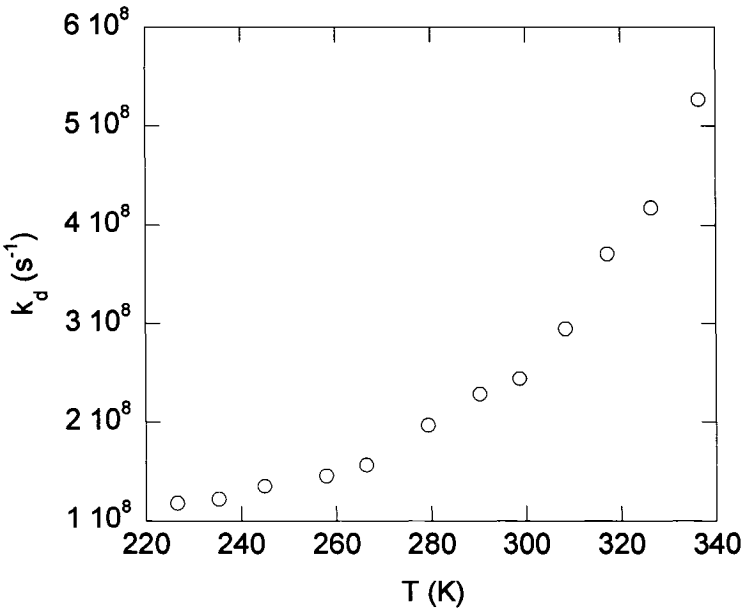

Figure 2.15. Dependence of the deactivation rate constant on the temperature for *p*-trifluoromethyltoluene 3p in AN

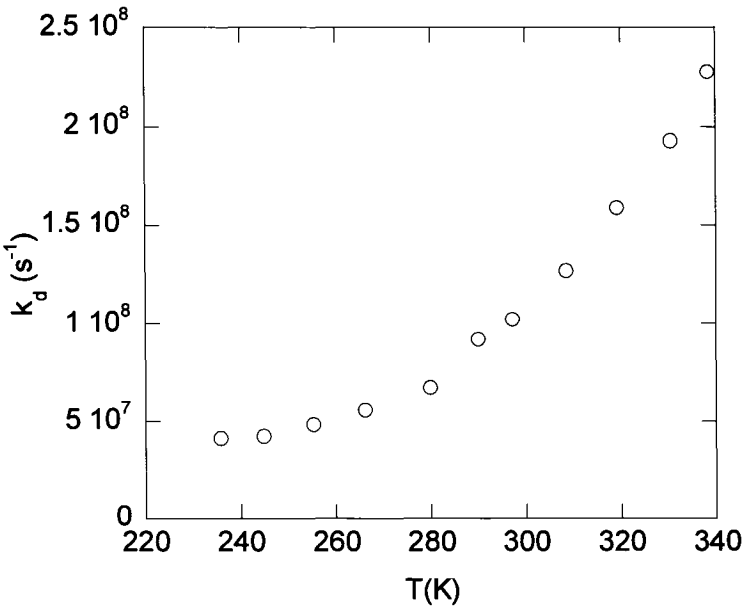

The deactivation rate constant for all the isomers increased with the temperature. This implies that at least one radiationless process is enhanced by an increase in temperature. The dependence of the k_d on the temperature can be related to the chemical reactivity of each isomer. For example, the deactivation rate constant of *o*-cyanotoluene **1o** in AN does not depend significantly on temperature; the total change in lifetime over the range of temperatures is only about 2 ns. Coincidently, after 20 hours of photolysis in AN only 8% of this isomer had isomerised to the meta- and para- isomers, **1m** and **1p**, Figure 2.16. For the *p*-cyanotoluene **1p**, which after 10 hours of photolysis is transformed into the other two isomers to about 90 % conversion, Figure 2.18, the singlet lifetime drops from 22 ns to 7ns. This last fact indicates that the chemical reactivity for **1p** is higher than that for **1o**. In every case investigated, the deactivation rate constants in TFE are greater than in AN. This suggests that at least one nonradiative process, probably the chemical reaction, is affected by the solvent. The increase in k_d of S_1 indicates that the activation energy for the temperature-dependent process is lower in the protic solvent TFE than in AN. Similar values of ϵ, wavelengths and 0,0 band were found for the isomers in both AN and TFE, indicating that this effect is not related to a different interaction between S_1 and the solvent, but rather between the solvent and the transition state; probably a stronger interaction takes place between the transition state and the solvent during the formation of the prefulvene intermediate.

2.4.3. Effect of the temperature on the chemical reactivity of compounds 1 and 3

In order to verify that the influence of temperature on the lifetimes of S_1 was due to the effect of the temperature on the reaction, the photolysis of **1o,m,p** and **3o,m,p** isomers were carried out at both 25 and 50 °C. Reactions for the phototransposition of these isomers were done in nitrogen-saturated solutions at a concentration of 1 mg/mL. A Rayonet reactor was used with 16 low-pressure Hg lamps (254.6 nm) using 100 mL of the solvent. Identification of the products was done by comparing the retention time obtained from gas chromatograms, and the corresponding mass spectra recorded by using a gas chromatograph instrument with a mass selective detector (GC-MS). The values for the retention time and the mass spectra for the photolysis products were compared to the same properties of a commercial sample of each isomer. The photolysis plots were obtained by gas chromatography with a flame-ionization detector (GC-FID). The GC-FID response was considered to be the same for each isomer. This allows for reporting the yields of each isomer in percent normalized to 100% with respect to the sum of the response of all three isomers on the GC-FID. The relatively high conversion for long photolysis times in AN for the para and meta isomer, in the case of the cyanotoluenes, **1p** and **1m**, and ortho and meta isomers in the case of the trifluoromethyltoluenes, **3o** and **3m**, and the absence of other signals in all the chromatograms indicates that these phototransposition reactions are clean. No secondary photochemistry was observed in any case. Plots of the results are shown in Figures 2.16-2.27.

Three major conclusions are obvious from these plots. First, the rate of isomerization is clearly isomer-dependent. For instance, at 25 °C, to reach 20% disappearance of the starting material requires 75 minutes for **1p**, 330 minutes for **1m**,

and 6000 minutes for **1o**.[29] The *p*-cyanotoluene isomer is the most reactive one in the series of the cyanotoluenes, whereas the ortho isomer is only slightly reactive at 25 °C. However, when the photolysis of **1o** was done at 50 °C, the chemical reactivity increased remarkably (20 % of this isomer had rearranged into products at around 500 minutes of photolysis), Figure 2.19. For the more efficiently reacting meta and para isomers (Figures 2.17 and 2.18), a photostationary state is approached at high conversions at 25 °C. When the temperature was increased to 50 °C, the time to reach the stationary state for the *o*- and *m*-cyanotoluene **1o** and **1m** was shortened. An enhancement in the chemical reactivity is clearly observed from the photolysis plots. For instance, the reactivity of the *o*-cyanotoluene increases by about a factor of 3 at 50 °C. The relative reactivity order continues to be **1p** > **1m**- >**1o** when the temperature increases.

In contrast to the results obtained for the reactivities of the cyanotoluenes, the reactivities of the trifluoremethyltoluenes are **3o** > **3m** > **3p** (the reverse of that observed for the cyanotoluenes **1o**,**m**,**p**). In addition, the reactions are considerably more efficient; the stationary state is reached in all cases before 500 minutes of photolysis time, Figures 2.22–2.24. The reason for this reversal in the order of reactivity must be related to the change in the substituents. The bulky $-CF_3$ substituent might increase the photochemical reactivity of the o-isomer due to a steric interaction between both ortho substituents, whereas the *p*-cyanotoluene could be the most reactive isomer due to the conjugative electron-withdrawing effect of the cyano-substituent in the para position. The influence of temperature in the phototransposition reactions of the *o*-, *m*-, *p*-trifluoromethyltoluene **3o**,**m**,**p** was similar to that for the cyanotoluenes. At 50 °C, the stationary states were reached earlier for all photolysis, and an enhancement in the chemical reactivity was also

observed. As expected, the rate constant of the reaction of the S_1 state depends on the temperature, just as that of a ground-state reaction does.

Figure 2.16. Conversion plot for the photolysis of isomer 1o in AN at 25 °C

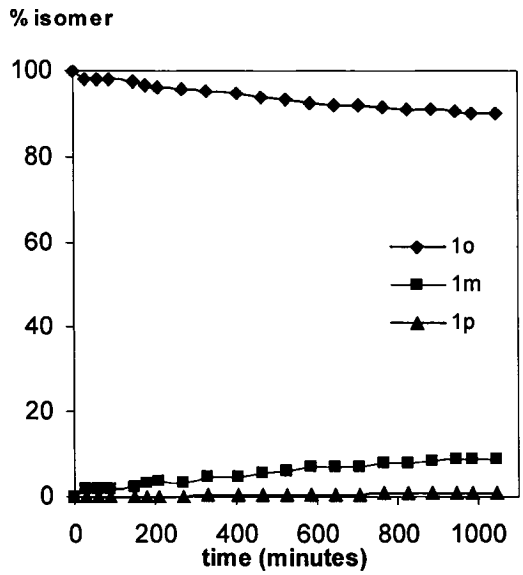

Figure 2.17. Conversion plot for the photolysis of isomer 1m in AN at 25 °C

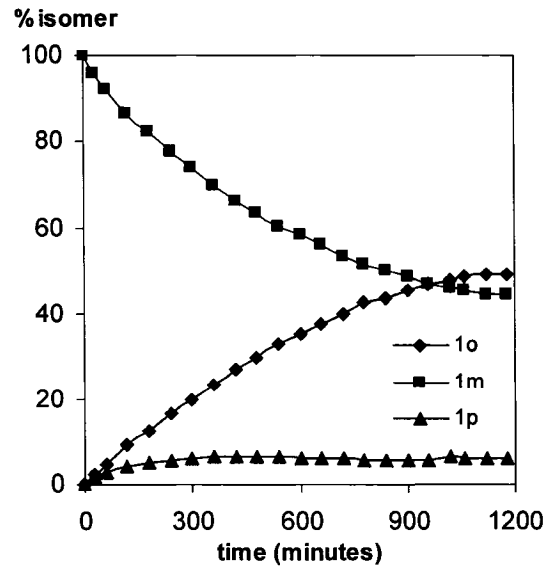

Figure 2.18. Conversion plot for the photolysis of isomer 1p in AN at 25 °C

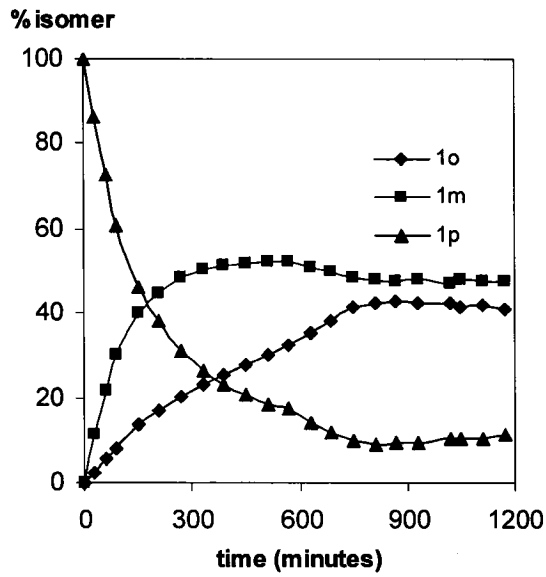

Figure 2.19. Conversion plot for the photolysis of isomer 1o in AN at 50 °C

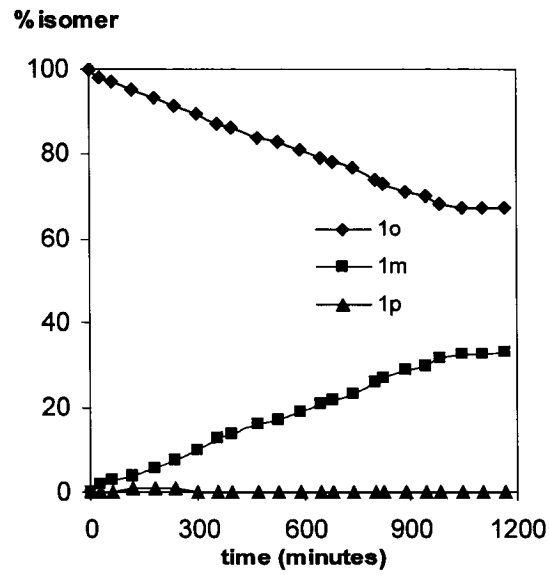

Figure 2.20. Conversion plot for the photolysis of isomer 1m in AN at 50 °C

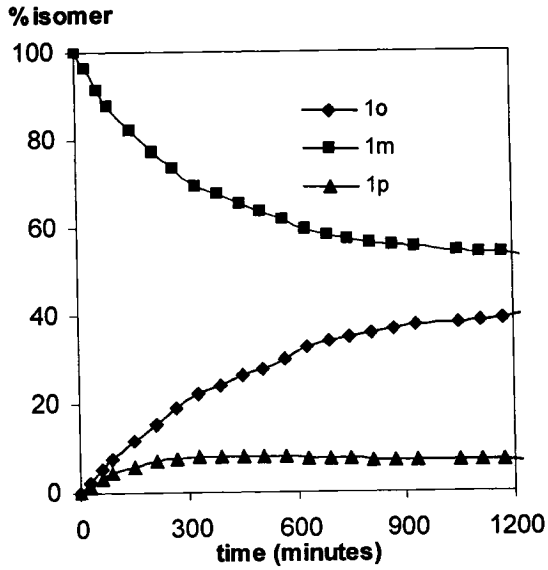

Figure 2.21. Conversion plot for the photolysis of isomer 1p in AN at 50 °C

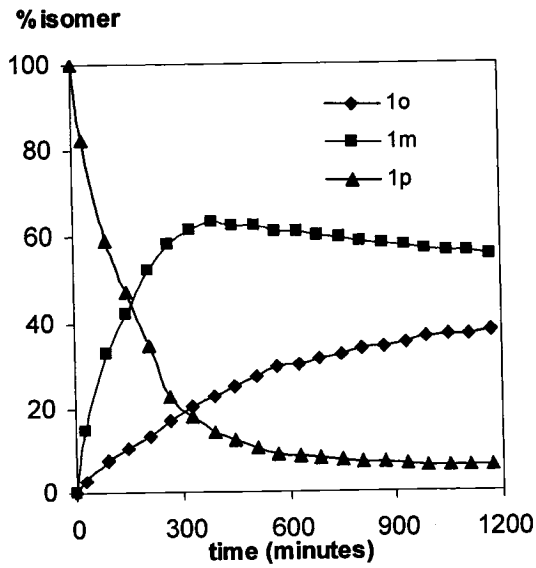

Figure 2.22. Conversion plot for the photolysis of isomer 3o in AN at 25 °C

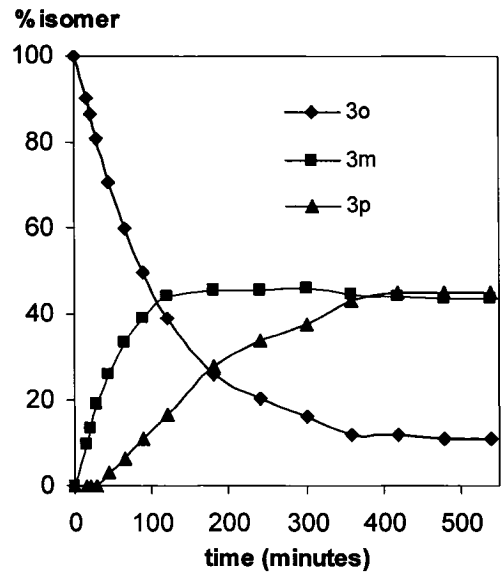

Figure 2.23. Conversion plot for the photolysis of isomer 3m in AN at 25 °C

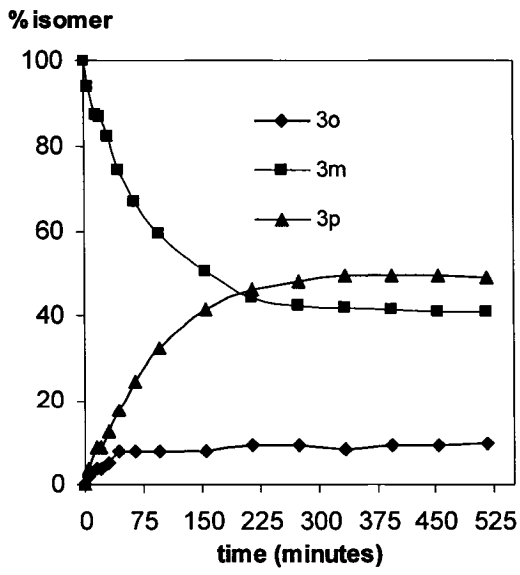

Figure 2.24. Conversion plot for the photolysis of isomer 3p in AN at 25 °C

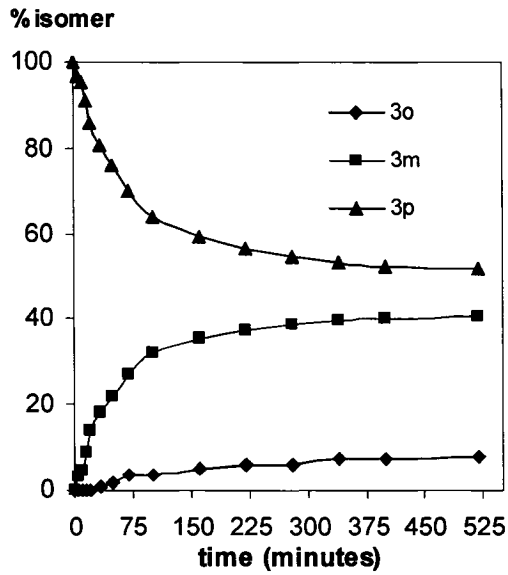

Figure 2.25. Conversion plot for the photolysis of isomer 3o in AN at 50 °C

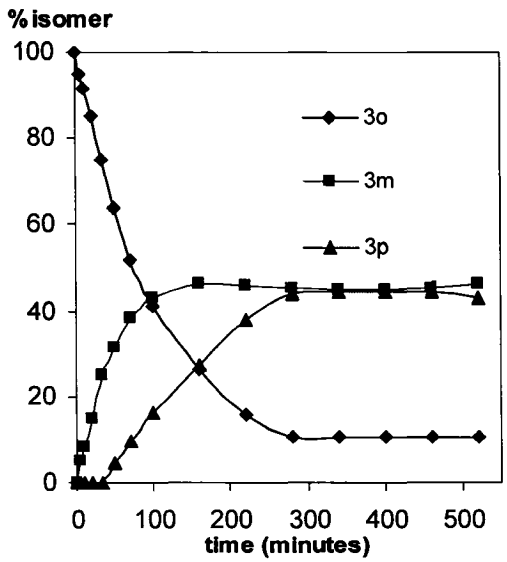

Figure 2.26. Conversion plot for the photolysis of isomer 3m in AN at 50 °C

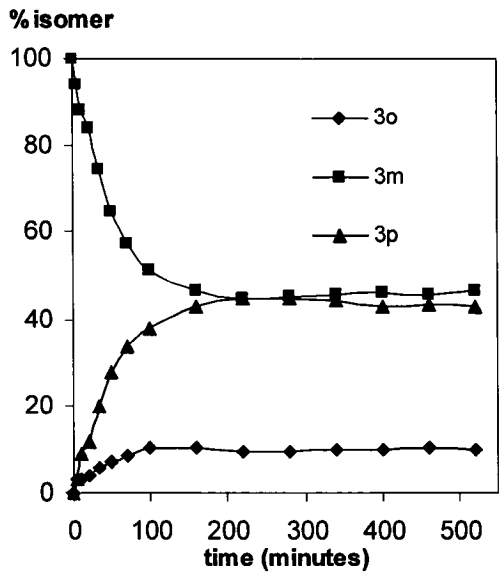

Figure 2.27. Conversion plot for the photolysis of isomer 3p in AN at 50 °C

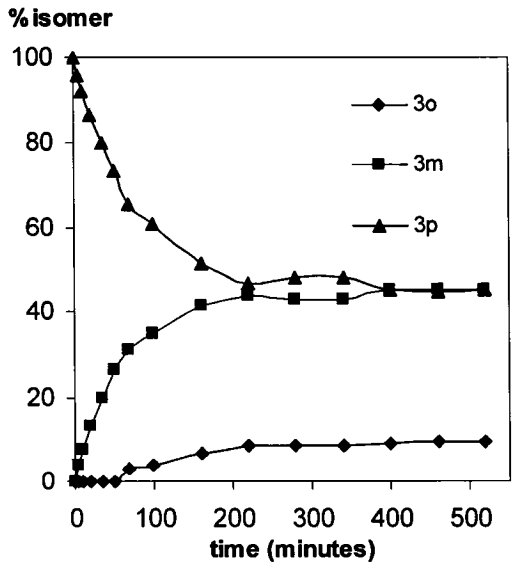

2.5. The Arrhenius equation as a means to estimate activation parameters, rate constants, and quantum yields of the processes of S_1 for benzene compounds

As outlined in Section 2.3, eq. 2.4 offers a convenient mathematical model to describe the dynamics of the singlet excited states of benzene compounds. Using the Arrhenius dependence of the kinetic rate constants of reaction on temperature, it is possible to rewrite eq. 2.4 as a function of temperature to eq. 2.16. This equation applies if the only activated chemical process that affects the decay of each isomer from the S_1 state is the formation of the biradical intermediate, and if the remaining rate constants of the physical processes of S_1 stay unchanged when the temperature varies.

Although there are not many studies on the dependence of fluorescence with respect to temperature, it is widely accepted that fluorescence rate constants are temperature independent. This will be discussed in more detail below. Whereas intersystem crossing can be an activated process, its typical Arrhenius parameter values are very small in comparison with those for reactions. These values are generally found to be for $A \sim 10^8\ s^{-1}$ and $E_{act} \sim 5 - 10$ kJ/mol.[77] The low A value reflects the fact that this process is spin forbidden ($S_1 - T_1$). The small kinetic barrier for intersystem crossing is a consequence of the proximity of both states on the energy surface that connects them. S_1 and T_1 are isoelectronic states that differ in spin multiplicity and, slightly, in energy.

$$k_d = k_f + k_{isc} + A\ exp\left(\frac{-E_{act}}{RT}\right) \tag{2.16}$$

In order to carry out a non-linear fitting that allows the determination of all the kinetic parameters of the processes of S_1, eq. 2.16 can be simplified to eq. 2.17.

$$k_d = B + A\,exp(\frac{-E_{act}}{RT}) \quad (2.17)$$

The parameter B is the sum of the rate constants of the non-activated photophysical process of S_1, fluorescence and intersystem crossing. As explained previously, the rate constant for internal conversion is ignored in this approach, as its value is very small in comparison to the values of rate constants of other photophysical processes and of the reaction. This last assumption is reasonable, as the energy gap between S_0 and S_1 for these benzene compounds is large enough to lead to unfavourable Franck-Condon overlap integral, and therefore to small values of k_{ic}. Rate constants for decay, k_d, were obtained from the singlet lifetimes τ_s, using eq. 1.4 as $k_d = 1 / \tau_s$. Experimental rate constants for fluorescence were obtained by using the measured quantum yields of fluorescence obtained on a fluorimeter and using eq. 1.21. The rate constants for intersystem crossing were obtained using the intercept of the curve at T = 0 K of the plots. This intercept is the sum of rate constants for fluorescence and intersystem crossing. k_{isc} is calculated by subtracting the experimental rate constant of fluorescence at 25 °C from B. Figures 2.28–2.30 show the Arrhenius plots and the parameters obtained for compounds **1o**, **m**, **p** in acetonitrile.

Figure 2.28. Non-linear fit to eq. 2.17 for 1o

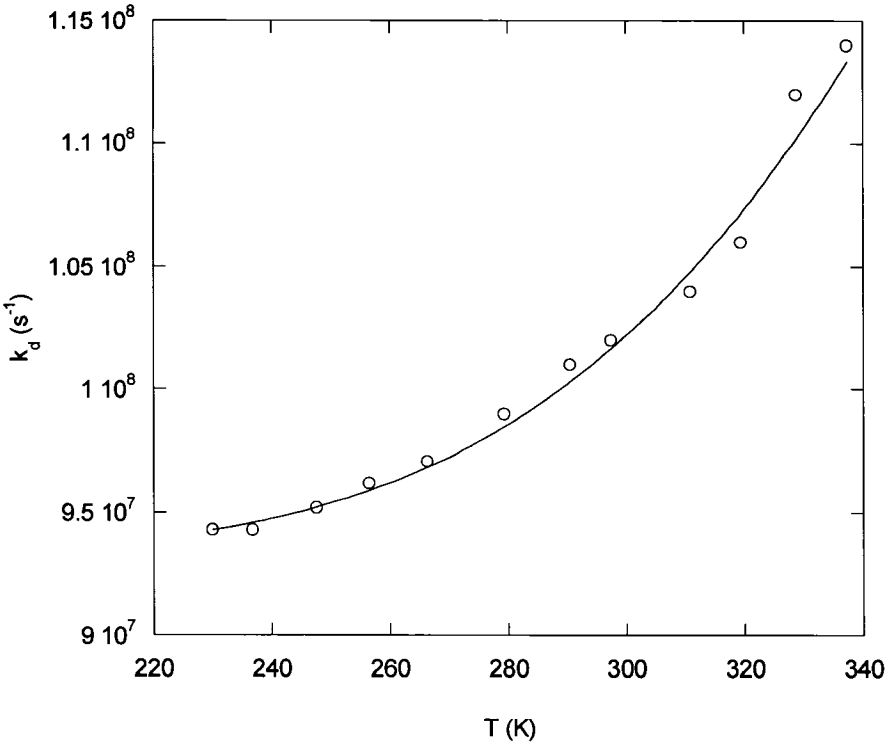

y = m1+m2*exp(-m3/(8.314e-3*...		
	Value	Error
m1	9.333e+07	8.5469e+05
m2	1.3551e+10	1.119e+10
m3	18.284	2.3637
Chisq	6.9434e+12	NA
R	0.99289	NA

Figure 2.29. Non-linear fit to eq. 2.17 for 1m

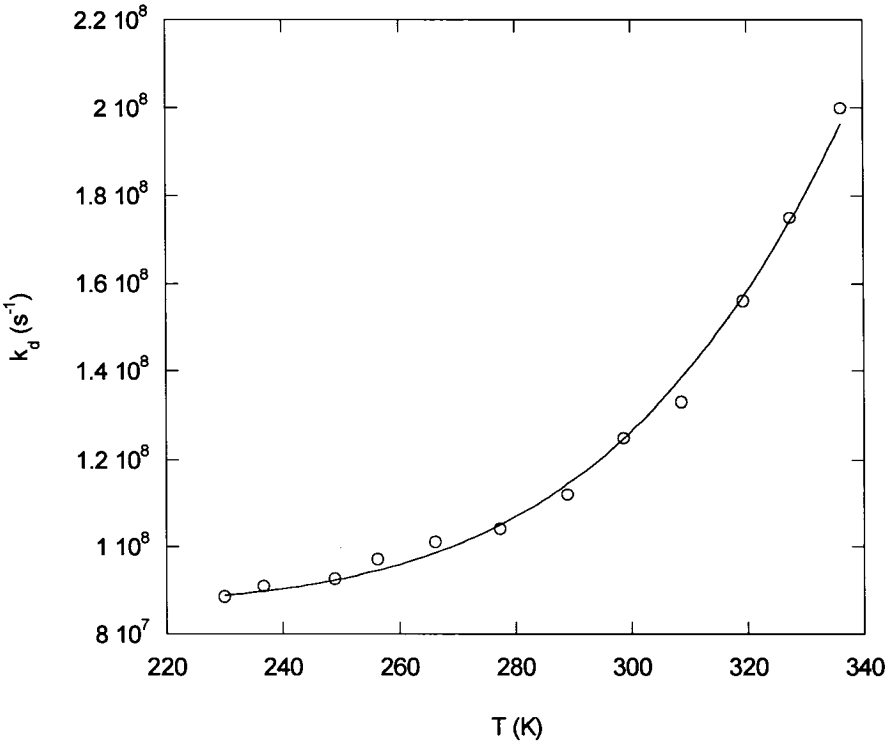

y = m1+m2*exp(-m3/(8.314e-3*...		
	Value	Error
m1	8.6489e+07	1.9603e+06
m2	4.8589e+11	2.5667e+11
m3	23.461	1.4854
Chisq	6.6068e+13	NA
R	0.99774	NA

Figure 2.30. Non-linear fit to eq. 2.17 for 1p

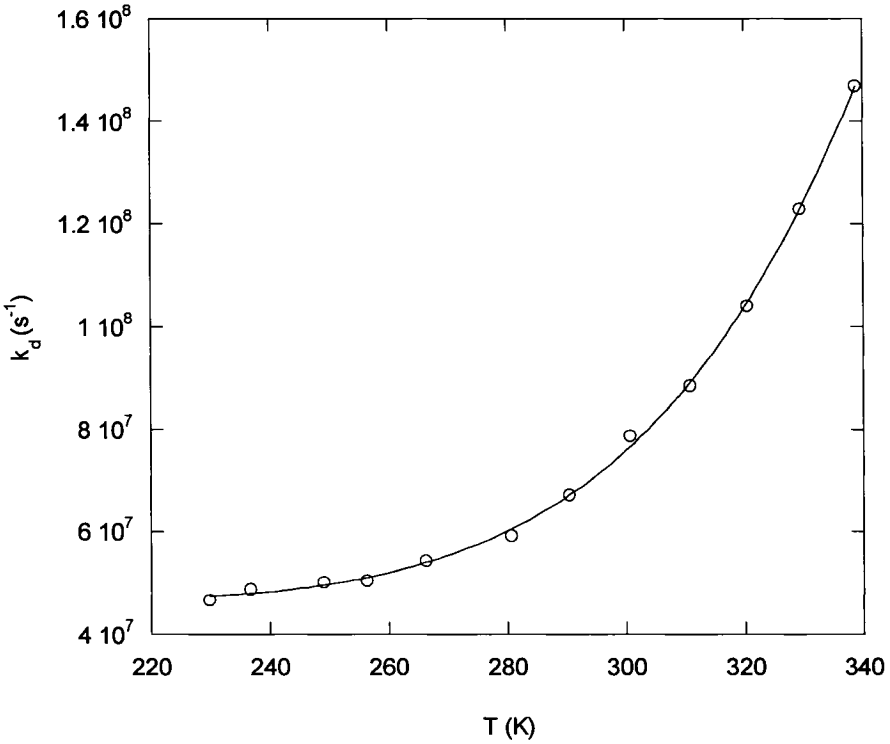

y = m1+m2*exp(-m3/(8.314e-3*...		
	Value	Error
m1	4.6371e+07	6.2959e+05
m2	1.3215e+12	3.0331e+11
m3	26.715	0.64674
Chisq	9.3615e+12	NA
R	0.99961	NA

2.5.1. The Arrhenius parameters, rate constants, and quantum yields for reactions and photophysical processes of 1,2,3

Table 2.5 contains a list of the kinetic parameters for the processes of S_1 for compounds **1** – **3** obtained by fitting the experimental values of k_d to the Arrhenius equation 2.17. The activation energies E_{act} and the pre-exponential factors A are listed along with values of $(k_f + k_{isc})$, k_f, k_{isc}, k_r, Φ_f, Φ_{isc}, and Φ_r calculated by using the non-linear fitting summarized in Section 2.5, or experimentally obtained at 25°C.

The quantum yields for all the processes of S_1 (Φ_i), eq. 2.18, were calculated using a similar equation to the one used to calculate the quantum yield for fluorescence Φ_f, eq. 1.21. The subscript i refers to a particular process of S_1, either a chemical reaction or photophysical deactivation of the singlet excited state.

$$\Phi_i = \phi_i \, k_i \, \tau_s \qquad (2.18)$$

ϕ_i is the efficiency of formation of the excited state that participates as the precursor of the process of interest. In direct excitation experiments, the efficiency of formation for the first singlet excited state of benzene compounds is unity. This means that every photon absorbed for a benzene compound molecule gives rise to a singlet excited state. k_i is the rate constant for the process being studied, chemical or photophysical, and τ_s is the lifetime of the state undergoing the process of interest, in this case, the first excited singlet state. k_r was calculated at 25 °C by using the Arrhenius expression for the rate constant of a reaction, and substitution of the values of A (s^{-1}) and E_{act} (kJ/mol) obtained from the output of the non-linear fits to the Arrhenius equation, and T was 298 K in all the cases. The values of Φ_f were measured by comparing the intensity of emission at a

particular λ of a standard of known Φ_f, anisole, and the intensity of emission of the sample of interest at the same λ, eq. 1.16. The values for k_f were obtained from eq. 1.21.

Table 2.2 Rate constants and quantum yields for the processes of S_1 for 1, 2, 3o,m,p at 25 °C in AN and TFE

	Solvent	A/ $10^{11}s^{-1}$	E_{act}/ kJ/mol	k_f+k_{isc}/ 10^7s^{-1}	k_f/ 10^7s^{-1}	Φ_f	k_{isc}/ 10^7s^{-1}	Φ_{isc}	k_r/ 10^7s^{-1}	Φ_r
1o	**AN**	0.13 (±0.11)	18 (±0.2)	9.3 (±0.1)	2.2 (±0.3)	0.22	7.1 (±0.3)	0.70	0.85	0.08
	TFE	0.02 (±0.09)	11 (±1)	9.6 (±0.3)	1.9 (±0.2)	0.17	7.7 (±0.3)	0.65	2.2	0.19
1m	**AN**	4.9 (±2.5)	24 (±1)	8.6 (±0.2)	2.7 (±0.3)	0.22	5.9 (±0.3)	0.51	3.1	0.27
	TFE	4.8 (±1.6)	23 (±1)	9.0 (±0.1)	2.1 (±0.2)	0.15	6.9 (±0.2)	0.51	4.6	0.34
1p	**AN**	13 (±3)	27 (±1)	4.6 (±0.1)	1.5 (±0.2)	0.16	3.1 (±0.2)	0.42	2.8	0.38
	TFE	5.8 (±1.0)	23 (±1)	4.6 (±0.1)	1.8 (±0.2)	0.14	2.8 (±0.2)	0.22	8.0	0.63
2o	**AN**	2.6 (±0.9)	22 (±1)	9.6 (±0.2)	2.1 (±0.2)	0.16	7.5 (±0.2)	0.57	3.5	0.27
	TFE	1.0 (±0.2)	15 (±0.1)	10.6 (±0.8)	1.8 (±0.2)	0.06	8.8 (±0.8)	0.27	21.9	0.67

Table 2.1. Continuation

2m	**AN**	2.3 (±0.3)	22 (±1)	7.7 (±0.1)	1.6 (±0.2)	0.14	6.1 (±0.2)	0.54	3.7	0.32
	TFE	0.36 (±0.06)	13 (±1)	6.3 (±0.5)	1.8 (±0.2)		4.5 (±0.5)	0.21	15.6	0.71
2p	**AN**	20 (±9)	27 (±1)	4.4 (±0.2)	0.8 (±0.1)	0.10	3.6 (±0.2)	0.46	3.4	0.44
	TFE	2.5 (±0.5)	17 (±0.6)	3.5 (±0.6)	0.9 (±0.1)	0.036	2.6 (±0.6)	0.11	21.4	0.86
3o	**AN**	4.3 (±1.0)	19 (±1)	7.8 (±0.6)	2.0 (±0.2)	0.08	5.7 (±0.6)	0.22	17.8	0.70
3m	**AN**	10 (±4)	21 (±1)	10.4 (±0.7)	2.1 (±0.2)	0.08	8.4 (±0.7)	0.30	17.7	0.63
3p	**AN**	3.2 (±1.0)	21 (±1)	3.1 (±0.3)	0.7 (±0.1)	0.07	2.4 (±0.3)	0.23	7.2	0.70

The experimental error for the fluorescence rate constant k_f was considered to be 10% of its value, on the basis of having to compare two spectra (the sample and the standard) of matched absorbances at the excitation wavelength. The standard error for the estimated intersystem crossing rate constant was calculated using the square root of the variance ($e^2(k_{isc}) = e^2(k_{isc} + k_f) + e^2(k_f)$, by a propagation of random errors. For E_{act} and A, the mathematical errors from the fits are reported. It is important to point out that when the k_d varies significantly with the temperature, the mathematical errors decrease appreciably.

2.5.2. The calculated rate constant for fluorescence using the Strickler/Berg Equation, eq. 1.12

Calculated values of k_f^{calc}, Table 2.2, were obtained using eq.1.12, the Strickler/Berg equation, which is an important relationship between theory and experiment. The expression relates the rate constant of fluorescence to the absorbance and fluorescence spectra and the refractive index of the solvent, by means of the expectation value for the frequency across the entire emission ($<\nu^{-3}>$) of the fluorescence spectrum, and it relates the sum of the contribution of all the different vibronic states of the singlet excited state by the integrated absorbance spectrum. Finally, this equation considers how the solvent affects the velocity of a beam of light passing through a sample using the refractive index n, which depends on the electronic ($n = (\varepsilon \times \mu)^{1/2}$) and physical properties of the solvent ($n = c / v$). This is discussed further in Section 2.5.3. The Strickler/Berg equation gives k_f^{calc} in units of s^{-1} if the frequency values are expressed in wavenumber (cm^{-1}), and molar absorptivity ϵ in the usual units ($M^{-1} cm^{-1}$). This equation is derived on the basis of Einstein's coefficients and their relation to the oscillator strength model, and the important assumption that the excited singlet state and the ground state have similar geometries. This equation has been used successfully in the past for simple aromatic compounds like benzene, toluene and *ortho*-xylene[78,79] and by Pincock *et al.* for aryl-substituted methyl, and allyl[80] and adamantyl ethers.[81]

$$k_f^{calc} = 2.88 \times 10^{-9} n^2 < \nu^{-3} >^{-1} g_i / g_u \int \epsilon \, d \ln \nu \qquad (1.12)$$

The correction for n^2 is necessary to obtain k_f^o, the solvent-independent, natural fluorescence decay-rate constant. For our purposes, the experimental k_f (not k_f^o) is the value of interest. The measurement of the experimental fluorescence rate constant as a function of temperature is complicated by the fact that the experimental quantum yield for fluorescence depends on the refractive index, and the refractive index of the solvent is temperature dependent. The complication is that the intensity of light reaching the emission slit of the monochromator is dependent on the square of the refractive index (n^2) of the solvent. The limited number of experimental values for the temperature dependence of the refractive index of solvents indicates that it decreases with increasing temperature by about 1 to 5% over the range of temperatures used.[82] This relatively small effect, leading to an increase in fluorescence intensity, is compensated for by the fact that as the temperature increases, the volume of solvent increases and the concentration of solute drecreases, leading to a decrease in the measured intensity. In fact, these two small effects have been shown essentially to cancel for *n*-pentane as solvent[83] and, consequently, this correction was ignored.

Calculated values of k_f^{calc} according to eq.1.12 for substrates **1–3** in AN are given in Table 2.2. The UV and fluorescence spectra were obtained at 25 °C using AN as solvent. Positive agreement between the measured and calculated values was obtained. The experimental rate constants for fluorescence are listed again for comparative purposes.

Table 2.3. Calculated values of k_f (k_f^{calc}) using eq. 1.12 and experimental values of k_f both in AN

compound	$k_f (= \Phi_f/\tau_s)/ 10^{-7}s^{-1}$	$k_f^{calc}/ 10^{-7}s^{-1}$
1o	2.2 ± 0.3	2.1
1m	2.7 ± 0.3	2.1
1p	1.5 ± 0.2	0.8
2o	2.1 ± 0.2	1.4
2m	1.6 ± 0.2	1.4
2p	0.8 ± 0.1	0.6
3o	2.0 ± 0.2	1.5
3m	2.1 ± 0.2	1.2
3p	0.7 ± 0.1	0.5

2.5.3. The rate constant for fluorescence and the temperature

Although, the Stricker/Berg equation for radiative deactivation assumes a dependence on temperature, as the refractive index depends on temperature, it is generally assumed that k_f is temperature independent. The explanation for this is related to the influence of the solvent and the temperature on the values of the dipole moment and dielectric constant of the solvent, and its influence on the electromagnetic properties of the emitting substrate. There is a universal interaction due to the additive influence of the solvent as a dielectric medium, with magnetic properties, with both the solute and the electromagnetic vector of the radiation. This electromagnetic property of the solvent can be affected by the temperature in two specific ways: by chemical or physical interactions.

The chemical factors are related to interactions among the molecules of both the solvent and the solute, such as hydrogen bonds, and association with the substrates, such as complexes and exciplets. As the chemical nature of the solvent changes, the influence of the continuous medium of dipoles will affect the electronic properties of the excited states. As well, temperature can modify the populations of the vibronic levels. The vibronic cooling of the substrate molecules could slightly delay the radiative deactivation. Another point to consider is that the change in density due to temperature can affect the velocity of the emitted photon. When the temperature decreases, a denser medium is produced and the emitted photos will be slowed. From the study of Cundal and Pereira,[79] for both reactive compounds and compounds featuring a temperature-dependent intersystem crossing, the lifetime for fluorescence (τ_f), which is by definition the reciprocal of k_f, is always slightly shorter at lower temperatures. This last study concludes that, at least for aromatic compounds, the corrected τ_f (τ_f^o) and therefore the corrected k_f^o are temperature independent. However, in all the cases investigated in the study of Cundal and Pereira,[79] the experimental lifetime for fluorescence is affected slightly by temperature.

The influence of the temperature on the k_f and quantum yield for fluorescence Φ_f for the cyanotoluenes **1** and methylanisoles **4** was studied. The results, similar to those of Cundal and Pereira,[79] are listed in Table 2.4. The rate constants for fluorescence vary slightly with temperature. For the cyanotoluenes, the values of k_f are slightly greater at lower temperatures, as expected, although the variation is not outside experimental errors. For the anisoles **4**, the variation is more random. For the reactive isomers of the cyanotoluenes **1**, the values of Φ_f vary appreciably with temperature. This is the result of

an enhancement of the chemical reactivity of these isomers as the temperature increases. For the non-reactive isomers of the methylanisoles **4**, the quantum yield for fluorescence is not affected substantially by a change in temperature. This result is consistent with the fact that these compounds do not react.

Table 2.4. Values of k_d, Φ_f, and k_f from eq. 1.24 as a function of temperature for the cyanotoluenes 1o,m,p and the methylanisoles 4o,m,p in AN

	T (°C)	k_d/ $10^7 s^{-1}$	Φ_f	k_f/ $10^7 s^{-1}$		T (°C)	k_d/ $10^7 s^{-1}$	Φ_f	k_f/ $10^7 s^{-1}$
1o	-25.6	9.6	0.25	2.4	**4o**	-22.6	13.9	0.23	3.1
	17.3	10.1	0.23	2.3		5.3	14.8	0.22	3.3
	25.0	10.2	0.22	2.2		25.0	15.0	0.22	3.3
	55.6	11.2	0.19	2.1		63.5	15.8	0.21	3.3
1m	-24.1	9.3	0.34	3.1	**4m**	-22.6	12.2	0.27	3.3
	15.9	11.3	0.25	2.8		5.3	12.8	0.26	3.3
	25.0	12.2	0.22	2.7		25.0	13.1	0.26	3.4
	63.0	20.0	0.12	2.4		63.5	14.0	0.24	3.4
1p	-24.1	5.0	0.30	1.5	**4p**	-22.6	15.1	0.21	3.2
	17.3	6.7	0.19	1.3		5.3	15.6	0.21	3.3
	25.0	7.5	0.16	1.5		25.0	15.8	0.19	3.0
	56.2	12.3	0.09	1.2		63.5	16.2	0.18	2.9

2.5.4. The influence of the temperature on the processes of S_1 for the methylanisoles

The methylanisoles **4o,m,p** were irradiated at both 25 and 50 °C in AN and TFE for 8 hours each. No products of photolysis were observed. The irradiated solution remained colorless and the GC-FID's for both the non-irradiated solution and the irradiated solutions were essentially the same. No other peaks were observed, and the response of the instrument with respect to the volume of solution injected and mass balance was the same. With no observed photochemistry up to 50 °C in either AN or TFE, the methylanisoles **4o,m,p** serve as a useful basis of comparison for the other reactive compounds **1**, **2**, **3**. Figures 2.31–2.33 show a plot of the dependence of the deactivation rate constant for the methylanisoles on the temperature.

Figure 2.31. Dependence of the singlet lifetime of S_1 on the temperature for compound 4o in AN

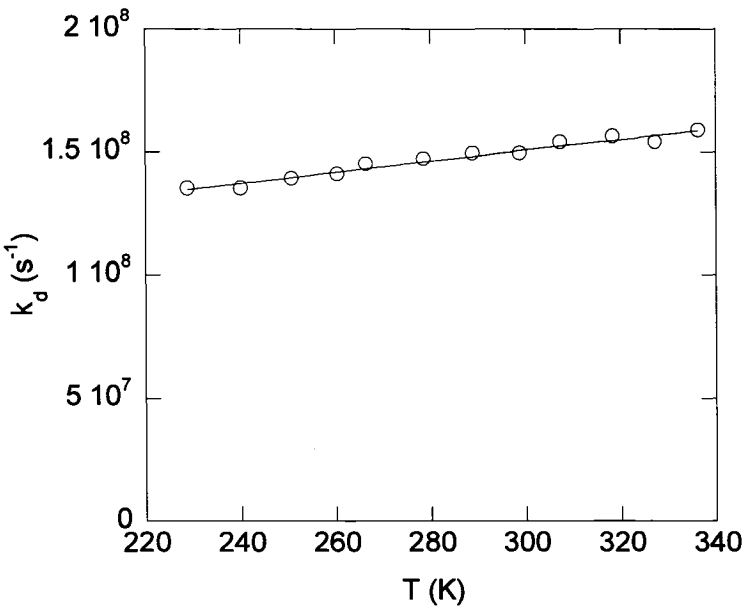

Figure 2.32. Dependence of the singlet lifetime of S_1 on the temperature for compound 4m in AN

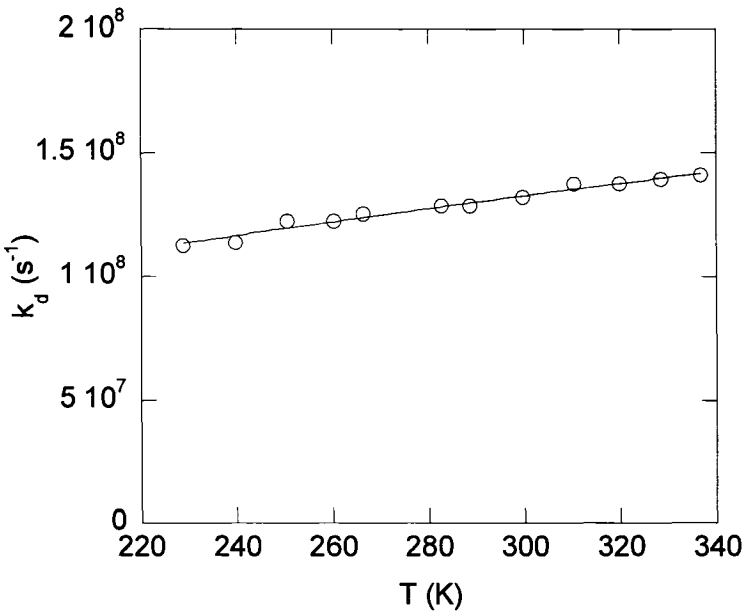

Figure 2.33. Dependence of the singlet lifetime of S_1 on the temperature for compound 4p in AN

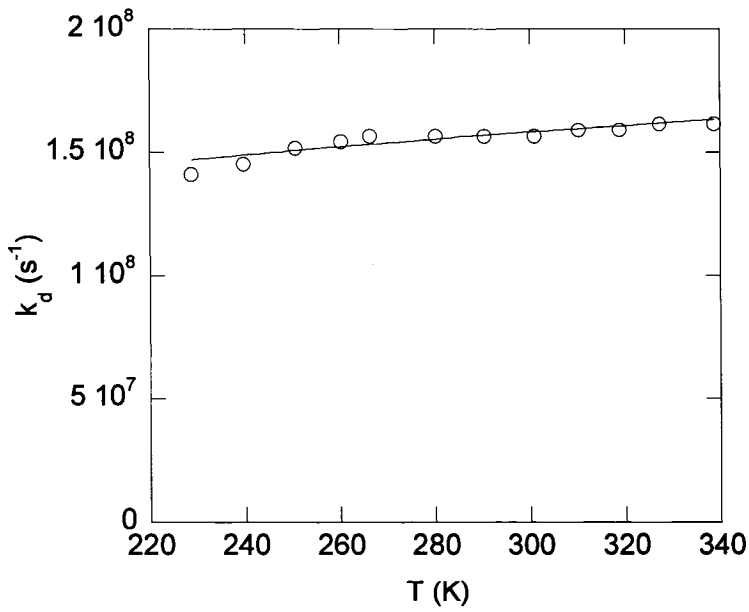

The plots are not entirely flat as there is a very small increase in k_d as the temperature decreases. A number of measurements in the same range of temperature were done in order to confirm this dependence and rule out the possibility of manipulation mistakes or instrumental problems. The results were identical, the values of τ_s were highly reproducible at each temperature. The photochemical stability of the methylanisole isomers **4,** along with the small temperature dependence, suggests that an activated photophysical process might be the cause of this behaviour. Activated intersystem crossing has been observed for other aromatic compounds, for instance, for naphthalene and, most recently in the detailed examples of Zacchariasse and co-workers, for arylamines.[77] In order to obtain the kinetic parameters associated with the processes of S_1 responsible for this dependence on temperature, fits of the values of τ_s to temperature were carried out by means of eq. 2.16. The objective of these fits was to obtain mathematical evidence to suggest which photophysical process was the temperature-dependent one. The values obtained are in Table 2.5.

Table 2.5. Fits to Eq. 2.6 of τ_s for 4 o,m,p: rate constants for the photophysical processes of S_1 and quantum yields at 25 °C in CH_3CN

compound	A_{isc}/ $10^8 s^{-1}$	E_{act}^{isc}/ kJ/mol	k_f+k_{isc}/ $10^7 s^{-1}$	k_f/ $10^7 s^{-1}$	Φ_f	k_{isc}/ $10^7 s^{-1}$	Φ_{isc}
4o	2±1	4±2	11±2	3.3±0.3	0.22	7±2	0.78
4m	2±1	4±2	8±2	3.4±0.3	0.26	5±3	0.74
4p	1±1	3±3	12±9	3.0±0.3	0.19	9±9	0.79

Due to the small change of k_d with T, fits of the data for compounds **4** to eq. 2.16 gave large errors for the activation parameters. Nevertheless, important information is obtained from the output. The A values are approximately three orders of magnitude lower (~3 x 10^{-8} s^{-1}) than for the other substrates, **1**, **2** and **3** (10^{10} to 10^{12} s^{-1}), and the E_{act} values are also very low (~ 4 kJ/mol). This is the range expected for an activated intersystem crossing process (k_{isc}).[84] For example, for naphthalene in hexane, A_{isc} is equal to 4 x 10^7 s^{-1}, and the E_{isc} is 2 kJ/mol. The small A_{isc} values are a consequence of the fact that the process is spin-forbidden, and the low E_{isc} values result from the fact that the process occurs either from the lowest vibrational level of S_1, or from a thermally populated vibrational level of S_1 to some unknown energy level in the triplet manifold. In either case, the activation energy will be small. Similar to the reactive isomers, the main process for decay of S_1 is intersystem crossing.

2.5.5. Reliability of the method

Before proceeding further, the reliability of the Arrhenius eq. 2.16 for determining the rate constants for the processes of S_1, as well as the activation parameters of the reaction for substituted benzene derivatives, must be assessed. It is necessary to prove that this equation can reproduce previously obtained experimental values for the processes of S_1, and also to demonstrate that the assumption that k_{isc} is temperature independent does not significantly affect the determination of k_r for reactive benzene compounds. The methylanisoles **4** most likely have an activated intersystem crossing processs, and so this latter issue is important. If by applying the Arrhenius equation to compounds previously studied, such as benzene, toluene and *o*-xylene, similar kinetic

parameter values to the experimental ones are obtained, and if it is possible to prove that, even if a reactive singlet excited state features an activated intersystem crossing, and that eq. 2.16 can reliably be used to analyze a compound that has two exponential terms, then the Arrhenius equation will be a powerful tool for estimating kinetic parameters.

An analysis of the literature values of τ_s in cyclohexane for benzene, toluene and *o*-xylene using eq. 2.16 was carried out.[79] For these compounds values of Φ_f and Φ_{isc} have been determined previously.[85, 86] Values at 25 °C of k_{isc} and k_f were calculated using eq. 2.16. The outcome for the fit of these reference compounds is listed in Table 2.5.

Table 2.6 Values of the kinetic parameters obtained for the reference compounds benzene, toluene and o-xylene in cyclohexane from fits to eq. 2.16

Compound	A/ $10^{11}s^{-1}$	E_{act}/ $kJmol^{-1}$	k_f+k_{is}/ 10^7s^{-1}	k_f/ 10^6s^{-1}	Φ_f	k_{isc}/ 10^7s^{-1}	Φ_{isc}	k_r/ 10^7s^{-1}	Φ_r
benzene	5.0 (±3.9)	23.8 (±2.3)	0.35 (±0.51)	2.2 (±0.2)	0.06	0.89 (±0.77)	0.25	3.2	0.69
toluene	4.3 (±2.4)	27.0 (±1.5)	1.6 (±0.1)	4.1 (±0.4)	0.14	1.5 (±0.4)	0.52	1.0	0.34
o-xylene	2.1 (±1.8)	25.4 (±2.6)	1.5 (±0.1)	5.0 (±0.5)	0.16	1.8 (±0.5)	0.58	0.70	0.26

The calculated values of the sum ($k_f + k_{isc}$) from the experimental quantum yields (1.1, 1.9, and 2.3 × 10^{-7} s^{-1} for benzene, toluene, and *ortho*-xylene, respectively) agree reasonably well with those from the Arrhenius plots (0.35 ± 0.51, 1.6 ± 0.1, and 1.5 ± 0.1 × 10^{-7} s^{-1}, respectively), especially considering the long extrapolation necessary for the latter. The k_r values can also be calculated at 25 °C using A and E_{act} and then summed into ($k_f + k_{isc}$) to give k_d ($1/\tau_s$). The calculated k_d values at 25 °C (3.6, 2.6, and 2.2 × 10^7 s^{-1} for benzene, toluene, and *ortho*-xylene, respectively) also agree remarkably well with those obtained from independent fluorescence lifetime measurements (3.6, 2.9, and 3.1 x 10^7 s^{-1}). This comparison of using either non-linear fits to the Arrhenius equation, or directly measured quantum yields for determining rate constants for the reactions of S_1, gives confidence that the Arrhenius plot method is reliable.

An important problematic issue is that eq. 2.14 assumes that k_{isc} is temperature-independent and ignores the fact that intersystem crossing, similar to k_{isc} for the anisoles, is likely a temperature-dependent process. The two processes, reaction and intersystem crossing, could be competitive at room temperature, because k_{isc} has a very low E_a (which leads to high values of k_{isc}), but also a low value of A (which leads to low values of k_{isc}). In contrast, the other process, k_r, has high values of both E_{act} and A. It has been shown by Zacchariasse and co-workers,[65] by doing measurements at a low enough temperature, that the latter process becomes negligibly slow, and reliable values of k_{isc} (T = 0 K) and A_{isc} can then be obtained. These values can then be used as input parameters to give reliable fits to eq. 2.16 at higher temperatures, where the two processes might be competitive. Since our laboratory does not have the equipment necessary to measure Φ_{isc} (and consequently k_{isc}), this property was investigated by using simulated data, calculated

by a new equation that includes an activated intersystem crossing process, eq. 2.19. Then, fits to the calculated data using eq. 2.16 (Arrhenius equation) were done.

$$k_d = 2x10^7 + \left[5x\ 10^7 + 2x10^8 \exp\left(\frac{5}{8.31xT}\right)\right] + 5x10^{11} \exp\left(\frac{E_{act}(reaction)}{8.31xT}\right) \qquad (2.19)$$

where E_{act} = 20 or 25 kJ/mol

Simulated data were calculated using eq. 2.19 over the same range of temperatures as for the experimental values, -30 °C – 65 °C. Fits to eq. 2.19 were first made assuming E_{act} was too high to allow the activated reaction process to compete with the other possible modes of decay of S_1, $E_{act} \rightarrow \infty$. Therefore, the second Arrhenius term does not contribute to k_d. Values used were: $k_f = 2 \times 10^7\ s^{-1}$, $k_{ic} = 0$, k_{isc} (T = 0) = $5 \times 10^7\ s^{-1}$, $A_{isc} = 2 \times 10^8\ s^{-1}$, and E_{isc} = 5 kJ/mol, typical of the temperature-dependent intersystem crossing values obtained for the methylanisoles. The plot of k_d *versus* T, shown in Figure 2.34, has a very shallow slope, similar to that of the plot for the k_d vs T of the methylanisoles **4** in Figures 2.31-2.33, with a slight increase in k_d over the temperature range of 250 to 350 K, as expected. Next, calculations of simulated data were made using eq. 2.19, including these typical intersystem crossing values plus values characteristic of an activated reaction, E_{act}. The aim of these fits was to verify that fits to eq. 2.16 (Arrhenius equation) of the simulated data give basically the same results. Two examples ($A = 5 \times 10^{11}\ s^{-1}$ and E_a = 20 or 25 kJ/mol) are shown in Figure 2.30. The fits are good and the values obtained are reasonably close to the input values (obtained : input value) for E_a = 20 kJ/mol: $k_f + k_{isc}$ ($8.5 \pm 0.1 : 7 \times 10^7\ s^{-1}$), A ($4.2 \pm 0.7 : 5.0 \times 10^{11}\ s^{-1}$),

E_a (19.2 ± 0.1 : 20 kJ/mol); and for 25 kcal/mol: $k_f + k_{isc}$ (9.0 ± 0.2 : 7 x 10^7 s^{-1}), A (3.7 ± 1.1 : 5.0 x 10^{11} s^{-1}), E_a (23.3 ± 0.9 : 25.0 kJ/mol). The largest deviation from the fits is for the intercept $k_f + k_{isc}$, perhaps because eq. 2.16 assumes that k_{isc} is a constant, and because of the large extrapolation required to obtain this parameter. Using similar fits to other simulated data calculated with different activation parameters, it was noted that the more correct eq. 2.19 (temperature-dependent k_{isc}) could be approximated reasonably by the simpler eq. 2.16 (temperature-independent k_{isc}) if A > 0.5 x 10^{11} s^{-1} and E_{act} < 25 kJ/mol. If both of these conditions are satisfied, then the larger values of k_r dominate the relatively insignificant changes in k_{isc} as a function of temperature. An examination of the data in Table 2.4 reveals that this is the case for the substrates **1**, **2** and **3** in both AN and TFE except for **1o**, the least reactive of all the substrates studied. In this case, the differences between k_{isc} and k_r are not large enough to obtain either reliably.

Figure 2.34. Simulated Arrhenius plots for a typical activated intersystem crossing process and two reactive isomers with different E_{act} values

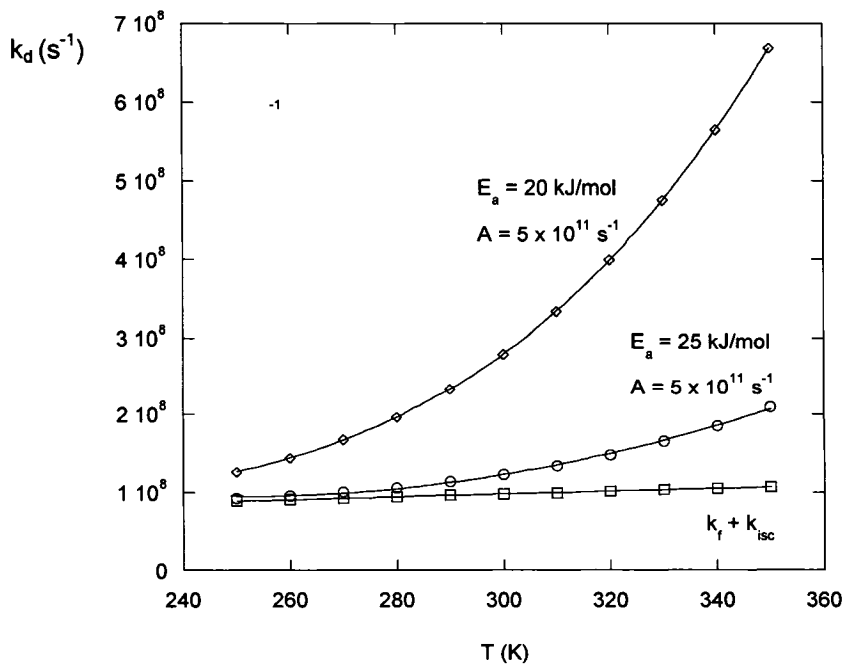

2.6. Discussion of results

The sum of all of the efficiencies of the process of S_1 is approximately 1.0 in all cases, as required by the mathematical approach used. In this way, the apparent incongruence with Ermonaloev's Rule is clarified and, therefore, related to the chemical reactivity of S_1. A more general form of Ermonaloev's Rule must consider all the processes of the excited states and be formulated as $\Sigma\ \Phi_i = 1$. The excellent fit of the experimental values of τ_s to eq. 2.14 guarantee that $k_d = k_f + k_{isc} + k_r$. However, any experimental error associated with the measurement of k_f will affect this sum. For example, if an incorrect measurement of Φ_f leads to an incorrect value of k_f, then the calculated value for k_{isc} will also be incorrect. This last fact reveals an interdependency of the kinetic rate constants of the processes of S_1 as they are obtained by a combination of an experimental technique and a mathematical fit. Only k_f and k_r are obtained independently; k_{isc} is obtained by the difference between $k_f + k_{isc}$ (from the intercept of the plots), and k_f from fluorescence quantum yields, eq. 1.21. Therefore, any error in k_f becomes incorporated into k_{isc}.

2.6.1. The Arrhenius equation as a tool to reveal details of the dynamics of the singlet excited states

Pincock *et al.* reported [8, 25, 27, 51, 52] that the quantum yields for product in the photochemical equilibrations of the **1**, **2**, and **3** isomers were surprisingly low. For example, the quantum yield for product formation for **1p** is 0.025.[8] In contrast, high values for Φ_r were obtained using eq. 216. This suggests that an activated internal return process through the prefulvene reactive intermediate, with a structure similar to **17,** offers

a mode for deactivation of S_1. This temperature-dependent route proceeds through the same intermediate as the one leading to products. In fact, this activated decay for internal conversion explains the failure of most substituted benzene derivatives such as toluene, tetralin, *o*-xylene, etc., to satisfy Ermonaloev's Rule. For polycyclic aromatics, the rule works very well, presumably because the geometric distortion required to form the RI **5** is no longer efficient, likely for both steric reasons and because the excitation energy is too low for the excited molecules to surmount the kinetic barrier that separates the energy surfaces of S_1 and the intermediate. Ermonaloev's Rule is obeyed nearly for some benzene compounds: ($\Phi_f + \Phi_{isc}$) for naphthalene (0.21 + 0.80 = 1.01) and anthracene (0.30 + 0.71 = 1.01), anisole (0.24 + 0.64 = 0.88), fluorobenzene (0.11 + 0.80 = 0.91), acetophenone (0.0+ 1.0 = 1.0), and aniline (0.17 + 0.75 = 0.91).[50] However, the sum of Φ_f and Φ_{isc} for toluene (0.14 + 0.5 = 0.64) , benzene (0.06 + 0.25 = 0.31), and *o*-xylene (0.16 + 0.58 = 0.74) indicates that these compounds do not obey Ermonaloev's Rule. As explained in Chapter 1, photolysis of benzene produces benzvalene and fulvene.[10, 11] *o*-xylene photoisomerizes when irradiated yielding principally *m*-xylene.[13,14,15] Logically, the chemical reactions that promote the formation of photolysis products have an activation energy.

Return to S_0 by an activated internal conversion process for compounds **1–3** seems to be a dominant mode for deactivation of S_1, along with intersystem crossing. This process explains why the experimental quantum yields of product formation, or relative reaction efficiencies, do not correlate with k_r. This can be illustrated by using the example of the cyanotoluenes **1**. The relative efficiencies of the phototransposition reaction in AN are **1o** : **1m** : **1p** = 1 : 4 : 32;[8] these values correctly explain the

photostationary state obtained after complete equilibration (**1o** : **1m** : **1p** = 67% : 26% : 7%).[8] Therefore, the most reactive isomer **1p** has the lowest final yield, as expected. The quantum yields of product formation, Φ_{prod}, also follow this trend (**1m** : **1p** = 0.003 : 0.025).[8] However, the k_r values listed in Table 2.1 do not follow the same order. The ratio of rate constants for reaction is as follows: **1o** : **1m** : **1p** = 0.85 : 3.1 : 2.8. Considering the rate constant for the formation of the prefulvene intermediate, the singlet excited state of the *m*-cyanotoluene is the most reactive of the three. An explanation for this order can be made by examining the prefulvene intermediates **70**, **71**, and **72** in Scheme 2.3. Intermediate **71** derived from the meta isomer should be the most stable because the methyl group is on the terminal position of the allylic moiety in the bicyclic structure, and will provide significant stabilization. Therefore, perhaps **71** is formed more efficiently (larger k_r) from **1m** but rearranges less efficiently (lower Φ_{prod} for formation of **1p**). Another explanation to justify the low Φ_{prod} in comparison with the para isomer can be found by analyzing the equilibration process of the RI from the meta-isomer. The prefulvene intermediate derived from **1m** has two possible prefulvene isomers **71** in which the breakage of the meta-bond can yield the meta-isomer again, Scheme 2.8. These processes will be invisible, as the product and the reactant are identical. In contrast, **72** may form less efficiently from **1p** but rearranges to **71** more efficiently because of the greater stability of this intermediate. Also, the compound **1p** does not form a prefulvene intermediate that can rearrange to one that can deactivate back to the para-isomer. Finally, **70** is the least stable of the three possible RI's, as the intermediate does not have electronic stabilization by the methyl group, and has the sterically unfavourable presence of the methyl group at the bridgehead position.

Scheme 2.8. Formation of two identical prefulvenes for the formation of 1m

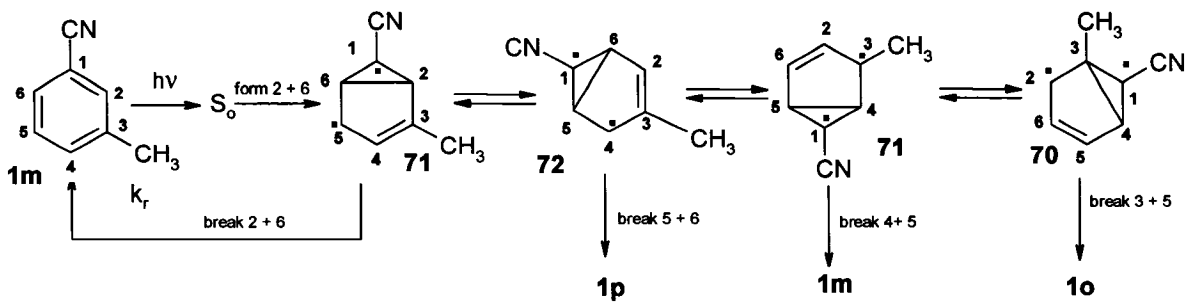

The boronate esters **2** feature almost the same reactivity for formation of the prefulvene biradical ($k_r \approx 10^7 s^{-1}$). They are more reactive than the cyanotoluenes, as the stationary state for the photolysis is reached more rapidly than for the cyanotoluenes (800 minutes versus 2000 minutes), and the percentage of conversion is reasonably high in all cases. For example, for the para-isomer **2p**, after 700 minutes of photolysis less than 10% of this compound remained.[51]

For the photolysis of trifluoromethyltoluenes **3** in AN, the situation is different. The percentage of isomer at the photostationary state for these compounds was **3o** : **3m** : **3p** = 7 : 32 : 61; for this set of isomers, the most reactive compound is the ortho-isomer **3o**.[52] The least reactive compound is the para isomer **3p**. The order of reactivity ($k_r / 10^7$ s^{-1}) for the trifluorotoluenes is **3o** : **3m** : **3p** = 17.8 : 17.7 : 7.2. This order indicates that the para-isomer is the least reactive, which agrees with the order of product disappearance observed on the photolysis plots of these compounds. However, the equal reactivity of **3o** and **3m** does not match their unequal values of isomer concentration at

equilibration. Again, efficiencies for product do not agree with the rate constants of reaction because of the intervention of a RI, followed by isomerization of the several prefulvene intermediates. The very high reactivity of **3o** ($17.8 \times 10^7 s^{-1}$) may now be partially a consequence of a steric acceleration, considering that a CF_3 group is certainly larger than a cyano group, and is also estimated to be considerably larger than a methyl group due to the lone electron pairs of the fluorine atoms. Previous studies of alkylbenzenes and methylbiphenyls[87] suggest that one of the driving forces for these photochemical reactions is the relief of the ortho interaction. This could be the explanation for the reversed order of reactivity of the trifluoromethyltoluenes **3** in comparison to compounds **1** and **2**. In contrast, the ortho-boronate ester **2o** is not particularly reactive in relation to the meta- and para- isomers, despite its large size. This observation is not surprising if we consider the fact that the boron substituent does not create a significant steric interaction, as the boron atom is sp^2 hybridized. A theoretical study (B3LYP 6-31G(d), Gaussian 98) indicated that the bond angle at the boron atom for the ortho methyl compound **2o** was still very close to the expected angle, B-C1-C2 = 124.5°, for sp^2 hybridized atoms.[51]

2.6.2. Solvent effects on the lifetimes and chemical reactivity of S_1 for 1, 2, 3o,m,p

The comparison between the two solvents, AN and TFE, offers important information on the structure of the transition state (TS) and the prefulvene intermediate. For both sets of isomers **1** and **2**, the rate constants of fluorescence and intersystem crossing are similar for any given compound in both solvents, as expected. However, the rate constants of reaction k_r are significantly higher in TFE than AN for any given

compound. The influence of the solvent on the deactivation rate constant k_d, and therefore k_r, for the isomers **2** is notable. An examination of the Arrhenius plots for the **2p** isomer in both solvents offers a convenient example of the effect of the solvent on the k_r, Figure 2.35. This rate difference (3.4×10^7 s^{-1} (AN) and 21.4×10^7 s^{-1} (TFE)) indicates that the prefulvene intermediates for the boronate ester isomers **2** presumably have some dipolar character. As the polarity of the solvent increases, the rate of formation of these intermediates increases as well. Although the two solvents have similar dielectric constants ($\varepsilon_{AN} = 1.344$ and $\varepsilon_{TFE} = 1.300$),[50] the more acidic TFE will stabilize the charged species to a greater extent, as indicated by their solvent ionizing power $Y_{OTS} = 1.77$ (TFE) and -3.21 (AN).[88] Therefore, the E_{act} values are lower for any given compound in TFE relative to AN presumably because a better solvation of the transition states for TFE decreases the kinetic barrier of this process. The A values are also lower, leading to more negative $\Delta S^{\neq}$ values, Table 2.7. The values of $\Delta S^{\neq}$ were calculated using the thermodynamic treatment of the transition state theory, eq. 2.20. The increased organization in the TS when TFE is the solvent, probably reflects the increased solvation of the TS in TFE relative to AN. This solvation process leads to an increase of the stability of the TS, and therefore of the rate constant for reaction.

$$\Delta S^{\neq} = R\,[\,\ln A - \ln\left(\frac{ekT}{h}\right)\,] \qquad (2.20)$$

Figure 2.35 Arrhenius plots of k_d versus T for 2p (AN) and 2p (TFE)

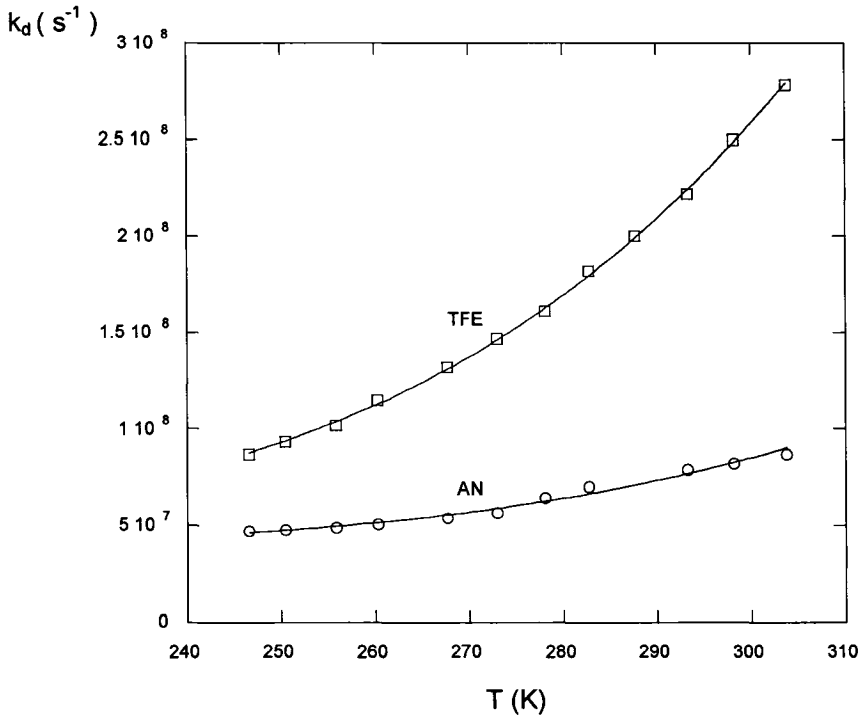

Table 2.7. Activation entropy values calculated using the thermodynamic treatment of the Transition State Theory

Compound	Solvent	$\Delta S^{\neq}$/ J/mol
1o	AN	-51
	TFE	-66
1m	AN	-21
	TFE	-21
1p	AN	-13
	TFE	-20
2o	AN	-26
	TFE	-34
2m	AN	-27
	TFE	-43
2p	AN	-9
	TFE	-26
3o	AN	-22
3p	AN	-15
3p	AN	-25

The very high reactivity of the boronate esters **2** in TFE was first observed because of the shorter times of irradiation required to reach complete equilibration in the phototransposition reaction relative to other substrates.[51] This high reactivity is now

confirmed by the higher values of k_r, the ratio of reactivity in TFE : AN = 6.2 (**2o**), 4.2 (**2m**) and 6.3 (**2p**), respectively. Initially, it was thought that this effect might be a consequence of a Lewis acid-base interaction between the trivalent boron atom (Lewis acid) and TFE oxygen (Lewis base), converting the substituent from neutral to negatively charged at the boron atom.[51] However, neither UV nor fluorescence spectra provided evidence to support a strong interaction of that type, either in the ground state or in S_1, for any of these isomers. For example, the values for ϵ ($S_0 \rightarrow S_1$) of **2o** were 769 $M^{-1}cm^{-1}$ in AN and 820 $M^{-1}cm^{-1}$ in TFE.[51] In addition, k_f's of **2o** have similar values in TFE and AN : 1.9 x 10^7 s^{-1} in AN and 2.1 x 10^7 s^{-1} in CH_3CN (Table 2.1). Another surprising observation for the boronate esters in TFE was that phototranspositions occur faster than photoadditions. It was reported that some peaks on the GC-MS could be due to the formation of photoadducts, but these isomers could not be separated from the reaction mixture.[51] Phototranspositions in TFE have been observed previously for one set of substrates: the ortho, meta and para isomers of the trifluoromethylbenzonitriles.[53] Therefore, the RI's in Scheme 2.4, for these two types of substituted benzene derivatives presumably do not undergo fast protonation to form cations. No satisfactory explanation for these observations is available at the moment.

2.7. Conclusions

Total rate constants of decay ($k_d = 1 / \tau_s$) as a function of temperature from -45 /-30 °C to +65 °C for compounds **1** and **2** in AN and TFE, and for **3** and **4** in AN were determined by fluorescence lifetime measurements. The data were fitted to a mathematical model that assumes that the rate constants of fluorescence, k_f, and intersystem crossing, k_{isc}, are temperature-independent, that $k_{ic} \approx 0$ due to small Frank-

Condon factor that results from the poor overlap between the vibronic wavefunctions of both S_1 and S_o states (Energy Gap Law), and that the rate constant of reaction, k_r, is temperature-dependent, according to the Arrhenius expression. For compounds **1–3**, values of k_f and k_{isc} were found to be basically independent of the solvent for any given compound, but, in contrast, k_r was consistently greater in TFE than in AN. For the methylanisoles **4**, the temperature effect was small but evident; indicating that no reaction occurs over the experimental range of temperatures studied, but suggesting that an activated intersystem crossing was the dominant temperature-dependent process. The k_r, A and E_{act} values obtained for compounds **1-3** can be rationalized in terms of their known photochemistry. The critical reactive intermediate in all cases is a bicycle[3.1.0]hexenyl biradical/zwitterion that is formed by an activated process from S_1. Due to the greater Φ_r in comparison to Φ_{prod}, the reactive intermediate must return to the starting material, and therefore an activated internal conversion is a major pathway for deactivation of S_1.

The method using the temperature dependence of fluorescence lifetimes provides information and mechanistic insight into the reactivity of S_1 that is unavailable from measurements of quantum yields of reaction, at a single temperature. As indicated by simulated data, measurements made over a limited range can only be used with confidence if, over that same temperature range, the rate of reaction is the dominant process. If quantum yields of reaction are also available, then the partitioning of a RI between product formation and return to starting material (activated internal conversion) can be determined. Moreover, any complications in interpreting quantum yields of reaction that might arise from parallel reactivity of S_1 and T_1 is avoided, as the measured lifetimes only considered the reactivity S_1.

The same type of photochemical isomerization has been observed for benzene compounds featuring different types of substituents. For example, the *o*-trifluoromethyltoluenes and *o*-xylene are very reactive, and, indeed, both compounds feature similar Arrhenius parameters. On the other hand, the para isomers of **1** and **2** are the most reactive ones for these series, in contrast to the trifluoromethyltoluenes. Surprisingly, while the cyanotoluenes isomers **1** are photochemically reactive, the *o*-, *m*- and *p*-dicyanobenzenes and the *o*-, *m*- and *p*-cyanoanisoles are not photoreactive in either AN or TFE. Therefore, it is important to recognize that little is known about how the substituents can affect the efficiency of these processes.

However, as shown in the qualitative reaction coordinate diagram, Figure 2.36, for **1p**, several barriers on the reaction co-ordinate diagram need to be considered: first, the one from S_1 to the intermediate **70** and, second, the ones that allow conversions between **70**, **71** and **72**. Which of these barriers is the most important can, at least partially, be assessed by examining the barrier separating S_1 and **70**. As stated before, small quantum yields of products, Φ_{prod}, are reported, and, in contrast, the quantum yields of reaction, Φ_r, obtained in this investigation are appreciably greater than the reported Φ_{prod}.[8, 25, 27, 51, 54] This could indicate that the heights of the kinetic barriers for the interconversion of the prefulvenes intermediates are greater than that for the formation of the prefulvene intermediate **70** from S_1.

The barriers on the energy surface, Figure 2.36, will not be determined easily experimentally, but perhaps can be modelled by high-level computational methods.

Figure 2.36. Kinetic barriers for the photochemical isomerization of 1p

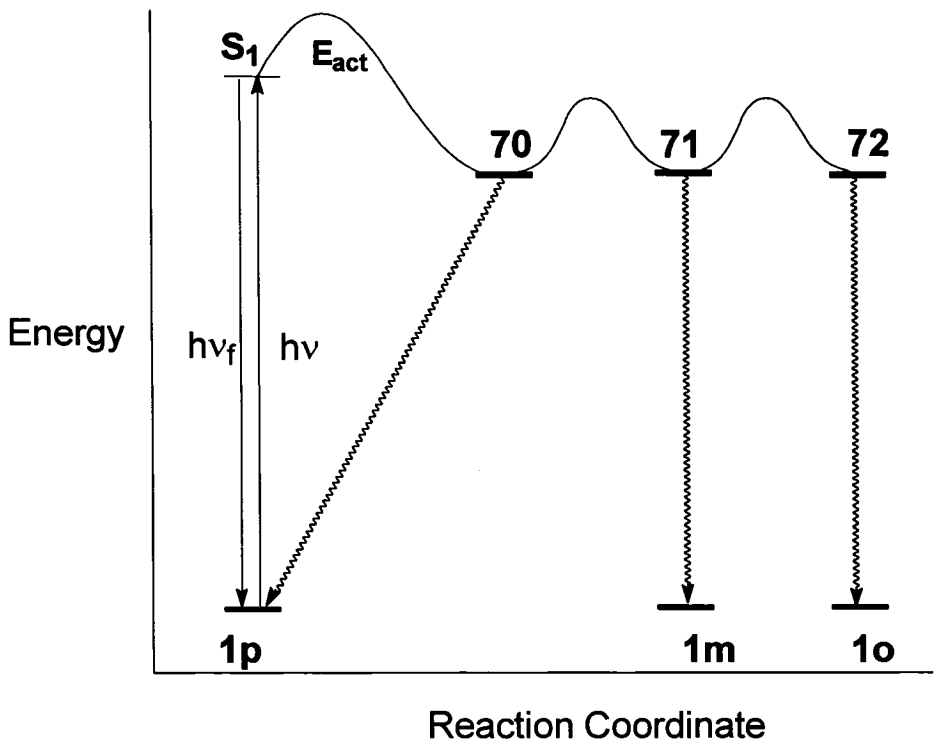

Chapter 3

Steric Effects in the Phototransposition Reaction of Dialkylbenzenes

3.1. Introduction

As shown in Chapter 2, the result of the phototransposition reactions of substituted benzene compounds depends on both the solvent and the substituent. For example, the compounds **1o,m,p** have different reactivities; **1o** is quite unreactive, whereas **1m** and **1p** are considerably more reactive. In contrast, for the trifluorotoluenes **3o,m,p**, the most reactive isomer is the ortho isomer. The calculated k_r's agree very well with the extent of conversion. The conclusion from these examples is that, occasionally, steric acceleration can result from the ortho interaction between the methyl group and a bulky group such as the trifluoromethyl substituent. The kinetic study of these series of compounds by the Arrhenius plot method to estimate kinetic parameters reveals details of the mechanism that extend the understanding of the dynamics of this type of photorearrangement. Another key point is the dependence of the product distribution on the solvent. For example, the photolysis of **1o,m,p** isomers in TFE yield only photoadducts, whereas for the compounds **2o,m,p** the main process continues to be the photoisomerization. Although the Arrhenius plots support the conversion results very well, they do not reveal the causes of these preferences. Designing experiments to

understand the causes is not easy. Perhaps high level *ab initio* calculations would provide a useful approach for understanding the complex potential energy surface connecting S_1 with the reactive intermediates.

Pincock *et al.* have investigated extensively the photochemistry of cyano-susbtituted benzene compounds.[8, 27, 89] In order to increase the understanding of the effect of the cyano substituent on the photochemistry of cyanobenzene derivatives, the compounds **5 - 10** were investigated, along with indan **115**, tetralin **116**, and *o*-xylene **18** as model compounds. Based on the previous results for **1o,m,p** and for the isomers of dimethylbenzonitrile (1,2-dimethylbenzonitrile **5**, 3,4-dimethylbenzonitrile **6**, 2,3-dimethylbenzonitrile **111**, 3,5-dimethylbenzonitrile **112**, 2,6-dimethylbenzonitrile **113**, and 3,5-dimethylbenzonitrile **114**), it has been very well established that these photoreactions proceed by migration of the cyano substituted carbon atom.[8, 27, 89] The aim of this chapter is to investigate how the substitution pattern affects the kinetics of these processes. For example, the neighbouring ring in compounds **7-10** may prevent the necessary distortion of S_1 through the required meta-bonding process that successfully connects to the energy surface that contains the prefulvene intermediate. If the kinetic barrier separating S_1 and the prefulvene intermediate for **7-10** is too high to allow the formation of the RI due to the steric effect of the neighboring ring, then the comparison with indan and tetralin will reveal the role of the cyano group in inhibiting the meta-bonding. For the cyano-derivatives a methyl substituent in the ortho position, which occupies the bridgehead position in the prefulvene intermediate, significantly inhibited the rate of photorearrangement.[8, 89]

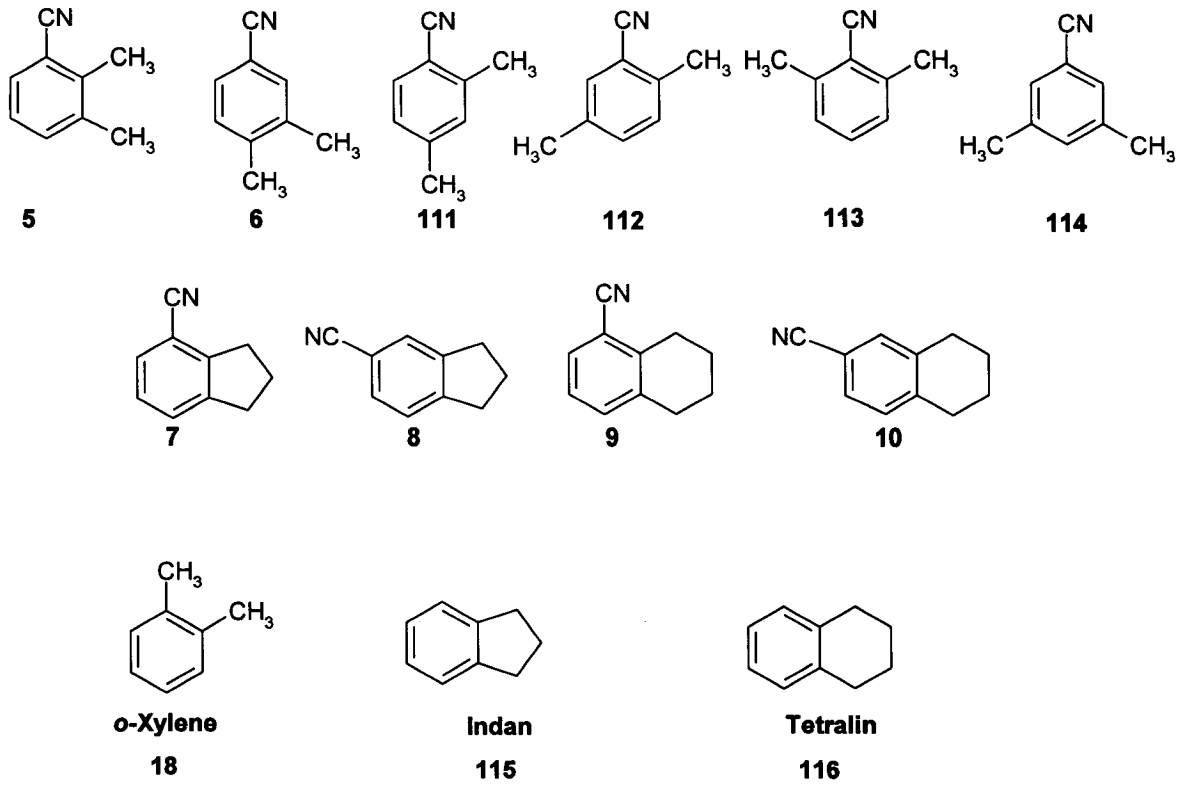

3.1.1. The phototransposition reaction in acetonitrile and the photoaddition of 2,2,2-trifluoroethanol to the isomers of dimethylbenzonitrile[89]

The photochemistry of dimethylbenzonitrile isomers **5**, **6** and **111-114** has been studied previously in our laboratory.[89] When the isomers **5**, **6** and **114** were irradiated in AN, at 254 nm and 25 °C, a photoisomerization process took place. The other isomers **111** - **113** were not reactive photochemically. The isomer **6** was found to be the most reactive; after 14 hours of photolysis almost 90% of the starting material had been converted into products. The main photolysis product was reported to be **5**, which showed the lowest chemical reactivity under the same conditions. For the photolysis of **6,** of the five possible isomers of the dimethylbenzonitriles, only **5** and **113** were formed.

This fact supports the mechanism of Molecular Acrobatics proposed by Pincock for the photorearrangement of substituted benzene compounds.[8, 25, 27, 51, 52, 53]

Scheme 3.1. Mechanism for the phototransposition of 5, 6 and 113 in AN

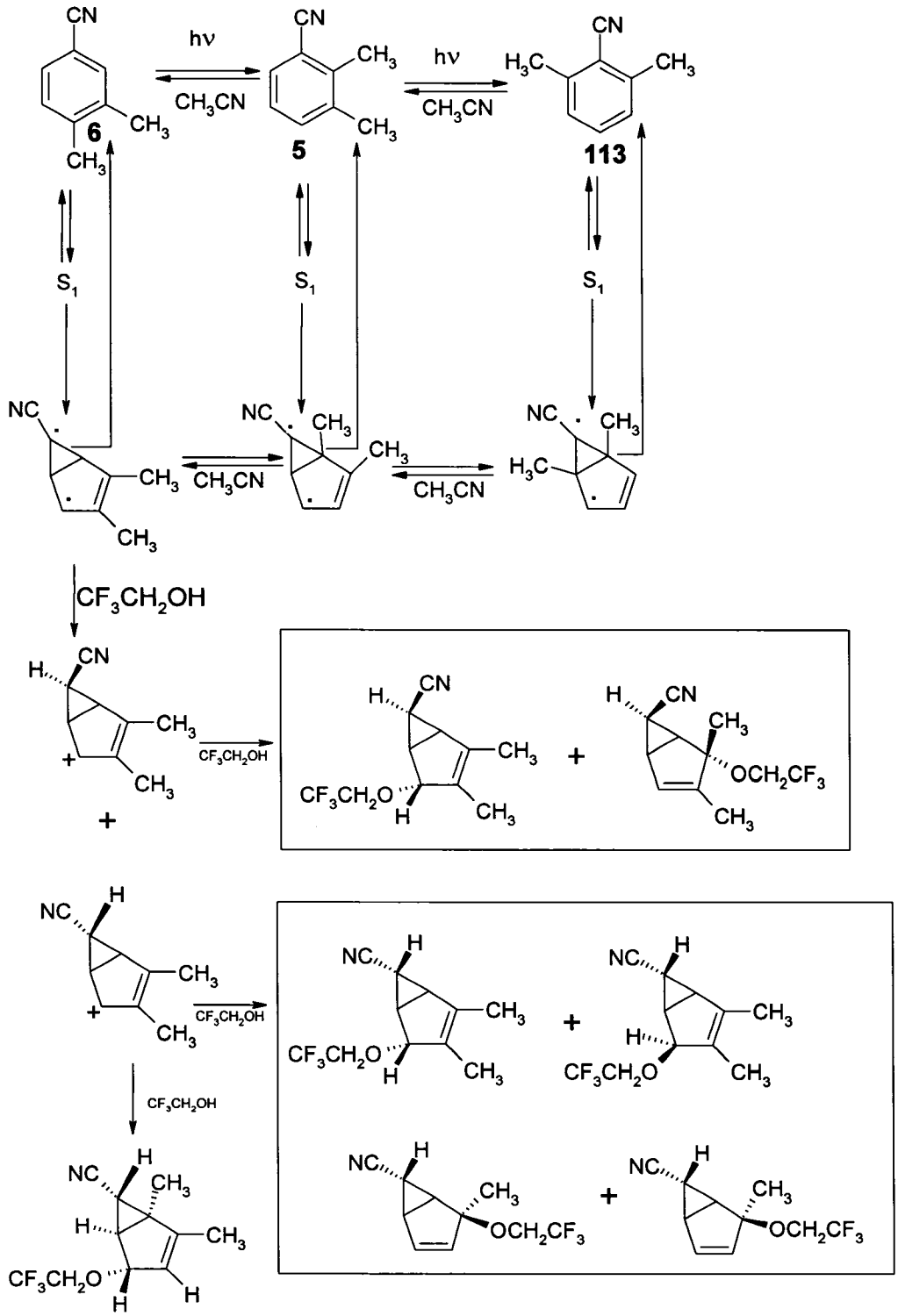

The process starts when electronic excitation of the reactive isomers leads to a prefulvene intermediate, Scheme 3.1. The phototransposition reaction in AN indicates that migration of the cyano-substituted carbon around the five-membered ring can only give two different positional isomers. Therefore only three isomers, including the starting material, will be present in the mixture when any of **6, 5** or **113** are irradiated. A similar observation was reported for the photolysis of the six isomers of dimethylpyridines,[90] where the six possible isomers were separated into two different triads. In contrast to the efficient reaction of **5**, less than 10 % of **6** was transformed into products after 14 hours, and **113** gave no observable phototransposition after 14 hours of photolysis. The same effect caused by the ortho-cyano substitution was observed in the photolysis of *o*-cyanotoluene **1o**,[8] in which substitution of a methyl group ortho to the cyano group leads to the lowest reactivity among the isomers investigated. This steric crowding will be maximised for **113**, resulting in a lack of photochemical reactivity at 25 °C.

In agreement with this mechanism, photolysis of **114** only gives **111** and **112**, demonstrating again that these isomers should be divided into two independent triads, eq. 3.1 and eq. 3.2. The dimethyl substituted isomers **111** and **112** were reported to be unreactive.

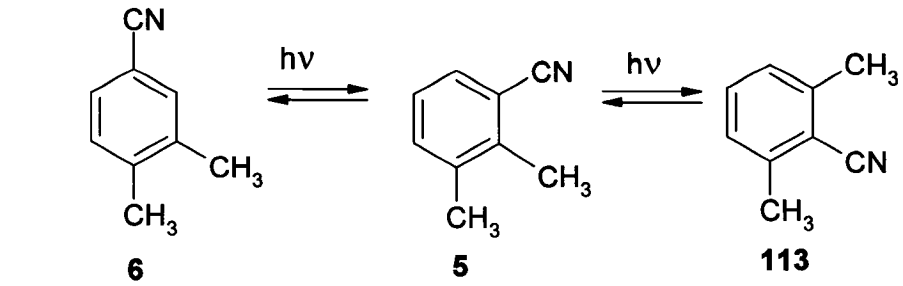

6 **5** **113**

(3.1)

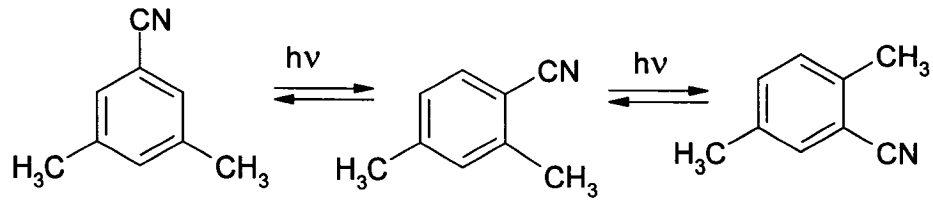

114 **111** **112**

(3.2)

On the basis of the results for the photochemistry in acetonitrile, **6** was examined in TFE with the idea that it would be the most reactive. Photolysis of **6** in TFE for 96 hours gives 9 photoaddition products: 6-cyano-x,y-dimethylbicyclo[3.1.0]hex-3-en-2-ol, Scheme 3.1. Under these conditions, no products from phototransposition were observed. The mixture was separated by flash chromatography and the products characterized by ^{1}H NMR and ^{13}C NMR. The regiochemistry of the isomers was assigned based on the observed coupling constants and splitting patterns.

3.1.2. Photochemistry of Benzocyclobutene[91]

Although formation of the prefulvene intermediate should be slowed by a fused ring, Turro *et al.* did observe a photoreaction for benzocyclobutene **117**.[91] Photolysis of **117** in pentane yielded 1,1-dihydropentalene **118** and 1,5-dihydropentalene **119**, eq. 3.3. The authors concluded that the mechanism for the formation of the isomeric

dihydropentalenes is consistent with the formation of a prefulvene biradical followed by the formation of a carbene intermediate.

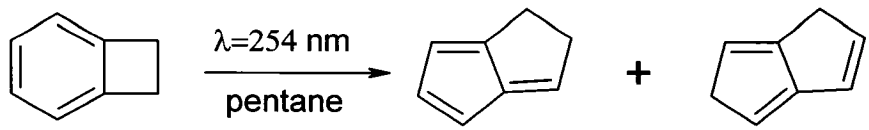

117 **118** **119** (3.3)

A solution of **117** in pentane (10^{-3} M) previously purged with Ar was irradiated in a typical Rayonet reactor equipped with sixteen 254 nm mercury lamps. Reaction products were analyzed by GC-MS and ^{1}H NMR. The products were separated by preparatory GC. The GC-MS spectrum indicated that isomers **118** and **119** were the main products. Hydrogenation of the mixture gave only a single product that was identified as bicycle[3.3.0]octane by comparison with a pure sample. The positions of the double bonds in **118** and **119** were established by ^{1}H-NMR. The chemical shifts for both isomers were compared with the values reported in the literature and were identical to those previously reported.[92, 93, 94, 95, 96]

α, α–Dideuteriobenzocyclobutene was used to provide information concerning the reaction mechanism of conversion of **117** to **118** and **119**, Scheme 3.3. The dideuterated compound was irradiated and the products analyzed by GC-MS, indicating that no deuterium was lost in the formation of the isomeric dihydropentalenes. ^{1}H NMR analysis indicated that the deuterium atoms did not migrate in the formation of the products. Based on these results the author proposed a mechanism similar to the photorearrangement mechanism for benzene and benzene derivatives.[11, 13, 14, 15] Two

prefulvene intermediates were suggested to be the primary photochemical intermediates. These intermediates can yield a secondary carbene intermediate by breaking one of the three-membered ring bonds. Successive 1,2-hydrogen shifts (but not deuterium) on this carbene yield the observed dihydropentalenes **118** and **119**.

Scheme 3.2. Mechanism for the formation of the 118 and 119 from benzocyclobutene

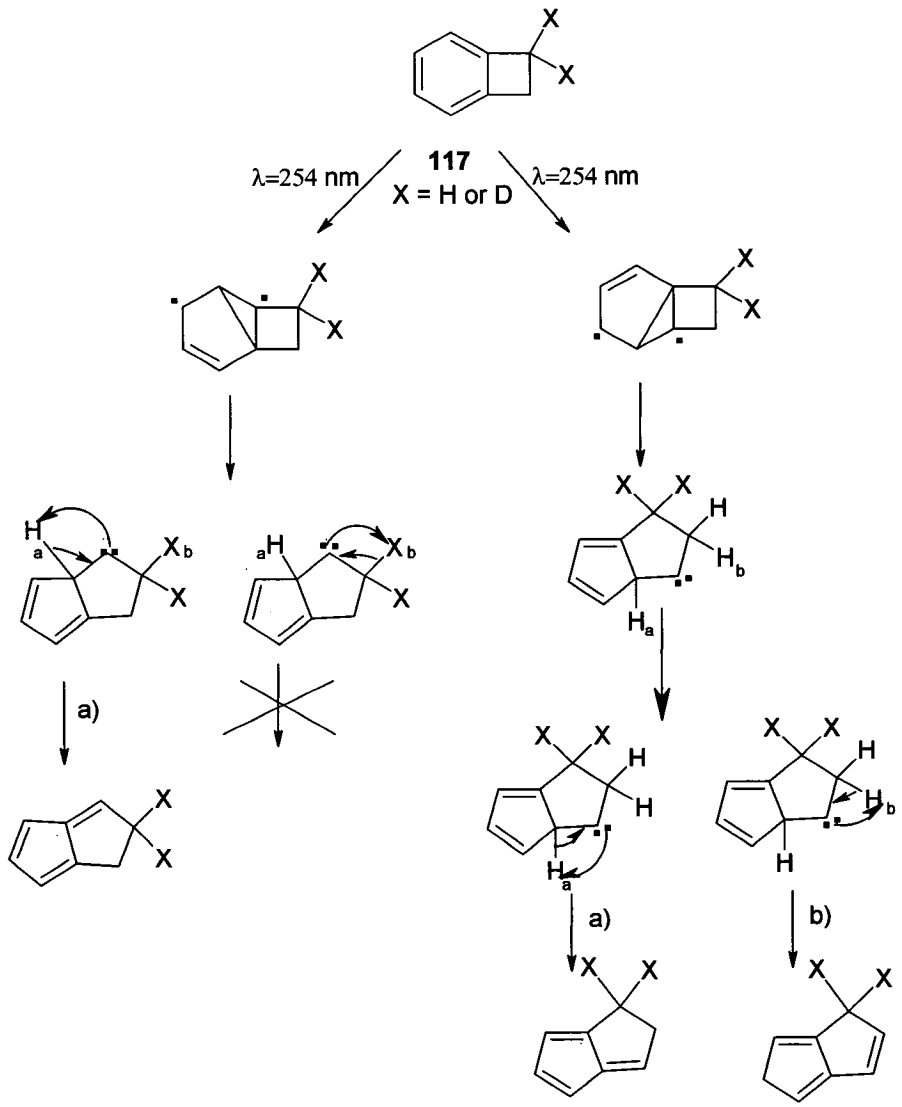

3.1.3. Project proposal

The literature that has been summarized above shows the importance of the cyano substituent in the photochemistry of benzene compounds. In these studies, it was observed that substrates with methyl groups ortho to the cyano substituted carbon were quite unreactive. For instance, the relative reactivity of **1p** : **1m** : **1o** = 32 : 4 : 1, and for **6** : **5** : **113** = 50 : 1 : 0.[8, 89] As explained before, these observations suggest that the conversion of S_1 to the prefulvene intermediate is slowed by the presence of a methyl group occupying a bridgehead position in the biradical. However, as explained in Section 2.7, Figure 2.6 for **1p**, several barriers on the reaction coordinate diagram need to be considered.

In order to probe this question, the photochemistry and photophysics of compounds **5-10**, **18**, **115** and **116** were examined. The aromatic hydrocarbons **18**, **115** and **116** were included to provide results for the cases without the cyano group, and because some previous literature values are available for comparison. The geometric changes required to form the bicyclic diradical intermediate (the important one in the phototransposition reactions) were expected to be inhibited for the compounds containing the neighbouring ring, **7-10**.

3.2. Results[97]

3.2.1. Synthesis of compounds 7-10

o-Xylene **18**, indan **116** and tetralin **117** are commercially available. Although dimethylbenzonitriles **5** and **6** have been prepared previously in Pincock's laboratory,[96] commercial samples were used with bulb-to-bulb distillation before use. Compounds **7-10** were synthesized from the commercially available amines by diazotization followed by reaction with cuprous cyanide, according to the Sandmeyer procedure, Scheme 3.3. Details are provided in Chapter 5. The yields obtained by using the Sandemyer reaction are rather low but adequate for the purposes of this investigation. The amine precursor for 6-cyanotetraline **10** was prepared by nitration of tetralin, followed by reduction of the mixture of 5- and 6-nitrotetralin with Sn/HCl and separation of the amines by column chromatography with Florasil as the stationary phase and 1% ethyl acetate in hexanes as eluent.

Scheme 3.3. Synthesis of 4-, 5-cyanoindan and 5-, 6-cyanotetralin

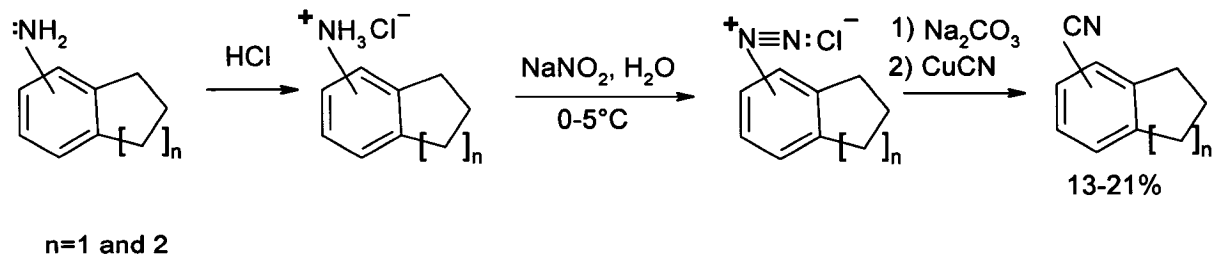

3.2.2. Photophysical properties of compounds 5-10, *o*-xylene 18, indan 115 and tetralin 117

All eight compounds being studied have the usual two bands with the former band being at a higher wavelength and a smaller molar absorptivity ϵ. This band corresponds to the $S_0 \rightarrow S_1$ transition, and the other to the $S_o \rightarrow S_2$ transition. The small value of ϵ for the $S_0 \rightarrow S_1$ band corresponds to the symmetry-forbidden character of this transition. A vibrational structure similar to the parent compound benzene can be observed in the UV spectra. All the compounds have emission spectra that show approximately the expected mirror symmetry. The values of λ_{max} and ϵ were obtained from the electronic spectra, and the energies of the 0,0 band, $E_{0,0}$, were obtained from the overlap of the fluorescence and excitation spectra. Experimental values of Φ_f were calculated using equation 1.16. Values of k_d ($= 1/\tau_s$) were obtained by a nanosecond single photon counting instrument, k_f from eq. 1.21 and k_f^{calc} from eq. 1.12. Photophysical data are given in Table 3.1. Compounds **5-10**, in comparison to **1o,m,p,** have a slight red shift in the zero-zero band, probably due to a larger hyperconjugation effect that arises from the second methyl, or methylene, substituent. For *o*-xylene **18**, the value of the extinction coefficient ϵ for the $S_0 \rightarrow S_1$ transition was very low, as expected on the basis of the values from the literature. The other photophysical data agreed with values previously reported.[78] For indan **115** and tetralin **116**, the values of the extinction coefficient ϵ for the $S_0 \rightarrow S_1$ transition were low in comparison to the cyano-substituted benzene compounds **5–10**, which are in accord with the typical low values of ϵ for alkyl-substituted aromatic compounds.[78]

For the compounds with the same substitution pattern, for example **5**, **7** and **9,** in which the alkyl substituent occupies position 2, the values for λ_{max} are very similar and

present higher ϵ coefficients than their isomers **6**, **8** and **10**. The same pattern can be identified for isomers **6**, **8** and **10**. The extinction coefficient for **7** seemed to be too high in comparison with the other compounds investigated. In order to confirm that this value was correct, a sample of **7** was purified by preparative chromatography-column twice, and then vacuum distilled. The sample was carefully analyzed by GC-FID and ^{1}H-NMR. Even though there was no evidence of impurities, the experimental value of ϵ for **7** seems anomalous in comparison with the rest of its homologues.

Table 3.1. Photophysical properties in AN of 5-10, indan 115, tetralin 116, and *o*-xylene 18, in AN at 25°C

Cmpd.	λ_{max} (nm)	ϵ_{max} ($M^{-1}cm^{-1}$)	$E_{0,0}$ (kJ mol^{-1})	Φ_f	τ_s (ns)	k_f (10^7 s^{-1})	$k_f^{calc.}$ (10^7 s^{-1})
5	280	1660	404	0.22	9.3	2.4	2.4
6	273	880	418	0.16	8.9	1.8	1.3
7	283	2600	404	0.23	8.8	2.6	3.8
8	275	880	417	0.21	9.9	2.1	2.1
9	282	1880	405	0.24	9.4	2.6	2.8
10	275	1320	414	0.18	10.9	1.7	1.8
o-xylene **18**	266	270	435	0.12	23.8	0.50	0.48
Indan **115**	265	580	432	0.24	17.5	1.4	1.5
Tetralin **116**	266	440	432	0.20	23.1	0.86	0.81

The agreement between the experimental values of k_f and the k_f^{calc} (eq. 1.12) is excellent and confirms that the singlet excited state of each of these compounds is a spectroscopic minimum with little change in geometry from the ground state. The conclusion is that eq. 1.12 offers a very good way to estimate k_f.[80, 81] The one exception in Table 2.1 is 4-cyanoindan **7**, with k_f^{cal} (3.8×10^7 s^{-1}) significantly larger than the experimental value (2.6×10^7 s^{-1}). However, the value of ϵ, which is directly related to the value of k_f^{calc} by eq. 1.12, also seems anomalously high.

$$k_f^{calc} = 2.88 \times 10^{-9} n^2 < v^{-3} >^{-1} g_i / g_u \int \epsilon \, d \ln v \qquad (1.12)$$

3.2.3. The photochemical reactivity of compounds 5-10

The photochemisty of 2,3-dimethylbenzonitrile **5**, 3,4-dimethylbenzonitile **6**, and isomers **111-113** has been studied previously.[89] Isomer **6** is the most reactive of this group of compounds. The phototransposition reactions of *ortho*-xylene have been described in the early literature[22] and have been repeated in AN by Pincock *et al.* more recently.[25] At very low conversion, the ratio of meta:para isomers was 11 : 1, indicating that both one-step and two-step phototranspositions are occurring in the primary photochemical event. This result is explained by rapid interconversion of the reactive intermediates as in Scheme 2.3 for the cyanotoluenes **1o,m,p**. Both tetralin and indan remain unchanged after irradiation in AN. However, any phototransposition reaction occurring would be undetectable.

Photolysis of compounds **5 - 10** was done in AN at both 25 and 50 °C. A Rayonet reactor was used with 16 low-pressure Hg lamps (254.6 nm) at both temperatures, using

100 mL of solutions containing 1 mg of solute / mL. For compounds **5** and **6** with well established photochemistry, the objective of the experiment was to verify that the photoisomerization is an activated process similar to the cyanotoluenes **1o,m,p**. The other compounds **5–10** were also irradiated under similar conditions to determine if they were photoreactive and if the process was an activated one. The photolysis of all the compounds was monitored by GC-MS.

Compounds **5** and **6** were photochemically reactive in AN, as expected, with an enhancement of the chemical reactivity when the temperature was increased, especially for **6**. Compounds **7, 8, 9** were photochemically stable for 8 hours at both temperatures. Compounds **7, 8, 9** were also irradiated in TFE to determine if a reactive intermediate had formed during the irradiation but had failed to isomerize due to geometry restrictions associated with the neighboring ring. However, these compounds were stable and no photoaddition products were observed, indicating that the prefulvene intermediate was not formed. Surprisingly, **10** was photochemically reactive, yielding **9**. The plots of the results are shown in Figures 3.1-3.5. The yields are reported in percent normalized to 100% with respect to the sum of all three isomers.

As described in Section 3.1.1, compound **5** is relatively unreactive to phototransposition but is slowly converted to a mixture of 2.8 % of **6** and 2.3% of **113** after 760 minutes of irradiation in AN. Photolysis at 50 °C is somewhat more efficient, giving 10.2 % of **6** and 1.3% of **113** after the same length of time, indicating that the phototransposition reaction is an activated process as expected. The cyclic analogues 4-cyanoindan **7** and 5-cyanotetralin **9** were photochemically stable.

Figure 3.1. Photolysis plot for the photoisomerization of 5 at 25 °C in An

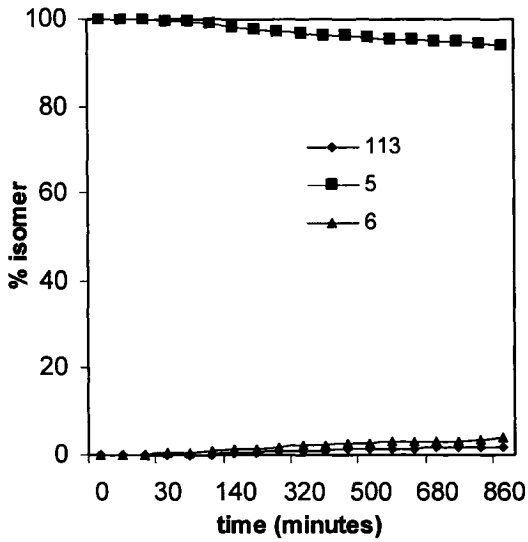

Figure 3.2. Photolysis plot for the photoisomerization of 5 at 50 °C in AN

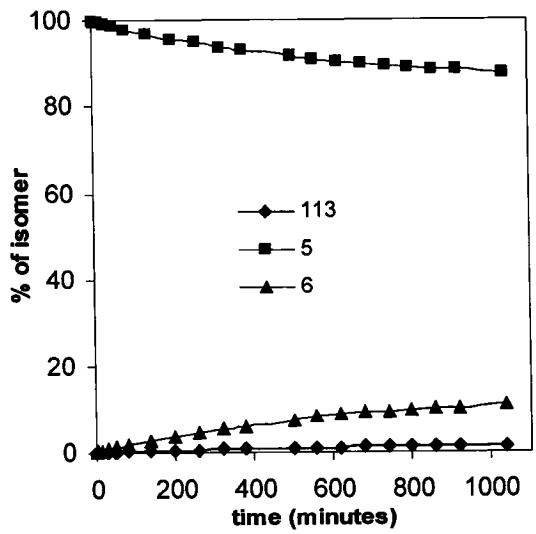

Figure 3.3. Photolysis plot for the photoisomerization of 6 at 25 °C in AN

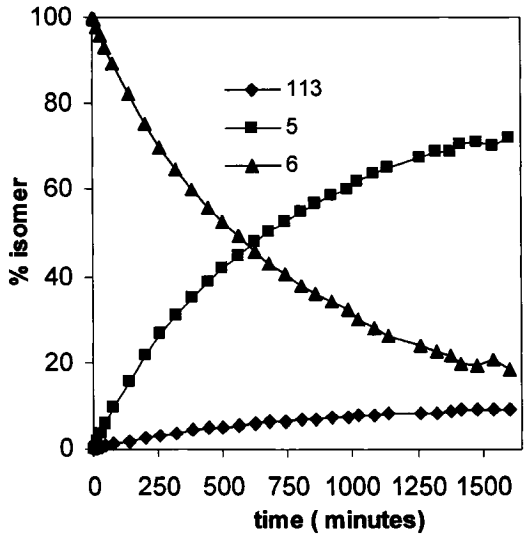

Figure 3.4. Photolysis plot for the photoisomerization of 6 at 50 °C in AN

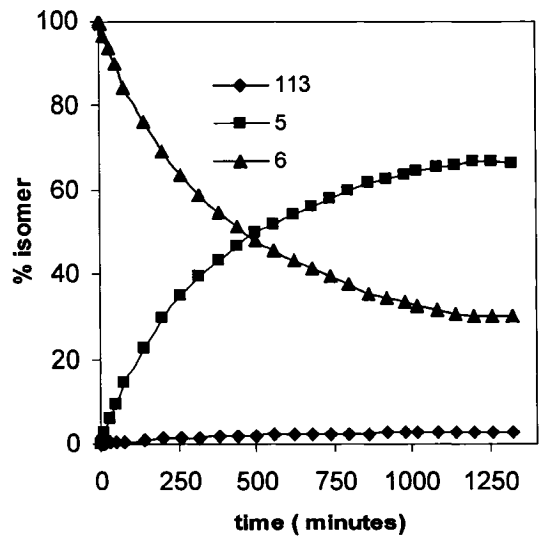

Compound **6** is quite reactive. For example, after 760 minutes of irradiation in AN at 25 °C, only 40% remained, giving 53% of **5** and 7% of **113**. At 50 °C, a very similar conversion is obtained after the same time of irradiation, but the stationary state is reached before 1500 minutes of irradiation. The analogous 6-cyanotetralin **10,** as stated before, reacts in AN giving the phototransposition product **9**, although not quite as efficiently as for **6**. For example, after 750 minutes of photolysis, only 36% of **10** had been converted into **9**, Figure 3.5. The intermediate for this photoisomerization process is presumably a biradical prefulvene, as shown in Scheme 3.1. After 2500 minutes, a photostationary state is reached with the ratio **6** : **5** = 41 : 59. No products from a secondary photoreaction were observed. The analogous 5-cyanoindan **8** does not undergo phototransposition in AN or photoaddition in TFE even at 50 °C.

Figure 3.5. Photolysis plot for the photoisomerization process of 10 in AN at 25 °

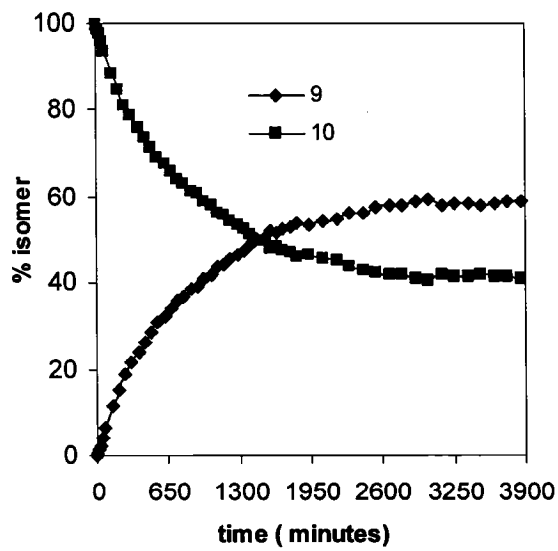

Scheme 3.4. Proposed mechanism for the formation of 5-cyanotetralin 9 from the photolysis of 6-cyanotetralin 10 in AN

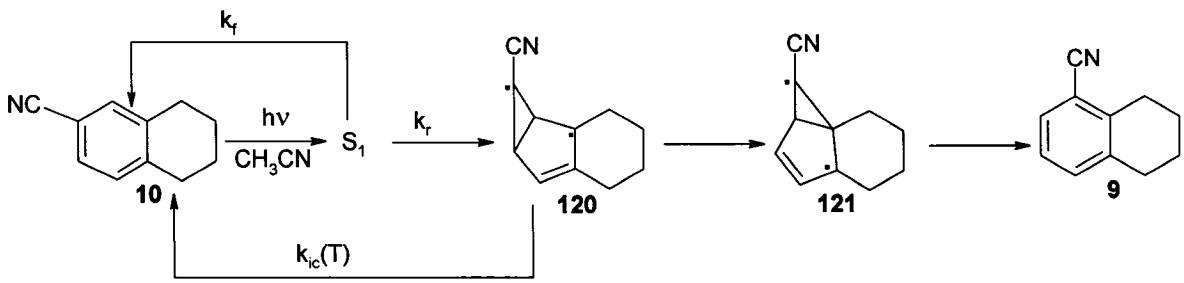

3.2.4. Temperature dependence of the lifetimes of the dialkylbenzonitiles 5-10 and *o*-xylene 18, indan 115, and tetralin 116

The influence of temperature and solvent on the rate constant of deactivation k_d of compounds **5-10** was measured using a nanosecond photon counting instrument (from – 25/-30 °C to 65 °C in AN). For *o*-xylene **18**, indan **115**, and tetralin **116** a more rapid method was used: Φ_f and τ_s were used to calculate k_f at 25°C, eq. 1.21, then measurement of relative fluorescence quantum yield over a range of temperatures (-25 °C to 65 °C) gives k_d , eq. 3.4. This method assumes that k_f is a constant, independent of the temperature. Data of k_d (T) for these different isomers are shown in Figures 3.6 – 3.14.

$$k_d(T) = \frac{1}{\tau_s(T)} = \frac{\phi_f(25°C)}{\tau_s(25°C) x \phi_f(T)} \qquad (3.4)$$

Figure 3.6. Deactivation rate constant vs. temperature for 2,3-dimethylbenzonitrile 5 in AN

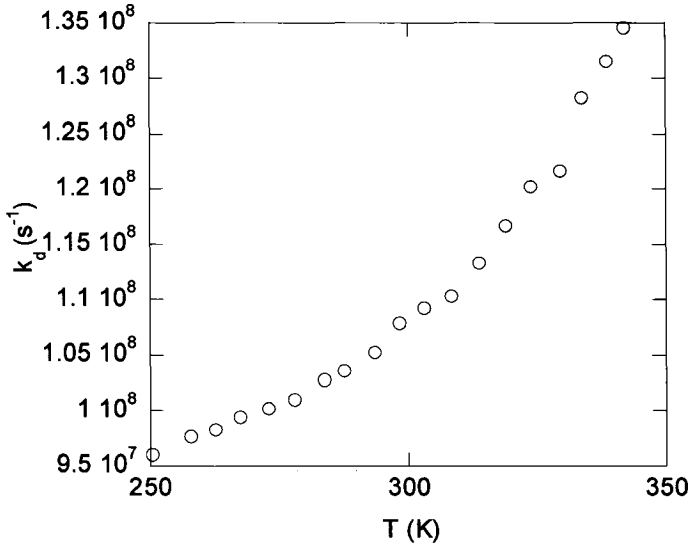

Figure 3.7. Deactivation rate constant vs. temperature for 3,4-dimethylbenzonitriles 6 in AN

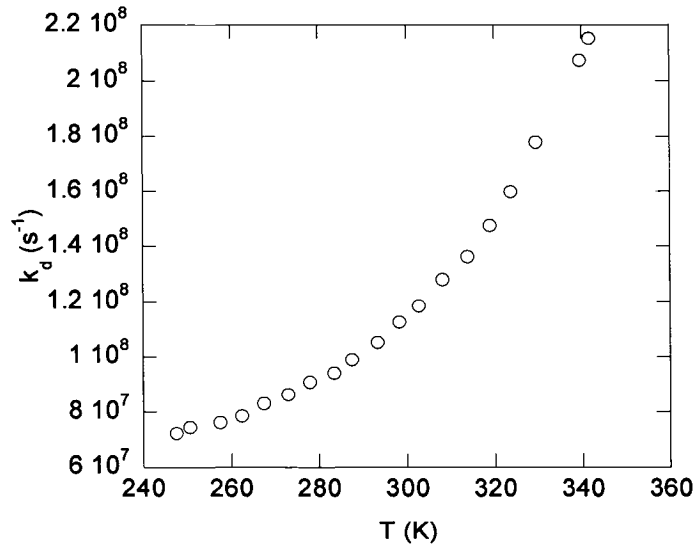

Figure 3.8. Deactivation rate constant k_d vs. temperature for 4-cyanoindan 7 in AN

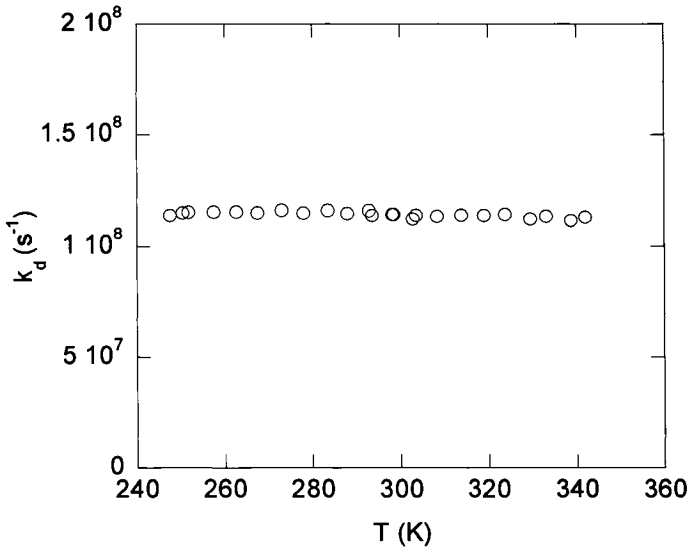

Figure 3.9. Deactivation rate constant k_d vs. temperature for 5-cyanoindan 8 in AN

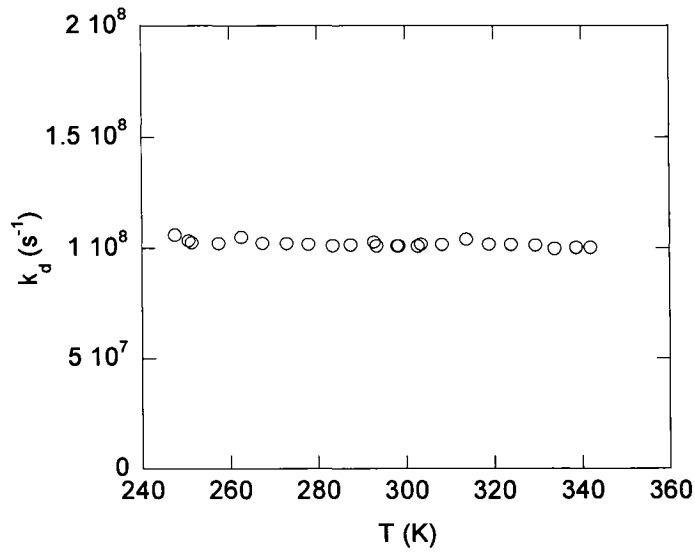

Figure 3.10. Deactivation rate constant k_d vs. temperature for 5-cyanotetralin 9 in AN

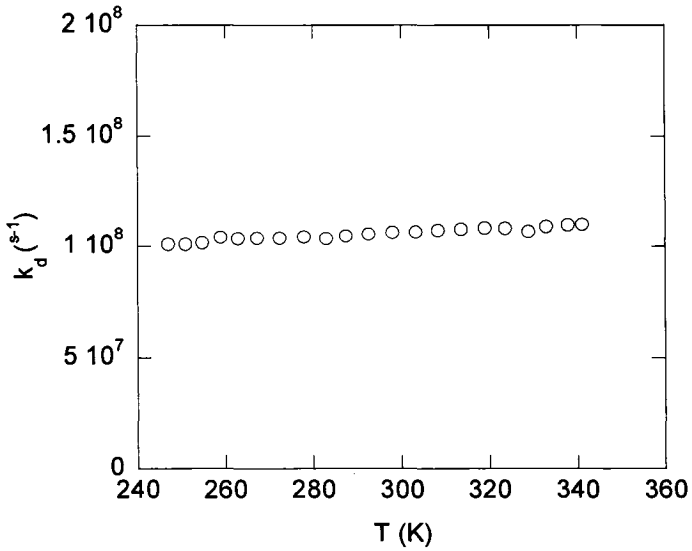

Figure 3.11. Deactivation rate constant k_d vs. temperature for 6-cyanotetralin 10 in AN

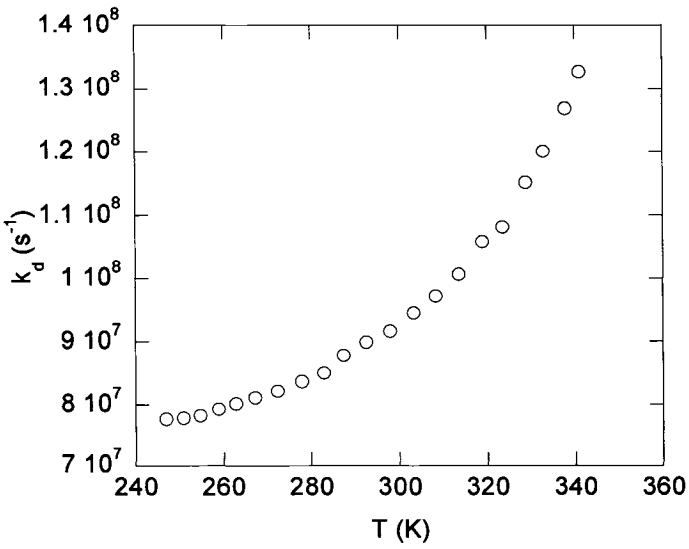

Figure 3.12. Deactivation rate constant k_d vs. temperature for *o*-xylene 18 in AN

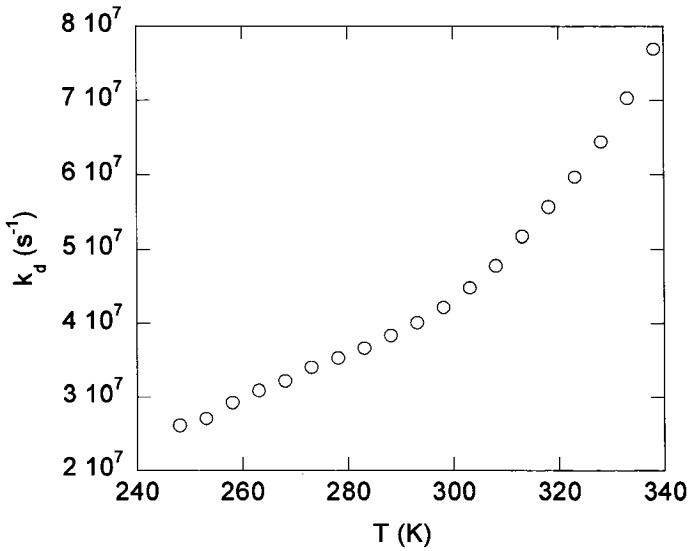

Figure 3.13. Deactivation rate constant k_d vs. temperature for indan 115 in AN

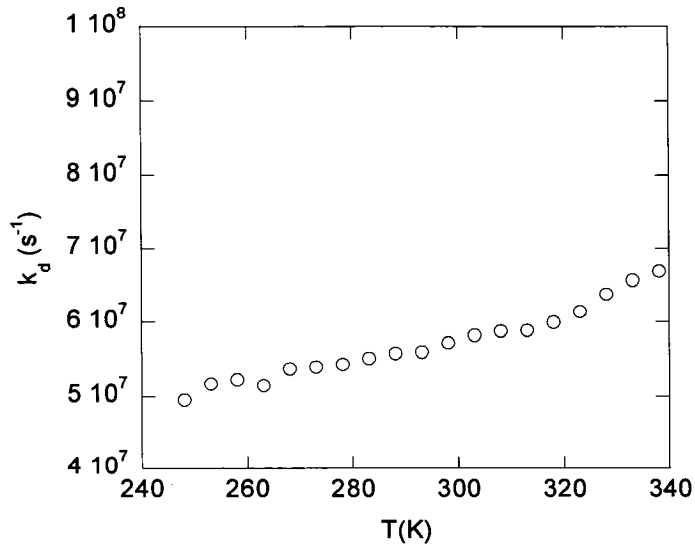

Figure 3.14. Deactivation rate constant k_d vs. temperature for tetralin 116 in AN

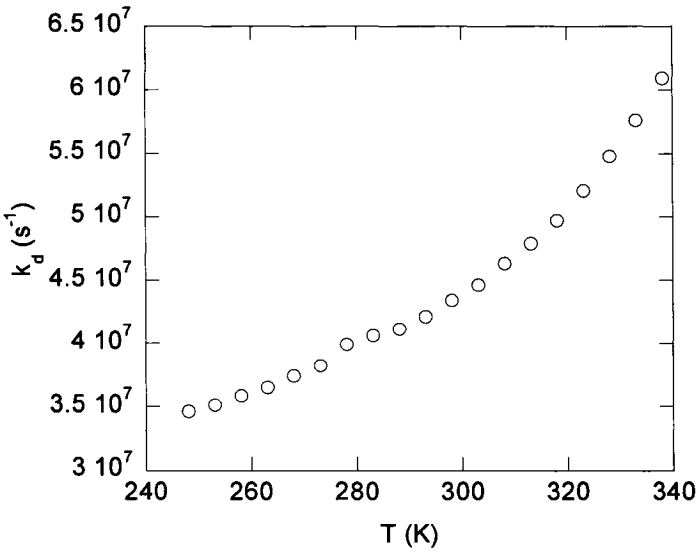

The rate constant for decay of the isomers **5**, **6** and **10** increased with temperature, implying that at least one radiationless process is enhanced. The dependence of k_d on the temperature can be related to the chemical reactivity of each isomer. For example, the rate constants of decay for **5** in AN do not depend significantly on the temperature; the total change in lifetime over the 90 °C range of temperatures is about 2 ns. Coincidently, after 20 hours of photolysis only 8% of this isomer had isomerised to the isomers **6** and **113**, Figure 3.1. For compound **6**, which after 10 hours of photolysis was about 60 % converted to the other two isomers, Figure 3.3, the singlet lifetime dropped from 22 ns to 7 ns, which means that the rate constant of deactivation k_d almost tripled over the 90 °C range of temperature, Figure 3.8. These facts indicate that the chemical reactivity for **6** is considerably higher than that for **5**.

3.2.5. Measurement of rate constants of reaction of S_1 by the temperature dependence of fluorescence

As explained in Chapter 2, Section 2.5, the measurement of singlet excited-state lifetimes τ_s (= 1 / k_d) as a function of the temperature provides a simple method for obtaining rate constants of reaction and other modes of decay of substituted benzene singlet excited states. In order to obtain the kinetic parameters of the processes of S_1 for compounds **5** - **10** and for indan **115**, tetralin **116**, and *o*-xylene **18**, the equation 2.17 was used again.

$$k_d = B + A\, exp\,(\frac{-E_{act}}{RT}) \qquad (2.17)$$

As a reminder, the parameter B is the sum of the rate constants of the non-activated photophysical process of S_1, fluorescence, and intersystem crossing. The rate constant for internal conversion is assumed to be relatively slow in comparison with the rate constants for the rest of the processes in competition, as explained previously.

The rate constants for intersystem crossing were calculated using the intercept of the plot at T = 0 K. This intercept is the sum of the rate constants for fluorescence and intersystem crossing, and is calculated by subtracting the experimental rate constant of fluorescence k_f at 25 °C from B. For comparative purposes, Arrhenius plots are shown below, in which k_d values for three different sets of compounds are plotted. Each set has the same substitution pattern of the methyl, or methylene, group. Set 1 is for compounds **5**, **7, 9**; set 2: for **6**, **8, 10** and set 3 for **18**, **115** and **116**. For those compounds with

significant curvature in the plots, the numerical values are also given. These values are also given in Table 3.2.

Figure 3.15. Arrhenius plots for set 1, compounds 5, 7, 9

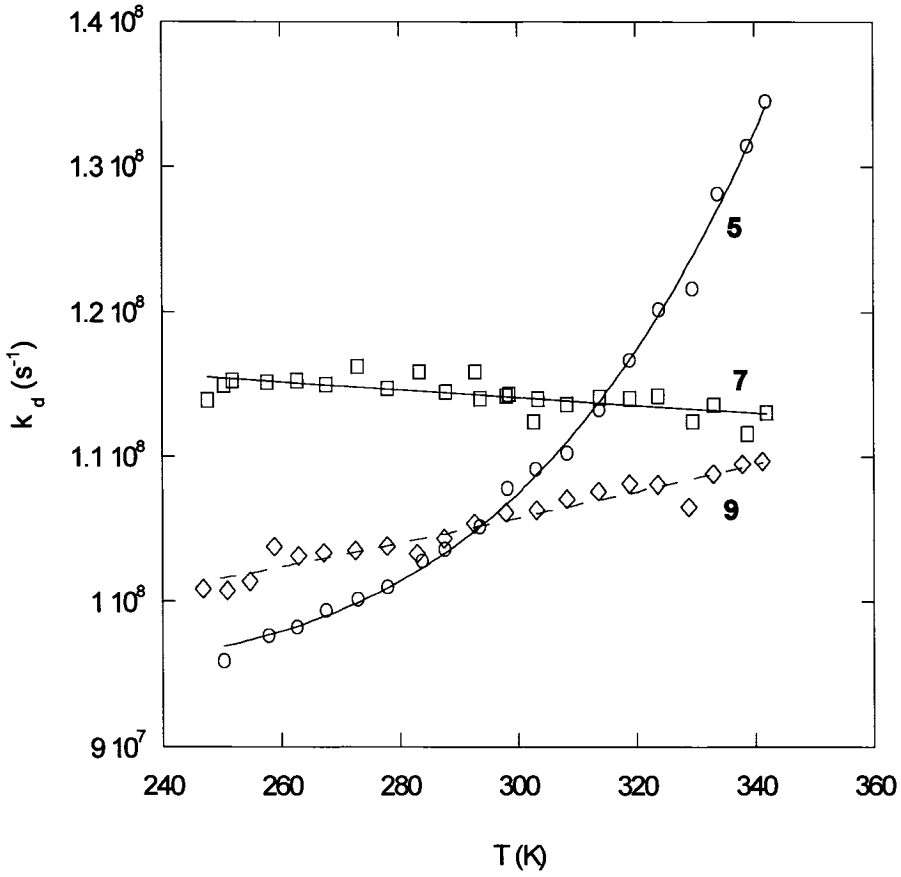

5

y = m1+m2*exp(-m3/(8.314e-3*...		
	Value	Error
m1	9.4989e+07	6.8891e+05
m2	1.413e+11	5.7395e+10
m3	23.285	1.1781
Chisq	9.9076e+12	NA
R	0.99808	NA

9

y = m1+m2*exp(-m3/(8.314e-3*...		
	Value	Error
m1	9.548e+07	5.4298e+06
m2	1.3907e+08	1.322e+08
m3	6.49	3.7183
Chisq	1.0511e+13	NA
R	0.96512	NA

Figure 3.16 Arrhenius plots for set 2, compounds 6, 8, 10

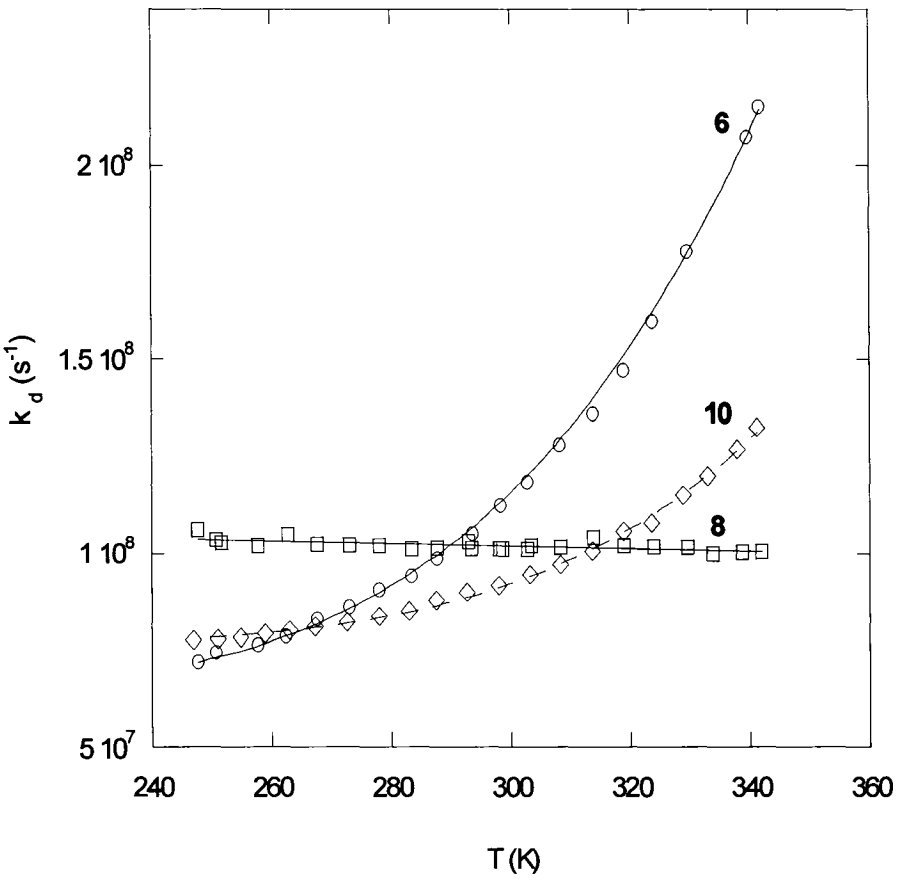

6

y = m1+m2*exp(-m3/(8.314e-3*...		
	Value	Error
m1	6.357e+07	1.5382e+06
m2	3.0433e+11	6.6375e+10
m3	21.628	0.63274
Chisq	5.1792e+13	NA
R	0.99927	NA

10

y = m1+m2*exp(-m3/(8.314e-3*...		
	Value	Error
m1	7.6345e+07	5.0806e+05
m2	4.6001e+11	1.2779e+11
m3	25.623	0.79493
Chisq	1.1305e+13	NA
R	0.99903	NA

Figure 3.17. Arrhenius plots for set 3 compounds 18, 115, 116

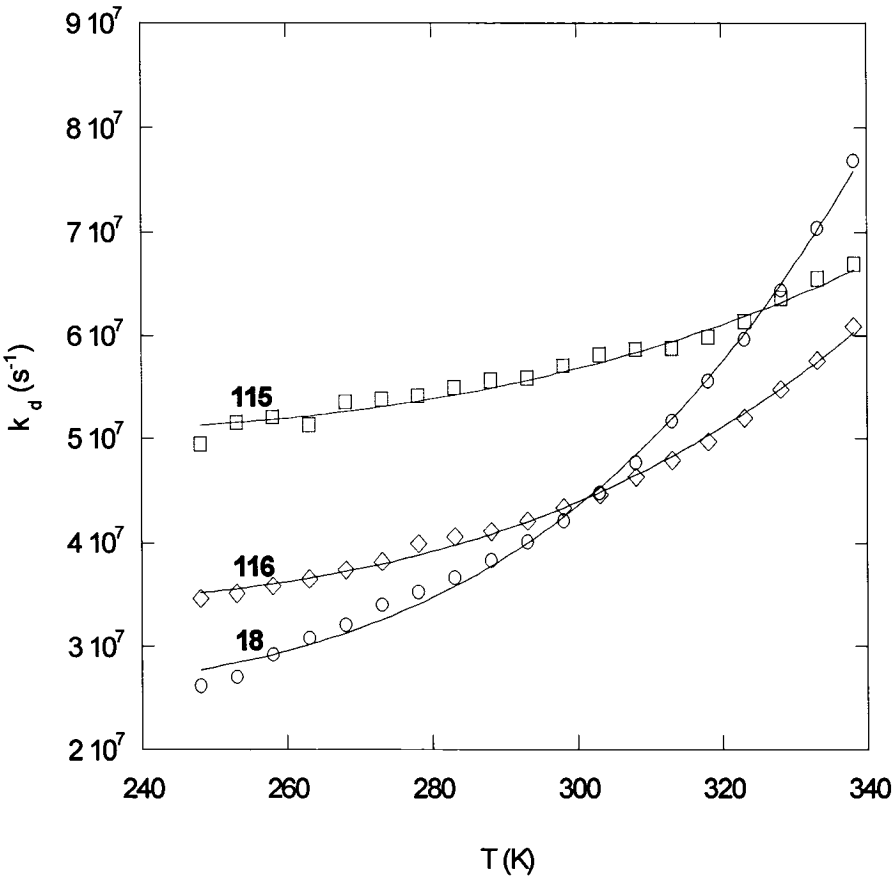

8

y = m1+m2*exp(-m3/(8.314e-3*...		
	Value	Error
m1	2.4822e+07	7.9724e+05
m2	1.381e+11	4.8288e+10
m3	22.218	1.0017
Chisq	1.2611e+13	NA
R	0.99845	NA

116

y = m1+m2*exp(-m3/(8.314e-3*...		
	Value	Error
m1	3.326e+07	4.9644e+05
m2	4.1117e+10	1.4781e+10
m3	20.601	1.036
Chisq	3.8859e+12	NA
R	0.99825	NA

115

y = m1+m2*exp(-m3/(8.314e-3*...		
	Value	Error
m1	4.9923e+07	9.1203e+05
m2	1.0553e+10	1.4009e+10
m3	18105	2.7491
Chisq	1.0354e+13	NA
R	0.98786	NA

The plots for the two cyanoindan derivatives **7** and **8** (Set 1 and Set 2) are different from the other compounds, as they have very small but negative slopes. Attempts to fit these plots to the Arrhenius model are not possible. Considering the experimental scatter, these slopes may not be significantly different from zero. However, the small negative slopes are, in fact, expected, even if all the rate constants for the

processes of S_1 are temperature independent. The reason for this is given in eq. 3.5, where n is the refractive index of the solvent. This equation indicates that k_f should decrease slightly with temperature, because n also decreases slightly with temperature.[82] Eq. 3.5 has been used previously to show that k_f^o is independent of temperature for aromatic compounds such as benzene, toluene, *o*-xylene, and tetralin in hydrocarbon solvents. For the other compounds discussed in Chapter 3 with significant dependence of k_d with temperature, the very small negative changes in k_f with temperature were ignored and k_f was assumed to be constant. The fact that the plots for the cyanoindan derivatives have slopes that are essentially zero indicates that the activation energy for any ring deformation that could lead to reactive intermediate prefulvene biradicals, like the bicyclic structures in Scheme 3.5, must be too high for this process to compete with fluorescence and intersystem crossing over the experimental range of temperatures studied. The higher values of k_d, which extrapolate to $k_f + k_{isc}$ at the lower temperatures for the indan derivatives, as compared to their tetralin and acyclic analogues of each set, must reflect faster rates of intersystem crossing.

$$k_f^o = k_f(T)\ n(T)^2 \tag{3.5}$$

For the remaining compounds studied, the plots have an obvious upward curvature, some more than others. Excellent fits of k_d to eq. 2.16 were obtained ($r > 0.998$ in all cases), giving an intercept equal to $k_f + k_{isc}$, assuming that $k_{ic} = 0$, and the Arrhenius parameters A and $E_{act.}$. The kinetic parameters are given in Table 3.2.)

Table 3.2. Arrhenius parameters, rate constants, and quantum yields at 25.0 °C for the compounds in sets 1-3 in acetonitrile

Cmpd.	A ($10^{11}s^{-1}$)	E_a (kJ/mol)	($k_f + k_{isc}$) (10^7s^{-1})	k_{isc} (10^7s^{-1})	Φ_{isc}	k_r (10^7s^{-1})	Φ_r	k_d (10^7s^{-1})
5	1.4 (±0.5)	23.3 (±1.2)	9.5 (±0.1)	7.1	0.66	1.1	0.10	10.8
7	--	--	11.4	8.8	0.77	0.0	0.0	11.5
9	0.001 (±0.001)	6.5 (±3.8)	9.6 (±0.5)	7.0	0.67	0.9	0.09	10.5
6	3.0 (±0.7)	21.6 (±0.6)	6.4 (±0.1)	4.6	0.40	5.0	0.45	11.2
8	--	--	11.2	9.1	0.79	0.0	0.0	10.1
10	4.6 (±1.3)	25.6 (±0.8)	7.6 (±0.1)	5.9	0.64	1.5	0.16	9.2
18	1.4 (±0.5)	22.2 (±1.0)	2.5 (±0.1)	2.0	0.45	1.8	0.42	4.2
115	0.11 (±0.14)	18.1 (±2.7)	5.0 (±0.1)	3.6	0.63	0.68	0.12	5.7
116	0.4 (±0.1)	20.6 (±1.0)	3.3 (±0.1)	2.4	0.56	1.0	0.23	4.3

The rate constants for reaction were calculated at 25 °C, using the parameters obtained from the fits. The quantum yields of all the processes of S_1 were calculated using eq.

2.14.

$$\Phi_i = k_i x\, \tau_s \qquad \text{(where i = f, isc, ic)} \qquad (2.14$$

Previous literature values for k_d obtained from -70 to +80 °C in methylcyclohexane for *o*-xylene **18**[7, 79] gave $(k_f + k_{isc}) = (1.5 \pm 0.1) \times 10^7\ s^{-1}$, $A = (2.1 \pm 1.8) \times 10^{11}\ s^{-1}$ and $E_a = (25 \pm 3)$ kJ/mol, which are in good agreement with the values in Table 3.2 in AN: $k_f + k_{isc} = (2.5 \pm 0.1) \times 10^7\ s^{-1}$, $A = (1.4 \pm 0.5) \times 10^{11}\ s^{-1}$, and $E_a = (22 \pm 1)$ kJ/mol. An important observation from similar measurements obtained previously for benzene is that although the k_f values obtained ($(0.16 \pm 0.02) \times 10^7\ s^{-1}$) are independent of the solvent, the Φ_f (0.06, 0.05, 0.04, 0.029, 0.025)[87] and τ_s values (34, 30, 28, 20, 15 ns)[79] decrease significantly as the solvent polarity increases (cyclohexane, methylcyclohexane, ethanol, methanol, acetonitrile, respectively). The reason for this must be that k_r, the rate of formation of the corresponding prefulvene biradical, increases with the solvent ionizing ability, due to a better stabilization of the transition state. Similar results were reported in Chapter 2 for the cyanotoluenes **1o,m,p** and arylboronate esters **2o,m,p** .

As stated above, the plot for indan **115** itself (Figure 3.17), in contrast to the other two cyano indan derivatives, does show a slight upward curvature, indicating that a temperature-dependent process is occurring. In Chapter 2, Section 2.5.5, artificial data was used to assess the reliability of the temperature versus fluorescence method for obtaining rate constants of reaction of S_1. The conclusion reached was that this experimental method, using a limited temperature range (-25 to +65 °C), can only give reliable values of k_r if $A > 0.5 \times 10^{11}\ s^{-1}$ and $E_a < 25$ kJ/mol in order that the chemical

reaction (k_r) contributes significantly enough over the temperature range examined to compete with the other modes of deactivation. In the case of 5-cyanotetralin **9**, the Arrhenius parameter values, E_{act} (1×10^8 s^{-1}) and A (6.5 kJ/mol), are consistent with an activated intersystem crossing process. In agreement with this conclusion, a photochemical reaction was not observed for this compound.

On this basis, the data for the Arrhenius parameters that appear in Table 3.2 for indan **115** and 5-cyanotetralin **9** do not satisfy the criteria that was established in Section 2.5.5. The data for **9** again indicate that an activated intersystem crossing is the dominant process. Therefore, the k_r value obtained from eq. 2.15 for 5-cyanotetralin **9** is expected to be the contribution that activated k_{isc} makes to intersystem crossing. At room temperature for **9**, the total rate of intersystem crossing will then be $k_{isc} + k_r$ (25 °C) = 7.9×10^7 s^{-1} and $\Phi_{isc} = 0.76$, the remainder of the deactivation of S_1 being fluorescence, $\Phi_f = 0.24$. The activation parameters for indan **115** suggest that some activated bond deformation is leading to a low value of k_r, which is a surprising observation in view of the complete lack of reactivity of the cyanoindan derivatives **7** and **8**. However, as indicated in Scheme 3.3, photolysis at 254 nm of the more highly strained benzocyclobutene yields two bicylo[3.3.0]octatriene derivatives (also known as dihydropentalenes) and the proposed mechanism included prefulvene biradicals (also known as "prebenzvalenes") as the critical intermediates.[91]

From the Arrhenius plot, reliable values of k_r at 25 °C can be obtained for **5**, **6**, **10, 18, 115** and **116**; these values are in Table 3.2. The first conclusion to be reached is one that reinforces the results of Chapter 2; although the k_r process results in significant quantum yields, the actual quantum yields of product (Φ_{prod}) are considerably smaller.

Therefore, in all the cases studied, internal return of the prefulvene biradicals is one of the dominant modes of deactivation of S_1 for substituted benzenes.

Also, the effect of ortho cyano substitution is very evident for the tetralin derivative **9**, with both the unsubstituted tetralin **116** and 6-cyanotetralin **10** having similar rates of reaction (1.0 and 1.5 x 10^7 s^{-1}, respectively), whereas for 5-cyanotetralin **9** this pathway is completely shut off and only intersystem crossing occurs. The preferred reaction pathway for cyano substituted benzene rings involves an intermediate with the cyano group at C6 of the bicylic intermediate, Scheme 3.4. This geometry change seems possible for the formation of the biradical **120** from **10** but, because of bridgehead strain, improbable for the formation of **121** from **9,** Scheme 3.4. For the acyclic cyano substituted cases **5** and **6**, a similar steric effect is present but much less severe: k_r for **6** (5.0 x 10^7 s^{-1}) is only a factor of five greater than for **5** (1.0 x 10^7 s^{-1}), in agreement with the observation from the preparative scale photochemistry that **10** is converted efficiently to **9**. Presumably, the adjacent ring in the cyanoindan **5**, **7** and **8**, and in the cyanotetralin derivatives **9** and **10** makes the required distortion of the geometry of S_1 to form the biradical prefulvene intermediate difficult.

3.2.6. Triplet state reactivity of 5 and 6

Because of the high quantum yields of intersystem crossing of 0.66 and 0.40 for **5** and **6,** respectively, the possibility of triplet state (T_1) reactivity must be considered. Previously it was shown that the cyanotoluenes **1p** and **1m** do not react from the triplet state and, therefore, S_1 was the reactive state for their phototransposition reactions.[8, 54] This was determined by selective quenching of T_1 by 2,3-dimethyl-1,3-butadiene. The

fluorescence in AN of **5** and **6** is also quenched by this diene, giving Stern-Volmer slopes ($k_Q \tau$), eq. 1.22, of 61.8 and 99.0 M^{-1}, respectively (Figure 3.17), and k_q values of 6.6 and 11.1 x 10^9 M^{-1} s^{-1}, respectively, close to the diffusional limit. Therefore, at a quencher concentration of 1.0 x 10^{-3} M, the percentage of excited singlet states that is being quenched is 6% for **5** and 11% for **6**. Making the usual assumption that T_1 will be much longer lived than S_1 and that the quenching of T_1 will also be diffusion controlled, the percentage of triplet states being quenched should be much higher. Irradiation of either **5** or **6** under these conditions resulted in only minor decreases in the efficiencies of the phototransposition reactions, suggesting that T_1 is, at most, a minor contributor to the phototransposition reactions of these two substrates. Irradiation of **6** at higher concentration of the diene resulted in cycloaddition products (determined only by GC/MS, m/z = 213), as expected for the quenching of the excited singlet states of substituted cyanotoluenes by dienes.

$$\frac{\phi_f^o}{\phi_f} = 1 + \tau_s k_Q [Q] \qquad (1.22)$$

Table 3.3. Quenching experiments for 5 and 6

Compound	photolysis time	[Quencher]/ M	composition of the mixture
2,3-dimethylbenzonitrile **5**	3h	0	**113** : 0.44% **5** : 98.59% **6** : 0.87%
	3h	1.0×10^{-3}	**113** : 0.23% **5** : 99.02 **6** : 0.75% No addition products
3,4-dimethylbenzonitrile **6**	3h	0	**113** : 3.65% **5** : 27.54% **6** : 68.81%
	3h	1.0×10^{-3}	**113** : 0.42% **5** : 13.5% **6** : 85.98% No addition porducts
	3h	21×10^{-3}	**113** : 0% **5** : 2.55% **6** : 90.27% a mixture of addition products of m/z = 213 [M(DMBN's) + M(Q)] = 213 g/mol

Figure 3.18. Stern-Volmer plots for compounds 5 and 6

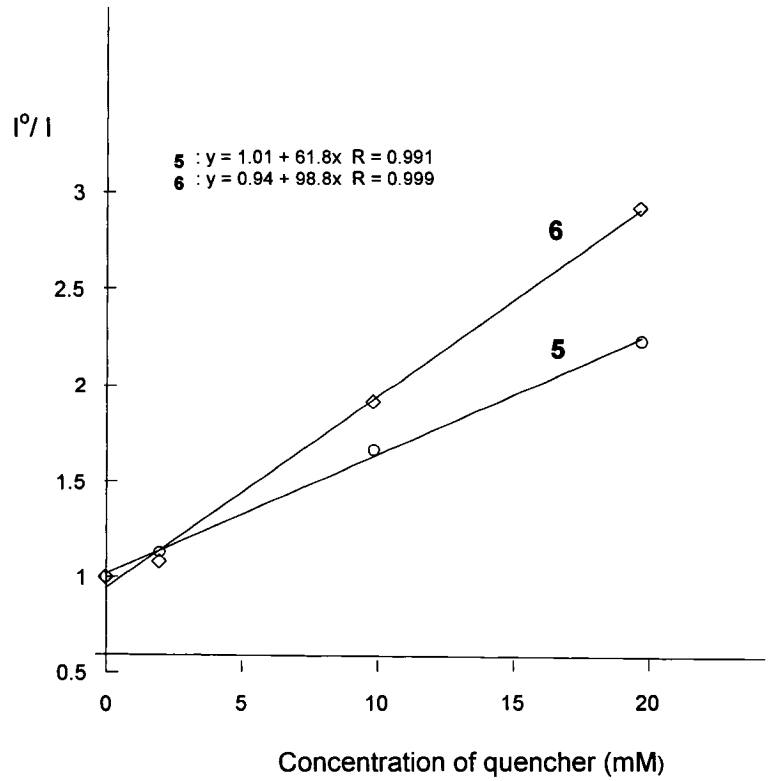

3.3. Conclusions

The results presented show that for those compounds that undergo phototransposition reactions, significant barriers exist on the surface that connects S_1 to the reactive intermediate. The major pathway for reaction of the substituted prefulvene biradical is the return to starting material by cleavage of the bond that was initially formed from S_1 (meta bonding). This conclusion is reached by comparison of the quantum yield of reaction (Φ_r) to the yield of product.[89] The quantum yield of product is, in all cases, very small in comparison with the value required to make the sum of all

quantum yields approximately unity (Ermolaev's rule). The first formed reactive intermediate equilibrates with its isomeric forms, allowing phototransposition to occur (Scheme 3.1). The barriers on this surface will not be easy to determine experimentally but perhaps can be modeled by high-level computational methods.

As expected, the effect of incorporating the substituted benzene into a bicyclic structure, as in tetralin and indan derivatives, decreases the efficiency of formation of the reactive intermediate, particularly for the cyanoindans **7** and **8**. Once again, the substitution of a methyl group ortho to the cyano group leads to low or no photochemical reactivity.[8, 89] This is the case for 2,3-dimethylbenzonitrile **5** and particularly for 5-cyanotetralin **9**.

These observations can perhaps be explained as a consequence of steric crowding in the bicyclic or tricyclic intermediate by the methyl, or methylene, group at the bridged position. The fact that the cyclic cyanobenzene derivatives have lower photochemical reactivity than their acyclic analogues could be a consequence of some geometry restriction imposed by the aliphatic ring with strong σ-bonds, and of the very well defined geometry associated with five- and six-membered rings.

Chapter 4

A Mechanistic Study of the Photochemical Addition of Alcohols to Methoxy-substituted 1,2-Diphenylethyne Derivatives

4. Introduction

4.1. The photophysics of 1,2-diphenylethyne 11 (tolan)

The photophysical properties of tolan **11** in solution have some special features; for example, tolan only fluoresces from the second excited singlet state, S_2. No fluorescence from the first excited singlet state has been reported in the condensed phase.[98] The S_2 state has a lifetime of only 9 ps at room temperature, and deactivates to S_1 by means of an activated internal conversion process, with an activation energy estimated at approximately 12 kJ/mol, independent of the solvent.[99] The solvent-independent activation barrier was observed by using solvents of quite different viscosities. This observation suggests that the activated internal conversion process is dominated by the electronic properties of this excited state and not by vibrational modes that may contribute to decay. The absence of any viscosity effect on the decay of $S_2 \rightarrow S_1$ may be taken as evidence against a structural change that might be involved in this process.

4.1.1. Electronic properties of tolan 11

Tolan has a strong electronic absorption band in the 300-250 nm region of the electromagnetic spectrum. This band presents a complex vibrational pattern and molar absorptivity ϵ_{max} of approximately 20000 M^{-1} cm^{-1}.[100] This vibrational structure could be the result of a long progression of C≡C stretching modes, which is an indication of a large displacement of the C≡C bond upon electronic excitation. Three different excited states, T_1, S_1, and S_2, have been observed using transient absorption measurements in condensed phase.[98] The $S_0 \rightarrow S_2$ state transition is fully one-photon allowed, suggesting that the band in the electronic spectra with high ϵ must be due to the $S_0 \rightarrow S_2$ excitation. The $S_0 \rightarrow S_1$ transition is symmetry forbidden and is considered to be absent in the UV spectrum of tolan. The S_2 state was assumed to be the emitting state because the decay rate constant for S_2, as observed by LFP, agrees with the decay rate constant obtained by fluorescence.[101] In addition, the mirror symmetry relationship of the electronic and emission spectra of **11** leads to the conclusion that the S_2 state is responsible for most, if not all, of the absorption in the lowest energy excitation band of tolan. Fluorescence from higher excited states is usually extremely weak because of the fast internal conversion process from $S_2 \rightarrow S_1$. This is a consequence of the small energy gap that separates these two excited states. Quantum yields of fluorescence Φ_f larger than 10^{-3} have been observed in only a few cases for $S_2 \rightarrow S_o$ deactivations. A well known example is azulene with ΔE ($S_2 \rightarrow S_1$) of 160 kJ / mol. For tolan, this gap is only 6 kJ / mol.[102]

The fluorescence quantum yield of tolan is estimated to be 0.01 in hexane at room temperature.[103] The harmonic oscillator strength, calculated in hexane by integration of the first absorption band in the electronic spectrum is 0.83.[104] The radiative lifetime, calculated from the Strickler – Berg relation, eq. 1.12, is 1.3 ns.[103]

4.1.2. Dynamics of the excited states of tolan 11

Picosecond transient absorption measurements of tolan revealed that, immediately after the laser pulse (295 nm), a strong narrow absorption band of a transient appeared at 500 nm.[98, 102, 103] This band, which was assigned to a $S_2 \rightarrow S_n$ transition, was rapidly replaced by two bands at 435 and 700 nm with increasing delay time. At delay times longer than 0.5 ns, the absorption spectrum features only a narrow, intense band at 415 nm. This transient absorption band was assigned to the T_1 state ($T_1 \rightarrow T_n$). The transient band at 700 nm originated from the S_1 state ($S_1 \rightarrow S_n$). The lifetime of the first band at 500 nm was estimated to be around 8 ps, which agrees with the fluorescence lifetime. The lifetimes of the triplet state absorption band and for the band at 700 nm ($S_1 \rightarrow S_n$) are both about 0.2 ns. No fluorescence with delay time of 0.2 ns was detected, indicating that the transient that absorbs at 700 nm is not an emitting state. From the analysis of the rise and decay times observed during the transient absorption experiments, it is possible to establish the dynamics of the excited states of tolan.

Scheme 4.1. Dynamics of the excited states of tolan[103, 104]

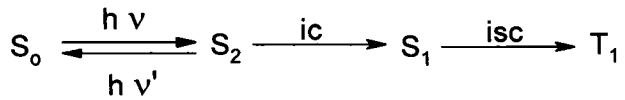

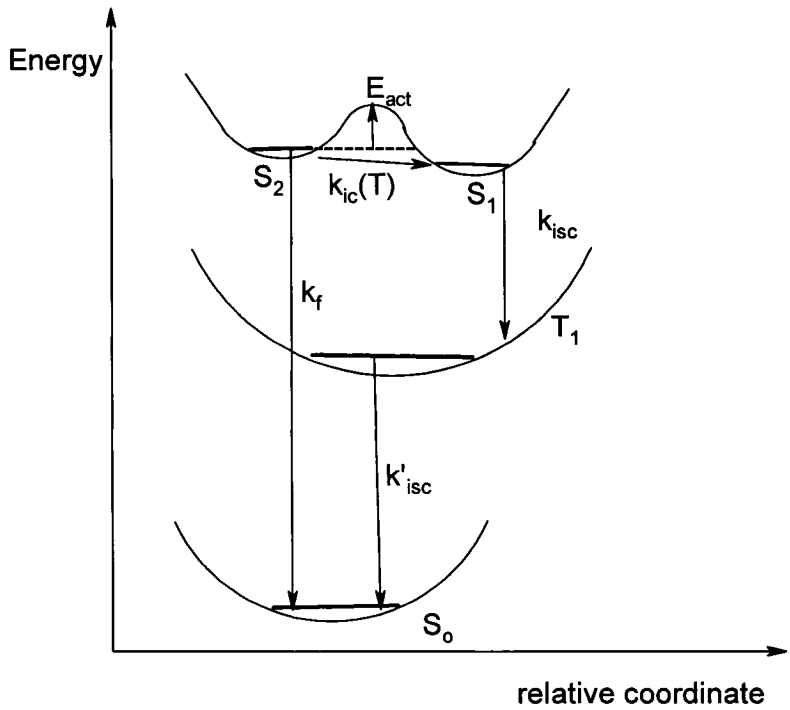

The lifetime of S_2 is particularly temperature-dependent. At lower temperatures than 130 K, the $S_2 \rightarrow S_1$ process no longer occurs. As the temperature decreases, the quantum yield of fluorescence increases remarkably. Because of the large energy gap between the singlet excited states and the ground state, internal conversion processes, $S_2 \rightarrow S_0$ and $S_1 \rightarrow S_0$, do not contribute appreciably to decay.

The internal conversion process, $S_2 \rightarrow S_1$, of various diphenylacetylene derivatives, such as the para compounds of 4-amino, 4-chloro and 4-methoxytolan, are temperature-dependent. The fluorescence quantum yields of 4-dimethylamino, 4-cyano and 4-

CH_3OOC- derivatives have been found to be almost temperature-independent, which indicates that, for these compounds, the $S_2 \rightarrow S_1$ internal conversion process is not an activated process.[104]

An Arrhenius plot for tolan was done in order to study the dependence of the quantum yield of fluorescence on temperature.[102] For the process $S_2 \rightarrow S_1$, Ferrante *et al.* reported an activation energy of 14 kJ/mol and a preexponential factor equal to 7.2×10^{13} s^{-1}. This last value agrees with the triple bond stretching vibration in the Raman spectrum, and might, therefore, be responsible for this process.

The very short fluorescence lifetime (8 ps) for tolan means that it is not possible to measure this lifetime using a nanosecond time-resolved fluorimeter (nanosecond lifetime instrument).

4.1.3. Photochemistry of phenylacetylene derivatives

The photochemistry of alkenes and phenylsubstituted phenyl alkenes has been a topic of great interest in the field of organic photochemistry. [37, 46, 105, 106, 107, 108, 109] However, the photochemistry of alkynes has been much less studied. A few examples can be found in the earlier literature.[28-33] The most common photochemical reactions in solution involving triple bonds are pericyclic reactions,[109] which frequently involve other unsaturated functional groups, such as carbonyl, nitro, phenyl, and C=C bonds, as well as redox reactions. With the exception of the study on the photohydration of phenylacetylenes **45** by McEwen and Yates,[37, 110] Scheme 2.5, no other reports on the photochemistry of phenylacetylenes in protic solvents were found.

Scheme 2.5. Mechanism for the photochemical hydration of phenylacetylene

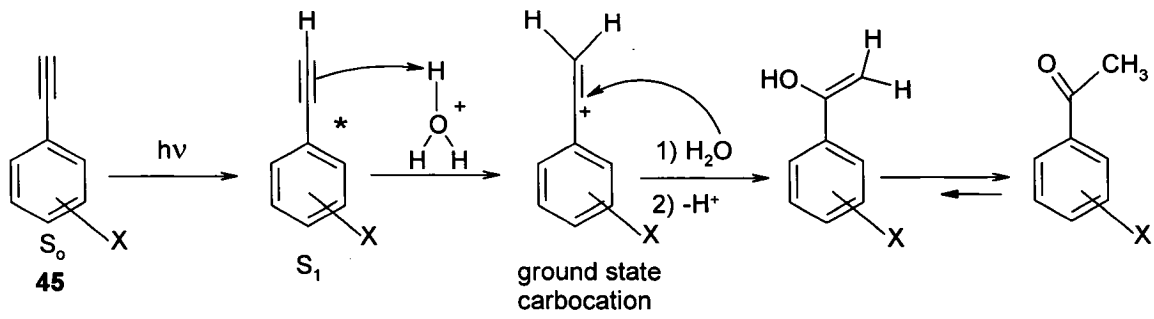

4.1.4. Research proposal

Pincock and Roberts recently reported on the influence of the meta-methoxy substitution on the photophysics and photochemistry of substituted stilbenes in protic media.[46, 111] With this in mind, the study of the photochemistry in protic solvents of their analog diphenylacetylenes was of interest.

As discussed above, the photophysics of tolan derivatives has been studied widely in the last decade, and the dynamics of the excited state of these compounds is well understood. However, the study of the photochemistry of these compounds is challenging because of the nature of their excited states. For example, many of these compounds do not fluoresce appreciably at room temperature, and the emitting excited state S_2 decays on the picosecond timing scale. Without equipment to measure deactivation rate constants of this order of magnitude, it was important to select substituted diphenylacetylenes on the basis of previous studies. An excellent precedent that allows for the selection of the compounds is the recent report by Pincock and Roberts on the photochemistry of methoxy-substituted *cis*- and *trans*-stilbenes. They reported

that meta methoxy substitution in *trans*-stilbenes increased the lifetime and the fluorescence quantum yield. Also the photochemical reactivity toward the addition of protic solvents such as methanol and TFE was observed to be enhanced for the meta methoxy compounds in comparison to the unsubstituted or para methoxy substituted stilbenes. These results were explained by proposing that the methoxy substituent in the meta position increased the electronic density on the carbon-carbon double bond in the excited state. The process consists of a photochemical addition of the alcohol to form ethers, Scheme 4.2.

Scheme 4.2. Photochemical addition of alcohols to trans-3, 4',5- trimethoxystilbene 122

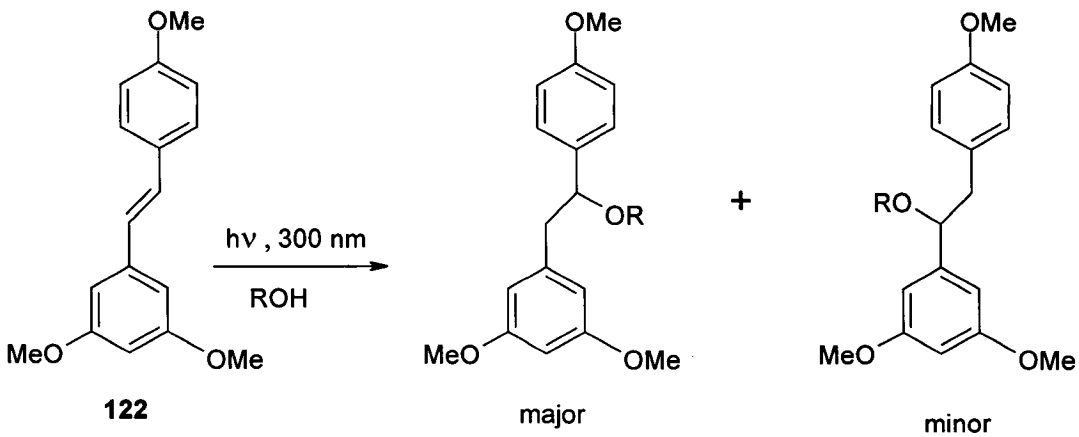

122 major minor

ROH = CH_3OH, CF_3CH_2OH

The product distribution was attributed to the electron donating effect of the methoxy substituent at the meta position in the excited state. This effect on the photochemical behaviour of stilbenes has been reported previously for the case of amino groups and was called "meta amino effect".[112] This study reported that *trans*-stilbene

derivatives with amino substituents in the ortho and meta positions have greater charge-transfer character, higher fluorescence quantum yields, and longer singlet lifetimes than the unsubstituted and para isomers. In contrast, these isomers with an abnormally high fluorescence quantum yield featured a small quantum yield of trans-cis isomerization. Scheme 4.3 shows the process for *trans*-3-aminostilbene **123**. The authors pointed out the possibility that electron-rich substituents in the ortho and meta positions produce an electronic restriction of the excited singlet state torsional barrier, which decreases the quantum yield of trans-cis isomerization. The geometric isomerization occurs from a singlet excited state that features an important charge-transfer character, by means of a twisting process around the double bond, to form a perpendicular intermediate that decays with almost equal probability to both geometric isomers.

Scheme 4.3. Trans–cis isomerization for trans-123

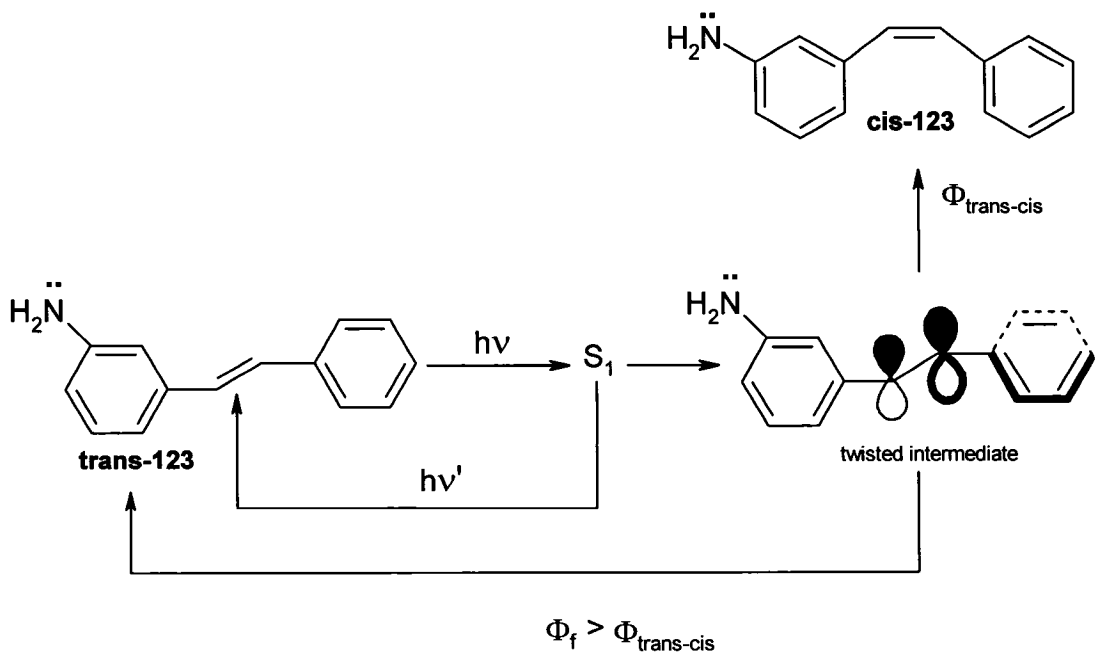

A historical study on the influence of the meta-methoxy substitution on the chemical reactivity of excited states was reported by Zimmerman *et al.* in 1963.[14] They performed Hückel Molecular Orbital calculations, using anisole as the reference, to predict the electronic effect of the methoxy substituent on its ground and excited states.[113] For the ground state, the results agree with the experimental observations that this substituent is an electron donor to the ortho and para positions. However, for the first excited singlet state, the calculations predicted an even greater electronic donation to the ortho and meta positions. Experimental confirmation of this prediction was obtained from the photolysis of methoxy-substituted benzyl acetates. For this experiment, they used 3-methoxy **124**, 4-methoxy **125**, and 3,5-dimethoxybenzyl acetate **126**. They found that **126** gave the greatest yield of ion-derived products, Scheme 4.4. The explanation is based on the fact that the electron donation of the meta methoxy substituent in S_1 could facilitate the elimination of the acetate ion, probably by means of a direct heterolytic cleavage.

In 1995, Zimmerman published a theoretical report on the meta-effect using *ab initio* calculations (Gaussian 92).[114] Predictions similar to the HMO calculations from 1963 were obtained.

Scheme 4.4. Photolysis of methoxy substituted benzyl acetates 124-126

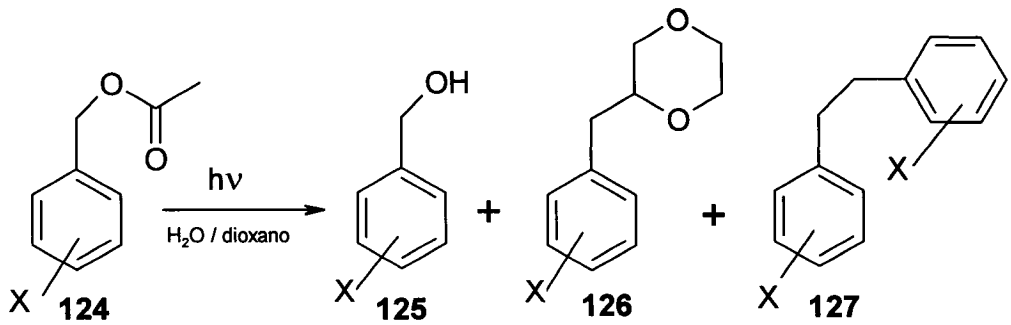

Percentage yields:		125	126	127	Quantum yield
x= m-OCH_3	**a**	29-35%	10%	8-18%	0.130
x= p-OCH_3	**b**	minor	23-31%	31-36%	0.016
x= 3,5-OCH_3	**c**	79%	0	0	0.100

In Section 1.7.1, a report by Roberts, Ardemagni, and Shechter on the photochemical addition of methanol to diarylacetylene **11**,[31] Scheme 1.5, was summarized. As explained before, the process consisted of the photochemical addition of methanol to tolan **11**. The reaction required a long photolysis time, 88 hours, and a product from a secondary photoreaction, phenanthrene **37**, was formed in a significant amount. Because the photoaddition reactions of the more acidic alcohol TFE to diphenylstilbenes were much faster than those in methanol,[111] TFE was chosen as a reactant for the experiments of this project. Tolan **11** and methoxy substituted tolans 12–**14** were chosen for study. The photophysics of compounds **11** – **14** was studied as well.

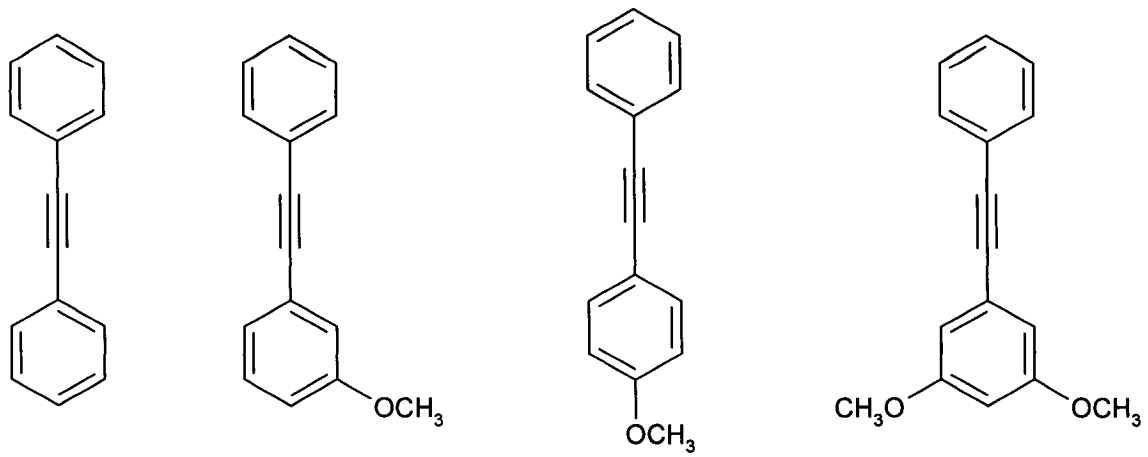

11 **12** **13** **14**

4.2. Results

4.2.1. Synthesis of methoxy substituted diphenylacetylenes

The methoxy-substituted diphenylacetylenes **12** – **14** were prepared by the Sonogashira coupling method[115] as described in a report by Chanteau and Tour.[116]

Scheme 4.5. The Sonogashira coupling method

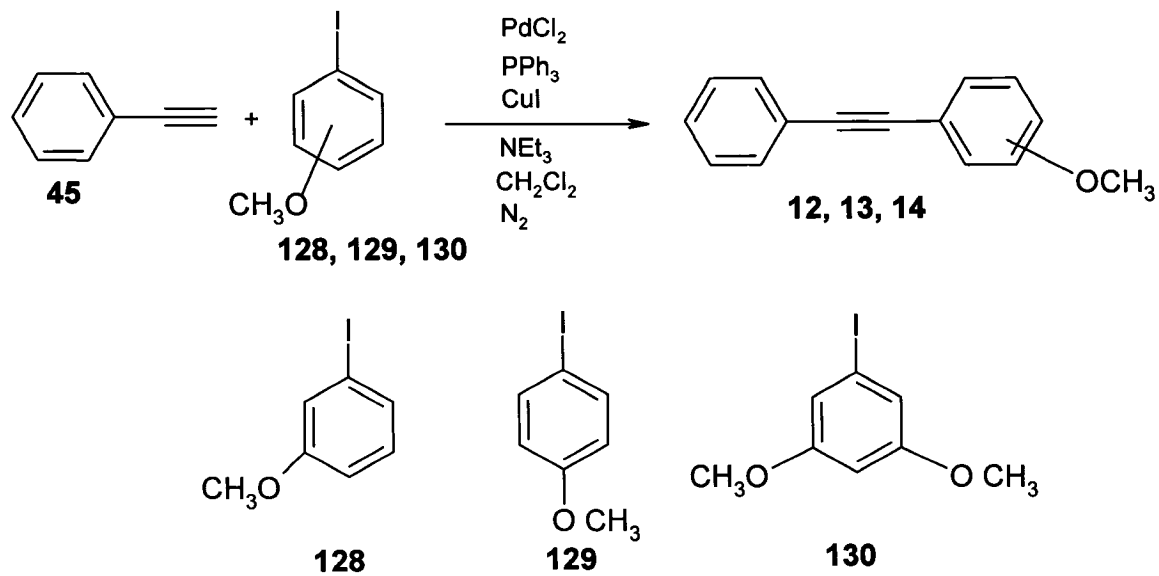

128 **129** **130**

The method provides a very simple synthesis. All the reagents are mixed together, starting by adding the iodobenzene derivative, phenylacetylene **45**, $PdCl_2$, and PPh_3 to tetrahydrofuran (THF), then the rest of the reagents. After 24 hours of stirring, the mixture changed from a yellow to a dark red color. The mixture was stirred for 36 hours at room temperature and then at 35 °C for 1 hour. Purification of the products was done by flash chromatography, followed by recrystallization of compounds **12** and **13** using a mixture of water and ethanol, and by bulb-to-bulb micro-vacuum distillation of liquid **14**. All three compounds have been prepared previously.[117]

The *meta*- and *para*-methoxyiodobenzenes **128**, **129** were commercially available, 3,5-dimethoxyiodobenzene **130** was prepared via a diazotation of 3,5-dimethoxyaniline, followed by the addition of the benzenediazonium chloride salt to a cold solution of KI. The 3,5-dimethoxyiodobenzene **130** was isolated by steam distillation followed by extraction with diethyl ether.

All the tolan products were characterized by ^1H NMR, ^{13}C NMR, and mass spectrometry. The synthesis procedure and characterization are described in Chapter 5.

4.2.2. Electronic properties of tolan 11 and methoxy substituted diphenylacetylenes 12-14

Table 4.1 contains a summary of the electronic properties for compounds **11 - 14**. The electronic spectra of the compounds being studied are typical of diphenylacetylenes. The lowest energy absorption band for all the compounds, corresponding to the allowed transition, is a broad band from about 240 nm to 300 nm or longer. The λ_{max} values are reported in Table 4.1. This band has been assigned to the $S_0 \rightarrow S_2$ transition that is both

spin and symmetry allowed.[100-104] The forbidden $S_0 \rightarrow S_1$ band is missing from the electronic spectra of all the compounds. In addition, the absorption spectra show a complicated vibrational pattern which has been related, as explained above, to a progression of the C≡C bond stretching modes, resulting in a large displacement of the C≡C bond length upon electronic excitation.[104]

Table 4.1. Electronic properties for compounds 11-14

compound	solvent	λ_{max}/ nm	ϵ_{max}/ $10^4 M^{-1}cm^{-1}$	f [a] ($S_0 \rightarrow S_2$)	$\Delta\mu(S_0 \rightarrow S_2)$ [b] D	$\lambda_{0,0}$ / nm [c]
tolan	CH_3CN	279	3.20	0.68	6.39	298
11	CH_3OH	278	3.62	0.77	6.82	
	TFE	275	3.67	0.78	6.82	
m-methoxytolan	CH_3CN	281	2.29	0.66	6.26	316
12	CH_3OH	281	2.61	0.66	6.32	
	TFE	280	2.61	0.69	6.46	
p-methoxytolan	CH_3CN	285	3.07	0.83	7.04	310
13	CH_3OH	283	3.16	0.87	7.20	
	TFE	282	3.09	0.87	7.20	
3,5-dimethoxytolan	CH_3CN	281	2.88	0.71	6.51	320
14	CH_3OH	280	3.07	0.77	6.80	
	TFE	279	3.04	0.78	6.82	

a. oscillator strength.
b. dipole moment of the transition.
c. zero-zero band wavelength.

The excitation wavelength, λ_{max}, for the meta-methoxy substituted diphenylacetylenes is similar in all the solvents, with the value for the para methoxy substituted derivative at a slightly longer wavelength. The experimental value for the molar absorptivity ϵ_{max}, and the calculated value for the oscillator strength *f* from eq.4.1, by integration of the electronic spectrum over the range of excitation wavelengths, are typical of allowed electronic transitions. In eqs. 4.1 and 4.2,[118] ν is the wave number of the transition. For tolan **11**, a value for the oscillator strength of 0.679 was reported by Ferrante and co-workers, a value identical to that reported in this thesis.[102] Ferrante used semi-empirical calculations in order to estimate *f*. For the compounds, the dipole moment of the transition $\Delta\mu$, calculated using eq. 4.2, indicates that the excited singlet state S_2 is more polar than the ground state. Both $\Delta\mu$ and *f* are slightly greater in the more polar, protic solvent TFE than in the other solvents, which indicates that, possibly, there is an interaction between the solvent and S_2. It has been reported that for tolan and derivatives intramolecular charge separation often occurs,[104] and therefore it is logical to expect an interaction between the solvent and S_2, as the polarity of the solvent increases. However, it is important to point out that, considering the experimental errors, these values are approximately the same in all solvents. If the equilibrium geometry for the S_2 of these compounds corresponds to a charge-transfer state instead of a Frank-Condon excited state, a better way to calculate $\Delta\mu$ is by investigating the effect of the solvent on the Stokes' shifts of fluorescence, *i.e.* using the Mataga-Lippert equation.

$$f = \frac{4\varepsilon_o m_e c^2 \ln(10)}{N_A e^2} \int \varepsilon(\nu) d(\nu) \qquad \text{eq. 4.1}$$

$$f = \frac{8\pi^2 m_e c}{3e^2 h} \nu |\Delta\mu|^2 \qquad \text{eq. 4.2}$$

The zero-zero band, $\lambda_{0,0}$, was also measured for all four compounds. For *m*- and *p*-methoxytolan, $\lambda_{0,0}$ is about the same, but for 3,5-dimethoxytolan **14**, it shifts slightly to the red because of the influence of two methoxy groups. Because of the very low Φ_f for *p*-methoxytolan **13** (≈ 0 at room temperature), its estimated $\lambda_{0,0}$ could have a large degree of error; however, the value in Table 4.1 agrees with the $\lambda_{0,0}$ values for the other isomers **11**, **12** and **14**.

4.2.3. Dependence of the fluorescence quantum yield of compounds 11-14 on temperature

The fluorescence quantum yields were determined using anisole as a standard. As explained before, the excitation wavelength was chosen based on the electronic spectra of both the standard and the compound being studied. This wavelength was chosen so that the absorbance of both compounds could be adjusted to the same value. The value of Φ_f was calculated by comparing the emission intensities and multiplying this fraction by the fluorescence quantum yield Φ_f of the standard. Values at 25 °C are given in Table 4.2.

Considering how small these values are for **11** and **13** and the effect that minor amounts of strongly fluorescent impurities might have, these two compounds have Φ_f values close to zero. Compounds **12** and **14** are more fluorescent. Fluorescence quantum yields for *p*- , *m*-methoxytolan and 3,5 dimethoxytolan, Figure 4.1, show a dependence on temperature, particularly for the meta methoxy compounds **12** and **14**. The same observation has been reported for tolan **11**.[102] The S_2 state of **11** has been found to be

essentially non-emitting at room temperature (Φ_f (RT) = 3.4 x 10^{-3}), but Φ_f approaches a value of 0.5 at about 100 K (-173 °C).[102,104] Similarly to tolan, *p*-methoxytolan **13** does not fluoresce appreciably over the range of temperature studied, although its fluorescence is slightly enhanced as temperature decreases to -25 °C. The S_2 states of compounds **12** and **14** do fluoresce at room temperature, Table 4.2, and as the temperature decreases, the quantum yield of fluorescence increases appreciably. For example, for compound **12**, at -25 °C (248 K), Φ_f equals 0.14 and for **14**, Φ_f equals 0.24. The enhancement of the fluorescence quantum yield for the meta substituted compounds **12** and **14** suggests that the meta effect is controlling the photophysical properties of the S_2 state for these compounds. As the fluorescence quantum yields for **12** and **14** are temperature dependent, an activated process must take place from S_2. Similar to tolan **11**, for **12** and **14**, $S_2 \rightarrow S_1$ internal conversion must be the process that is affected by temperature. The Φ_f increases as the temperature drops because the internal conversion is activated.

Figure 4.1. Dependence of fluorescence quantum yield on temperature in AN for compounds 12 - 14

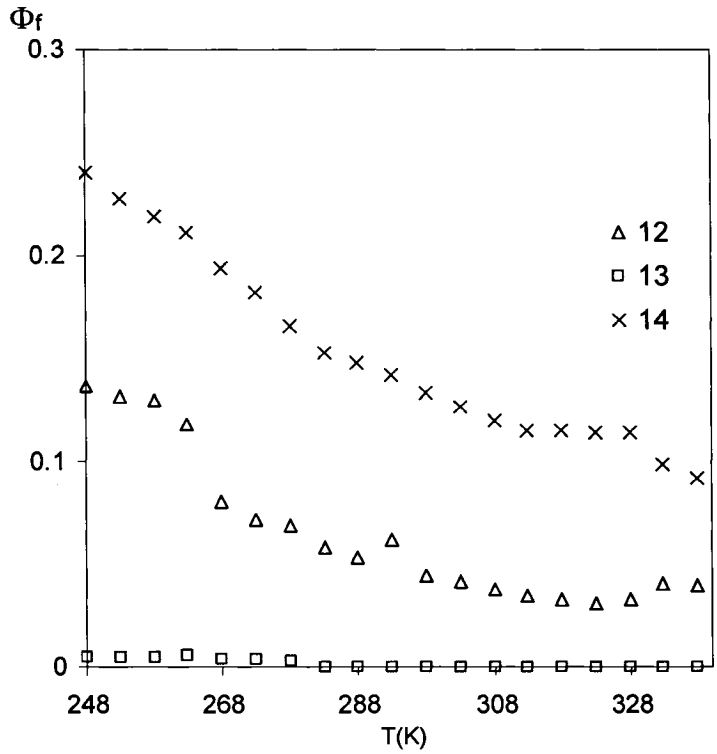

For *m*-methoxytolan **12**, the fluorescence rate constant k_f was calculated from the Strickler/Berg relation, eq. 1.12, Table 4.2. Because tolan **11** and *p*-methoxytolan **13** do not fluoresce appreciably at room temperature, it was not possible to calculate their k_f using eq. 1.12. For 3,5-dimethoxytolan **14**, it was possible to obtain an experimental value of k_f because the decay rate constant for the S_2 state is in the nanosecond timing scale (5.4 ns).

$$\Phi_f = k_f \tau_s \tag{1.21}$$

Table 4.2. Fluorescence properties for compounds 11-14 at 25 °C

compound	Φ_f (25 °C)	k_f^{calc}/ 10^7 s^{-1} (decay from S_2)[a]	k_f/ 10^7 s^{-1} (decay from S_2)	τ_s/ns (S_2)
tolan **11**	< 0.01	76.9[103]		0.008[104]
m-methoxytolan **12**	0.03	4.5		0.7[b]
p-methoxytolan **13**	< 0.01			0.006[104]
3,5-dimethoxytolan **14**	0.07		1.3[b]	5.4[c]

a. k_f calculated using the Strickler / Berg equation, eq. 1.12.
b. τ_s calculated using eq. 1.21.
c. τ_s measured using a ns time-resolved single photon-counting fluororimeter.

The reported values of singlet lifetimes, τ_s, at 286 K for tolan **11** and *p*-methoxytolan **13** are 8 and 6 ps respectively.[104] The fast deactivation of S_2 for **12** did not allow the measurement of its rate constant of deactivation (k_d = 1 / τ_s) by means of a nanosecond lifetime instrument (time-resolved fluorimeter), but it was possible to estimate its value using both the Strickler/Berg equation (eq. 1.12), and eq. 1.21. The singlet lifetimes for **12** and **14**, listed in Table 4.2, indicate that the presence of meta methoxy substituents increases the lifetime of the S_2 state. This is another result that indicates that the meta effect has an influence on the photophysics of these excited states.

4.2.4. Photolysis of tolan 11 and methoxytolan derivatives 12 – 14 in TFE

Photolysis of a nitrogen-saturated solution (1mg / mL) of compounds **11–14** at 25 °C was done in a Rayonet reactor using 16 lamps of 300 nm. These lamps insured that absorption corresponds to the $S_0 \rightarrow S_2$ transition of the UV spectra. For compounds **12–14,** the process resulted in a mixture of four isomers, and for tolan **11,** two isomers. The

photolysis products are a mixture of geometric and positional isomers resulting the addition of TFE to the triple bond, Scheme 2.6

Scheme 4.6. Photochemical addition of TFE to compounds 11 - 14

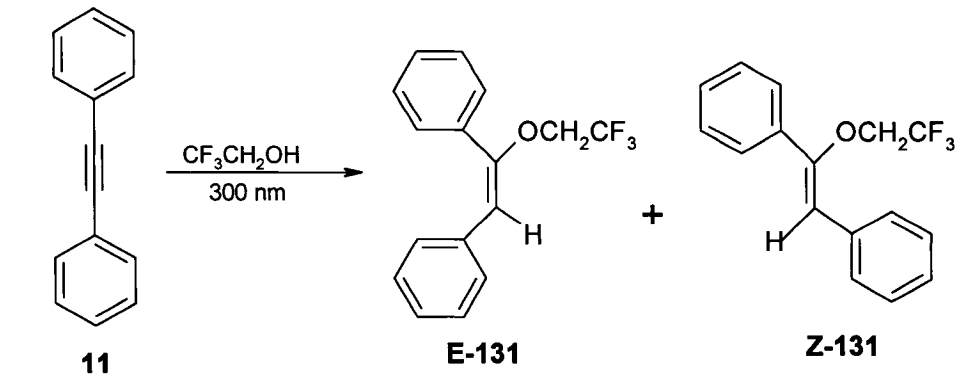

11 **E-131** **Z-131**

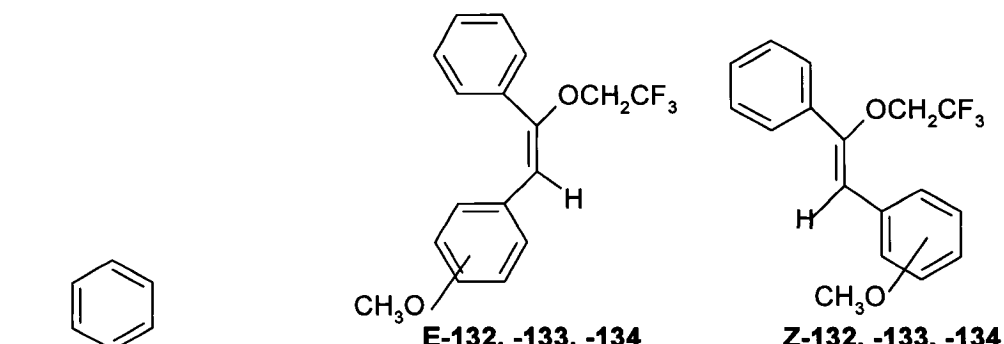

E-132, -133, -134 **Z-132, -133, -134**

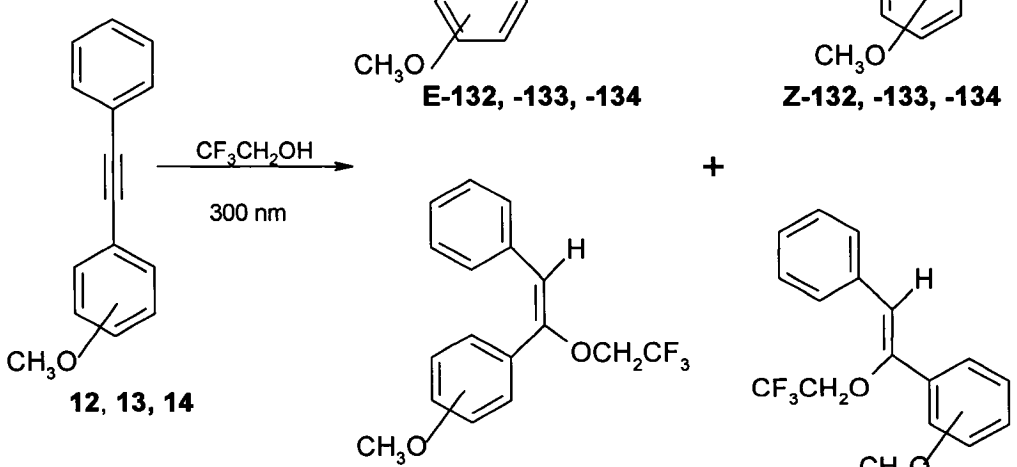

12, 13, 14 **E-135, -136, -137** **Z-135, -136, -137**

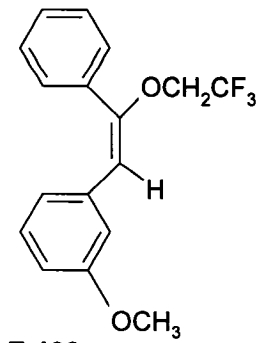

E-132

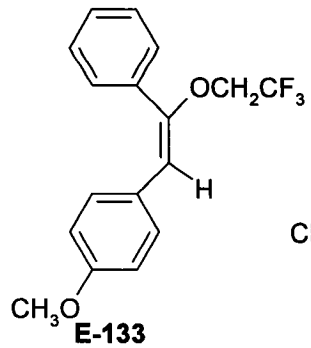

E-133

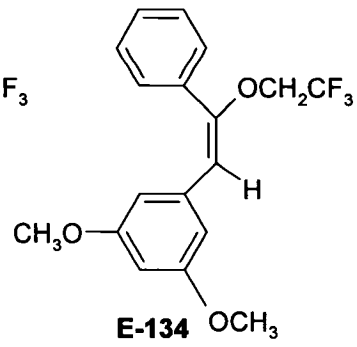

E-134

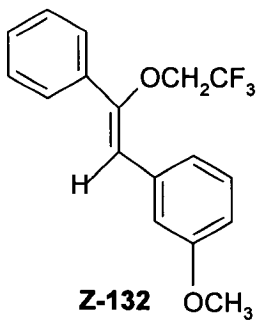

Z-132

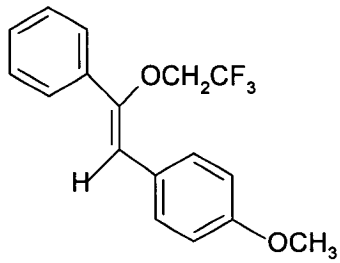

Z-133

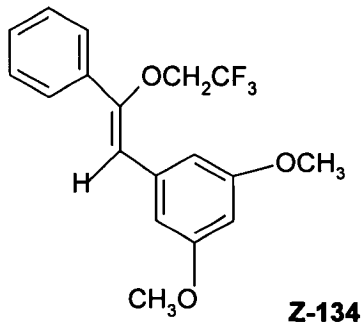

Z-134

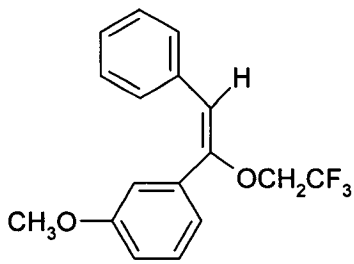

E-135

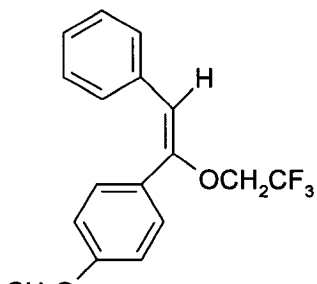

E-136

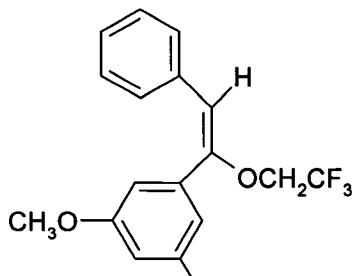

E-137

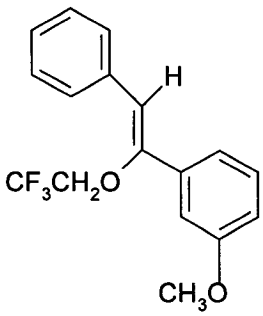

Z-135

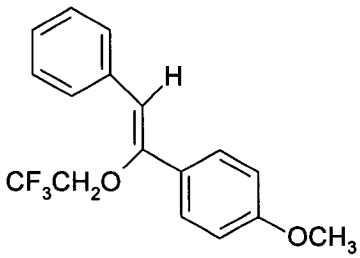

Z-136

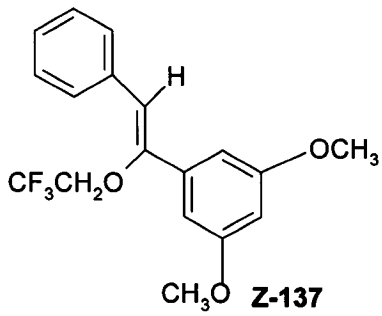

Z-137

Photolysis plots were obtained by monitoring the process by GC-FID. For the photolysis of tolan, two new peaks, **E-** and **Z-131**, were observed with retention times of 13.52 (**E-131**) and 14.62 minutes (**Z-131**), Figure 4.3. The retention time for tolan **11** was 14.34 minutes. Similarly, two sets of two peaks were found for compounds **12 – 14,** as in Figure 4.5. Logically, the two components of each pair represent similar stereochemistry, Z or E isomers, as they only differ from each other in the position of the methoxy substituent on the benzene ring, which presumably does not remarkably affect the boiling point and therefore the GC retention time. The more difficult task was to match each component of the mixture with its vinyl ether isomer.

In order to assign the relative position of the chemical shifts for the olefinic protons of both isomer peaks, the products from the photolysis of tolan **11**, **Z-131** and **E-131**, were separated by column chromatography. The objective of this experiment was to identify which isomer, Z or E, would elute first in the GC–FID, and match this to the chemical shift of the corresponding trans- or cis-olefinic proton. To carry out this assignment, 2D-NOESY spectra of the vinyl ethers, **E-131** and **Z-131**, were obtained, Figures 4.6 and 4.7. The results indicated that the peak with shorter GC retention time corresponded to the E-isomer. This conclusion was reached because of the presence of a cross peak between the signals that corresponds to the proton on the sp^2 carbon of the double bond (5.96 ppm) and the quartet that corresponds to the sp^3 proton from the alkoxy group -CH_2- (4.26 - 4.21 ppm). In addition, this confirms that the olefinic proton from the E-isomer appears at lower chemical shift, 5.96 ppm, compared to the olefinic proton from the Z-isomer at 6.18 ppm. Giving these facts, it is most probable that photolysis products of **12**, **13**, and **14** with shorter retention times correspond to the E-

isomers, and the set with longer retention corresponds to the Z-isomers. ^{1}H NMR spectra of the irradiated samples were done to relate the GC peaks to the isomers. Calculation of the normalized integration of both the signals of the olefinic protons in the ^{1}H NMR and the signals in the GC-FID plot showed that the photolysis products from the compounds **11**, **12,** and **13** have approximately the same integration (normalized with respect to the major component) as the integration of signals of these same components on the GC-FID plot, Table 4.3. The spectra of the photolysis samples from **14** did not provide conclusive information as it was not possible to locate the signals from the very minor component of the mixture, and the signals from the aromatic ring of the 3,5-dimethoxy substituted tolan **14** were mixed with the alkene hydrogen.

Figure 4.2. GC –FID plot for tolan 11 at irradiation

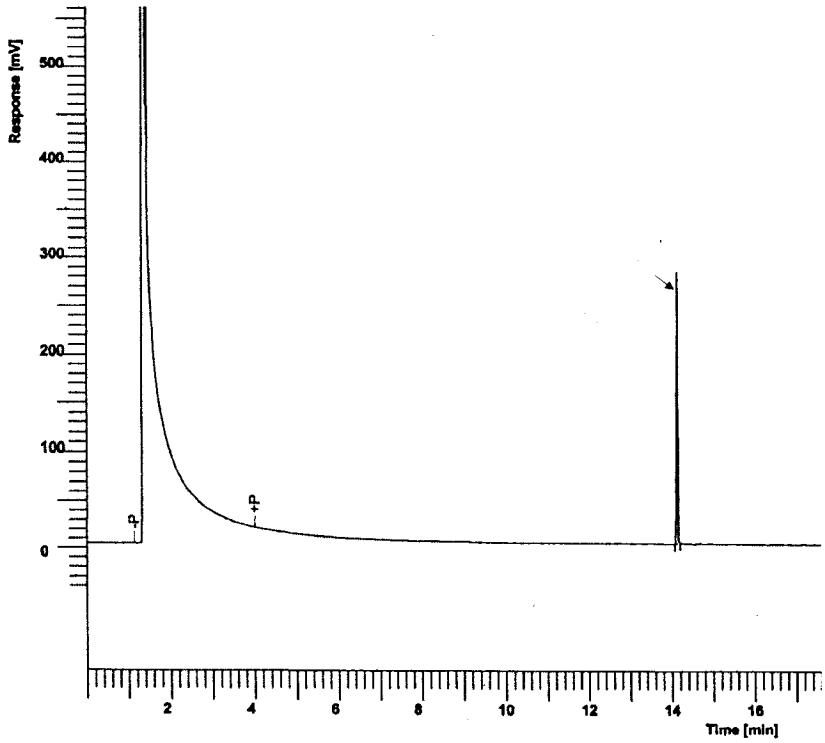

Figure 4.3. GC–FID plot for tolan 11 at irradiation time t_R = 120 minutes in TFE

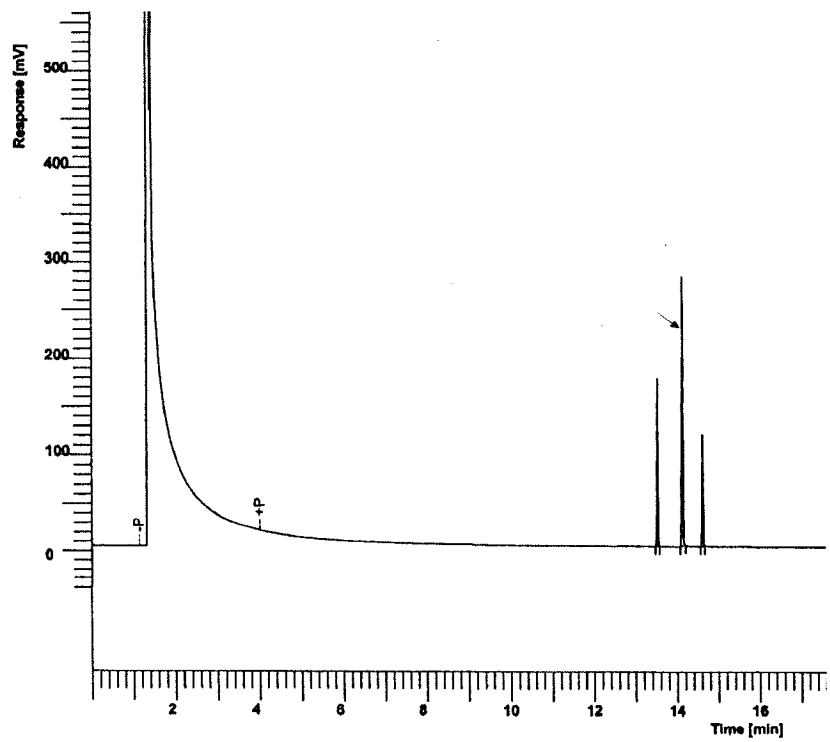

Figure 4.4. GC–FID plot for *m*-methoxytolan 12 at irradiation time $t_R = 0$ in TFE

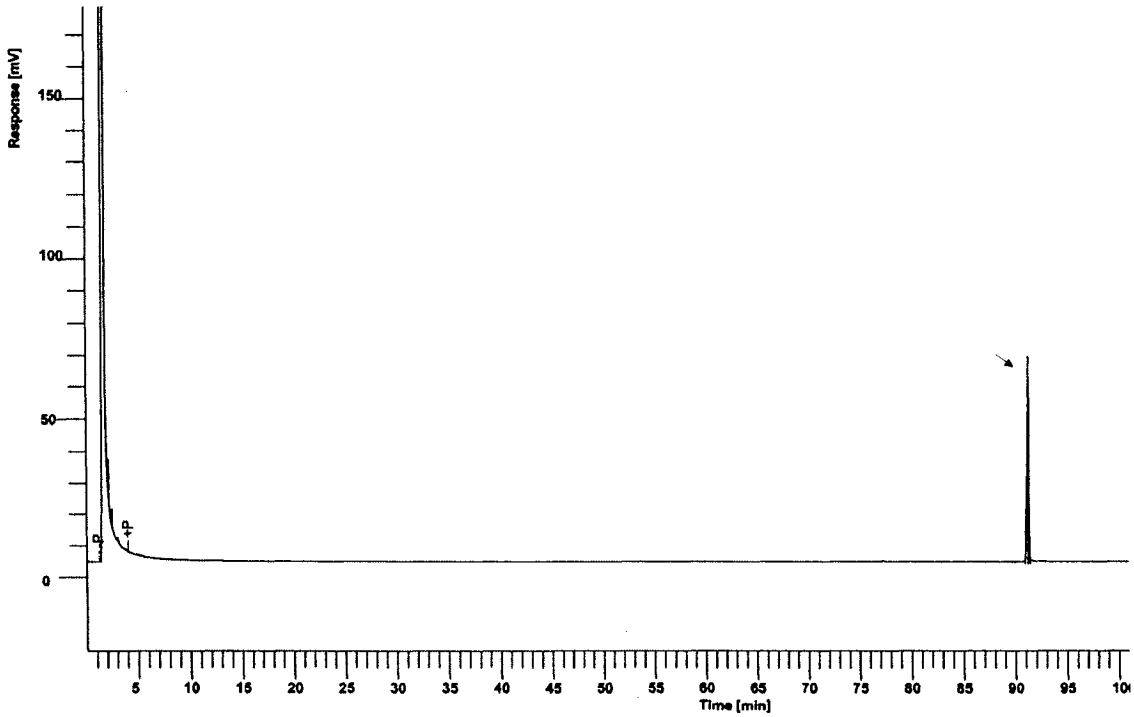

Figure 4.5. GC–FID plot for *m*-methoxytolan and 12 at irradiation time $t_R = 120$ minutes in TFE

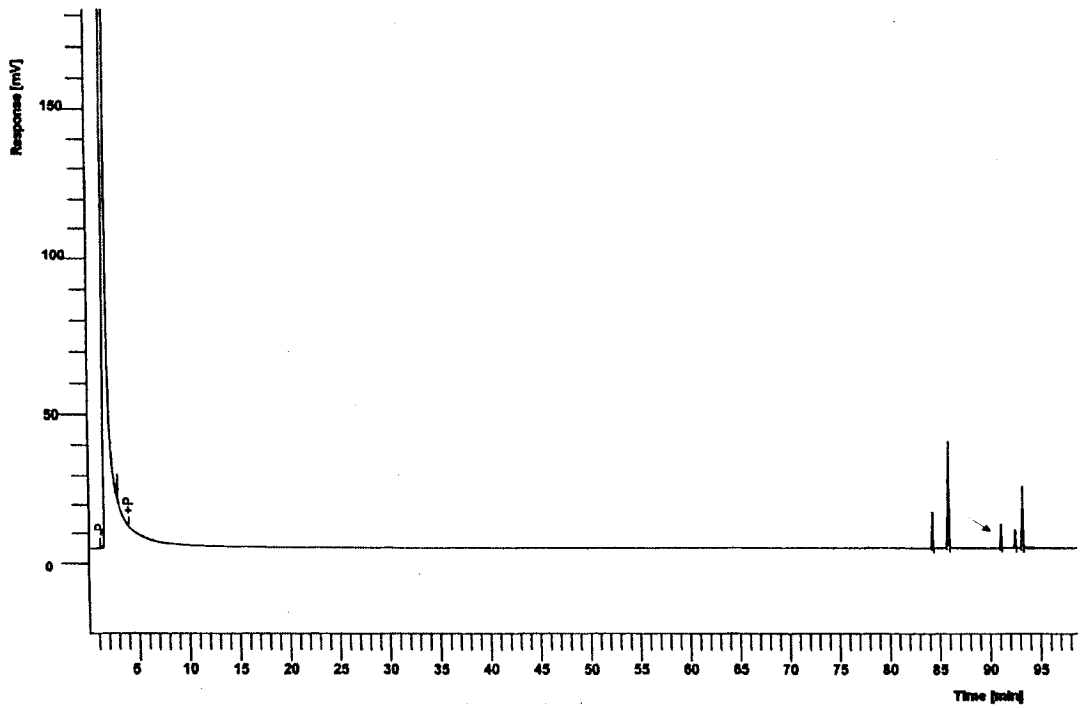

Figure 4.6. 2D-NOESY spectrum for compound E-131 (shorter R_t)

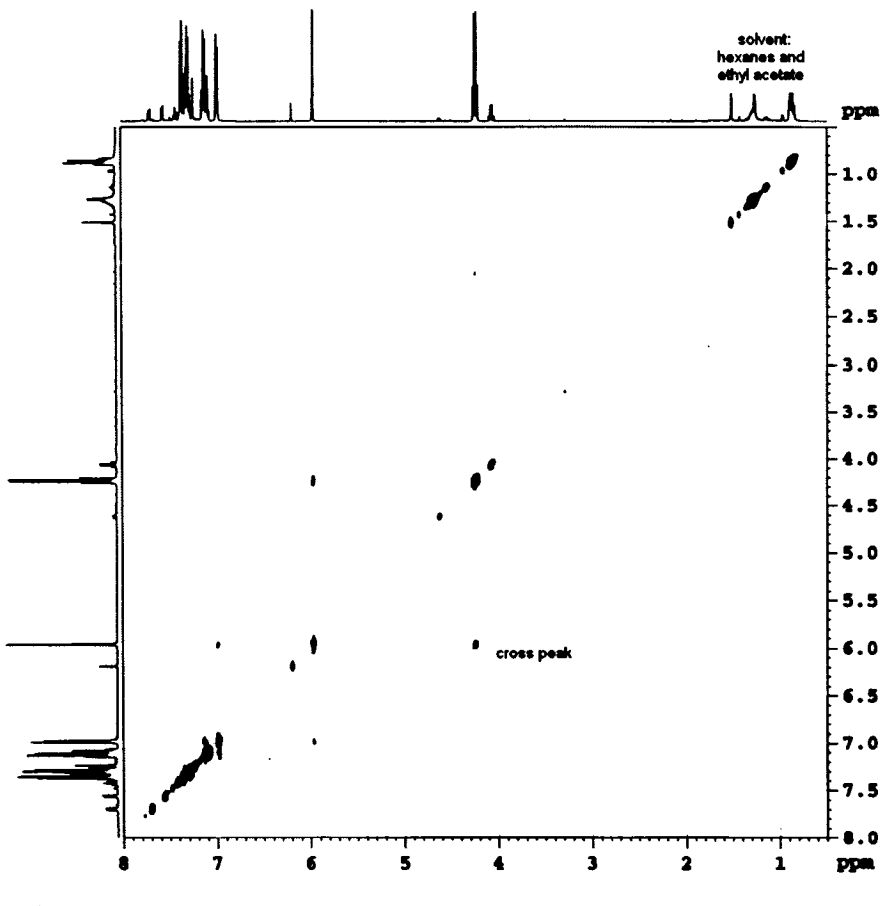

Figure 4.7. 2D-NOESY spectrum for compound Z-131 (longer R_t)

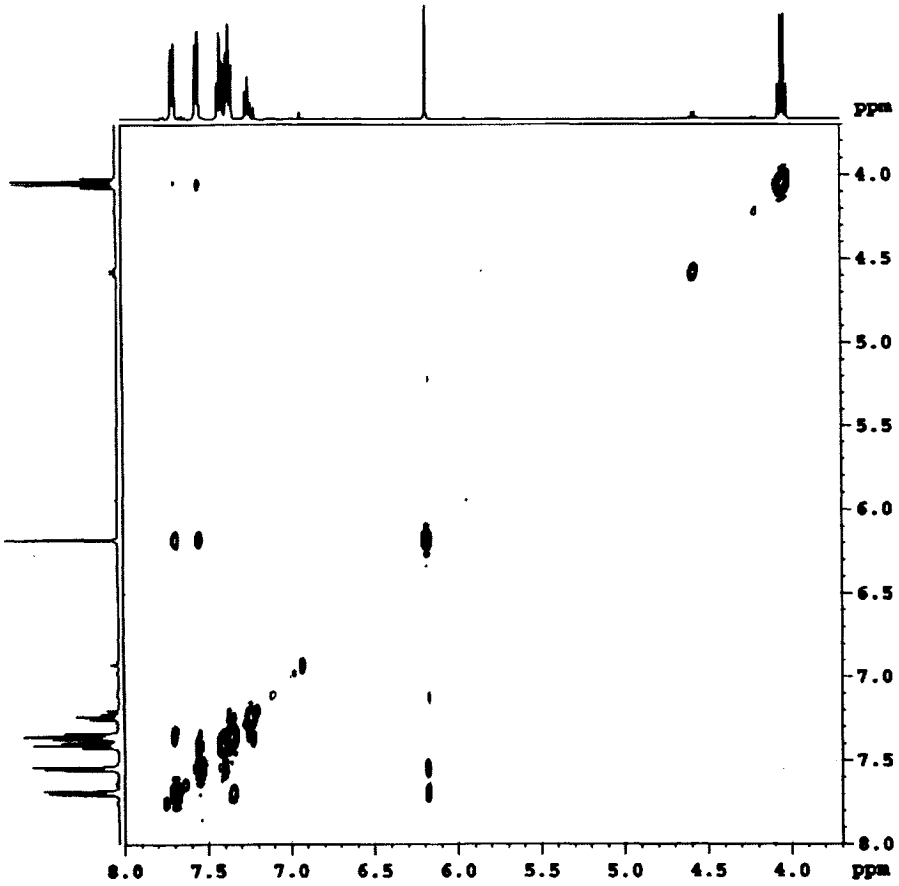

Table 4.3. Product composition calculated by GC-FID and ^{1}H NMR

compound	Normalized integration from GC-FID	Normalized integration from ^{1}H-NMR
11	1 : 0.58[a]	1 : 0.51[a]
12	1 : 0.45 : 0.27 : 0.17[b]	1: 0.41 : 0.24 : 0.10[b]
13	1 : 0.81 : 0.91 : 0.55[b]	1 : 0.60 : 0.84: 0.54[b]

a. The ratio corresponds to the E : Z isomer abundance.
b. The first two values correspond to the E isomers and the last two to the Z isomers.

With the E,Z stereochemistry established, the next task was to establish the regiochemistry of each component of the mixtures. Hydrogenation of the mixtures from the photolysis reactions was done using $PdCl_2$ as a catalyst. Scheme 4.7 shows the hydrogenation process for the 2,2,2-trifluoroethoxy derivatives of **12, 13, 14**. Each one of any given E/Z pair gives a single product. In this way, evidence of the chemical connectivity of the vinyl ethers **132** – **137** is obtained as well. The structures of the expected hydrogenation products have been previously studied by Roberts and Pincock in an investigation on the photochemical addition of TFE to methoxystilbenes, **138** – **140**. [46, 111] They identified the regioisomers of the products in TFE, **141** – **146**, by mass spectrometry, analyzing the fragmentation pattern of such ethers, Scheme 4.8. It is important to point out that in each set of two peaks from the chromatogram (GC–FID), one component has a higher response than the others. It is logical to state that both major components, one Z and one E isomer, arise from the same intermediate, which must be the more abundant of the two possible regioisomeric intermediates, Scheme 4.9. This was proved by analyzing the fragmentation pattern of the reduced samples from the photolysis process, Scheme 4.8.

Scheme 4.7. Products of the reduction process of the vinyl ethers derivatived from compounds 12 – 14

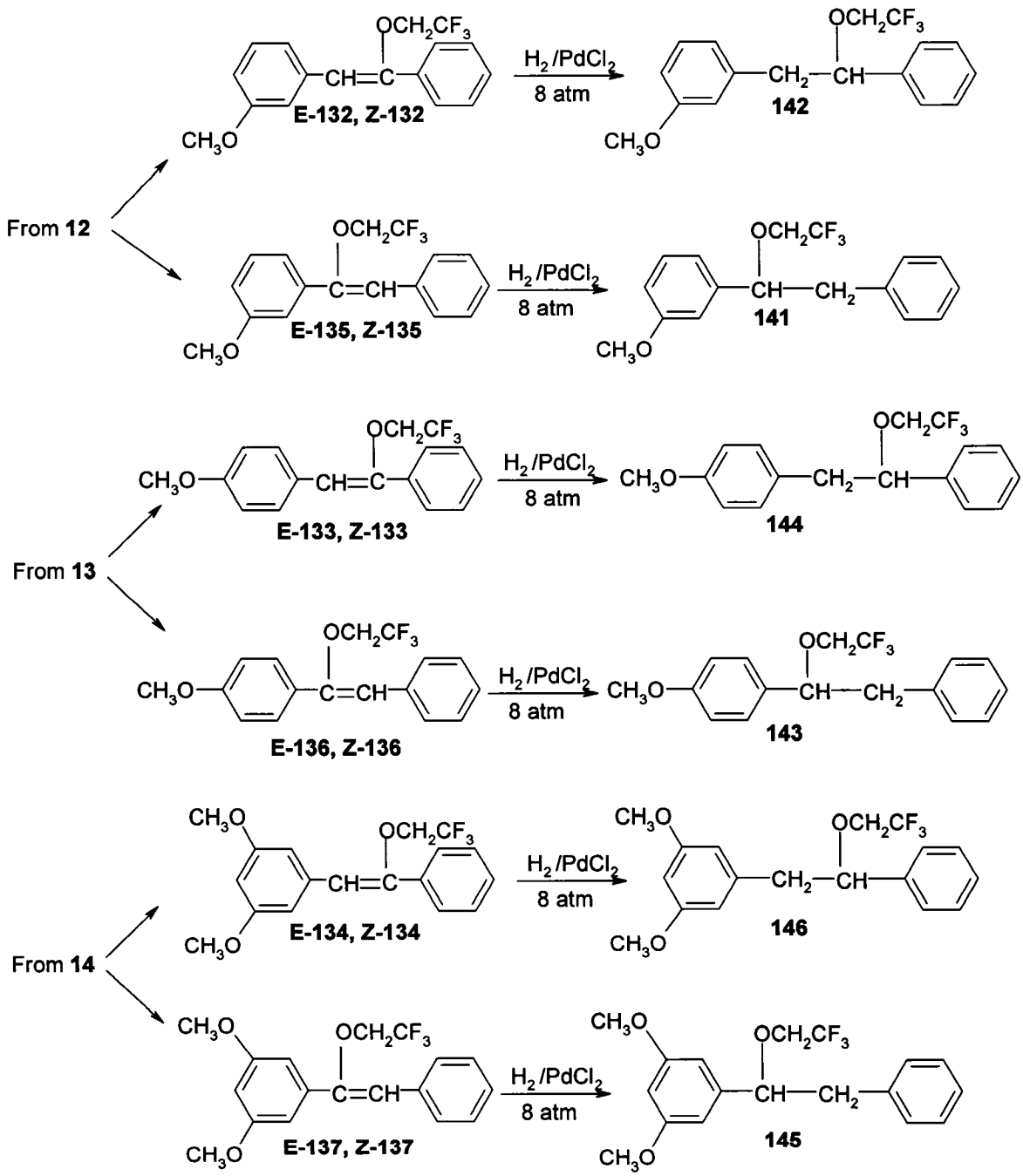

Scheme 4.8. Main fragmentation pattern for ethers 141 - 146

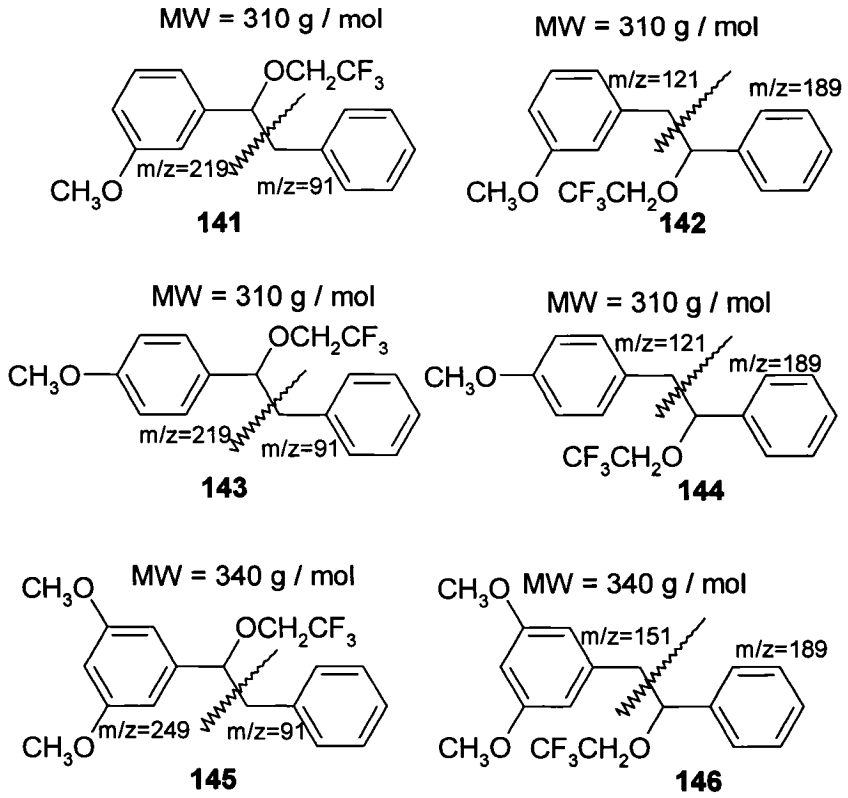

Scheme 4.9. Common intermediate for the most abundant Z/E isomers for 12

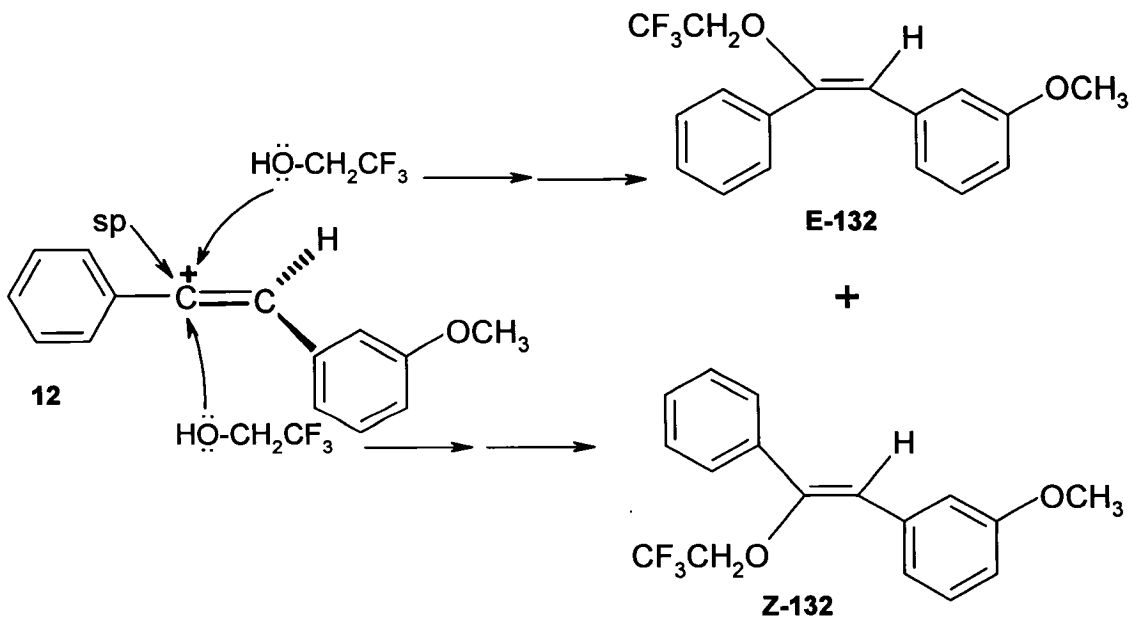

The ethers from the reduction process for **132** – **137** have a fragmentation pattern in which the single C-C bond, connecting the two benzene moieties, cleaves efficiently. The basic idea is that the radical cation of the diaryl ethanes will fragment to give a radical (invisible) and a cation (visible) with a preference for the cation formation on the 2,2,2-trifluoromethoxy fragment. For instance, the GC-MS chromatogram for the hydrogenated sample of the *m*-methoxytolan photolysis addition products showed two signals in a ratio 76:26. For the main component (76 %), the mass spectrum showed the molecular ion (6%) and the base peak with m/z equal to 189; this must be ether **142.** This suggests that the major regioisomers arising from the photolysis of **12** have the alkoxy substituent (CF_3CH_2O-) directly bonded to the carbon attached to the unsubstituted benzene ring. The GC-MS chromatogram for the hydrogenated sample of the *p*-methoxytolan photolysis products showed two signals of m/z equal to 310 in a ratio 59:41. For the main component, the molecular ion was found (3%) as well as a very intense peak of m/z = 219 (68%); this must be ether **143**. In contrast with the results for **12**, this indicates that the major regioisomers arising from the photolysis of **12** have the alkoxy substituent directly bonded to the carbon attached to the methoxy substituted benzene ring. For the analysis of the reduced sample from the photolysis of 3,5-dimethoxytolan **14**, the GC-MS chromatogram showed two peaks in a ratio 88:12, with a molecular ion with m/z equal to 340. The MS of the major component showed a peak of m/z equal to 189 (base peak). This means that the major regioisomers arising from the photolysis of **14** have the alkoxy substituent directly bonded to the carbon attached to the unsubstituted benzene ring. As stated before, a rationalization of these fragmentation

patterns is shown in Scheme 4.8. Plots of product yields *versus* irradiation times are given in Figures 4.8 – 4.11.

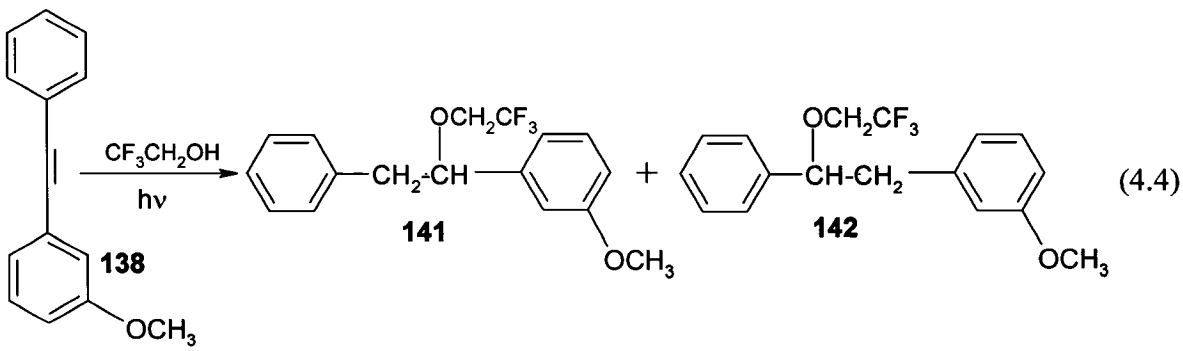

(4.4)

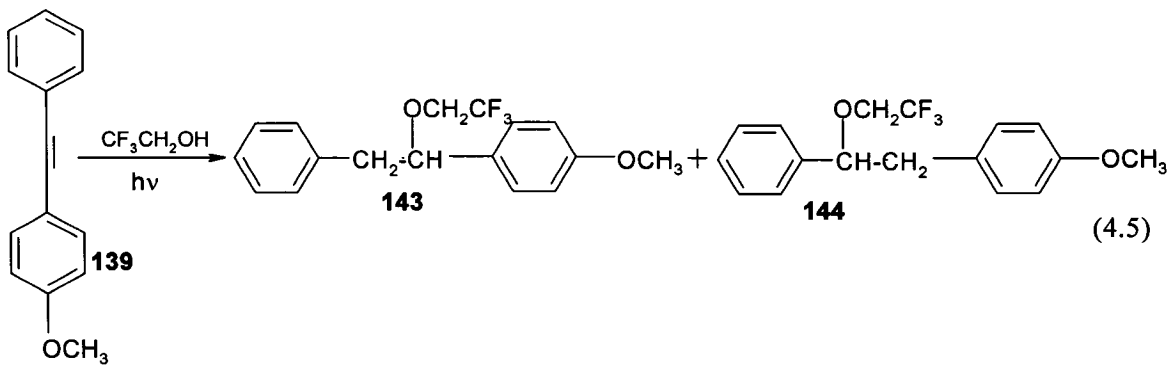

(4.5)

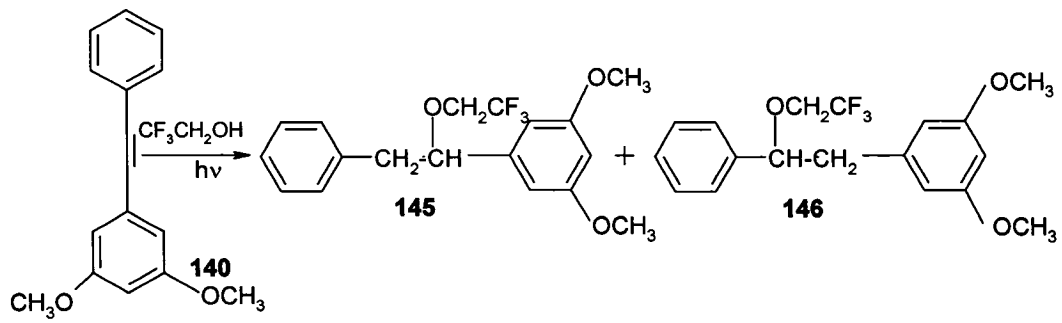

(4.6)

The major E and Z isomer pair in each set was assigned on the basis of their reduction to the most abundant ether. Table 4.4 shows the product distribution at low product conversion (10 %). Table 4.5 shows the product distribution when the irradiation

was stopped. In agreement with the ^1H NMR results for photolysis products of tolan **E-131** and **Z-131**, which as explained before were isolated and characterized, the two peaks at lower retention time were considered to be the E isomers and the last two the Z isomers. Plots of product yields versus irradiation times are given in Figures 4.8 – 4.11.

Table 4.4. Product distribution at 10% of conversion

compound	ratio of product (E : Z)[a]
11	1.7 : 1
12	4.5 : 1 : 3 : 0
13	1.3 : 1 : 1.3 : 0
14	6 : 1 : 2 : 0

a. The first two values correspond to the E isomers and the last two to the Z isomers.

Table 4.5. Relative abundance normalized to 100% of the isomers when the photolyses were stopped

compound	E + Z [a] (methoxy)	E + Z [b] (hydrogen)
11		100 %
12	81.9 %	18.1 %
13	40.5 %	59.5 %
14	85.3 %	14.7 %

a. Nucleophile (CF_3CH_2O-) on the benzylic carbon next to the methoxy substituted ring.
b. Nucleophile (CF_3CH_2O-) on the benzylic carbon next to the unsubstituted ring.

Figure 4.8. Plot of % isomer vs. irradiation time for the photolysis of 11 in TFE

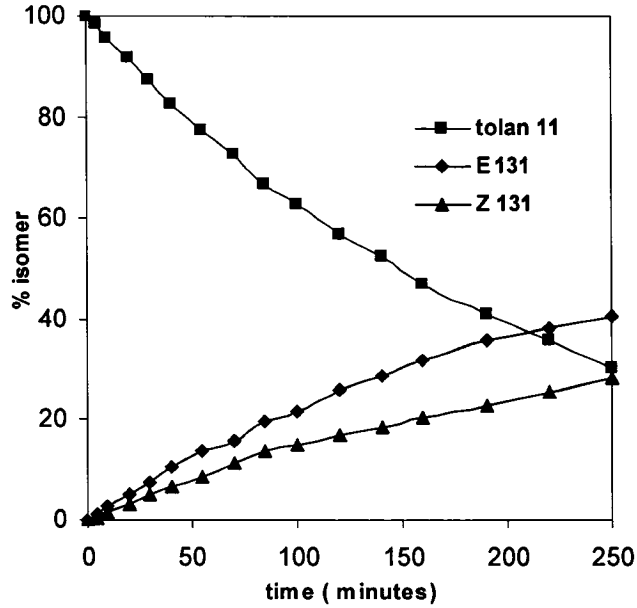

Figure 4.9. Plot of % isomer vs. irradiation time for the photolysis of 12 in TFE

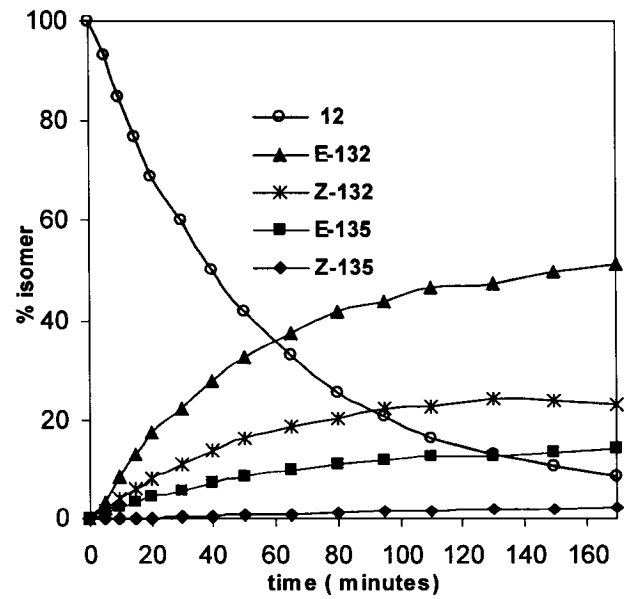

Figure 4.10. Plot of % isomer vs. irradiation time for the photolysis of 13 in TFE

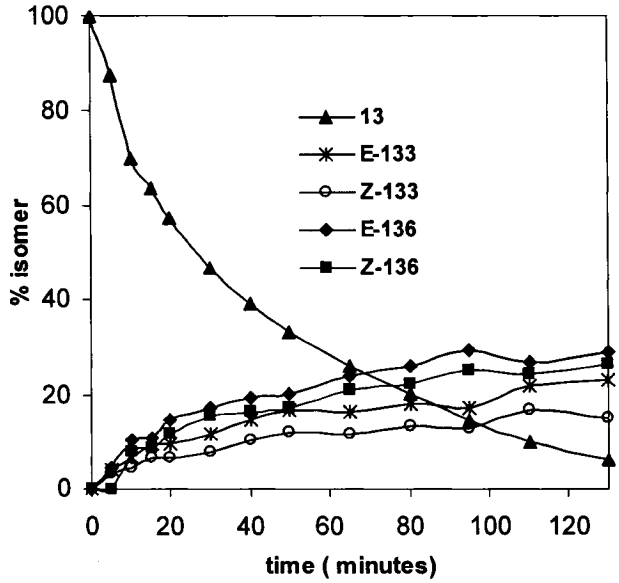

Figure 4.11. Plot of % isomer vs. irradiation time for the photolysis of 14 in TFE

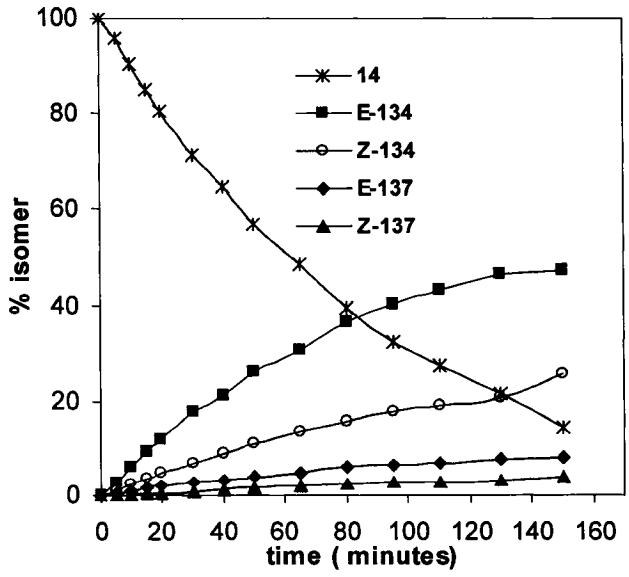

From the photolysis plots, it is apparent that the photoaddition for the methoxy-substituted tolans **12**, **13** and **14** is faster than for tolan **11**. The difference in the relative reactivity of the three methoxy-substituted tolans **12**, **13** and **14** is small because all of them are about 80 % consumed within 120 minutes of irradiation. At photolysis time longer than 120 minutes, it is not safe to make conclusions with respect to the chemical reactivity as a yellowing of the photolysis solution, of different intensities for each isomer, appeared during the process. However, the time taken for 20 % conversion was approximately 16 minutes for **12**, 10 minutes for **13** and 20 minutes for **14**. A better way to estimate the chemical reactivity would be, for example, by means of Stern–Volmer quenching plots.

4.2.5. Details regarding the mechanism for the photochemical addition of alcohols (TFE, TFED, and MeOH) to the excited state of compounds 11–14

In this section, mechanistic details for the reaction pathway of the photochemical addition of 2,2,2–trifluoroethanol (TFE), deuterated 2,2,2–trifluoroethanol TFED, and methanol MeOH to tolans **11–14** will be summarized. As explained in Section 1.3.2, the Stern-Volmer plot, eq. 1.22, is a convenient and powerful tool to estimate lifetimes. However, it is also an indirect method of estimating rate constants for the quenching process which is, in this case, a photochemical reaction of the excited state, and not an energy transfer process. If the lifetime of the excited state being quenched is known, emission–quenching methods are easily carried out and offer the possibility of making Stern-Volmer plots in which the Stern-Volmer coefficient (τ_S x k_Q) can be directly estimated. The only disadvantage of this method, eq. 1.22, is that the excited states being

studied must fluoresce. It is important to point out that fluorescence is not the only property that could be used in estimating either lifetimes or quenching rate constant. Ratios of any process occurring from S_1 (Φ^o_i/Φ_i), including ratios of quantum yields for photochemical products, are candidates for this mechanistic probe, eq. 4.7. In this investigation, the most convenient property is the fluorescence quantum yield as a function of quencher concentration (Q = TFE, TFED, MeOH). The problem with this method is that compounds **11** and **13** do not fluoresce appreciably at room temperature and therefore they cannot be studied. Nevertheless, the mechanistic details that are obtained by studying compounds **12** and **14** presumably apply to their homologues **11** and **13**.

$$\frac{\phi_f^o}{\phi_f} = 1 + \tau_s k_Q [Q] \tag{1.22}$$

$$\frac{\phi_i^o}{\phi_i} = 1 + \tau_s k_Q [Q] \tag{4.7}$$

Plots of Φ^o_f/Φ_f vs. [ROH] were done using a series of ROH/CH_3CN mixtures (0 – 100 %). Figures 4.12 – 4.15 show the Stern – Volmer plots for compounds **12** and **14** using volume percentage of alcohol, % ROH, instead of quencher concentration [Q]. In all cases, at low quencher concentration (or percentage), the plots were linear. The quenching plots for TFE and TFED present considerable upwards curvature at higher percentages of alcohol. This is the result of the change in solvation power of the mixture of solvents, along with the change in % ROH. As the concentration of the quencher increases, the dielectric constant of the medium, as well as its solvation power, changes.

Perhaps the most important consideration is the ionization power of the mixture of solvents (equivalent to the solvation power) and its influence on the stabilization of the transition state of the photochemical addition. The photochemical reaction discussed in this thesis possibly involves charged intermediates, *i.e.* carbocations. The effect of the mixture of solvents on the stabilization of the transition state will be more important as the ionization power increases. The increase of the percentage of alcohol results in an increase in the ionization power of the mixture (Y_{OTs} (AN) = -3.21, Y_{OTs} (TFE) = 0.92, Y_{OTs} (MeOH) = -0.92)[119] and in a more efficient quenching of fluorescence resulting from an increase in the rate constant of the quenching process, as suggested by the strong upwards curvature observed at higher % ROH. This results in a better solvation of the transition states, with a reduction in the activation energy of the process. The nature of the quenching process of the excited states of tolans **12** and **14** is probably a proton transfer followed by rapid trapping of the vinyl carbocations by solvent. Possibly the conjugated base of the alcohols interacts with the vinyl carbocation as well. It is well established that this type of photochemical addition involves an early transition state. Therefore, the interactions between the quencher and the excited state of **12** and **14** (S_2) must be very important in determining the regiochemistry of the process. The nucleophile could be either the conjugate base of the alcohol ($CH_3CH_2O^-$ or CH_3O^-) or the neutral solvent itself because of the formation of both geometric isomers Z and E. In Table 4.3, the Stern-Volmer coefficients and the calculated quenching rate constants are listed.

Figure 4.12. Stern-Volmer plot for m-methoxytolan 12

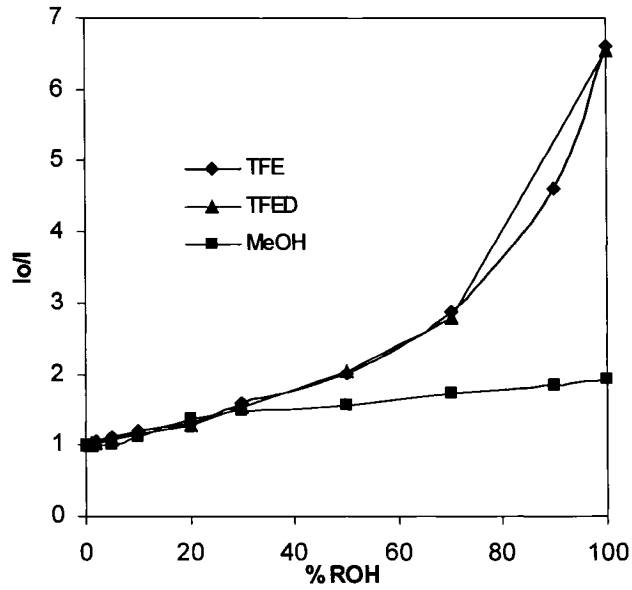

Figure 4.13. Stern-Volmer plot for m-methoxytolan 12 at low quencher concentration

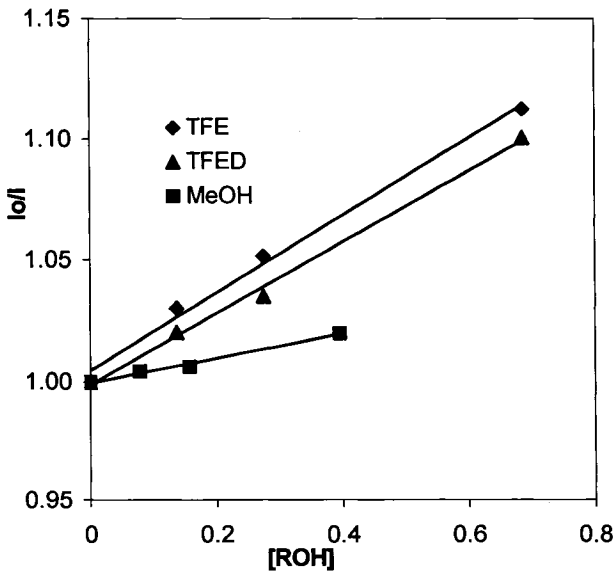

Figure 4.14. Stern-Volmer plot for 3,5-dimethoxytolan 14

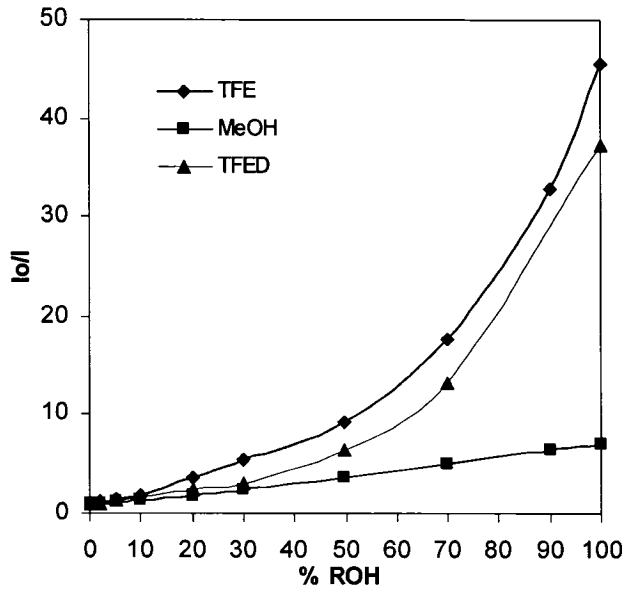

Figure 4.15. Stern-Volmer plot for 3,5-dimethoxytolan 14 at low quencher concentration

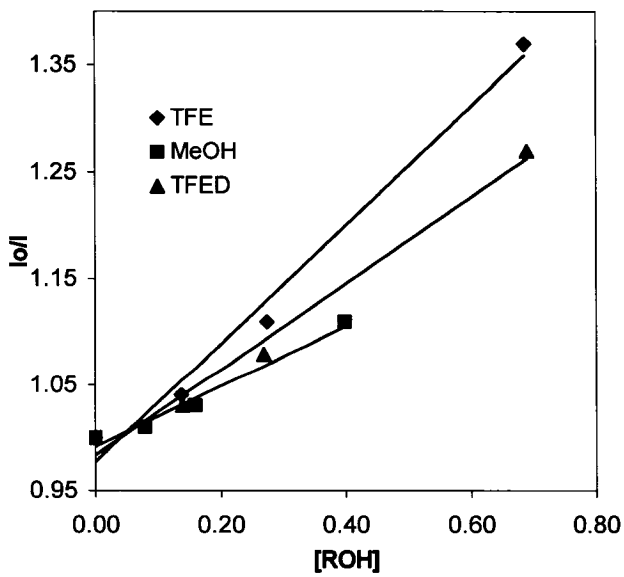

Table 4.6. Stern-Volmer coefficients (C_{sv}), quenching rate constants (k_Q), and isotopic effect ratios (k_H / k_D) for compounds 12 and 14

Compound	C_{sv}^a / M^{-1}	k_Q^a / 10^8 M^{-1} s^{-1}	C_{sv}^b / M^{-1}	k_Q^b / 10^8 M^{-1} s^{-1}	k_H / k_D
12					
TFE	0.16	2.3	1.44	20.6	1.15[a]
TFED	0.14	2.0	0.91	13.0	1.58[b]
MeOH	0.13	1.9	0.11	1.57	
14					
TFE	0.56	1.0	9.26	17.2	1.35[a]
TFED	0.40	0.74	5.79	10.7	1.60[b]
MeOH	0.29	0.54	0.88	1.63	

a. Low quencher concentration.
b. Average slope between the points at the highest quenching concentration:
$k_Q = \{[(I_o/I)_2 - (I_o/I)_1] / (C_2 - C_1)\} / \tau_s$

The calculated isotopic effects indicate that the rate-limiting step for these photochemical reactions is possibly a proton-transfer process. The values of k_H / k_D indicate that the transition state of the process is an early transition state. The calculated values of k_Q are higher in the more acidic alcohol TFE which is the expected result for a process that involves the cleavage of a hydrogen–oxygen bond. The quenching rate constants increase considerably at higher quencher concentration, perhaps as the result of an increase in the ionization power of the solvent, resulting in a better stabilization of the transition states. At both low quencher concentration and high quencher concentration,

the calculated values of k_Q indicate that the processes are near the diffusion-controlled limit. In all the cases investigated, the order of quenching rate constants agrees with the acidity of the quencher. It does not seem that the presence of two methoxy substituents in the meta position with respect to the triple bond enhance the rate of the photochemical reaction although, as explained in Section 4.2.3, it does enhance appreciably the quantum yield of fluorescence. The rate constants for the photochemical addition process k_Q are slightly higher for **12** than for 14.

4.3. Conclusion

The presence of meta methoxy-substituents changes considerably the photophysical properties of the tolan derivatives. First, for **12** and **14,** an enhancement of the quantum yield of fluorescence is observed. Second, the lifetimes of the emitting excited state S_2 of **12** and **14** are longer, in agreement with previous results.[46, 111, 112] The quantum yields of fluorescence for **12**, **13** and **14** are temperature-dependent which, based on previous investigations,[102-104] suggests that an activated internal conversion process occurs, presumably an $S_2 \rightarrow S_1$ internal conversion.

The excited states of compounds **11-14** are photochemically reactive toward the addition of TFE, Figures 4.8 – 4.11. The regiochemistry of this process depends on the substitution pattern. The para methoxy substituent affects the photophysics and photochemistry of these substrates in a form opposite to the meta-methoxy substituent, *i.e.*, very weak fluorescence at room temperature ($\Phi_f < 0.01$), a very fast deactivation rate constant for S_2, as well as a different effect on the electronic configuration of the excited states S_2. The latter, furthermore, affects the regiochemistry of the

photochemically initiated electrophilic addition of TFE (different orientation for the attack of the incoming electrophile **H**-OR). An explanation for the different regiochemistry of the photoadducts as a function of the substitution pattern needs to be addressed. Reactions of the excited states are usually assumed to have an early transition state. The Hammond postulate proposes that, for this type of process, the effects that stabilize the intermediates are less important as the transition state is more like the reactant. This suggests that a kinetic control rather than a thermodynamic control (energy of the intermediate) governs the pathway for the photo-addition reaction discussed in this chapter. The meta-methoxy effect which is, as stated before, an increase in the electron density on the neighbouring meta positions in a benzene ring with methoxy substituents, could increase the electronic density on the carbon atom of the triple bond next to the meta methoxy substituted benzene ring, Scheme 2.10. This could possibly result in a fast proton transfer process, resulting in vinyl carbocations. The final result is a product distribution in which, for compounds **12** and **14**, the alkoxy group is next to the unsubstituted benzene ring. As the same substituent effect does not occur for the *para*-methoxytolan **13**, a different regiochemistry is found for the photolysis process.

Scheme 4.10. Mechanism for the photochemical addition of TFE to *m*-methoxytolan 12

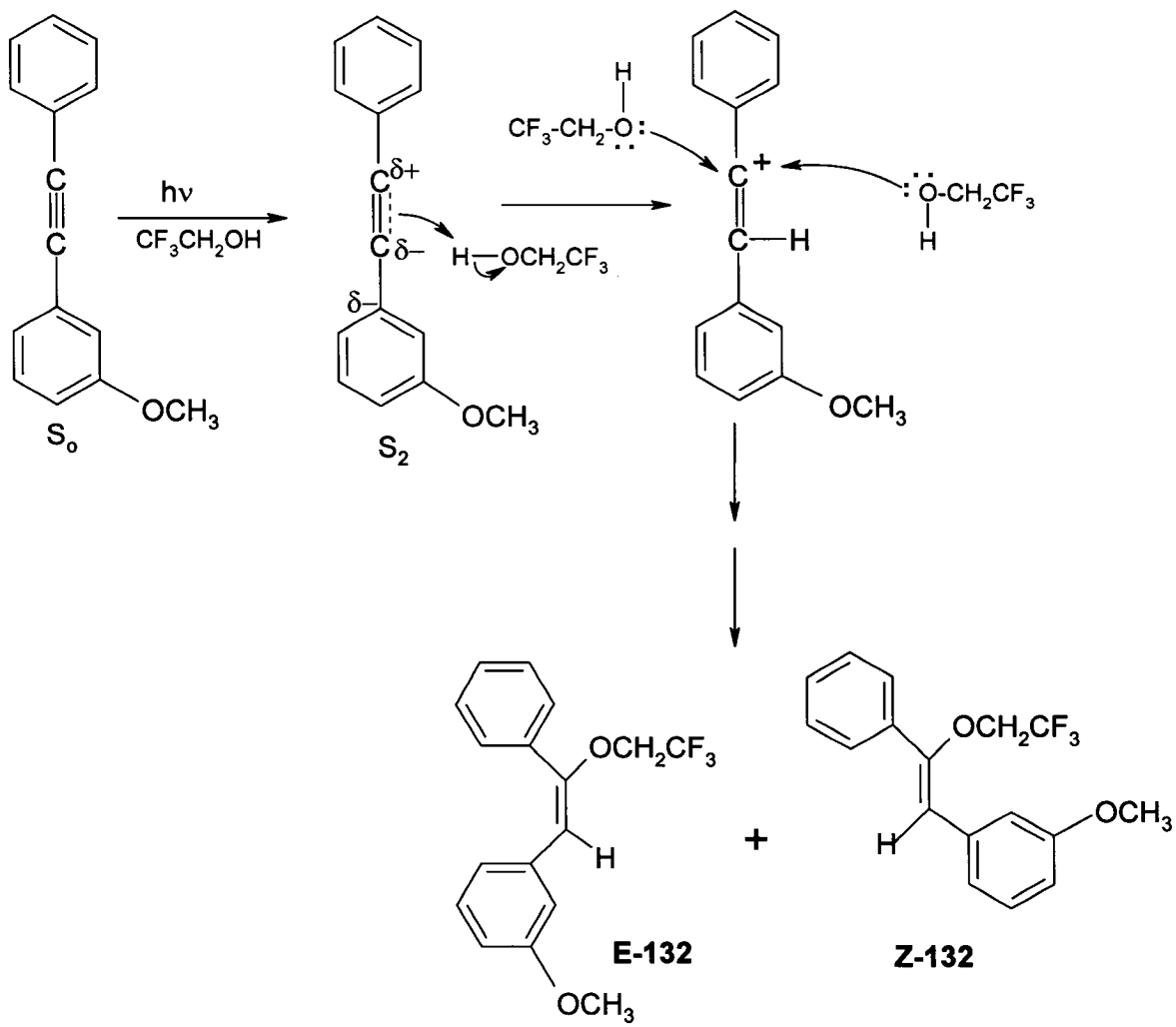

Chapter 5

Experimental Details

This chapter provides details regarding the synthetic procedures and instrumental measurements described in Chapters 2–4. Sections 5.2-5.4 will give experimental details on methods and results related to the corresponding Chapter.

5.1. General experimental methods

5.1.1. Photophysical measurements

Ultraviolet spectra were recorded on a Varian–Cary Bio 100 spectrometer, at 1 nm resolution, using a cuvette of path length of 1 cm with samples thermostated at 25 °C. Baseline correction for the solvent was always done. The fluorescence spectra were recorded with a PTI Model L201M fluorescence spectrometer (steady–state fluorimeter) with dual model 101 monochromators, a 75 W Xenon lamp, and a model 814 photomultiplier detector. All the fluorescence spectra were corrected with respect to the response of the instrument and the intensity of the lamp as a function of the emitted wavelengths. Singlet lifetimes were measured by monitoring fluorescence decay with a time-resolved fluorimeter in the

nanosecond time domain. The time–resolved fluorimeter, model PRA system 3000, was equipped with a hydrogen filled model 510 PRA arc lamp operating at 30000 Hz. The pulse width at half-height was approximately 1.8 ns. The lamp profile was recorded following each measurement to obtain the 'pure' emission profile of the sample by deconvoluting the lamp profile from the sample profile. The temperature was controlled by circulating water or methanol (below 0 °C) from an external constant temperature bath and checked by measurement in the fluorescence cuvette with a digital thermocouple probe. The singlet lifetimes τ_s were determined using the MatLab 6.5 software package. All the fluorescence data (steady-state and time-resolved) were obtained using a cuvette with a path length of 1 cm. All the samples were degassed by three freeze-pump-thaw cycles and then thermostated at the appropriate temperature. Fitting of the k_d ($= 1 / \tau_s$) versus T data, Chapters 2 and 3, was done using the KaleidaGraph program, Version 3.5b5, March 22, 2000, Synergy Software. In Chapter 4, Section 4.2 3, plots of Φ_f versus T were done with Microsoft Excel for Windows XP 2000.

5.1.2. Structure analysis instrumentation

^1H and ^{13}C NMR spectra were recorded in deuterated chloroform on a Bruker AC 250F instrument, Chapter 3, or a Bruker AVANCE 500 MHz instrument, Chapter 4. Chemical shifts δ are reported as parts per million (ppm) relative to the tetramethylsilane internal standard. Gas chromatography was performed on a Perkin-Elmer Autosystem XL instrument (controlled by a computer with TurboMass and TurboChrom software) with one Turbomass detector and one flame ionization detector (both columns: Supelco 30 m / 0.25 mm MDN-5S 5% phenyl methylsiloxane, film thickness 0.50 μm). For GC-MS, the

injection volume was 3 μL with no attenuation in the response of the instrument; mass spectral data are reported as mass to charge ratios (*m/z*) with intensities relative to the base peak (100 %). For characterization purposes, the temperature program used was: 60 °C / 1min.; 20 °C / min. to 240 °C; 240 °C / 10 min. For GC-FID, the injection volume was 5 μL. For the photolysis plots, several temperature programs were used in order to resolve the signals of isomeric compounds with very similar retention time. The photolysis plots were done, in all cases, using Microsoft Excel for Windows XP 2000.

5.1.3. Laboratory solvents and chromatography solid supports

For synthesis procedures and preparative column chromatography, solvents such as methanol, ethyl acetate, and hexanes were all distilled prior to use. Dichloromethane, benzene, diethyl ether and 2,2,2-trifluoroethanol were all reagent grade solvents that were used without further purification. For photochemical studies, acetonitrile, methanol, and 2,2,2-trifluoroethanol were all spectrophotometric or HPLC grade solvents. All starting materials required for synthesis were supplied by Aldrich Chemicals unless a different provider is reported. Thin layer chromatography was performed using plates from Eastman-Kodak. Preparative chromatography was performed using 60-250 mesh silica gel from Silicycle. Separation of both 5- and 6-amino tetralin, Section 3.2.1, was carried out by column chromatography with Florisil (Fisher Scientific Company) as the stationary phase.

5.1.4. Determination of fluorescence quantum yields

For the measurement of fluorescence quantum yields, the standard used, anisole, was purified twice by a bulb-to-bulb vacuum distillation from a reagent grade sample. The actual equation used to determine the fluorescence quantum yield is one derived from eq.1.16, in which the fluorescence quantum yield of a standard is used to compare the emission intensities of both the standard and the sample at a particular wavelength in which both solutions have the same absorbance, eq. 5.1.

$$\Phi_f = \frac{I_f}{I_{abs}} \tag{1.16}$$

$$\Phi_f = \frac{I_f(sample)}{I_f(standard)} x \Phi_f(standard) \tag{5.1}$$

The fluorescence quantum yield of the standard is the corrected one with respect to the refraction index and was determined in cyclohexane (Φ_f= 0.24).

5.2. Procedures for Chapter 2

5.2.1. Irradiation procedures

Solutions of **1o,m,p** and **3o,m,p** of approximately 90 mg of the compound in 100 mL of acetonitrile were purged with nitrogen and then irradiated in a Rayonet photochemical reactor using 16 lamps (75 W, 254 nm). The temperature was controlled at the desired value (25°C and 50°C) by circulating water in an immersion tube. The solution was stirred during

the irradiation. The reaction progress was monitored by GC-MS. Samples taken during the photolysis were analyzed by GC-FID to determine percentage of products. The photolysis plots are displayed in Excel charts.

5.2.2. Photophysical characterization procedures

The ϵ_{max} values for compounds **1**, **2**, **3** and **4**, Table 2.1, were calculated at the maximum excitation wavelength using the absorbance spectra. All the solutions had an absorbance between 0.2 and 0.3. The integrated spectra needed to obtain the k_f^{calc} values from eq. 1.21 were obtained by summing the 1 nm incremental areas (the absorbance values were converted to ϵ by dividing by the molar concentration) over the complete absorption band $S_0 \rightarrow S_1$. These areas are somewhat uncertain at the short wavelength end because of overlap with the long wavelength tail of the S_2 band, hence the absorbance does not reach zero. Therefore, the wavelength for the minimum in absorbance was used as the cut-off point for the S_1 band. To calculate $\int \varepsilon \, d \, ln$, the trapezoidal method for the calculation of the area under a curve was used.

The fluorescence spectra for all the twelve compounds, **1, 2, 3, 4o,m,p**, were obtained using the same solutions as for the calculation of ϵ and k_f from eq.1.12.

The $E_{0,0}$ listed in Table 2.1 were calculated using Planck's equation, eq. 5.2. The values of $\lambda_{0,0}$ (zero-zero band) for calculation of $E_{0,0}$ were the wavelength of overlap for the normalized excitation and fluorescence spectra.

$$E_{0,0} = h\,\nu_{0,0}\,N = h\frac{c}{\lambda_{o,o}}N \qquad (5.2)$$

$N = 6.02\ 10^{23}\ mol^{-1}$

5.3. Procedures for Chapter 3

5.3.1. Synthetic procedures and characterization of compounds 7-10

Compounds **7**, **8** and **9** were synthetisized from the commercially available amines **147-149**; the amine precursor of **10** was prepared by a nitration followed by reduction with Sn/HCl. The cyanoderivatives **7-10** were synthetized by diazotization followed by reaction with cuprous cyanide according to the Samdmeyer procedure,[120] Scheme 3.3. First, a solution of CuCN in water was prepared as follows: a solution of $Na_2S_2O_7$ (0.008 mol) and NaOH (0.01 mol) in 10 mL of water was added to a solution of $CuSO_4x5H_2O$ (0.016 mol) and NaCl (0.019 mol) in 20 mL of hot water. To this was added a solution of potassium cyanide (0.043 mol) in water (8 mL). The aqueous phase was decanted from the solid; 8 mL of water was then added to the solid and the mixture was chilled to 0 °C. The preparation of the diazonium salt of the amine precursors of **7**, **8, 9**, and **147-149** was done as follows: a solution of $NaNO_2$ (0.012 mol) in 2 mL of water was added dropwise to the hydrochloric salts of **147-149**, which were prepared by adding 3 mL of concentrated hydrochloric acid and 5 mL of water to 0.012 mol of the corresponding amine. This mixture was neutralized with sodium carbonate. Next, to a mixture of the CuCN solution and toluene (10 mL) at 0 °C, was added dropwise the diazonium salt solution, keeping the temperature below 5 °C. After the addition, the mixture was allowed to warm to room temperature, then heated to 50-60 °C for 1 hour, and then left at room temperature over an 18-hour period. The resulting reaction

mixture was filtered and the solid residue washed with diethyl ether. The filtrate was then extracted several times with diethyl ether. The combined diethyl ether solutions were washed with saturated NH_4Cl solution, dried with Na_2SO_4, and concentrated *in vacuo*. The residue was purified twice by column chromatography on silica gel using 0.5 % of ethyl acetate in hexanes as eluant. Finally, the product was distilled by bulb-bulb vacuum distillation. The final yield of product was 18-21%.

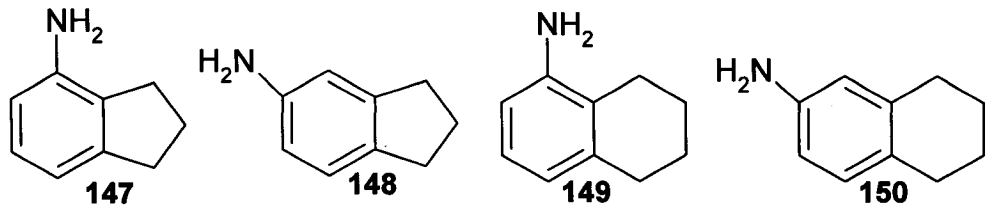

147 **148** **149** **150**

The amine precursor for **10** was prepared by nitration of tetralin, follows by reduction of the mixture of 5- and 6-nitrotetralin to the mixture of amines with Sn/HCl, and separation of the amines by column chromatography with Florisil and 1% ethyl acetate in hexanes as eluant.

The preparation of the nitro derivatives of tetralin, **151** and **152**, was done as follows:[121] 35 mL of concentrated HNO_3 was placed in a 500mL round-bottom flask immersed in ice water bath and equipped with a magnetic stirrer, and then 40 mL of concentrated H_2SO_4 was added in small portions. Benzene (30 mL) was introduced in portions of 2-3 mL. The temperature was kept below 55 °C. The mixture was refluxed at 60 °C for 45 minutes. The reaction mixture was transferred into a beaker containing 500 mL of cold water (~10°C), and the beaker contents were stirred vigorously. The layers were decanted as much as possible. The organic material was transferred to a separatory funnel to

remove the rest of the acidic solution. The organic layer was washed with water (2 x 50 ml) and dried with 5g of $CaCl_2$. The yield of the mixture of isomers was 81%.

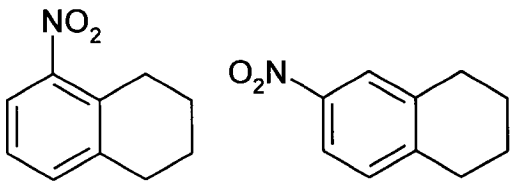

151 **152**

The reduction of the mixture of nitrotetralins was done as follows:[122] To a round-bottom flask equipped with magnetic stirrer and reflux condenser and containing the mixture of nitrotetralins (0.12 moles), and 12 g of granulated tin, 30 ml of concentrated hydrochloric acid was added in small portions. After 10 minutes, the reaction was refluxed at 100 °C until the nitro compound was consumed. When the reaction ended, the mixture of hydrochloric salts of the aminotetralins was made alkaline with 20% NaOH solution. The amines were isolated by steam distillation. Finally, the mixture of 5- and 6-aminotetralin was separated, as explained above, by column chromatography with Florisil.

4-cyanoindan, **7**: ^{1}H NMR ($CDCl_3$) δ 7.39-7.43 (2H, m), 7.18-7.24 (1H, m), 3.10 (2H, t, J = 7.3 Hz), 2.98 (2H, t, J = 7.3 Hz), 2.18 (2H, quintet, J = 7.3 Hz); ^{13}C NMR ($CDCl_3$) δ 24.6, 32.4, 32.9, 108.5, 118.1 (-CN), 126.8, 128.8, 129.5, 145.6, 148.3; m/z (GC-MS):144 (38), 143 (93), 142 (100), 141 (21), 140 (66), 117 (32), 116 (77), 115 (86), 114 (32), 113 (31), 103 (13), 102 (10), 91 (12), 90 (18), 89 (60), 88 (27), 87 (22), 86 (11), 77 (18), 76 (230), 60 (26), 74 (17), 71 (72), 65 (22), 64 (25), 63 (61), 62 (38), 61 (14), 59 (16), 57 (430), 52 (150, 51 945), 50 (21); HRMS calculated for $C_{10}H_9N$: 143.0735; found: 143.0728.

5-cyanoindan, **8**: ^{1}H NMR ($CDCl_3$) δ 7.48 (1H, s), 7.42 (1H, d, J = 8.0 Hz), 7.30 (1H, d, J = 8.0 Hz), 2.93-2.96 (4H, m), 2.12 (2H, quintet, J = 7.0 Hz); ^{13}C NMR ($CDCl_3$) δ 25.1, 32.6, 33.2, 109.7, 119.6 (-CN), 125.1, 127.9, 130.3, 145.4, 150.0; m/z (GC-MS):144 (10), 143 (100), 142 (98), 140 (20), 116 (49), 115 (50), 114 (10), 89 (19), 71 (10), 63 (23), 62 (13), 51 (16); HRMS calculated for $C_{10}H_9N$: 143.0735; found: 143.0732.

The nitrotetralins **151** and **152** were identified by comparing the corresponding mass spectra of the peaks from the GC-MS with those for the 5- and 6-nitrotetralins reported in the NIST Library and Chemical Structures V1.0 Micromass LTD. 1998, (for 5-nitrotetralin **151,** reference number 16913, for 6-nitrotetralin **152**, reference number 16897).

5-nitrotetralin **151**: m/z (GC-MS): 177 (12), 160 (34), 159 (64), 132 (37), 130 (100), 128 (46), 127 (22), 114 (45), 115 (64), 105 (13), 104 (21), 103 (22), 92 (9), 91 (55), 89 (21), 78 (14), 77 (41), 76 (9), 65 (18), 63 (24), 53 (12), 51 (29).

6-nitrotetralin **152**: m/z (GC-MS): 178 (11), 177 (100), 161 (11), 160 (70), 149 (21), 147 (18), 132 (9), 131 (75), 130 (55), 129 (37), 128 (30), 127 (14), 116 (33), 115 (55), 103 (24), 102 (13), 92 (8), 91 (99), 89 (12), 77 (42), 76 (9), 65 (16), 63 (26), 53 (16), 51 (29).

5-cyanotetralin, **9**: ^{1}H NMR ($CDCl_3$) δ 7.43 (1H, d, J = 7.5 Hz), 7.27 (1H, d, J = 8.0 Hz), 7.16 (1H, t, J = 7.5 Hz), 2.95 (2H, t, J = 6.0 Hz), 2.78 (2H, t, J = 6.0 Hz), 1.89-1.79 (4H, m); ^{13}C NMR ($CDCl_3$) δ 22.5, 22.5, 28.0, 29.7, 112.7 (-CN), 118.2, 125.8, 130.2, 133.6, 138.7, 140.8. m/z (GC-MS):157 (61), 156 (26), 142 (17), 130 (13), 129 (100), 128 (14), 116 (19); HRMS

calculated. for $C_{11}H_{11}N$: 157.0891; found: 157.0897.

6-cyanotetralin, **10**: ^{1}H NMR ($CDCl_3$) δ 7.33- .34 (2H, m), 7.13 (1H, d, J = 8.5 Hz), 2.77-2.80 (4H, m), 1.79-1 83 (4H, m); ^{13}C NMR ($CDCl_3$) δ 22.6 (two signals), 29.0, 29.7, 109.1 (-CN), 119.4, 128.9, 129.9, 132.8, 138.5, 143.0; m/z (GC-MS):159 (21), 158 (86), 157 (86), 156 (68), 154 (11), 142 (58), 141 (11), 140 (30), 130 (42), 129 (100), 128 (56), 127 32), 126 (13), 117 (12), 116 (73), 115 (34), 114 (12), 103 (28), 102 (53), 101 (20), 89 (33), 88 (10) 78 (25), 77 (49), 76 (32), 75 (27), 74 (15), 71 (10), 65 (14), 64 (24), 63 (47), 62 (16), 52 (17), 51 (50), 50 (22); HRMS calculated for $C_{11}H_{11}N$: 157.0891; found: 157.0896.

5.3.2. Irradiation and photophysical characterization procedures

Irradiations and photophysical characterization were carried out using the same experimental methods and instruments that were described for Chapter 2 in Sections 5.2.1 and 5.2.2.

The Stern-Volmer plots for compounds **5** and **6** were done using 2,3-dimethyl-1,3-butadiene as a quencher. For this experiment, solutions of identical cyano-derivative concentration with different quencher concentrations were prepared. Plots of I_f ([Q]=0)/I_f were linear with respect to [Q]. The slope of the line divided by the lifetime gives the kinetic rate constant for the quenching process k_Q.

5.4. Procedures for Chapter 4

5.4.1 Synthetic procedures and characterization for compounds 12-14

The methoxy-substituted tolans **12** – **14** were prepared by the Sonogashira coupling method.[115, 116] A solution of triethylamine (20 mL), phenylacetylene (8.8 mmol), and THF (20 mL) was added by means of a canula to a solution of the iododerivative, **128** - **130**, (9.0 mmol), $PdCl_2$ (0.4 mmol), PPh_3 (0.7 mmol), and CuI (0.7 mmol) in THF. The mixture was stirred for 24 hours at RT and at 35 °C for 1hour. The product was purified by column chromatography (silica gel) twice, using 5% ethyl acetate in hexanes as eluent. The solid was crystalized from a mixture of water/ethanol (80 : 20), and the liquid 3,5-dimethoxytolan **14** by microvaccumm distillation.

The iodo-substituted anisoles **128** and **129** were commercially available (Merck). They were purified by column chromatography using silica gel as stationary phase and 5 % ethyl acetate in hexanes as eluant. 1-iodo-3,5-dimethoxybenzene **130** was prepared by diazotization of 3,4-dimethoxyaniline, followed by reaction of the diazonium salt with KI. The synthesis procedure used is as follows: the hydrochloric salt of 3,5-dimethoxyaniline **152** was prepared using 0.013 mole of the amine, 6 mL of concentrated HCl, and 6 mL of water. This mixture was cooled to 0 °C. A solution of $NaNO_2$ was prepared with 0.02 mole of the salt and 8 mL of water. The $NaNO_2$ solution was added dropwise to the hydrochloric salt of 3,4-dimethoxyaniline. The temperature was kept about 5 °C. The solution of the diazonium salt was added dropwise to a solution of 0.02 mole of KI and 10 mL of water in a 25 mL round-bottom flask equipped with a magnetic stirrer. The reaction mixture was allowed to stand for 12 hours. The iododerivative was separated by steam distillation. The distillated was transferred to a separatory funnel and the organic layer separated. Diethyl ether (20 mL)

was added to the iodo derivative and the solution was dried with $CaCl_2$. After filtration, the solution was concentrated *in vacuo*. The yield of product was 80 %.

m-methoxytolan **12** (1-(3-methoxypheny)-2-phenylethyne). Yield 87 %; ^{1}H-NMR ($CDCl_3$) δ 3.82 (s, 3H), δ 6.88-6.91 (ddd, 1H), δ 7.06-7.08 (dd, 1H), δ 7.12-7.14 (dt, 1H), δ 7.24-7.27 (t, 1H), δ 7.33-7.36 (m, 3H) δ 7.52-7.54 (m, 2H). ^{13}C NMR ($CDCl_3$) 55.33, 89.22, 89.33, 114.98, 116.39, 123.24, 124.22, 124.31, 128.32, 128.37, 129.43, 131.66, 159.40; m/z (GC-MS): 209 (16), 208 (100), 179 (8), 178 (30), 165 (34), 164 (14), 163 (13), 152 (6), 139 (11), 126 (6), 115 (6), 89 (4), 87 (4), 77 (2), 74 (4), 63 (7), 62 (3); m. p.: 72 - 74 °C.

p-methoxytolan **13** (1-(4-methoxyphenyl)-2-phenylethyne). Yield 81%; ^{1}H-NMR ($CDCl_3$) δ 3.83 (s, 3H), δ 6.86-6,89 (m,1H), δ 7.26 (s, 1H) δ 7.30-7.35 (m, 3H), δ 7.48–7.46 (m, 1H), δ 7.46–7.48 (dd, 1H), δ 7.49–7.52(m, 2H). ^{13}C NMR ($CDCl_3$) 55.33, 89.38, 114.03, 115.44, 123.64, 127.4, 128.32, 131.48, 133.08, 159.66.; m/z (GC-MS): 209 (17), 208 (100), 194 (9), 193 (63), 176 (4), 166 (6), 165 (58), 164 (20), 163 (14), 150 (4), 139 (17), 126 (5), 115 (20), 104 (6), 98 (4), 89 (5), 88 (5), 87 (7), 86 (5), 75 (4), 74 (5), 63 (10), 62 (3), 51 (5); m.p. 56-59 °C.

1-iodo-3,5-dimethoxybenzene **130**. Yield 86 %; m/z (GC-MS): 265 (27), 264 (100), 248 (2), 235 (3), 234 (22), 233 (10), 222 (2), 221 (36), 218 (13), 206 (4), 205 (4), 203 (5), 191 (4), 177 (4), 165 (3), 152 (3), 138 (9), 137 (64), 136 (19), 132 (15), 127 (40), 123 (16), 122 (87), 110 (3), 109 (37), 108 (68), 107 (74), 106 (12), 105 (5), 95 (4), 94 (48), 93 (15), 92 (55), 91 (24), 90 (4), 81 (5), 80 (7), 79 (66), 78 (37), 77 (70), 76 (13), 75

(19), 74 (30), 73 (7), 69 (68), 66 (55), 65 (24), 64 (47), 63 (71), 62 (62), 61 (34), 59 (18),54 (33), 51 (65); m.p.: 74-75 °C.

3,5-dimethoxytolan **14** (1-(3,5-dimethoxyphenyl)-2-phenylethyne). Yield 78 %; ^{1}H-NMR ($CDCl_3$) δ 3.80 (s, 6H), δ 6.46-6.47 (t, 1H), δ 6.69–6.70 (d, 2H), δ 7.32–7.36 (m, 3H) δ 7.52–7.54 (m, 2H). ^{13}C NMR ($CDCl_3$) 55.46, 89.40, 89.97, 101.89, 109.42, 123.15, 124.60, 128.38, 131.69, 160.60; m/z (GC-MS): 239 (20), 164 (100), 210 (4), 209 (27), 208 (15), 207 (4), 195 (10), 194 (23), 193 (2), 180 (7), 179 (10), 178 (30), 177(8), 176 (5), 167 (3), 166 (12), 165 (37), 164 (9), 163 (13), 153 (5), 152 (38), 151 (14), 150 (7), 139 (7), 127 (4), 126 (29), 119 (20), 115 (7), 102 (5), 98 (7), 91 (21), 89 (9), 82 (7), 76 (9), 75 (5), 74 (4), 63 (7), 51 (3).

5.4.2. Irradiation and photophysical characterization procedures for Chapter 4

Irradiations and photophysical characterization were carried out using the same experimental methods and instruments that were described for Chapter 2 in Sections 5.3.1 and 5.2.2.

The Stern-Volmer plots for compounds **12** and **14** were done using solutions of identical tolan derivative concentration. The slope of the curve divided by the lifetime gives the kinetic rate constant for the quenching process.

5.4.3. Products of photochemistry of tolans 12 - 14

The *E*- and *Z*-1-(2,2,2-trifluoroethoxyde)-1,2-diphenylethene **131** were prepared by photolysis of a solution of tolan **10** (50 mg) in 2,2,2-trifluoroethanol (100mL). The products were isolated and purified by column chromatophy on silica gel

E-1-(2,2,2-trifluoroethoxy)-1,2-diphenylethene, **E-131**:

^{1}H-NMR ($CDCl_3$) δ 7.36- 7.24 (6H, m), 7.14-7.08 (6H, m), 6.98-6.97 (1H,d, J = 7.3 Hz), 5.96 (1H, s), 4.26-4.21 (2H, J_{HF} = 8.2 Hz) ^{13}C NMR ($CDCl_3$) δ 65.9 (1C, q, J^2_{C-F} = 35.5 Hz), 106.3, 123.6 (1C, q, J^1_{C-F} = 278.8 Hz), 126.3, 128.3, 128.5, 129.1, 129.3, 129.7, 134.2, 135.7, 155.0; m/z (GC-MS): 279 (18), 278 (100), 277 (3), 195 (6), 194 (2), 180 (2), 179 (13), 178 (12), 177 (4), 176 (5), 168 (11), 167 (73), 166 (20), 165 (60), 164 (4), 163 (2), 159 (10), 153 (5), 152 (38), 151 (5), 150 (2), 141 (2), 139 (4), 128 (4), 105 (17), 102 (2), 91 (2), 90 (6), 89 (12), 88 (2), 83 (8), 82 (3), 77 (12), 76 (5), 75 (2), 74 (2), 65 (2), 64 (3), 63 (6), 62 (2), 51 (11), 50 (2).

Z-1-(2,2,2-trifluoroethoxy)-1,2-diphenylethene, **Z-131**:

^{1}H-NMR ($CDCl_3$) δ 7.70- 7.68 (2H, d, J = 7.4 Hz), 7.55-7.53 (2H, m) 7.42-7.34 (4H, m), 7.25-7.20 (1H, m), 6.18 (1H, s), 4.07-4.02 (2H, J_{HF} = 8.5 Hz) ^{13}C NMR ($CDCl_3$) δ 66.5 (1C, q, J^2_{C-F} = 35.1 Hz), 114.5, 123.6 (1C, q, J^1_{C-F} = 278.7 Hz), 126.7, 127.4, 128.6, 129.0, 129.1, 134.9, 135.2, 153.4; m/z (GC-MS): 279 (17), 278 (100), 277 (3), 196 (2), 195 (9), 194 (2), 180 (3), 179 (16), 178 (15), 177 (5), 176 (5), 168 (13), 167 (93), 166 (25), 165 (74), 164 (5), 163 (2), 159 (13), 153 (6), 152 (47), 151 (7), 150 (2), 141 (2), 139 (5), 129 (2), 128 (5), 126 (2), 118 (2), 115 (7), 109 (3), 106 (2), 105 (30), 102 (4), 97 (2), 91 (3), 90 (10), 89 (20), 88

(4), 87 (2), 83 (15), 82 (8), 77 (19), 76 (8), 75 (3), 74 (2), 65 (3), 64 (4), 63 (9), 62 (2), 52 (2), 51 (15), 50 (3).

GC-MS of products detected from the photolysis of **12** in TFE:

E-1-(2,2,2-trifluoroethoxy)-2-(3-methoxyphenyl)-1-phenylethene, **E-132**:
m/z (GC-MS): 309 (18), 308 (100), 307 (7), 225 (5), 210 (2), 209 (3), 198 (2), 197 (17), 183 (2), 182 (17), 181 (10), 179 (2), 178 (2), 169 (2), 167 (4), 166 (12), 165 (35), 164 (4), 163 (2), 154 (7).

Z-1-(2,2,2-trifluoroethoxy)-2-(3-methoxyphenyl)-1-phenylethene, **Z-132**:
m/z (GC-MS): 309 (11), 308 (78), 307 (3), 225 (7), 209 (5), 198 (2), 197 (34), 195 (2), 194 (3), 183 (5), 182 (44), 181(26), 179 (5), 178 (4), 169 (6), 167 (9), 166 (32), 165 (100), 164 (10), 163 (3), 154 (23).

E-1-(2,2,2-trifluoroethoxy)-1-(3-methoxyphenyl)-2-phenylethene, **E-135**:
m/z (GC-MS): 309 (14), 308 (100), 225 (4), 210 (3), 209 (7), 197 (30), 194 (6), 183 (3), 182 (35), 181 (28), 179 (3), 178 (2), 169 (4), 167 (5), 166 (27), 165 (76), 164 (9), 163 (4), 159 (3), 154 (16).

Z-1-(2,2,2-trifluoroethoxy)-1-(3-methoxyphenyl)-2-phenylethene, **Z-135**:
m/z (GC-MS): 309 (9), 308 (100), 296 (2), 289 (3), 287 (2), 265 (2), 254 (2), 239 (2), 238 (2), 235 (3), 229 (3), 209 (4), 202 (3), 197 (29), 183 (38), 181 (29), 180 (3), 177 (2), 169 (3),

166 (25), 165 (97), 164 (5), 163 (2), 154 (14).

GC-MS of products detected from the photolysis of **13** in TFE:

E-1-(2,2,2-trifluoroethoxy)-2-(4-methoxyphenyl)-1-phenylethene, **E-133**:
m/z (GC-MS): 309 (9), 308 (71), 209 (6), 208 (2), 198 (9), 197 (77), 195 (6), 194 (3), 193 (2), 183 (2), 182 (31), 181 (25), 179 (2), 178 (3), 167 (9), 166 (34), 165 (100), 164 (9), 163 (3), 158 (13), 154 (35).

Z-1-(2,2,2-trifluoroethoxy)-2-(4-methoxyphenyl)-1-phenylethene, **Z-133**:
m/z (GC-MS): 309 (4), 308 (73), 291 (2), 225 (27), 209 (4), 198 (7), 197 (100), 182 (16), 181 (2), 180 (2), 169 (3), 167 (2), 166 (14), 165 (49), 154 (9).

E-1-(2,2,2-trifluoroethoxy)-1-(4-methoxyphenyl)-2-phenylethene, **E-136**:
m/z (GC-MS): 309 (8), 308 (53), 226 (2), 225 (22), 198 (16), 197 (100), 183 (2), 182 (19), 181 (12), 167 (6), 166 (17), 165 (53), 164 (5), 163 (2), 154 (20).

Z-1-(2,2,2-trifluoroethoxy)-1-(4-methoxyphenyl)-2-phenylethene, **Z-136**:
m/z (GC-MS): 308 (61), 300 (2), 293 (3), 239 (2), 197 (77), 193 (2), 182 (14), 181 (14), 179 (6), 177 (2), 167 (9), 166 (23), 165 (100), 159 (8), 154 (30).

GC-MS of products detected from the photolysis of **14** in TFE:

E-1-(2,2,2-trifluoroethoxy)-2-(3,5-dimethoxyphenyl)-1-phenylethene, **E-134**:
m/z (GC-MS): 339 (16), 338 (100), 337(16), 323 (3), 307 (21), 269 (13), 255 (18), 239 (11), 233 (14), 227 (6), 225 (5), 224 (5), 213 (3), 212 (26), 211 (5), 209 (9), 208 (3), 197 (19), 196 (29), 195 (15), 194 (3), 183 (2),182 (5), 181 (19), 180 (10), 179 (2), 169 (12), 168 (4), 167 (5), 166 (5), 165 (23), 164 (2), 154 (3).

Z-1-(2,2,2-trifluoroethoxy)-2-(3,5-dimethoxyphenyl)-1-phenylethene, **Z-134**:
m/z (GC-MS): 339 (16), 338 (100), 337(14), 323 (2), 307 (19), 269 (14), 255 (19), 240 (6), 239 (10), 233 (16), 227 (6), 225 (3), 224 (4), 212 (28), 211 (6), 209 (9), 208 (2), 197 (21), 196 (30), 195 (16), 194 (3), 182 (3), 181 (20), 180 (9), 169 (13), 168 (3), 167 (6), 166 (6), 165 (25), 154 (2).

E-1-(2,2,2-trifluoroethoxy)-1-(3,5-dimethoxyphenyl)-2-phenylethene, **E-137**:
m/z (GC-MS): 339 (6), 338 (100), 337(2), 255 (4), 240 (3), 239 (11), 227 (6), 212 (13), 197 (3), 196 (13), 195 (2), 181 (4), 169 (2), 165 (27).

Z-1-(2,2,2-trifluoroethoxy)-1-(3,5-dimethoxyphenyl)-2-phenylethene, **Z-137**:
m/z (GC-MS): 339 (3), 338 (100), 255 (7), 255 (7), 240 (2), 239 (14), 227 (8), 212 (30), 202 (4), 197 (8), 196 (31), 195 (8), 181 (11), 169 (8), 165 (49).

Hydrogenation of the photolysis samples of **12**, **13** and **14** was done using a Parr 4560 mini-bench reactor (equipped with a 4836 controller for heating and steering) as follows: a sample of 25 mL of the irradiated solution and a small amount of $PdCl_2$ were added directly into the vessel. The system was closed, and the air was evacuated using nitrogen. The hydrogen (ultra-pure, from PraxAir company) was introduced into the reactor until the internal pressure reached 8 atmospheres. The vinyl ethers were reacted with hydrogen for 24 hours with mechanical stirring. The resulting 1,2-diphenylethane derivatives have been characterized previously in our laboratory.[46, 47, 111]

GC-MS of products detected following hydrogenation of the irradiated sample from **12**:

1-(2,2,2-trifluorethoxy)-1-(3-methoxyphenyl)-2-phenylethane, **141**:

m/z (GC-MS): 310 (1), 220 (98), 219 (100), 211 (2), 165 (4), 150 (2), 139 (3), 137 (2), 136 (26), 135 (25), 121 (2), 109 (2), 108 (2), 107 (6), 105 (2), 105 (23), 103 (2), 92 (4), 91 (16), 90 (2), 89 (3), 83 (2), 79 (18), 78 (4), 77 (9), 76 (2), 65 (10), 64 (3), 63 (4).

1-(2,2,2-trifluorethoxy)-2-(3-methoxyphenyl)-1-phenylethane, **142**:

m/z (GC-MS): 310 (7), 190 (15), 189 (100), 179 (2), 178 (3), 165 (4), 152 (3), 141 (2), 122 (2), 121 (8), 115 (2), 110 (2), 109 (21), 107 (3), 106 (3), 105 (23), 103 (2), 92 (3), 91 (21), 90 (3), 89 (5), 83 (9), 79 (18), 78 (12), 77 (22), 76 (3), 65 (6), 64 (2), 63 (4), 52 (3), 51 (7), 50 (2).

GC-MS of products detected following hydrogenation of the irradiated sample from **13**:

1-(2,2,2-trifluorethoxy)-1-(4-methoxyphenyl)-2-phenylethane, **143**:

m/z (GC-MS): 310 (3), 220 (7), 219 (64), 211 (3), 210 (5),190 (4), 189 (39), 178 (2), 167 (3), 166 (2), 152 (4), 136 (9), 135 (22), 122 (9), 121 (100), 115 (2), 109 (5), 107 (2), 106 (2), 105 (7), 103 (2), 92 (2), 91 (12), 90 (2), 89 (4), 83 (3), 79 (5), 78 (8), 77 (15), 76 (2), 65 (6), 64 (2), 63 (3), 52 (2), 51 (6).

1-(2,2,2-trifluorethoxy)-2-(4-methoxyphenyl)-1-phenylethane, **144**:

m/z (GC-MS): 190 (10), 189 (100), 143 (4), 141 (2), 129 (4), 128 (4), 117 (3), 115 (4), 109 (8), 105 (12), 104 (18), 103 (3), 91 (17), 83 (4), 81 (2), 79 (11), 78 (5), 77 (12), 65 (3), 58 (3), 57 (3), 56 (2), 55 (12), 54 (2), 53 (3), 51 (6).

GC-MS of products detected following hydrogenation of the irradiated sample from **14**:

1-(2,2,2-trifluorethoxy)-1-(3,5-dimethoxyphenyl)-2-phenylethane, **145**:

m/z (GC-MS): 250 (2), 249 (22), 167 (3), 166 (20), 165 (15), 153 (2), 152 (3), 137 (4), 135 (6), 128 (2), 122 (3), 115 (3), 109 (4), 107 (3), 103 (2), 95 (5), 92 (9), 91 (100), 89 (7), 83 (4), 79 (4), 78 (7), 77 (11), 76 (2), 69 (4), 66 (3), 65 (28), 64 (5), 63 (10), 62 (2), 52 (3), 51 (2)

1-(2,2,2-trifluorethoxy)-2-(3,5-dimethoxyphenyl)-1-phenylethane, **146**:

m/z (GC-MS): 341 (3), 340 (18), 190 (9), 189 (100), 165 (4), 153 (2), 152 (4), 151 (8), 141 (2), 128 (2), 121 (2), 115 (2), 109 (10), 108 (2), 107 (2), 106 (2), 105 (14), 103 (2), 91 (13),

89 (3), 83 (6), 79 (15), 78 (13), 77 (23), 76 (2), 69 (3), 65 (8), 64 (2), 63 (5), 52 (2), 51 (9), 50 (2).

Apendix for Chapter 2:

Table A1. Singlet lifetimes (ns) *versus* temperature (°C) for the cyanotoluenes 1o, 1m and 1p in AN and TFE.

1o AN		**1m** AN		**1p** AN	
t (°C)	τ (ns)	t (°C)	τ (ns)	t (°C)	τ (ns)
-43.1	10.6	-43.1	11.3	-43.3	21.4
-36.4	10.6	-36.4	11.0	-36.4	20.5
-25.6	10.5	-24.1	10.8	-24.1	19.9
-16.7	10.4	-16.8	10.3	-16.8	19.8
-6.9	10.3	-6.9	9.9	-6.9	18.4
6.1	10.1	4.2	9.6	7.4	16.9
17.3	9.9	15.9	8.9	17.3	14.9
24.3	9.8	25.5	8.0	27.5	12.7
37.7	9.6	35.5	7.5	37.7	11.3
46.3	9.4	46.2	6.4	47.3	9.6
55.6	8.9	54.3	5.7	56.2	8.1
64.2	8.8	63.0	5.0	65.6	6.8

1o TFE		**1m** TFE		**1p** TFE	
t (°C)	τ (ns)	t (°C)	τ (ns)	t (°C)	τ (ns)
-22.3	9.5	-22.3	10.0	-22.3	18.6
-16.7	9.4	-16.7	10.0	-16.7	18.6
-10.8	9.3	-10.8	9.6	-10.8	17.9
-5.6	9.2	-5.6	9.3	-5.6	17.1
5.1	9.0	5.1	8.6	5.1	15.9
9.4	8.8	9.4	8.4	9.4	14.1
15.4	8.7	15.4	8.0	15.4	13.5
25.8	8.5	25.8	7.4	25.8	12.4
36.3	8.3	36.3	6.4	36.3	10.5
46.0	7.9	46.0	5.7	46.0	8.9
56.4	7.7	56.4	5.1	56.4	7.5
63.6	7.5	63.6	4.6	63.6	6.3

Table A2. Singlet lifetimes (ns) *versus* temperature (°C) for the boronate esters 2o, 2m and 2p in acetonitrile (AN) and 2,2,2-trifluoroethanol (TFE)

2o AN		**2m** AN		**2p** AN	
t (°C)	τ_s (ns)	t (°C)	τ_s (ns)	t (°C)	τ_s (ns)
-27.2	10.0	-27.6	12.1	-27.8	21.3
-22.7	9.7	-23.0	11.9	-23.0	21.1
-17.5	9.5	-18.5	11.7	-18.5	20.5
-12.6	9.5	-12.7	11.5	-12.5	19.8
-6.0	9.3	-7.6	11.1	-7.0	18.6
-0.2	8.7	-0.3	10.7	0.0	17.7
4.9	8.7	7.1	10.2	7.6	15.6
9.7	8.6	14.8	9.6	14.9	14.3
14.6	8.2	20.1	9.2	20.3	13.9
20.0	7.9	25.2	8.8	23.1	12.7
25.0	7.2	29.8	8.4	25.5	12.2
35.2	7.0	35.5	7.9	29.9	11.5
35.9	6.9	42.2	7.3	35.5	10.9
39.1	6.6	47.9	6.8	39.5	10.0
46.0	6.2	53.5	6.4	45.1	9.2
52.2	6.0	59.9	6.0	52.7	7.9
53.3	5.9	64.5	5.6	57.7	6.7
58.3	5.5			63.6	6.0
58.8	5.4				
63.5	5.1				
66.4	4.9				

2o TFE		**2m** TFE		**2p** TFE	
t (°C)	τ_s (ns)	t (°C)	τ_s (ns)	t (°C)	τ_s (ns)
-27.2	6.0	-26.2	8.7	-26.6	11.5
-22.7	5.8	-22.7	8.4	-22.7	10.7
-17.3	5.4	-17.3	7.9	-17.3	9.8
-12.6	5.1	-12.8	7.5	-12.8	8.7
-5.5	4.7	-5.5	7.0	-5.5	7.6
-0.2	4.4	-0.2	6.5	-0.2	6.8
4.9	3.8	4.9	6.0	4.9	6.2
9.6	3.8	9.6	5.6	9.6	5.5
14.5	3.5	14.5	5.3	14.5	5.0
20.1	3.3	20.1	4.9	20.1	4.5

Table A2 (Continued)

25.0	3.0	25.0	4.5	25.0	4.0
30.6	2.8	30.6	4.3	30.6	3.6
35.2	2.7	35.2	4.0	35.2	3.2
39.1	2.5	35.9	4.0	39.1	3.0
44.7	2.4	39.1	3.8	44.7	2.8
50.5	2.2	41.8	3.7	47.0	2.7
53.3	2.1	44.7	3.6	50.5	2.4
58.8	1.9	50.5	3.3	53.3	2.3
64.2	1.8	53.3	3.2	58.6	2.1
		58.3	3.1	64.2	1.9
		58.8	3.0		
		64.2	2.8		

Table A3. Singlet lifetimes (ns) *versus* temperature (^{o}C) for the trifluoromethyltoluenes 3o, 3m and 3p in acetonitrile (AN).

3o		**3m**		**3p**	
t (^{o}C)	τ_s (ns)	t (^{o}C)	τ_s (ns)	t (^{o}C)	τ_s (ns)
-44.2	10.1	-46.6	8.5	-37.3	24.3
-35.2	9.6	-37.8	8.2	-28.3	23.5
-25.4	8.7	-28.2	7.4	-17.8	20.8
-17.3	7.8	-15.2	6.9	-7.1	18.0
-8.8	6.8	-6.8	6.4	6.7	14.9
6.6	5.6	6.2	5.1	16.8	10.9
18.2	4.4	17.1	4.4	24.0	9.8
27.2	3.8	25.4	4.1	35.4	7.9
36.9	3.2	35.2	3.4	46.0	6.3
45.4	2.7	44.1	2.7	57.3	5.2
53.3	2.4	53.3	2.4	65.2	4.4
63.5	1.9	63.3	1.9		

Table A4. Singlet lifetimes (ns) *versus* temperature (^{o}C) for the methylanisoles 4o, 4m and 4p in acetonitrile (AN)

4o		**4m**		**4p**	
t (^{o}C)	τ_s (ns)	t (^{o}C)	τ_s (ns)	t (^{o}C)	τ_s (ns)
-44.3	7.4	-44.3	8.9	-44.3	7.1
-33.2	7.4	-33.4	8.8	-33.4	6.9
-22.6	7.2	-22.6	8.2	-22.6	6.6
-13.0	7.1	-13.0	8.2	-13.0	6.5
-6.8	6.9	-6.8	8.0	-6.8	6.4
5.3	6.8	9.6	7.8	6.9	6.4
15.5	6.7	15.5	7.8	17.3	6.4
25.5	6.7	26.5	7.6	27.8	6.4
34.0	6.5	37.2	7.3	37.0	6.3
45.2	6.4	46.7	7.3	45.7	6.3
54.0	6.5	55.3	7.2	54.0	6.2
63.0	6.3	63.5	7.1	65.5	6.2

Apendix for Chapter 3:

Table A5. Singlet lifetimes (ns) as a function of temperature for the compounds in Set 1 in acetonitrile.

2,3-dimethylbenzonitrile **5**		4-cyanoindan **7**		5-cyanotetralin **9**	
t (°C)	τ_s (ns)	t (°C)	τ_s (ns)	t (°C)	τ_s (ns)
-25.5	10.69	-26.2	9.91	-25.5	8.78
-22.7	10.42	-22.1	9.93	-22.7	8.71
-15.2	10.24	-18.3	9.86	-21.3	8.68
-10.4	10.18	-14.2	9.63	-15.5	8.69
-5.6	10.06	-10.1	9.70	-10.4	8.68
-0.1	9.99	-5.9	9.68	-5.6	8.70
4.9	9.90	-0.6	9.66	-0.1	8.61
10.7	9.73	4.9	9.63	4.9	8.72
14.5	9.66	9.9	9.68	10.3	8.63
20.4	9.51	14.4	9.58	14.7	8.73
25.2	9.27	19.5	9.49	19.7	8.63
30.0	9.16	24.9	9.42	20.5	8.77
35.3	9.07	30.1	9.41	25.0	8.76

Table A5 (Continued)

40.7	8.83	35.2	9.34	25.4	8.75
45.8	8.57	40.5	9.29	29.6	8.89
50.8	8.32	45.8	9.25	30.3	8.77
56.4	8.23	50.5	9.25	35.2	8.80
60.7	7.80	55.8	9.39	40.7	8.77
65.6	7.61	59.9	9.19	45.8	8.77
68.8	7.43	64.8	9.13	50.6	8.76
		68.1	9.12	56.4	8.90
				60.0	8.81
				65.6	8.96
				68.8	8.85

Table A6. Singlet lifetimes (ns) as a function of temperature for the compounds in Set 2 in acetonitrile

3,4-dimethylbenzonitrile **6**		5-cyanoindan **8**		6-cyanotetralin **10**	
t (^{o}C)	τ_s (ns)	t (^{o}C)	τ_s (ns)	t (^{o}C)	τ_s (ns)
-25.5	13.92	-26.2	12.93	-25.5	9.42
-22.4	13.45	-22.1	12.85	-22.4	9.67
-15.5	13.12	-18.3	12.78	-21.6	9.75
-10.7	12.73	-14.2	12.61	-15.5	9.79
-5.6	12.06	-10.1	12.48	-10.4	9.54
-0.1	11.63	-5.9	12.34	-5.6	9.76
4.9	11.06	-0.6	12.17	-0.1	9.79
10.3	10.64	4.9	11.95	4.9	9.80
14.5	10.14	9.9	11.76	10.3	9.86
20.4	9.52	14.4	11.39	14.5	9.86
25.2	8.90	19.5	11.13	19.7	9.71
29.6	8.46	24.9	10.91	20.3	9.87
35.1	7.82	30.1	10.58	25.0	9.89
40.7	7.35	35.2	10.30	25.4	9.89

Table A6 (Continued)

45.8	6.80	40.5	9.94	29.6	9.90
50.6	6.27	45.8	9.45	30.3	9.80
56.4	5.63	50.5	9.26	35.2	9.84
60.9	4.87	55.8	8.69	40.7	9.62
66.5	4.83	59.9	8.34	45.8	9.80
68.6	4.65	64.8	7.88	50.8	9.83
		68.1	7.54	56.4	9.84
				60.7	10.02
				65.6	9.97
				68.8	9.96

Table A7. Quantum yields of fluorescence and derived k_t values as a function of temperature for the compounds of Set 3 in acetonitrile

t (°C)	*ortho*-xylene, **18**		indan, **115**		tetralin, **116**	
	Φ_f	k_d[a]/ 10^7 s^{-1}	Φ_f	k_d[a]/ 10^7 s^{-1}	Φ_f	k_d[a]/ 10^7 s^{-1}
-25	0.19	2.61	0.25	3.46	0.28	4.95
-20	0.19	2.70	0.25	3.51	0.27	5.16
-15	0.17	2.92	0.24	3.58	0.26	5.21
-10	0.16	3.08	0.24	3.65	0.27	5.14
-5	0.16	3.21	0.23	3.74	0.26	5.36
0	0.15	3.40	0.23	3.82	0.25	5.39
5	0.14	3.52	0.22	3.99	0.25	5.42
10	0.14	3.66	0.21	4.06	0.25	5.50
15	0.13	3.83	0.21	4.11	0.25	5.57
20	0.13	4.01	0.21	4.21	0.25	5.59
25	0.12	4.21	0.20	4.34	0.24	5.71
30	0.11	4.48	0.19	4.46	0.24	5.82
35	0.11	4.77	0.19	4.63	0.23	5.87
40	0.10	5.17	0.18	4.79	0.23	5.88
45	0.09	5.56	0.17	4.97	0.23	5.99
50	0.08	5.96	0.17	5.20	0.22	6.14
55	0.08	6.44	0.16	5.48	0.22	6.37
60	0.07	7.03	0.15	5.76	0.21	6.56
65	0.07	7.69	0.14	6.09	0.20	6.69

a. calculated using eq. 3.4

$$k_d(T) = \frac{1}{\tau_s(T)} = \frac{\phi_f(25°C)}{\tau_s(25°C) x \phi_f(T)} \qquad (3.4)$$

Bibliography

1. March, J. *Advanced Organic Chemistry.* Jonh Wiley and Sons Ltd. New York. **1992**, *273.*

2. Hughes, E. D. and Ingold, C. K. *J. Chem. Soc.* **1935**, *244.*

3. Turro, N. J *Modern Molecular Photochemistry.* The Benjamin Cumming Publishing Company, Inc. **1978.**

4. Strickler, S.J. and Berg, R. A. *J. Chem. Phys.* **1962**, 37, *814.*

5. Birks, J. B. and Dyson, D. J. *Proc. Roy. Soc., A.* **1963**, 275, *135.*

6. Ware, W. R. and Baldwin, B. A. *J.Chem. Phys.* **1964**, 40, *1703.*

7. Gonzalez, C. M.; Pincock, J. A. *J. Am. Chem. Soc.* **2004**, 126, *8870.*

8. MacLeod, P. J.; Pincock, A. L.; Pincock, J. A.; Thompson, K. A. *J. Am. Chem. Soc.* **1998**, 120, *6443.*

9. Kaplan, L.; Rausch, D. J.; Wilzbach, K. E. *J. Am. Chem. Soc.* **1972**, 94, *8638.*

10. Bagot, J.; Gilbert, A. *Essentials of Molecular Chemistry.* CRC Publications, **1991**, *355.*

11. Kaplan, L.; Wilzbach, K. E.; Brown, W. G.; Yang, S. S. *J. Am. Chem. Soc.* **1965**, 87, *675.*

12. Wilzbach, K. E.; Kaplan, L. *J. Am. Chem. Soc.* **1965**, 87, *4004.*

13. Barlow, M. G.; Dingwall, J. G.; Haszeldine *J. Chem. Soc. Chem. Comm.* **1970**, *1580.*

14. Ward, H. R. *J. Am. Chem. Soc.* **1967**, 89, *2367.*

15. Anderson, D. *J. Phys. Chem.* **1970**, 74, *1686.*

16. Den Besten, I. E.; Kaplan, L.; Wilzbach, K. E. *J. Am. Chem. Soc.* **1968**, 90, *5868.*

17. Ishikawa, M.; Sakamoto, H.; Kametani, F.; Minato, A. *Organometallics.* **1989**, 8, *2767.*

18. Bryce-Smith, D.; Gilbert, A. *Tetrahedron Lett.* **1976**, 32, *1309.*

19. Kaplan, L.; Ritscher, J. S.; Wilzbach, K. E. *J. Am. Chem. Soc.* **1966**, 88, *2881.*

20. Farenhorst, E.; Bickel, A. F. *Tetrahedron Lett.* **1966**, 47, *5911.*

21. Berson, J. A.; Hasty, N. M. *J. Am. Chem. Soc.* **1971**, 93, *1551.*

22. Wilzbach, K. E.; Kaplan, L. *J. Am. Chem. Soc.* **1974**, 86, *2307.*

23. Wilberg, K. B.; Szeimies, G. *J. Am. Chem. Soc.* **1970**, 92, *571.*

24. Katz, T. J.; Wang, E. J.; Acton, N. *J. Am. Chem. Soc.* **1971**, 93, *3782.*

25. Foster, J.; Pincock, J. A.; Rifai, S.; Thompson, K. A. *Can J. Chem.* **2000**, 78, 1019.

26. Wilzbach, K. E.; Harkness, A. L.; Kaplan, L. *J. Am. Chem. Soc.* **1968**, 90, *2881*

27. Foster, J.; Pincock, A.L.; Pincock, J. A.; Thompson, K. A. *J. Am. Chem. Soc.* **1998**, 120, *13354.*

28. Buchi, G.; Perry, C. W.; Robb, E. W. *J. Org. Chem.* **1962**, 27, *4106.*

29. Chapman, O. L.; Lenz, G. *Organic Photochemistry.* Vol. I, Inc., New York, **1967**, *283.*

30. Wilson, J. W.; Stubblefield, V. S. *J. Am. Chem. Soc.* **1968,** 90, *3423.*

31. Roberts, T. D.; Ardemagni, L.; Shechter, H. *J. Am. Chem. Soc.* **1969**, 91, *6185.*

32. Zimmerman, H. E.; Pincock, J. A. *J. Am. Chem. Soc.* **1973**, 95, *3246.*

33. McEwen J.; Yates K. *J. Am. Chem. Soc.* **1986,** 50, *2881.*

34. Zimmerman, H. E.; Baum, A. A. *J. Am. Chem. Soc.* **1971**, 93, *3646.*

35. Zimmerman, H. E.; Pratt, A. C. *J. Am. Chem. Soc.* **1970**, 92, *6259.*

36. Zimmerman, H. E.; Mariano, P. S. *J. Am. Chem. Soc.* **1969**, 91, *1718.*

37. McEwen, J.; Yates, K. *J. Am. Chem. Soc.* **1987**, 109, *5800.*

38. Noyce, P. S.; Schiavelli, M. D. *J. Am. Chem. Soc.* **1968**, 90, *1020.*

39. Bott, R. W.; Eaborn, C.; Walton, D. R. M. *J. Chem. Soc.* **1965**, *384.*

40. Noyce, D. S.; Matesich, M. A.; Schiavelli, M. D.; Peterson, P. E. *J. Am. Chem. Soc.* **1965**, 87, *2295.*

41. Simandoux, J. C.; Torck, B.; Hellin, M.; Coussemant, F. *Bull. Soc. Chim. Fr.* **1972**, *4410* .

42. Chiang, Y.; Chwang, W. K.; Kresge, A. J.; Robinson, L. H.; Sagatys, D. S.; Young, C. I. *Can. J. Chem.* **1978**, 56, *456.*

43. Wan, P.; Culshaw, S. C.; Yates, K. *J. Am. Chem. Soc.* **1982**, 104, *2509.*

44. Wan, P.; Yates, K. *Rev. Chem. Intermed.* **1984**, 5, *157.*

45 Wan, P.; Yates, K. *J. Org. Chem.* **1983**, 48, *869.*

46 Roberts, J. C. The Formation of Carbocations from Excited States: The meta Methoxy Effect in Photofragmentation and Photoadditions. PhD Thesis. Dalhousie University. **2005.**

47. Roberts, C. J.; Pincock, J. A. *J. Org. Chem.* **2006**, 71, *1480.*

48. Lewis, F. D.; Kalgutkar, R. S.; Yang, J. S. *J. Am. Chem. Soc.* **1999**, 121, *12045.*

49. Ermolaev, V. L.; Sveshnikova, E. B. *Acta Phys. Pol.* **1968**, 34, *771.*

50. Murov, S. L., Carmichael, I., Hug, G. L. *Handbook of Photochemistry*, 2nd ed., Eds., Marcel Dekker: New York, **1993**; Table 1, *5-53.*

51. Cameron, K. S., A. L. Pincock, J. A. Pincock and A. Thompson *J. Org. Chem.* **2004**, 69, *4954.*

52. Foster, A.; Pincock, A.; Pincock, J. A.; Rifai, S.; Thompson, K. A. *Can. J. Chem.* **2000**, 78, *1019.*

53. DeCosta, D. and J. A. Pincock *J. Org. Chem.* **2002**, 67, *9484.*

54. Pincock, J. A. In *CRC Handbook of Organic Photochemistry and Photobiology*, 2nd ed.; Horspool, W., Lenci, F., Eds.; CRC press: New York, **2004**; 46, *1.*

55. Foster, A.; Pincock, A.; Pincock, J. A.; Thompson, K. A. *J. Am. Chem. Soc.* **1998**, 120, *13354.*

56. Lewis, F. D.; Zuo, X. *The Spectrum*; **2003**, 16, *8.*

57. Syage, J. A.; Adel, F. A.; Zewail, A. H. *Chem. Phys. Lett.* **1983**, 103, *15.*

58. Bearpark, M. J.; Bernardi, F.; Olivucci, M.; Robb, M. A. *J. Phys. Chem.* A **1997**, 101, *8395.*

59. Condirston, D. A.; Laposa, J. D. *Chem. Phys. Lett.* **1979**, 63, *313.*

60. Ni, T.; Caldwell, R. A.; Melton, L. A. *J. Am. Chem. Soc.* **1989**, 111, *457.*

61. Lewis, F. D.; Zuo, X.; Kalgutkar, R. S.; Warner-Brennan, J. M.; Miranda, M. A.; Font-Sanchis, E.; Perez-Prieto, J. *J. Am. Chem. Soc.* **2001**, 123, *11883.*

62. Zimmerman, H. E. *Org. Phtochem.* **1991**, 11, *1.*

63. Hixon, S. S. *J. Am. Chem. Soc.* **1976**, 98, *1271.*

64. Beesley, R. M.; Ingold, C. K.; Thorpe, J. F. *J. Chem. Soc.* **1915**, *1080.*

65. Druzhining, S. I.; Yung-Bao, J.; Demeter, A.; Zachariasse, K. A. *Phys. Chem.Chem. Phys.*, **2001**, 3, *5213.*

66. Zachariasse, K. A.; Grobys, M.; Tauer, E. Tauer, *Chem. Phys. Lett.* **1997**, 274, *372*

67. Demeter, A.; Druzhining, S.; George, M.; Haselbach, E. L.; Roulin, J. L.; Zachariasse, K. A. *Phys. Chem.* **2000**, 214, *1597.*

68. Rückert, I.; Hebecker, A.; Parusel, A. B. J.; Zachariasse, K. A. Z. *Phys. Chem.* **2000**, 214, *1563.*

69. Druzhinin, S. I.; Uzhinov, B. M. *Theor. Exp. Chem.* **1982**, 18, *565.*

70. Suzuky, K; Tanabe, H.; Tobita, S.; Shizuka, H. *J. Phys. Chem. A.* **1997**, 105, *373.*

71. Suzuky, K; Demeter, A.; Kühnle W.; Tauer, E.; Zachariasse, K.A.; Tobita, S.; Shizuka H. *Phys. Chem.Chem. Phys.* **2000**, 2, *981.*

72. Druzhinin, S.; Demeter, A.; Niebuer, M.; Tauer, E.; Zachariasse, K. A. *Res. Chem. Intermed.* **1999**, 25, *531.*

73. Bernardi, F.; Olivucci, M; Robb, M. A. *Chem. Soc. Rev.* **1996**, 25, *321.*

74. Zachariasse, K. A.; Grobys, M.; Tauer, E. *Chem. Phys. Lett.* **1997**, 274, *372.*

75. Zachariasse, K. A.; Von deer Haar, T.; Leinhos, U.; Kühnle, W. *Pure Appl. Chem.* **1993**, 65, *1745.*

76. Gonzalez, C. M; Pincock, J. A. *J. Photochem. and Photobio.* **2005**, 82, *301.*

77. Rücker, I.; Demeter, A.; Morawski, O.; Kühnle, W.; Tauer, E.; Zachariasse, K. A. *J. Phys. Chem. A.* **1999**, 103, *1958.*

78. Birks, J. B.; *Photophysics of Aromatic Molecules*, Wiley, London, John Miley and Sons Ltd. **1970**, Table 4.2, *122.*

79. Cundal, R. B. and Pereira, L.C. *J.C.S., Faraday. Trans.* **1970**, 92, *6259.*

80. Pincock, A. L.; Pincock J. A.; Stefanova R. *J. Am. Chem. Soc.* **2003**, 124, *9768.*

81. Pincock, A. L. and Pincock J. A. *Can. J. Chem.*, accepted. **2005**

82. Timmermans, J. *Physic–Chemical Constants of Pure Organic Liquids.* Vol.1, Elsevier, New York. **1950**.

83. Strickler, S. J. and R. A. Berg . *J. Chem. Phys.* **1962**, 37, *814.*

84. Birks, J. B.; *Photophysics of Aromatic Molecules*, Wiley, London, John Miley and Sons Ltd. **1970**, Table 5.2,*180.*

85. Carroll, F. A.; Quina, F. H. *J. Am. Chem. Soc.* **1976**, 98, *1.*

86. Quina, F. H.; Carroll, F. A. *J. Am. Chem. Soc.* **1976**, 98, *6.*

87. Mende, U.; Laseter, J. L.; Griffin, G. W. *Tetrahedrom Lett.* **1970,** 43, *3747.*

88. Bentley, T. W., Llewellyn G. *Yx* scales of solvent ionization power. In progresss in *Physical Organic Chemistry* Vol 17. (Edited by R. W. Taft), J. Wiley and Sons, New York, *121-158.*

89. Howell, N.; Pincock, J. A.; Stefanova, R. *J. Org. Chem.* **2000**, 65, *6173.*

90. Pavlik, J. W.; Kebede, N.; Thompson, M.; Day, A. C.; Barltrop, J. A. *J. Am. Chem. Soc.* **1999**, 121, *5666.*

91. Turro, N. J.; Zhang, Z.; Trahanovsky, W. S.; Chou, C. H. *Tetrahedron Lett.* **1988**, 29-21, *2543.*

92. Meier, H.; Pauli, A.; Koldhorn, H.; Hochhan, P. *Chem. Ber.* **1987**, 120, *1607.*

93. Pauli, A.; Koldhorn, H.; Meier, H. *Chem. Ber.* **1988**, *1611.*

94. Tschesche, H.; Obermeier, R.; Kupfer, S. Angew. *Chem. Intern. Ed. Engl.* **1970**, 9, *893.*

95. Katz, T. J.; Rosenberger, M.; O'Hara, P. *J. Am. Chem. Soc.* **1964**, 86, *249.*

96. Martin, H. D.; Pfohler, P.; Urbanek, T. Walsh, R. *Chem. Ber.* **1983**, 86, *1415.*

97. Gonzalez, C. M.; Pincock, J. A.. *Can J. Chem.* **2006**, 84 (1), *10.*

98. Hirata, Y.; Mataga, N.; Nomoto, *J. Phys. Chem.* **1992**, 96,*6569.*

99. Ishibashi, T, Okamato, H, .Hamaguchi, H. *Chem Phys. Lett.* **2000**. 325, *212.*

100. Taniaki, Y.; Inoue, H.; Hoshi, T.; Shiraishi. J. Z. *Phys. Chem.* **1971**, 74, *45.*

101. Ishibashi, T, Okamato, H, .Hamaguchi, H. *J. Phys Chem. A.* **1998**. 102, *2263.*

102. Ferrante, C.; Kensy, U.; Dick, B. *J. Phys Chem.* **1993**, 97, *13457*

103. Hirata, Y. Bull. *Chem. Scoc. Jpn.* **1999**, 72, *1674.*

104. Hirata Y.; Okada, T. *Chem Phys. Lett.* **1993**, 209, *397.*

105. Turro, N. J "*Modern Molecular Photochemistry*",The Benjamin Cumming Publishing Company, Inc. **1978**, *415.*

106. Bagot, J.; Gilbert, A. *Essentials of Molecular Chemistry.* CRC Publications, **1991**, *229.*

107. Schubert, W. M.; Keeffe, J. R. *J. Am. Chem. Soc.***1972**, 94, *559.*

108. Koshy, K. M.; Royd, D.; Tidwell, T. T. *J. Am. Chem. Soc.***1979**, 101, *357.*

109. Horspool, W.; Song, P. (Edts), CRC Handbook of Organic Photochemistry and Photobiology. **1995**.

110. McEwen, J.; Yates, K. *J. Phys. Org. Chem.* **1991**, 4, *193.*

111. Roberts, J. C.; Pincock, J. A. J. Org. Chem. **2004**, 69, *4279.*

112. Lewis, F. D.; Yang, J. S. *J. Am. Chem. Soc.***1997**, 119, *3834.*

113. Zimmerman, H. E.; Sandel, V. R. *J. Am. Chem. Soc.***1963**, 85, *915.*

114 Zimmerman, H. E. *J. Am. Chem. Soc.***1995**, 117, *8988.*

115. Sonogashira, K., Tohda, Y., *Tetrahedron Lett.* **1975**, *4467.*

116. Chanteau, S.H., Tour, J.M. *J. Org. Chem.* **2003**, 68, *8750.*

117. Shen, W., Wang, L. *J. Org. Chem.* **1999**, 64, *8873.*

118. Bagot, J.; Gilbert, A. *Essentials of Molecular Chemistry.* CRC Publications. **1991**, *85.*

119. March, J. *Advance Organic Chemistry*. 4th Eddition, John Wiley & Sons. **1992,** *361.*

120. Vogel, A. I. *Texbook of Practical Organic Chemistry*. Longman Scientific & Technical. 5th Edition. **1989**, *983.*

121. Vogel, A. I. *Texbook of Practical Organic Chemistry*. Longman Scientific & Technical. 5th Edition. **1989**, *895.*

122. Vogel, A. I. *Texbook of Practical Organic Chemistry*. Longman Scientific & Technical. 5th Edition. **1989**, *1281.*